Influence of input motion selection and soil variability on nonlinear ground response analyses

Yusuf GUZEL

A thesis submitted for the degree of Doctor of Philosophy (PhD)

Newcastle University

School of Engineering

December 2018

Abstract

This thesis studies the influence of input motion selection strategies on nonlinear site response analyses of soft clay soil deposits. It also investigates the role of elastic and nonlinear soil properties in nonlinear site response predictions. The research adopts a fully-coupled finite element (FE) procedure, employing an advanced kinematic hardening soil model. In addition, the results of equivalent linear site response analyses are considered for comparison purposes.

Firstly, the research validates the performance of the advanced soil constitutive model as implemented in the FE code. For this purpose, the free-field response at the Lotung Large-Scale Seismic Test (LSST) site in Taiwan is modelled in two dimensions. The best-fit shear modulus values according to in-situ data are used and the remaining soil model parameters are calibrated against experimental data from samples retrieved at different depths at the site. One weak (LSST11) and one strong (LSST7) input motion recorded along the downhole array are simulated. The predictions from the nonlinear FE approach at 17 m, 11 m, 6 m and at ground surface are compared with the corresponding recordings in terms of acceleration time histories, spectral response and maximum acceleration profiles. The accumulation of excess pore water pressures obtained from the FE nonlinear analyses is also compared to the recorded data.

Secondly, the research investigates the influence of five input motion selection strategies on nonlinear site response predictions. In particular, the effect of Peak Ground Acceleration (PGA) scaling, spectral acceleration scaling at T_1 ($Sa(T_1)$), where T_1 is the natural period of the soil column,, $0.2T_1$-$2T_1$ scaling, Mean Squared Error (MSE) scaling and spectral matching selection strategies is studied by modelling an ideal soft clay soil deposit with soil class D properties according to Eurocode 8 (EC8). Sets of seven input motions are formed for each selection strategy with lower (0.15g) and higher (0.35g) seismic intensity levels. The target response spectra are constructed based on the EC8 prescription. The selection strategies are evaluated with respect to $Sa(T_1)$, PGA profile and amplification factors. Moreover, they are assessed based on relative displacement, PGA and $Sa(T_1)$ at the ground surface (referred to as Engineering Demand Parameters, EDPs).

Finally, the research investigates the impact of the variability of the elastic (shear wave velocity, V_s) and dynamic (shear modulus reduction, G/G_o, and damping, D, curves) soil

properties on nonlinear site response predictions. The same soil model and input motions used for the deterministic analysis of the LSST site are adopted for nonlinear Monte Carlo Simulations (MCS) of the site. The results are evaluated in terms of spectral response, PGA profile and maximum shear strain profile, and the median values are compared with the recorded data.

Overall, the research verifies the capacity of the advanced constitutive soil model within a fully-coupled nonlinear FE procedure to correctly predict the free-field ground response at a given site, including the accumulation of excess pore water pressures. It also concludes that the spectral matching method is the best choice amongst the investigated selection strategies, as it leads to the least scatter in the EDP response. Moreover, seven input motions are found to be sufficient to obtain a stable response at ground surface. Lastly, the impact of variability of the V_s profile and G/G_o and D curves is shown to be dependent on both seismic intensity level and the adopted numerical approach. (e.g. equivalent linear code vs fully-coupled nonlinear code).

Acknowledgements

I, first of all, acknowledge my sponsor, the Turkish National Education Ministry, for giving me an opportunity to study at Newcastle University. I appreciate their effort during the time of completing my degree. I will forever be grateful to them.

I should acknowledge the priceless help and guidance of my supervisors, Dr Gaetano Elia and Dr Mohamed Rouainia, allowing me to gain in-depth understanding of the research area which I have been dreaming of. Their contributions to my academic and personal lives have been immeasurable in many aspects. It has been a great honour for me to study with them and I wish to carry on many cooperative researches with them for many years to come. I also thank Dr Carmine Galasso for his advices at the beginning of the research and Dimitrios Karofyllakis for his contributions to Chapter 4.

I should express my gratitude to my wife and my daughter whose presence in my life is my happiness to feel and my strength to stand strong. Living two years far from them was something to endure but acknowledging this right now is something to feel. I wholeheartedly thank them for their patience and for being considerate. I also appreciate the full support of my parents and the rest of my extended family. I wish them happy and healthy long life.

Last, but not least, is to acknowledge my office mates, Tom Charlton, Lowell Cabangon, and Alfred Opukumo. Long-lasting and deep discussions with them helped me to look at the geotechnical engineering problems in different ways. Making such friendship with them is also something to honour and remember in the future. I wish them all the best in the rest of their lives.

Table of Contents

Table of Figures

Table of Tables

List of Symbols

AF	Amplification factor
A, m and n	Plasticity index dependent stiffness parameters
a_g	Design ground acceleration on type A ground
a_{max}	Maximum peak ground acceleration
$\bar{\alpha}$	Centre of the bubble yield surface
$\hat{\alpha}$	Centre of the structure surface
α_R and β_R	Mass and stiffness related Rayleigh damping coefficients
A^*	Parameter controlling relative proportion of distorsional and volumetric destructuration
β_1 , β_2 , β_1^*	First two parameters solid phase and last one fluid phase Newmark parameters
B	Stiffness interpolation parameter
b	Normalised distance between bubble and structure surface
b_{max}	Maximum value of b
CDF	Cumulative density function
CMS	Conditional mean spectrum
COSMOS	Consortium of Organizations for Strong Motion Observation Systems
COV_{G_0}, COV_A	Coefficient of variance for G_0 or Viggiani stiffness parameter A
CSS	Cyclic simple shear test
c_u	Undrained shear strength of soil
d_{ij}	Distance between point i and point j
$D_{5\text{-}95}$	Dobry's duration
DSHA	Deterministic seismic hazard analysis
e	Void ratio
EDP	Engineering demand parameter
EERA	Equivalent-linear Earthquake site Response Analysis
EPRI	Electric Power Research Institute
ESM	European Strong-Motion Database

E-W, N-S and U-P	East-west, north-south and up-down directions for the recorded earthquake data
f^s, f^p	Force matrices for solid and fluid phases, respectively
F, f_r, f_b	Structure, reference and bubble surfaces
FFT	Fast Fourier transform
g	Acceleration of gravity
GMPE	Ground motion prediction equation
GNjp	Generalized Newmark scheme for the dynamic response solutions at each time step
G_0	Initial shear modulus
G/G_0	Normalised shear modulus
G, D	Material shear stiffness and material damping
H_i, V_i	Thickness (m) and shear wave velocity of the ith layer out of N
H	Plastic modulus
H_c	Plastic modulus at conjugate stress
$\boldsymbol{I}$	Second rank identity tensor
I_a	Arias intensity
$\{I\}$	Unit vector
IFFT	Inverse fast Fourier transform
IM	Intensity measure
k	Parameter controlling rate of loss of structure with damage strain
K	Bulk modulus
K_o	Coefficient of earth pressure at rest
lnv : lnp plane	Logarithmic volume – logarithmic mean stress compression plane
L	Correlation length used for the spatial distribution of V_s
LSST	Large-Scale Seismic Test
Δl_{node}	Distance between the element nodes
M	Magnitude
M	Slope of the critical state line
MCE	Maximum credible earthquake
MCSs	Monte Carlo Simulations
$[M]$, $[C]$ and $[K]$	Mass, viscous and stiffness matrix

M_θ	Dimensionless scaling function for deviatoric variation of critical state stress ratio
MSE	Mean squared error
M_w, M_s and M_L	Moment, surface and Richter local magnitudes
$\bar{\boldsymbol{n}}$	Normalised stress gradient on the bubble
N	Number of soil layers at the top 30 m of the soil deposit
NEHRP	National Earthquake Hazards Reduction Program
NLDA	Nonlinear dynamic analysis
N_{SPT}	Standard penetration resistance
OCR	Over consolidation ratio
p	Mean effective stress
p	Pore pressure matrix
p_c	Stress variable controlling size of the surfaces
p_r	Reference stress
PDF	Probability density function
PEER	Pacific Earthquake Engineering Research Centre
PGA, PGV and PGD	Peak ground acceleration, peak ground velocity and peak ground displacement
PI, LL	Plasticity index and liquid limit
PSHA	Probabilistic seismic hazard analysis
q	Scalar deviator stress
$[Q], [S]\ and\ [H]$	Coupling, compressibility and permeability matrix
r	Parameter describing ratio of sizes of structure and reference surfaces
r_0	Initial value of r
R	Ratio of sizes of bubble and reference surface
R	Site to source distance
RMSE	Root mean square error
RMW	Rouainia and Muir Wood
$\boldsymbol{s}$	Tensorial deviator stress
S	Soil factor
Sa	Spectral acceleration

$Sa(T_1)$	Spectral acceleration at the fundamental period of the single degree of freedom system
Sa_{arb}	Arbitrary single horizontal component of an event
$Sa_{g.m}$	Geometric mean of two horizontal components of an event
SDOF, MDOF	Single and multiple degree of freedom systems
SM2D	Soil model testing program in 2D
SR	Spectral shape factor
SWANDYNE	SWANsea DYNamic program version II
TPC	Taiwan Power Company
T_1, T_2	First and second modes of soil models
μ	Positive scalar of proportionality
$\{\ddot{u}\}$, $\{\dot{u}\}$ and $\{u\}$	Vector of nodal relative acceleration, velocity and displacement
$\ddot{u}_g$	Acceleration at the bottom of the soil layer
μ_{G_0}, μ_A	Mean value of G_0 or Viggiani stiffness parameter A for a soil element
μ_{lnG_0}, μ_{lnA}	Logarithmic mean value of G_0 or Viggiani stiffness parameter A for a soil element
UHS	Uniform hazard spectrum
USGS	United States Geological Survey
v	Poisson's ratio
V_s	Shear wave velocity
$V_{s,30}$	Average shear wave velocity at the top 30 m of a soil deposit
V_p	Compression wave velocity
ω_m and ω_n	Mass and stiffness related angular frequencies
τ, γ	Shear stress and strain
$\gamma_{eff}, \gamma_{max}$	Effective and maximum shear strains
λ	Slope of the compression line
λ_m	Rate of earthquake occurrence with magnitudes larger than m
λ_{min}	Minimum wave length
λ*	Slope of normal compression line in ln$v$: ln$p$ compression plane
κ	Slope of the swelling line
κ*	Slope of swelling line in lnv : lnp compression plane
Σ_{ij}	Covariance function between data in point i and pont j

E	Distant measurement between the spectral acceleration of an input motion and the mean value from the ground motion prediction equation at a given period
$\boldsymbol{\Sigma}$	Effective stress tensor
$\boldsymbol{\sigma}_c$	Conjugate stress
σ_h	Lateral total stress
$\sigma_{lnG_0}, \sigma_{lnA}$	Logarithmic standard deviation of G_0 or Viggiani stiffness parameter A for a soil element
σ_{lnSa}	Logarithmic standard deviation of Sa
ϕ	Soil angle of internal friction
ξ	A normally distributed random variable
$\boldsymbol{\eta}_0$	Dimensionless deviatoric tensor (anisotropy of structure)
Ψ	Stiffness interpolation exponent

Chapter 1. Introduction

1.1 Background and Motivation

Structures are designed to function for particular purposes within a projected lifespan. They are expected to ensure the capacity of resisting internal (self-weight) and external (earthquake, wind, human activity, etc.) forces, while retaining functionality with respect to serviceability limit states. Of particular importance is the load from earthquake events, which should be carefully considered, as this has the potential to cause great damage to earth structures, resulting in enormous economic and, more seriously, human losses. The consideration of seismic forces in geotechnical design requires an understanding of fault mechanisms, seismic wave propagation through rigid earth structures and, finally, local site conditions where the geotechnical structures are located.

Whereas the first two considerations mentioned above (fault mechanisms and seismic wave propagations) are the concern of the discipline of geology, the last one is dealt by geotechnical engineering and soil dynamics. The local site conditions significantly influence the characteristics of seismic motions, travelling from the bedrock to the ground surface through layered soil deposits (Kramer, 2014). Modern seismic design code provisions (EC8, NEHRP, etc.) include the effects of soil deposits on the construction of design response spectra for different soil conditions, which are thought to be a good proxy for future potential earthquake events at any site of interest. However, the inclusion of soil factors in the construction of a design response spectrum cannot guarantee that the local site effect is properly accounted for (Pitilakis *et al.*, 2012). This is especially true when soil deposits are characterised by low shear wave velocity (V_s), as the dynamic properties of the soils control the seismic oscillations of the deposit and can produce a considerable alteration in the frequency content of the bedrock motions. For this reason, it is suggested to always closely study local site effects in areas located over soft soil deposits.

One way of studying local site effects is to conduct ground response analyses of the deposit subjected to bedrock input motions. While the use of equivalent linear or nonlinear numerical approaches can affect the response predictions at the surface, there are three other major factors that play an important role: 1) bedrock input motions; 2) adopted V_s profiles; and 3) adopted shear modulus reduction (G/G_o) and damping (D) curves

(Andrade and Borja, 2006). These three site response analysis inputs involve aleatory and epistemic uncertainties that may influence the variability in the predictions at surface (Phoon and Kulhawy, 1999). To overcome uncertainty due to the bedrock input motions, selection and modification strategies can be used, allowing the acquisition of a stable response at the surface from fewer analyses (Shome *et al.*, 1998; Iervolino and Cornell, 2005). The selection of bedrock input motions firstly requires the determination of a target response spectrum, which can be based on site-specific seismic hazard analyses or acquired imposed by design code provisions (e.g. EC8, NEHRP). Secondly, bedrock input motions can be modified according to a specific selection strategy. This topic of selecting and modifying input motions is relatively understudied in the geotechnical earthquake engineering field, compared to the research implemented in the nonlinear dynamic analysis of structures (Baker and Allin Cornell, 2006; Baker and Cornell, 2006; Galasso, 2010; Galasso and Iervolino, 2011; Haselton *et al.*, 2012). This may be due to "poorly documented and unclear parameter selection and code usage protocols" of nonlinear site response analyses, as stated by Stewart and Kwok (2008).

To quantify the uncertainty in site response prediction at the surface sourcing from the V_s profile and G/G_o and D curves, a series of site response analyses can be conducted by randomising these input parameters. The influence of their variability on site response can be associated with the numerical procedures adopted (i.e. frequency or time domain equivalent linear approaches, and time domain nonlinear approaches). In addition, as the soil behaviour is mostly dependent on the seismic intensity of the input motion, the site response will definitely be affected. While there are several studies that have dealt with this topic (Roblee *et al.*, 1996; Bazzurro and Cornell, 2004; Kwok *et al.*, 2008; Li and Assimaki, 2010; Rota *et al.*, 2011), it is still not clear whether it is appropriate to include the soil variability in site response analyses, as no obvious benefit over response predictions from deterministic analyses has been observed (Rathje *et al.*, 2010). Therefore, the topic needs further research particularly concerning the application of input motion selection, modification strategies and the influence of variability in soil properties.

1.2 Aim

The aim of this study is to provide guidance to engineering practitioners and geotechnical researchers about the selection and modification of the bedrock input motions and the role of elastic and nonlinear soil properties adopted in nonlinear site response analyses of soft clay deposits.

1.3 Objectives

The aim will be achieved through the following objectives:

1) To examine existing earthquake databases in order to assess whether the median response spectrum of actual input motions, especially those recorded on soft soil deposits (class D), matches well the design response spectrum proposed by EC8.
2) To identify key parameters that will give an indication of the efficiency of the input motion selection/scaling strategies for ground response analysis.
3) To clarify the best earthquake selection strategy from amongst the widely known selection methods, in terms of the response parameters identified in Objective 2.
4) To assess, within a probabilistic framework, the reliability of the EC8 design response spectrum with respect to ground response predictions for soft clay soil deposits.
5) To provide guidelines to engineering practitioners and researchers about the selection and scaling strategies of bedrock input motions for nonlinear ground response analysis.
6) To model a downhole array site that has been rigorously characterised from a soil dynamics point of view and which includes sufficient data to enable a study on the variability of the soil properties.
7) To randomise the soil properties by using available measured in-situ and laboratory data for the site under consideration.
8) To determine the contribution of variability in soil properties to the uncertainty in the site response predictions at the ground surface.

1.4 Structure of the Thesis

In this section, the general contents of the chapters that shape the thesis are explained.

Chapter 2 deals with earthquake databases around the world. Objective 1 will be achieved by considering the earthquake ground motions recorded on soft soil deposits, and evaluating them in a probabilistic way to test the suitability of the EC8 design response spectrum. The main idea of the chapter is to highlight the impact of soft soil deposits on the characteristics of ground motions that cannot be accounted for by a smooth design response spectrum. This will allow the ideal soft clay deposits discussed in Chapter 5 to be studied in terms of the influence of input motion selection and modification strategies in free-field nonlinear site response analyses. In addition, some suggestions about the EC8 design response spectrum will be given, based on the results, in terms of predicted spectral response values.

Chapter 3 contains a review of the concept of input motion selection and modification strategies, particularly from a structural engineering perspective. It also highlights the lack of research on this topic in the geotechnical engineering discipline. Subsequent to that, the focus of geotechnical research on the simulation of seismic waves propagation through the soil deposit is expressed via equivalent linear or nonlinear codes, incorporating different soil constitutive models. Several previous studies have tackled the impact of certain input sources (e.g. elastic and nonlinear soil properties, numerical models and thickness of soil deposits) bringing uncertainty to site response predictions at the surface. Emphasis is placed on the need for further research in this area. This chapter essentially presents clear documentation justifying the motivation for this thesis, and addresses Objective 2.

Chapter 4 documents the performance of the nonlinear numerical finite element code, SWANDYNE II, employed in Chapters 5 and 6 with the kinematic hardening soil model *RMW*. The Large-Scale Seismic Test site in Lotung (Taiwan) is considered for the free-field nonlinear site response analyses. One weak and one strong input motion recorded at the site are simulated and the predictions from the analyses are compared with actual data from different depths, along with the results from equivalent linear analyses. Overall, this chapter demonstrates the capacity of the code in simulating seismic wave propagation and the reliability of the results presented in the following chapters.

Chapter 5 deals with the implementation of five selection strategies used in nonlinear site response analyses which are well established in the nonlinear performance analysis of

structures. For this purpose, ideal soft clay soil deposits are modelled in the FE code and the analyses are carried out under sets of seven input motions, with lower and higher seismic intensity levels. Herein, the results are evaluated at the surface, with respect to spectral response and Engineering Demand Parameters (EDPs), i.e. relative displacement, peak ground acceleration (PGA) and spectral acceleration at a fundamental period of the soil deposits. The influence of the number of input motions for each selection strategy is also discussed. Moreover, a statistical test is conducted to check whether the medians of the selection strategies results can be found to be equal. Lastly, the level of correlation between the Arias intensity/Dobry duration of the bedrock input motions and EDPs are evaluated. This chapter reports on the achievement of Objectives 3, 4 and 5.

Chapter 6 focuses on the effects of variability in the elastic and nonlinear soil properties in nonlinear site response analyses. It uses the same soil model and bedrock input motions adopted in Chapter 4. This enables an investigation of the role of the inclusion of soil properties variability in conjunction with the influence of the seismic intensity level in site response prediction. The site response analyses are conducted by nonlinear Monte Carlo Simulations (MCSs). Spectral response predictions are considered for evaluation purposes, in conjunction with their logarithmic standard deviations. Equivalent linear MCSs are also performed to study the model-to-model variability. This chapter reports on Objectives 6, 7 and 8.

Finally, Chapter 7 outlines the methodologies used in each chapter. The conclusions from each chapter are summarised, and the overall findings and recommendations for future work are reported.

Chapter 2. Earthquake Databases on Class D Soils

2.1 Introduction

Earthquake events are one of the natural disasters that can cause the utmost damage to earth structures, leading to high levels of human and economic loss. By designing earth structures to accommodate potential seismic events, earthquake hazards can be minimised. The interest of the practitioners of earth structures, in terms of earthquake events, is the spectral accelerations of ground motions to be used in their designs. Since the characteristics of each ground motion are different, they have unique spectral accelerations. Therefore, it is difficult to rely only on spectral accelerations of a single past earthquake event when an earth structure at another site is designed. In order to deliver resistance of an earth structure to a future earthquake event, it is reasonable to use a standard spectral response shape (i.e. design response spectrum) that can include past, and represent future, earthquake events for the site of interest.

From the early stage of the concept of a standard (or smooth) design response spectrum until now, there has been ongoing discussion on the reliability of their use in structural design (Biot, 1941; Housner, 1941). The basics of the smoothed design response spectrum originate from the spectral accelerations of real earthquake events, which are the maximum response (i.e. acceleration, velocity or displacement) of all possible single degree of freedom systems to an applied input motion with a specific damping level. In the early stages, as Biot (1934) expressed, when a reasonable number of real earthquake motions have been obtained, a standard response spectrum can be constructed from their shapes, which can be adopted in assessing/designing the dynamic performance of existing or new structures (Trifunac, 2008). The studies of Blume *et al.* (1973) and Newmark *et al.* (1973a), for example, proposed smooth response spectra, based on probabilistic computations of the real earthquake response spectra.

The design response spectrum is governed mainly by peak ground acceleration, velocity and displacement (PGA, PGV, and PGD, respectively) of seismic motions. Based on these three earthquake parameters, the response spectrum is separated into three discrete regions—the acceleration, velocity and displacement domain regions, at frequency ranges of around 3-8

Hz, 0.3–3.0 Hz and 0.1–0.3 Hz, respectively (Mohraz, 1976). In each frequency range, the dominant parameter of seismic motion drives the response spectrum. The dominance of each parameter at a certain range of frequencies is due to their distinct greater amplifications at certain frequency ranges. Moreover, PGA, PGV and PGD are well correlated with spectral acceleration at long, medium and short frequencies (Malhotra, 2006), as spectral acceleration is accepted as a good proxy for the representation of earthquake intensity and the corresponding structural response.

The impacts of the surface soil features, such as density, layering, layer thicknesses, depth to firm soil, water table level, primary and secondary V_s profiles, and soil linear/nonlinear behaviour on the characteristics of the seismic motions, and thus on the shape of the design response spectrum, have also been studied (Blume *et al.* (1973) Newmark *et al.* (1973b) Seed *et al.* (1976). Amplification factors with different damping levels (i.e. 0, 2, 5, 10 and 20) have been developed to form a design response spectrum at the ground surface by using the PGA, PGV and PGD values of the seismic motions (Newmark *et al.*, 1973b; Mohraz, 1976). A greater amplification at softer sites has also been clearly observed, although characterisation of the sites where the accelerograms were installed was not rigorously identified at the time of the studies mentioned above.

Spectral responses are the product of ground motions. The seismic hazard of a ground motion to a site is mainly dependent on three factors –magnitude, distance to the fault and local site conditions. As reported below, firstly, these factors were studied to provide a better understanding of the concept of seismic hazard analysis in shaping the design response spectra that are included in modern seismic design codes. Secondly, the approaches to seismic hazard analysis are given, in conjunction with the Newmark and Hall (1973b) method. The results of the response spectra for real earthquake events, as recorded in soft soils and included in the earthquake databases, are presented.

2.2 Factors Affecting Ground Motion

2.2.1 Magnitude

The magnitude of an earthquake event influences the relative frequency content and the duration of ground motions. The greater the magnitude of an earthquake, the higher the

spectral accelerations produced at lower and higher frequencies. Another event with a smaller magnitude, recorded on the same accelerometers, may be characterised by lower spectral amplitudes at higher frequencies, and at the longer periods. In parallel, the greater the magnitude of an earthquake, the longer the seismic excitation a site can be exposed to. Three earthquake events recorded by the Guerrero accelerometer (Mexico) clearly indicate the relation between magnitude and duration (Figure 2.1) or between magnitude and the spectral accelerations at the longer periods (Figure 2.2).

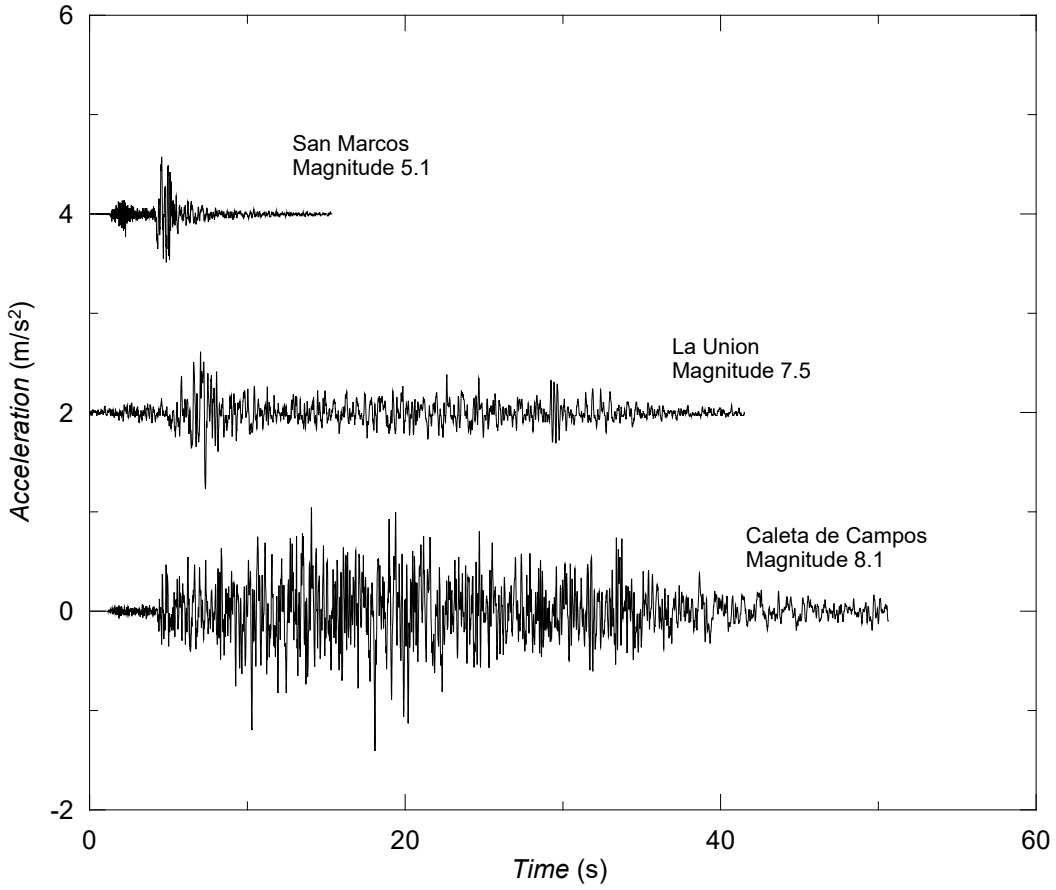

Figure 2.1 Acceleration-time histories of three different earthquake events, as recorded by the Guerrero accelerometer, Mexico (after Anderson and Quaas, 1998).

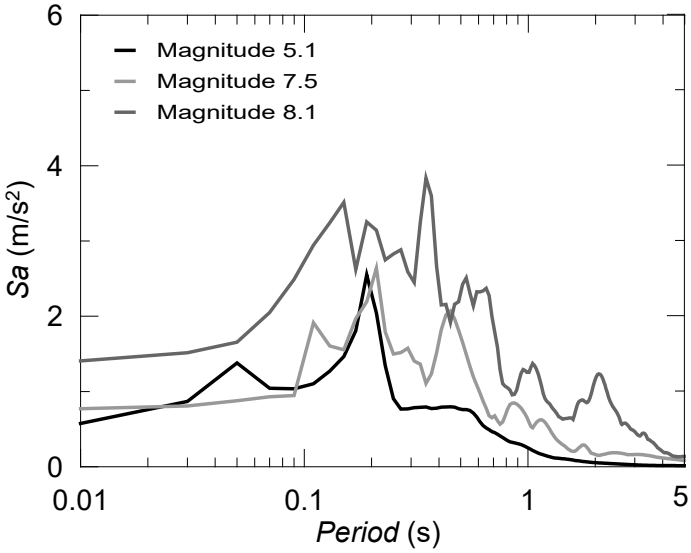

Figure 2.2 The 5% damped response spectra of the acceleration–time histories shown in Figure 2.1.

2.2.2 Distance

The distance between the location of the accelerometers (or sites) and the epicentre of the earthquake does affect the frequency content of ground motions. An earthquake recorded by several accelerometers in the same soil type at different locations can clearly describe such an effect on the ground motion. The spectral amplitudes of ground motions are expected to show a reduction at higher frequencies and an increase at the longer periods with increasing distance from the epicentre.

Figure 2.3 represents the recordings of the October 17 Loma Prieta earthquake at different distances from the epicentre. It is clear that the spectral responses of the recordings show great discrepancy at periods of less than 1 s. The ground motions recorded at 45 km and 4.3 km from the epicentre have spectral accelerations at periods greater than 1 s that are similar to those recorded at 98 km and 11 km, respectively. As expected, further distant recordings are characterised by greater spectral accelerations at the longer periods, while short distant recordings have greater spectral accelerations at the shorter periods.

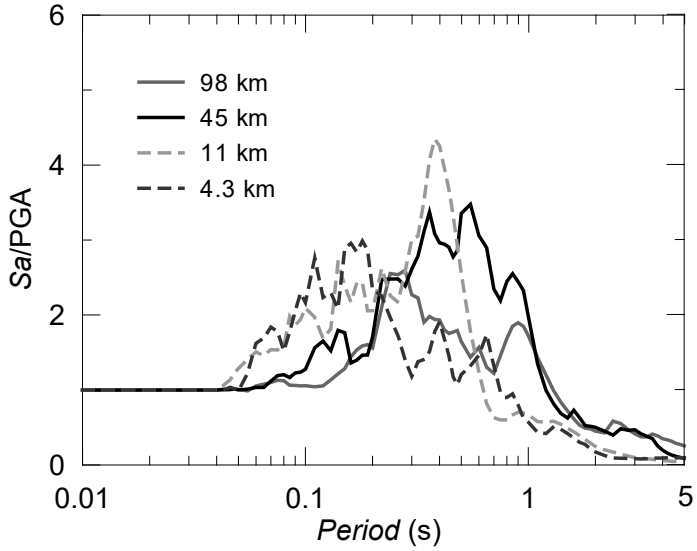

Figure 2.3 Influence of the epicentral distances on the spectral shapes of the October 17, 1989 earthquake recorded at different locations in stiff soil deposits (rock).

When a site is within 10 to 15 km of the epicentre, the energy of the ground motion pulses from medium to long periods. These near-epicentre events are known as pulse-like type events, in which the earthquake energy develops towards a site. This type of earthquake events is also characterised by a directionality effect, where the fault-normal component of the ground motions expresses higher earthquake parameters than the fault-parallel component. The recording of the 1994 Northridge earthquake is a good example, with respect to illustrating the features of near-fault ground motions, as demonstrated in Figure 2.4.

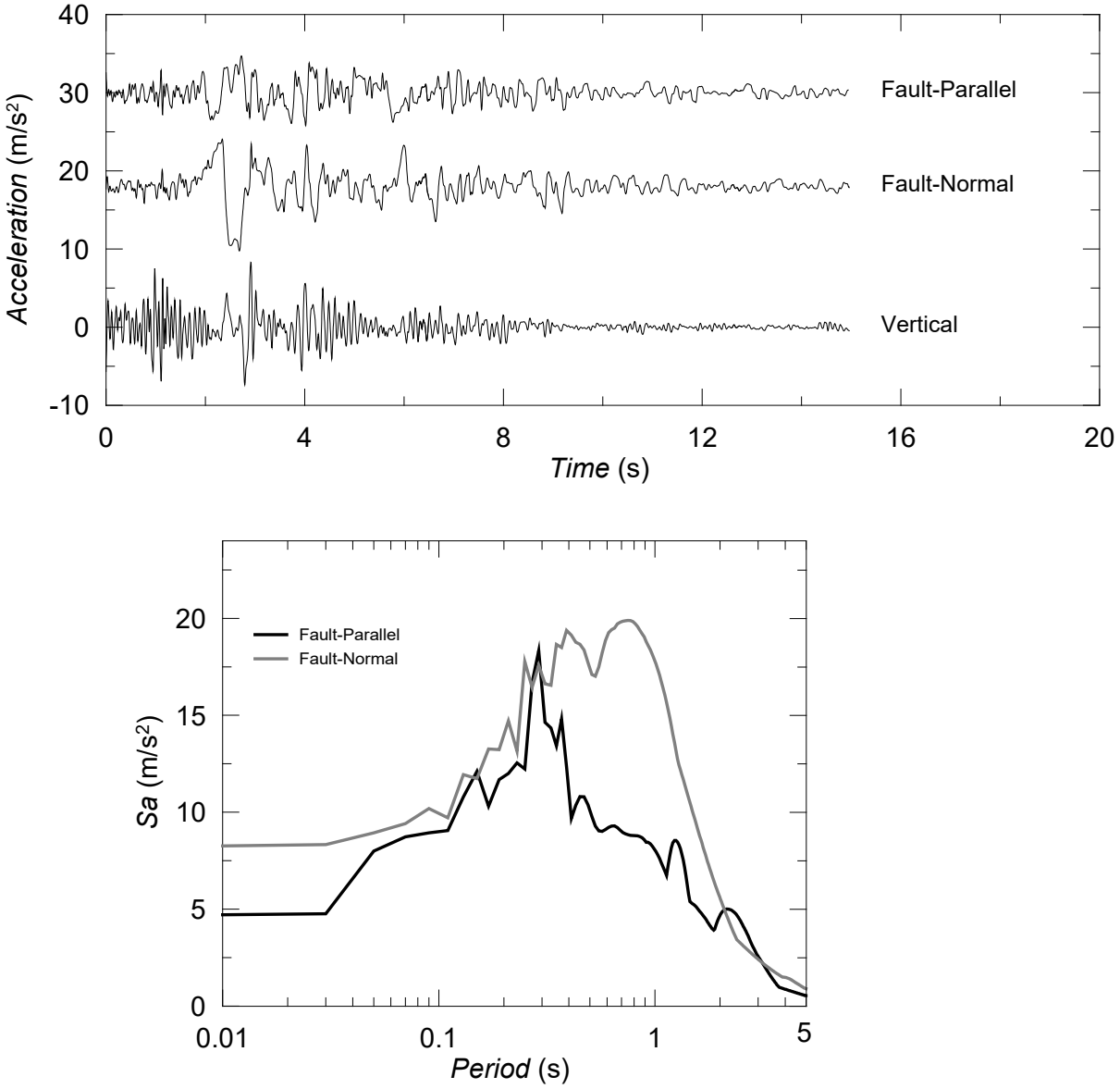

Figure 2.4 Acceleration-time histories of, and 5% damped spectral responses to, the 1994 Northridge earthquake event, California in horizontal (fault-normal and fault-parallel) and vertical directions, as recorded by an accelerometer situated 7.5 km away from the epicentre (after Somerville et al., 1997).

2.2.3 Local site conditions

It has been well established that the propagation of ground motions through soil deposits can affect the level and characteristics of spectral responses. Remarkable exemplary ground motions, showing local site effects, can be seen in the 1985 Mexico and the 1989 Loma Prieta earthquake events, where recordings in different soils show great differences.

The effects of site conditions on ground motion depend on the seismicity level of the earthquake event and the elastic and dynamic characteristics of the soil. If the soil is

relatively loose, and the seismicity level is greater than 0.4g, the spectral values at higher frequencies will tend to de-amplify due to soil nonlinearity, but will still amplify at the longer periods, which may be less than the amplifications observed at lower seismicity levels (Engineers, 1999). Figure 2.5 shows the spectral responses to the 1989 Loma Prieta earthquake in soft ($V_{s,30}$, 158 m/s) and relatively stiff ($V_{s,30}$, 314 m/s) soil deposits. It is clear that the ground motion was more amplified in the soft soil (Gilroy-1 site) than in the stiff soil (Santa Teresa Hills site).

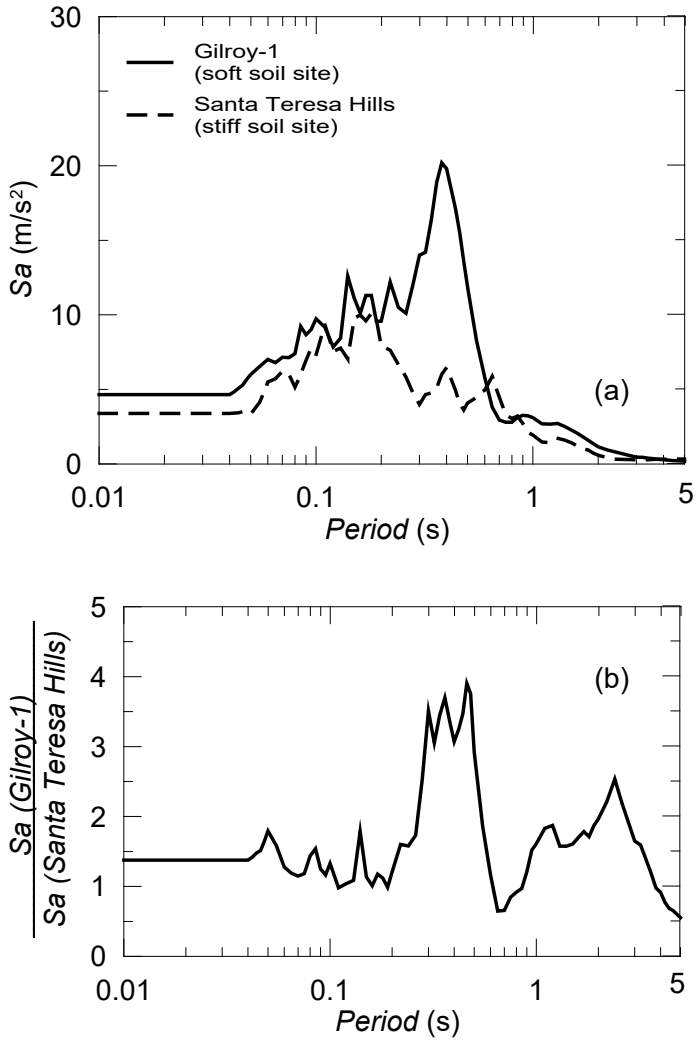

Figure 2.5 Spectral responses to ground motions of the 1989 Loma Prieta earthquake recorded in soft (Gilroy-1) and stiff (Santa Teresa Hills) soils (a), and their spectral ratios (b) (after Engineers, 1999).

2.3 Development of Site-Specific Response Spectra

The ultimate desire of site response analyses involving ground motions is to verify the performance of a structure in resisting the intensity of the shaking experienced. One fundamental question is: what level of shaking intensity should be applied to the structure at a site. The magnitude, location and other earthquake properties (e.g. shaking intensity) cannot be precisely determined for a potential earthquake event, but can only be assumed. To do this, it is necessary to define the annual rate of exceedance of a specific intensity of ground motions for a range of shaking intensities.

Figure 2.6 indicates that low intense ground shaking is frequently exceeded, while high intense ground shaking is rare. It may be feasible to consider annual rate of exceeding ground shaking with high intensity for thousands of years, by means of observatory earthquake data; however, this is not possible, due to a lack of information on earthquake events with low exceedance interest, or with high intensity. Moreover, there is great uncertainty associated with the size, location and intensity of an earthquake event, such that extrapolated assumptions cannot totally be relied on. On account of that, seismic risk analysis should involve mathematical models, which can predict the possible magnitude and distance of a future earthquake event at a site with potential ground motion intensities.

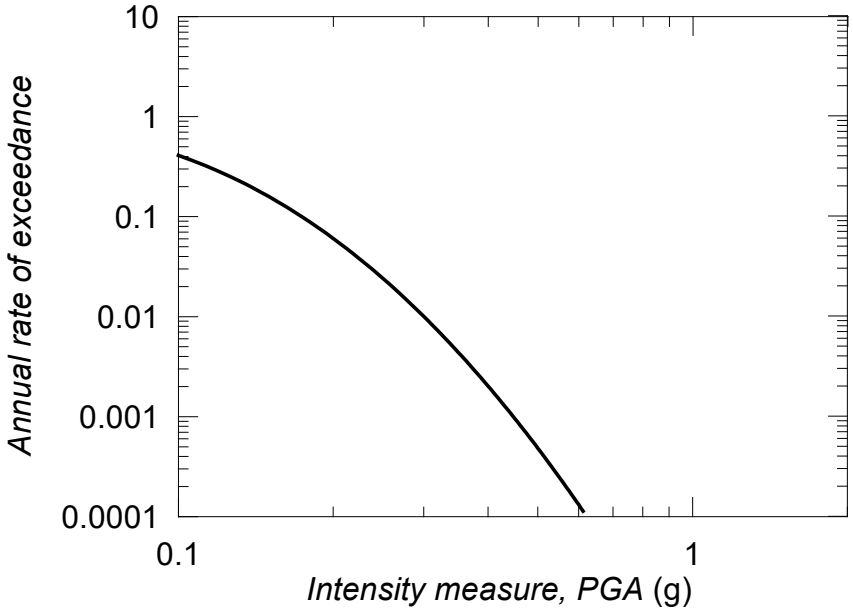

Figure 2.6 Probability of ground motion exceedance rate at various predicted intensity levels, based on the model of Campbell and Bozorgnia (2008).

Two main approaches have been developed to determine ground motion for a potential earthquake event at a site –deterministic and probabilistic. These approaches are known to form the fundamentals of modern seismic-resistant design codes. In the following section, the concept of DSHA will, firstly, be given. Then, the framework of probabilistic seismic hazard analysis (PSHA) will briefly be presented.

2.4 Deterministic seismic hazard analysis (DSHA)

DSHA estimates the ground motions from an earthquake event of a certain size, emanating from an epicentre at a certain distance from the site. This approach considers the worst-case earthquake scenario that the site can experience. Such an earthquake event is called a maximum credible earthquake (MCE). Alternatively, in order to consider a potential maximum earthquake event closer to the site of interest, a deterministic approach can sometimes be regarded as the mean maximum considered earthquake. There are two main methods leading to a deterministic ground motion estimation.

a) **Anchoring the response spectral shape to PGA:** This method consists of three steps: 1) estimation of PGA; 2) selection of spectral shape; and 3) multiplication of spectral shape with peak ground parameters to obtain the response spectra. Estimations of PGA, PGV and PGD can be obtained by using suitable ground motion data, along with attenuation models for the site under consideration. The amplification factors for three different regions (the acceleration, velocity and displacement domain regions) in the spectral shape were provided by Newmark and Hall (1978) for different *D* levels. The response spectra can then be constructed by using estimated ground motion parameters and amplification factors, shown in Table 2.1.

Structural *D* ratio	Amplification factors for:		
	Displacement	Velocity	Acceleration
0	2.5	4.0	6.4
2	1.8	2.8	4.3
5	1.4	1.9	2.6
10	1.1	1.3	1.5
20	1.0	1.1	1.2

Table 2.1 Amplification factors for different *D* levels following (after Newmark-Hall, 1978).

b) Direct estimation of the spectrum: There are three ways of estimating the response spectrum directly: 1) by using attenuation laws; 2) by performing statistical analyses of ground motion data; and 3) by simulating ground motion using numerical models. Attenuation laws have been developed for different site conditions in order to compute the spectral values at the period ranges of interest through statistical regression and theoretical analyses. The spectral values computed from these attenuation laws are generally damped at 5%. Spectral values at other damping levels have been calculated by using the spectral ratios given in the Newmark and Hall (1978, 1982) model.

By statistically analysing the ground motion data for specific magnitude and distance ranges, the spectral responses at each period can be estimated. If there is not enough earthquake data available for statistical analyses to be conducted for the desired magnitude and distance, attenuation relationships can be used instead to scale ground motions to the desired values, in terms of magnitude and distance. Lastly, numerical ground motion models are able to simulate the earthquake rupture, seismic wave propagation from the fault to the site, and the influence of local site conditions. This method of direct spectrum estimation is useful if earthquake events are rarely encountered, and no similar event is available from earthquake databases. Band Limited White Noise/Random Vibration Theory (BLWN/RVT) (Hanks and

McGuire, 1981) is one example of a simple numerical technique that is capable of simulating earthquake rupture and seismic wave propagation from source to site.

By using one of the approaches outlined above, it is possible to determine ground motion from an earthquake event with the maximum possible magnitude at the closest fault to the site under consideration. Even though this philosophy seems to be simple and straightforward, some problems can arise in its application. To make the concerns with the deterministic approach obvious, one ideal site with two faults, located 10 km and 20 km away, are considered. It is assumed that the MCE from the nearer fault is 6.5, and at the farther fault, it is 7.5. The median spectral responses are predicted by using the Campbell and Bozorgnia (2008) model, shown in Figure 2.7.

It is obvious that the earthquake with the smaller magnitude at the shortest distance from the site will produce greater spectral values at short periods, whilst the earthquake with larger magnitude at the furthest distance leads to higher spectral amplitudes at longer periods. Hence, it is difficult to determine a single worst-case event, given the highest spectral values at all interested periods, but enveloping two spectral curves will provide a reasonable approximation for considering the level of hazard risk of a site.

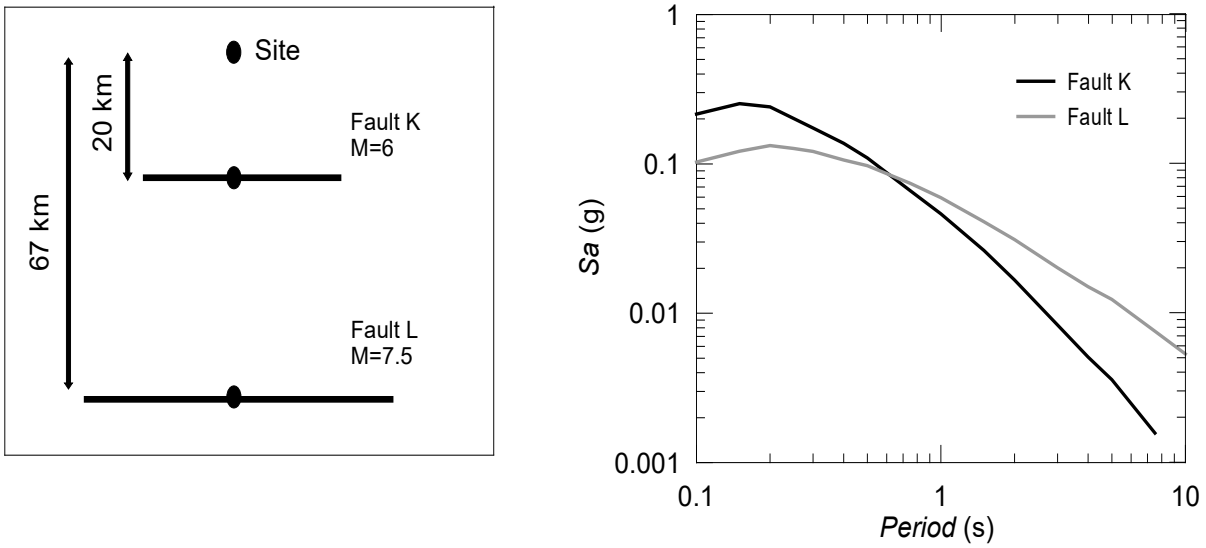

Figure 2.7 Ideal site with two faults capable of producing magnitude 6 and 7.5 earthquakes at 20 km and 67 km distances, respectively, and their predicted spectral responses, based on the model of Campbell and Bozorgnia (2008).

In addition, the deterministic approach can become even more challenging due to the fact that such a worst-case earthquake event has a variety of ground motion intensity. In this regard, it is necessary to determine the worst-case ground motion intensity. Although Figure

2.7 indicates the median spectral responses from an empirical model, the actual ground motion intensities of an earthquake event will show great scatter around the median values. In order to consider this scatter, mean plus and minus one standard deviation curves can be plotted. This will account for about two-thirds of the potential ground motion intensities at measured sites.

2.4.1 Probabilistic seismic hazard analysis (PSHA)

Some challenges in determining ground motion intensity from a single worst-case earthquake event in order to obtain seismic hazard risks for a site have been discussed above. Rather than neglecting the other potential earthquake scenarios that can cause damage to a site, inclusion of those events in describing ground motion may allow a more reasonable replication of the actual case. This procedure will bring more uncertainty into the site response analysis, but, at the same time, it will provide a better opportunity to evaluate the seismic risks for a given site.

PSHA can be described as the consideration of all potentially damaging earthquake events, with their associated occurrence levels, aimed at identifying a ground motion with the desired exceedance rate (Baker, 2008). In its simple form, five basic steps are sufficient to conduct PSHA for the site under consideration. These consist of:

1. identifying earthquake sources capable of producing damaging ground motions;
2. configuring the distribution of earthquake magnitudes, with respect to occurrence rates;
3. characterising the distribution of potential earthquake events, in terms of source-to-site distances;
4. predicting the distribution of ground motion intensities by adopting an empirical model; and
5. combining all the uncertainties given above by employing a total probability theorem, leading to the exceedance of intensity measures (*IMs*) at different levels.

The procedures for accomplishing the above five steps towards the determination of potential ground motion intensity, is explained in the following sections.

2.4.2 Identification of earthquake sources

Whilst DSHA focuses only on the worst-case earthquake event from a single fault point, PSHA incorporates all the potential earthquake sources into the hazard analysis of a site. The geological formation and location of past earthquake events can be used to determine earthquake sources around the site of interest. If the sources are not present at the location of interest, which may be the case for less seismically active regions, it can be assumed that an event could occur anywhere, within a certain distance of the site. When all the potential earthquake sources have been revealed, the distribution of magnitude and source-to-site distances for events at each source can be identified.

2.4.3 Distribution of earthquake magnitudes

Earthquake events produced at tectonic faults show various magnitudes. From past earthquake events, it has been found that the distribution of earthquake magnitudes at a site follow a specific distribution (Gutenberg and Richter, 1944), formulated as:

$$\log \lambda_m = a - bm \tag{2.1}$$

where λ_m is the rate of earthquake occurrence with magnitudes larger than m, and a and b are constant parameters. They are predicted by using statistical analysis of past earthquake events expressing the overall rate of occurrences, and the ratio of small to large earthquakes, respectively. Equation 2.1 is one of the empirical models describing the distribution of earthquake magnitudes and known as *Gutenberg-Richter recurrence law*. The formulation of the law does not have an upper limit to the predictions for the recurrences of earthquakes with greater magnitudes; however, the physical limitations of fault ruptures constrain the maximum level of earthquake magnitudes possible at a site. Consideration of the upper limit in the analytical calculation of earthquake magnitude distribution is described by the *bounded Gutenberg–Richter recurrence law*. The probability density function (PDF) distributions of both recurrence laws are presented in Figure 2.8, in which a good agreement with the return period of the observed earthquake events around Duzce, Izmit, Turkey can be seen.

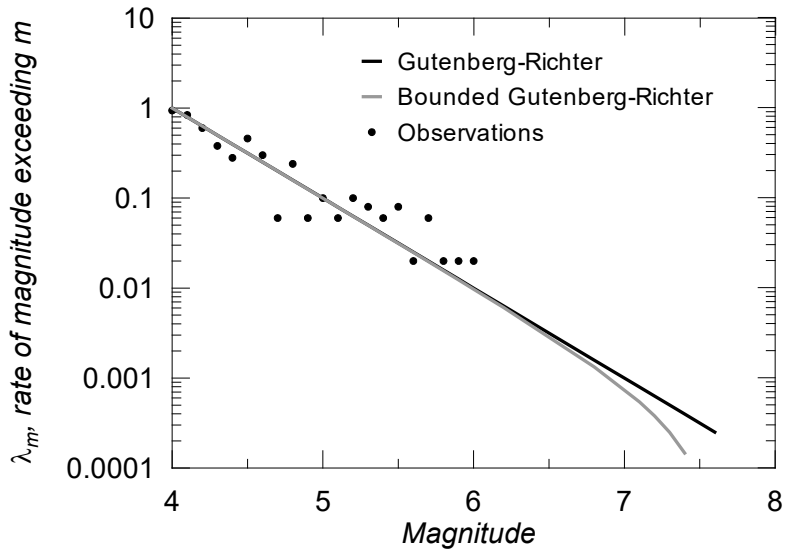

Figure 2.8 Predictions of the annual rate of exceedance of earthquake magnitudes, based on the Gutenberg–Richter and Bounded Gutenberg–Richter recurrence laws, and actual earthquake data for a site (Duzce, Izmit) over 50 years, using European Strong-Motion Database.

2.4.4 Characterisation of site-to-source distances

The distribution of distances between the site of interest and the earthquake sources should be identified in order to define potential ground motion intensity. It is suggested that, for any given source, there is an equal probability of earthquake occurrences at any point along the fault. Since the fault points are uniformly distributed, the distance can easily be computed by simple geometrical calculations.

2.4.5 Prediction of ground motion intensity

As long as the size and distance distributions of earthquake events at a site can be predicted, the only objective to be achieved in producing ground motion is to identify the distribution of intensities. The prediction of ground motion intensities is made by empirical models involving magnitude, distance, fault mechanism, near-fault effects, etc. These models are generally developed based on statistical regression analysis of past earthquake events, in terms of ground motion intensities.

It has been established that the ground motion intensities of an earthquake event at different measured locations can show great discrepancies (Figure 2.9 shows an example for the 1999

Duzce earthquake). Hence, ground motion prediction models should be capable of producing *IM* at different levels.

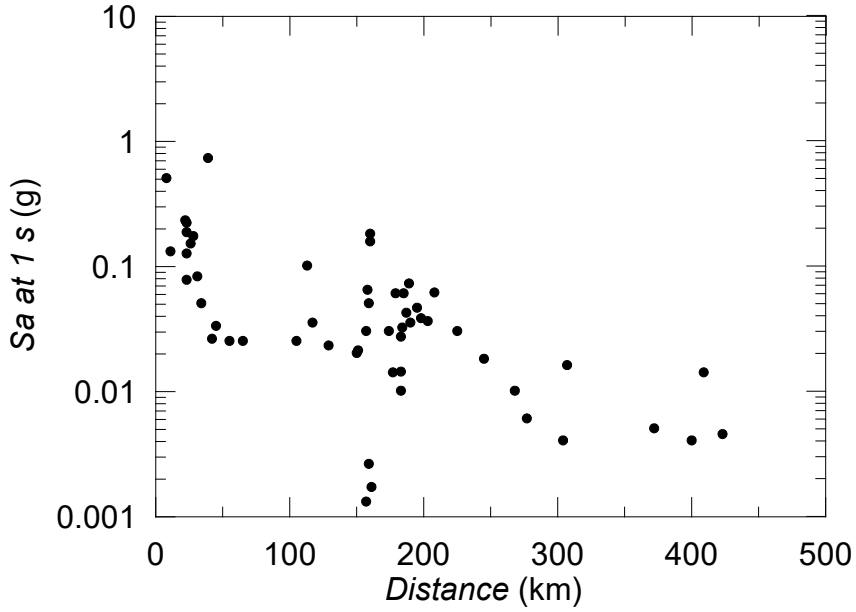

Figure 2.9 Spectral acceleration of ground motions recorded at various distances from the fault of the 1999 Duzce earthquake event, using European Strong-Motion Database.

A common formula used in the prediction models for describing the probability distribution is:

$$lnIM = \overline{lnIM}(M, R, \theta) + \sigma(M, R, \theta)\varepsilon \tag{2.2}$$

where $lnIM$ is the natural logarithm of the ground motion *IM* (such as PGA), and is a random variable with normal distribution. The terms on the right-hand side of Equation 2.2 are the outcomes of the prediction models, where $\overline{lnIM}(M, R, \theta)$ is the mean and $\sigma(M, R, \theta)$ is the standard deviation of $lnIM$, incorporating the magnitude (M), distance (R) and other earthquake parameters (which are generally represented by the symbol θ). ε is a standard normal random variable representing the change in $lnIM$.

2.4.6 Combining all information

Once the probability distributions of earthquake magnitudes and distances have been identified (individual or joint distributions), and the probability of the exceedance level of the *IM* has been predicted using ground motion prediction models, the PSHA equations can

be readily implemented. Before giving the full formulation of PSHA, in defining the rate of exceedance *IM* for a site, two additional sub-steps are provided so that the fundamental of the concept can be well understood.

Taking a single source of an earthquake, the probability of the *IM* exceedance level of *x* for a given magnitude and distance can be predicted by ground motion prediction models. Even if the magnitude and distance (which are the main inputs for the models) of a potential earthquake event cannot be precisely known, their probability distributions can be determined, as discussed above. So, reflecting these variables (or probability distributions) into the total probability theorem will give (Kramer, 2014):

$$P(IM > x) = \int_{m_{min}}^{m_{max}} \int_{0}^{r_{max}} P(IM > x|m,r)\, f_M(m) f_R(r) dr dm \tag{2.3}$$

where $P(IM > x|m,r)$ is the output of the ground motion prediction model, and $f_M(m)$ and $f_R(r)$ are the probability density functions (PDFs) of the magnitudes and distances. Integral operations allow the consideration of the overall probability of exceedance from the possible magnitudes and distances at an earthquake source.

Equation 2.3 only gives the probability of the specific *IM* exceedance level, but does not give any information about the rate of earthquake occurrence from the single source of interest. By modifying the equation, the rate of the *IM* exceedence level of *x* can be computed:

$$\lambda(IM > x) = \lambda(M > m_{min}) \int_{m_{min}}^{m_{max}} \int_{0}^{r_{max}} P(IM > x|m,r)\, f_M(m) f_R(r) dr dm \tag{2.4}$$

where $\lambda(M > m_{min})$ is the rate of earthquake occurrence exceedance, m_{min}, and $\lambda(IM > x)$ is the rate of *IM* greater than *x*.

Since the above formulation gives the rate of *IM* exceedance with a certain amplitude at a single source, combining all the sources from a site leads to the total exceedance rate:

$$\lambda(IM > x) = \sum_{i=1}^{n_{sources}} \lambda(M_i > m_{min}) \int_{m_{min}}^{m_{max}} \int_{0}^{r_{max}} P(IM > x|m,r)\, f_{M_i}(m) f_{R_i}(r) dr dm \quad (2.5)$$

where $n_{sources}$ represents the number of earthquake sources, and f_{M_i} and f_{R_i} are the magnitude and distance distributions at source *i*, respectively.

Equation 2.5 is the character of PSHA incorporating the rates of earthquake occurrences and the distributions of the associated magnitudes, distances and ground motion intensities. These input variables of PSHA are identified based on information from past earthquake events. Computing the exceedance rate of an *IM*, in the end, is vital in reducing the hazard risks of sites. PSHA also allows the prediction of the rate of occurrence of earthquake events that are rare (low-rate), and have not been recorded before. Figure 2.10 is an example of results of PSHA showing the annual rate of exceedance of PGA and Sa at a range of periods obtained by using an OpenSHA program (Field *et al.*, 2003) for an ideal site, applying an attenuation model of Campbell and Bozorgnia (2008).

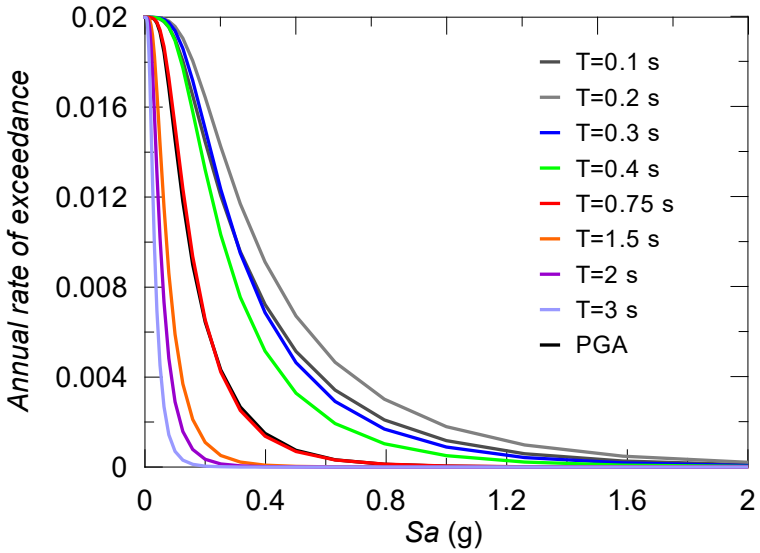

Figure 2.10 Example of PSHA results for an ideal site showing exceedance rates of spectral accelerations at different periods of interest predicted by using the model of Campbell and Bozorgnia, 2008.

2.5 Evaluation of the EC8 Design Response Spectra

The technological developments have been enabled to better record earthquake events, and better investigation of soils and fault mechanisms. In parallel, the available earthquake data has been increased with time, assisting the development of comprehensive attenuation laws (the basic framework of which was explained in the previous section). With these advancements, the standard design response spectrum is covered by the modern seismic design codes that must be complied with in performance-based structural design. In the current implementations of EC8, two types of horizontal and vertical design response spectra with 5% damping are described, based on the magnitude of an earthquake event. When the earthquake magnitude is higher than 5.5, it is regarded as Type 1, and if it is equal to or lower than 5.5, it is categorised as Type 2.

In the Type 1 seismicity, the energy content of an earthquake event is more pronounced at the long periods observed in high-seismicity regions. Type 2 seismicity has higher amplification at short period ranges, and lower energy content at long periods, compared to Type 1, and is suggested for low- and moderately-seismic regions (Pousse *et al.*, 2005). Five main soil types (A, B, C, D and E) are classified in EC8, with respect to the average V_s of the upper 30 m of the soil deposit ($V_{s,30}$), standard penetration resistance ($N_{SPT(\text{blows/30cm})}$) and undrained shear strength (c_u) values of the soil.

The soil can be directly classified when the 30 m V_s profile of the soil is available (based on Equation 2.6), otherwise the last two soil properties should be taken into consideration. For each soil type, the Type 1 and Type 2 elastic design response spectra are provided over a range of periods as seen in Figure 2.11. It is clear that stiffer soil classes (A, B and C) have spectral response shapes with less amplitude and narrower plateaus, whereas softer soil classes (D and E) are characterised by higher spectral values and wider plateaus in both seismicity types. Moreover, the period elongation of soft soil deposits with a strong earthquake event (i.e. seismicity Type 1) is clearly considered in the design response spectrum of EC8, as the spectral shapes shift to the longer periods from soil classes A to D. In the case of the seismicity Type 2 spectral shapes, this pattern is not as evident as in seismicity Type 1, due to the seismic intensity level. More information regarding the construction of EC8 design response spectra can be found in Appendix A-1.

$$V_s = \frac{30}{\sum_1^N \frac{H_i}{V_i}} \tag{2.6}$$

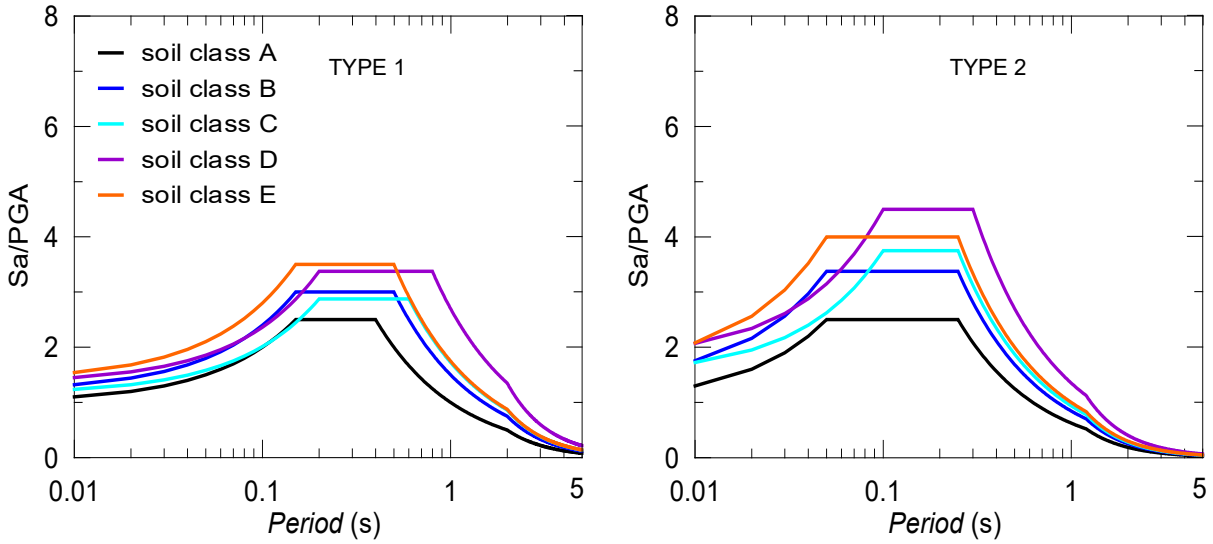

Figure 2.11 Types 1 and 2 design response spectra applied in EC8 for different types of soils.

The horizontal design response spectra given by EC8 for seismicity Types 1 and 2 have recently been investigated by Pitilakis *et al.* (2012). The spectral accelerations from earthquake events recorded in soil classes A, B, C, D and E have been compared to the associated EC8 design response spectra. Based on the study, the EC8 elastic design response spectra provided for soil classes A, B and C were shown to be good representations of an earthquake event, as they were in good agreement with the 84th percentile of the real spectral accelerations. As for soil classes D and E, the spectral shapes included in EC8 could not be evaluated confidently, as the number of real earthquake accelerograms is insufficient in the earthquake database considered. Nevertheless, the EC8 seismicity Type 1 elastic response spectrum for soil class D is not able to represent the peak over the plateau, based on the spectral values of four earthquake events, and the seismicity Type 2 spectrum is insufficient to capture the spectral values at longer periods (> 0.5 s).

In the remaining part of the chapter, the EC8 elastic design response spectra are examined by considering the earthquake events measured only by stations on soil class D in the national and international databases. This specific interest in the earthquake records in soft soils is, firstly, due to concerns about the inadequacy of the associated EC8 design response spectrum in accurately representing the spectral responses, as highlighted above. Secondly, the phenomena of local site effects on the characteristics of input motions is strongly linked to the characteristics of soft soils. Thus, a detailed look at the earthquake events propagated

through soft soils may help to justify the focus of ongoing research, in terms of soil class considered.

2.6 Investigation and Discussion of Earthquake Databases

The Italian Accelerometric Archive (ITACA) version 2.0, European Strong-Motion Database (ESD), Pacific Earthquake Engineering Research Centre (PEER) ground motion database, United States Geological Survey (USGS) earthquake database, Consortium of Organizations for Strong Motion Observation Systems (COSMOS) database, GeoNet, and the Kyoshin (K-NET) and Kiban Kyoshin (KiK-net) networks were investigated. These include most of the global earthquake events, along with the devastating and historical ones, such as the 1989 Loma Prieta, the 1994 Northridge and the 2011 Christchurch earthquakes.

Only earthquake magnitude, soil type and the type of housing at the stations were extracted from the earthquake records. The magnitude parameter, ranging from 3 to 5.5 (including 5.5), and from >5.5 to 10, was used to compare the results with the EC8 Type 1 and Type 2 design response spectra. Moment magnitude (M_w) was generally sought, but in the absence of M_w-based measurements, the surface (M_s), or Richter local (M_L) magnitudes were taken into consideration. The ITACA, PEER and ESD databases provided the direct soil classes of the stations, classified in accordance with the EC8 criteria, but for the rest, V_s values for soil less than 30 m deep were checked to determine the soil class. As for housing types, free-field stations, the ground level of buildings, bridge piers and ground surface of the geotechnical arrays were considered.

Except from K-NET and KiK-net, the processed spectral acceleration-time histories of the records can be obtained from all of the accessed databases. The appropriate processed spectral acceleration data for the earthquake events included in the K-NET and KiK-net databases is available on the NEEShub website, as the databases only contain raw earthquake data (Dawood *et al.*, 2014). The spectral acceleration values were normalised, with respect to the PGA values. The PGA normalisation process is carried out to compare earthquake records on a rational basis, as each ground motion has a different intensity (Riddell, 1996).

The median, mean plus one standard deviation (84th percentile) and mean minus one standard deviation (16th percentile) of the 5% damped spectral accelerations of the

earthquake events were plotted with the EC8 response spectra. The earthquake records were considered separately in two horizontal directions, and then the geometric means were plotted. It is worth noting that the overall results from the datasets in one direction do not differ substantially from the results of the other direction. For brevity, the geometric mean shapes are represented in this chapter but the results from the two individual directions can be found in Appendix A-2. The earthquake records in the PEER database were excluded from this process, since the spectral accelerations given in the Excel sheet were not provided with any specification of the horizontal components. Thus, the given values are regarded as the geometric means of the earthquake motions. The description of soil class D in EC8 refers to the soil class E in NEHRP and NZS1170.5, with respect to the V_s values, as shown in Table 2.2 (Khose *et al.*, 2012).

Soil type	NEHRP	EC8	NZS1170.5
A	>1500	>800	>1500
B	760–1500	360–800	360–1500
C	360–760	180–360	150–360
D	180–360	<180	150–360
E	<180	-	<150

Table 2.2 Soil classifications from NEHRP, EC8 and NZS1170.5, based on $V_{s,30}$ (m/s) values.

2.6.1 ITACA

The ITACA version 2.0 web-based earthquake database has approximately 7,500 processed three-component waveforms, produced from about 1,200 earthquakes having a magnitude of more than 3. Both the processed and unprocessed acceleration-time histories are available to users. Furthermore, the 5% damped spectral acceleration values of the earthquake events can also be directly downloaded.

ITACA provides detailed information for each station, including soil type. The available number of earthquake events measured by accelerogram on soil class D are eight and 47 for seismicity Types 1 and 2, respectively. According to the results shown in Figure 2.12, the smooth spectral curve for Type 1 in EC8 is in reasonably good agreement with the 84th percentile of the empirical records, although it should be borne in mind that they are small in number. Moreover, peaks in the short and medium periods, and beyond 2 s, cannot be fully captured in the current EC8 practice. For seismicity Type 2, the design response spectrum of EC8 seems not to be conservative, especially above the period of 0.4 s (Figure 2.12), as it is even considerably below the median of the empirical data of a relatively considerable number of earthquake events.

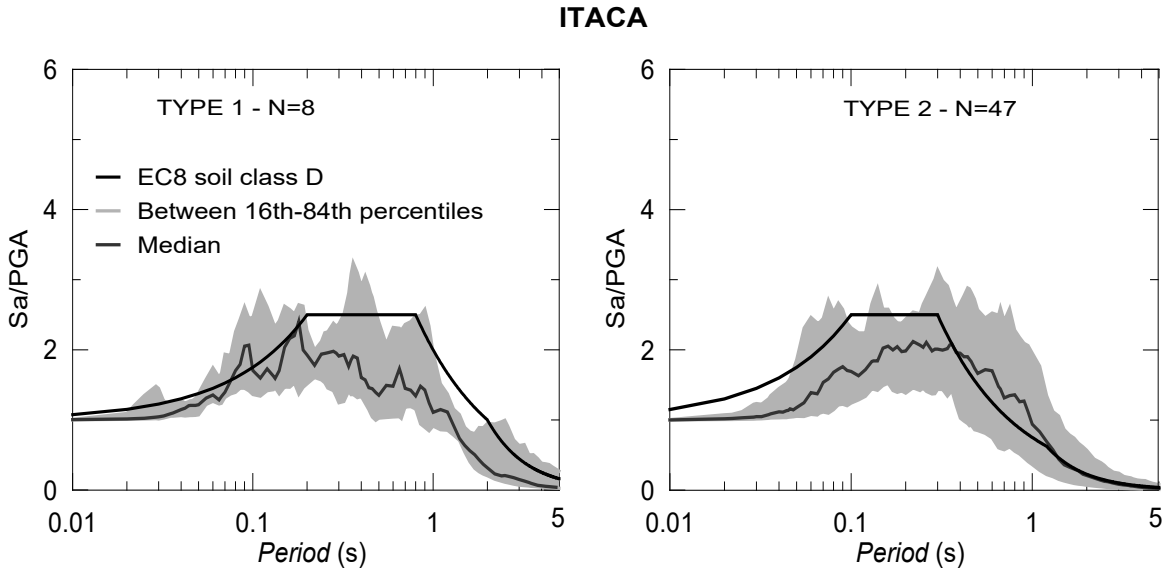

Figure 2.12 Probabilistic empirical earthquake spectral results from the ITACA database with corresponding EC8 spectral acceleration shapes.

2.6.2 ESD

The earthquake records presented in this database are from Europe, the Mediterranean and the Middle East. It includes over 2,000 earthquake accelerograms, which are available online, in raw and processed data formats. As with the European-based strong-motion database, data measured by stations on soil class D can be easily derived with 5% damped spectral acceleration values; however, for some records, the spectral acceleration values have not been provided in the database. To obtain the 5% damped spectral acceleration values of those records, the acceleration-time histories must be processed via the Equivalent-linear Earthquake site Response Analysis (EERA) code. More information about the code is presented in Chapter 3 (Section 3.3.1).

From the results of the empirical data shown in Figure 2.13, the Type 1 EC8 design response spectrum can be regarded as a good representative of probable earthquake events, as it captures the 84th percentile of the real events. With respect to the Type 2 results, the design response spectrum shows good agreement with the 84th percentile of the real events; however, it should be noted that, for both seismic intensities, the design response spectrum still does not cover 16% of the earthquake events or the spectral peaks in the medium and long period ranges.

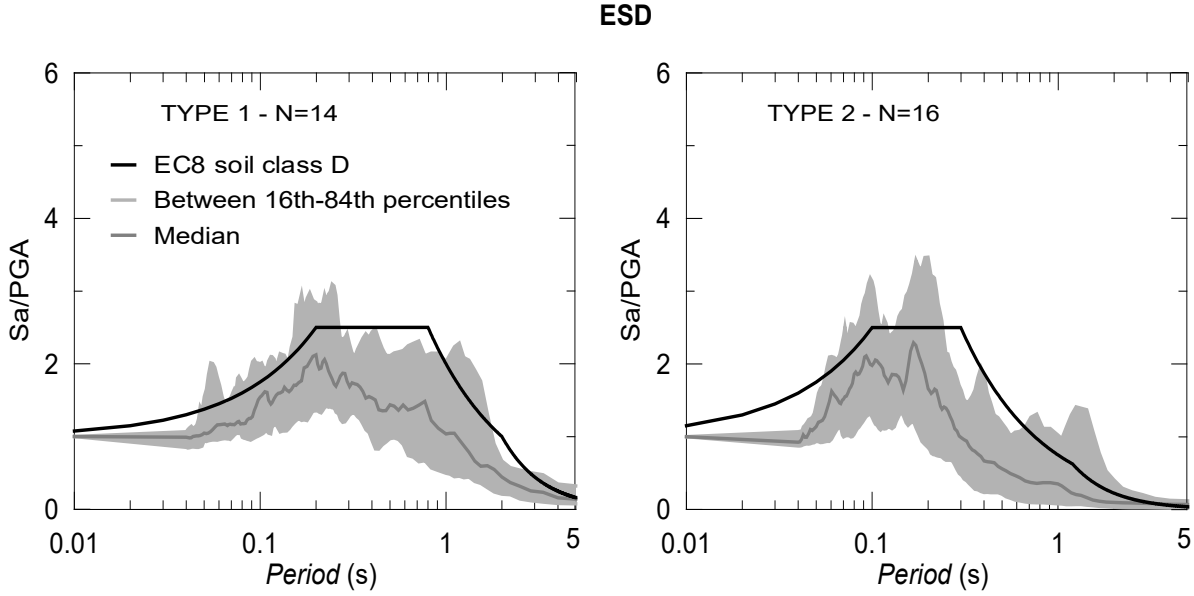

Figure 2.13 Probabilistic empirical earthquake spectral results from the ESD database with corresponding spectral acceleration shapes from EC8.

2.6.3 PEER

The PEER ground motion database includes spectral accelerations of the records with various damping ratios, including 5%. It contains over 21,000 three-component earthquake signals from around the world (Campbell, 2013). The number of earthquake motions recorded in soft soil class D is 10 for seismicity Type 1 and eight for seismicity Type 2.

Based on the results of the normalised spectral accelerations of the records, as shown in Figure 2.14, the elastic design response spectra of EC8 are positioned well, between the median and the 84th percentile of the records, at almost all ranges of periods in both seismicity cases; however, at short and medium periods, the Type 1 design response spectrum of EC8 is not able to represent certain earthquake scenarios. This may also be a concern for the Type 2 design response spectrum, between 0.1 and 0.2 s and 0.4 and 1.6 s.

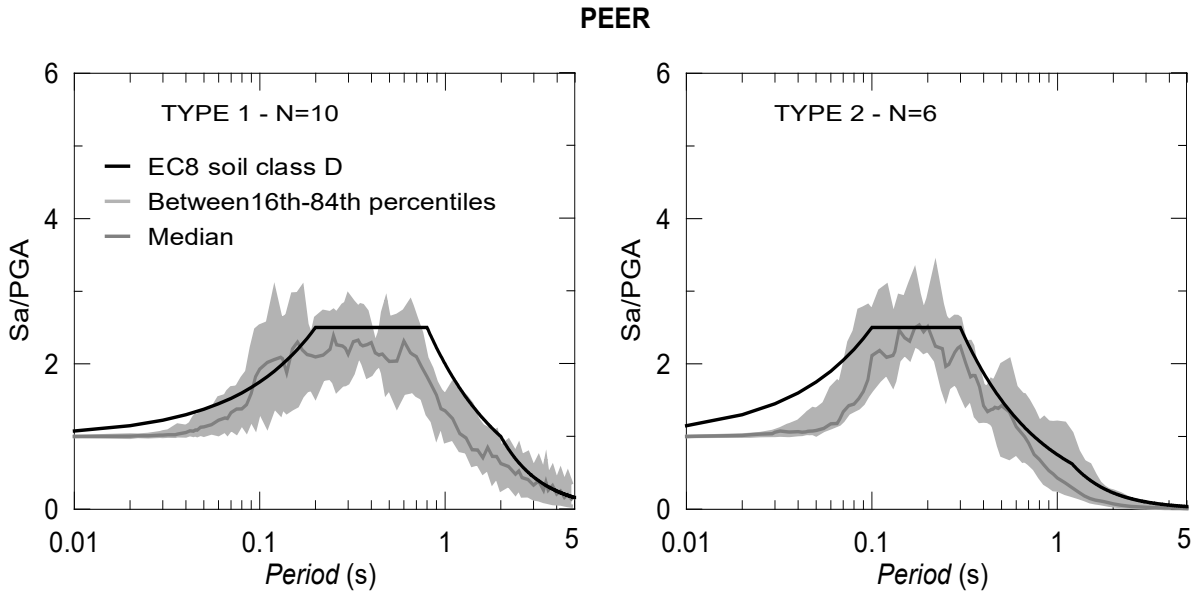

Figure 2.14 Probabilistic empirical earthquake spectral acceleration results from the PEER earthquake database with corresponding spectral acceleration shapes from EC8.

2.6.4 USGS

The USGS earthquake database provides both processed and raw data on global earthquake events to be used for earthquake-related studies. The spectral acceleration values of the seismic motions are given, with varied damping levels, including 5% damping. As this is a US-based database, the soil classifications for the stations have been assigned in compliance with the NEHRP criteria. Thus, stations on soil class D, with respect to the EC8 soil

classification criteria, were determined with respect to the given V_s values of the soil deposits down to 30 m.

Based on the results plotted in Figure 2.15, smooth spectral acceleration shapes provided by EC8 can be a good proxy for potential earthquake events with low or moderate seismic intensities; however, the peaks for the 84th percentile of the empirical data are, again, not captured by the EC8 design response spectra, especially for the Type 2 seismicity level. This may not be strongly supported because of the small number of earthquake samples in both seismicity cases.

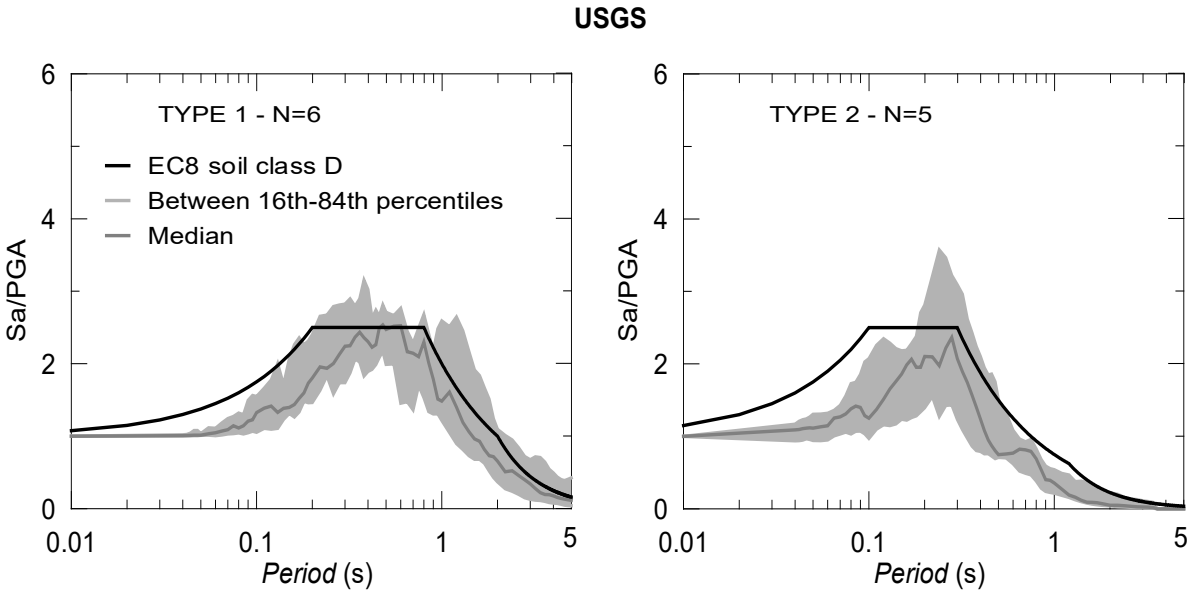

Figure 2.15 Probabilistic empirical earthquake spectral results from the USGS database with corresponding spectral acceleration shapes from EC8 and NEHRP.

2.6.5 COSMOS

Worldwide strong-motion earthquake data are easily accessible from the COSMOS earthquake database. It allows the user to search earthquake records in specific regions via many filtering options (for example, earthquake magnitude, PGA, housing type, soil type and fault mechanism). Detailed information about the stations is also provided, and 5% damped spectral acceleration values are easily obtainable.

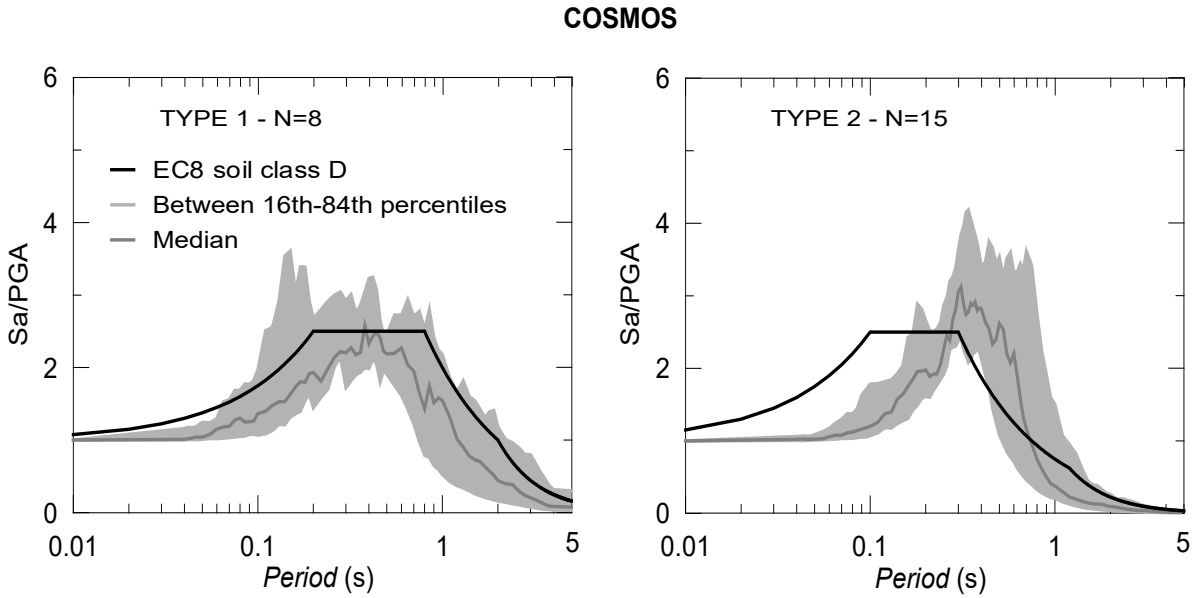

Figure 2.16 Probabilistic empirical earthquake spectral results from the COSMOS database with corresponding spectral acceleration shapes from EC8.

Referring to Figure 2.16, the design response spectrum included in EC8 does represent most of the potential earthquake scenarios for the Type 1 seismicity level, but does not consider some of the earthquakes carrying energy at short and at medium periods. As for seismicity Type 2, the smoothed spectral shape becomes unreliable in the period range of between about 0.3 and 2 s. This clearly indicates the need of the plateau to be shifted to the longer period, below and above which the spectral shape of EC8 is a reasonable response spectrum.

2.6.6 Geonet

Geonet is the New Zealand national geological hazard monitoring network that records information of earthquake, volcano and tsunami activities. It includes all of the processed earthquake data from 1966 onwards, including 5% damped spectral acceleration values.

Unlike the previously investigated global and national databases, Geonet includes a considerable number of earthquake records measured on soil class D—104 records for seismicity Type 1, and 515 records for seismicity Type 2. The resultant spectral shapes (16th, 84th and median shapes of the records) from these earthquake records indicate that the Types 1 and 2 seismicity design response spectra given by EC8 are able to represent the spectral values at periods greater than 1 and 2 s, respectively (Figure 2.17). But, at medium and short periods, they only show a good match with the medians of the earthquake events. This means that 50% of the spectral accelerations are not captured by the design response spectra.

Considering that the number of earthquake events in this database is relatively considerable, the results may be more reliable.

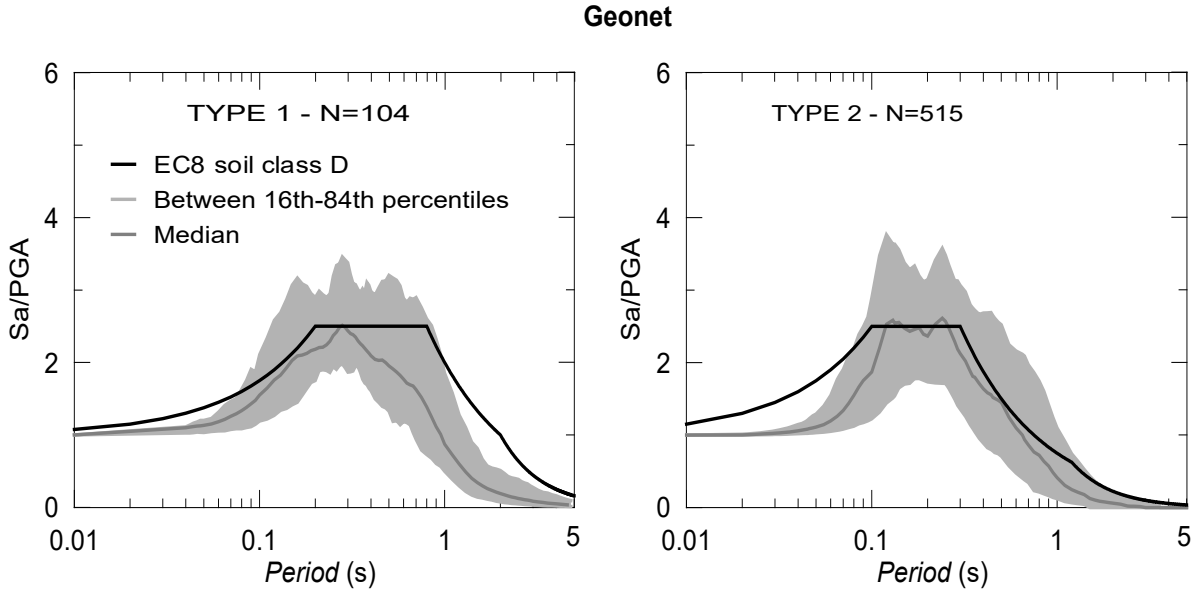

Figure 2.17 Probabilistic empirical earthquake spectral results from Geonet with corresponding spectral acceleration shapes from EC8.

Of equal important to highlight, the spectral acceleration shapes of the earthquake event of 22 February, 2011, with a magnitude of 6.3 recorded by stations on soil class D around the Christchurch Central Business District, New Zealand, exceeded the design response spectrum with a 2,500-year return period in the NZS1170 code. This observation is surprising because a design response spectrum with 500 years of return period is the general building design consideration in that region (Kaiser *et al.*, 2012). Another essential finding of the study is that when the Geonet database applies filtering with a 0.25 Hz to 25 Hz band-pass, it may not have been possible to capture the peaks in the long periods. If a wider pass band of 0.1 Hz and 50 Hz is regarded to process raw earthquake data, then the peak at long periods was represented.

To investigate whether the band-pass filter of 0.25 Hz and 25 Hz impacted on these results, data from 22 earthquakes from the Geonet database, with raw and processed spectral accelerations, were extracted. The impact of filtering on the spectral acceleration shapes at long periods was not observed, as can be seen in Figure 2.18, where this issue is better expressed at short or medium periods. Nevertheless, this impact has been clearly illustrated for individual earthquake records (Figure 2.19). This case does not change the overall shapes

of the spectral acceleration at longer periods, as some records are over the 84th percentile and some of them are well below the spectral shape.

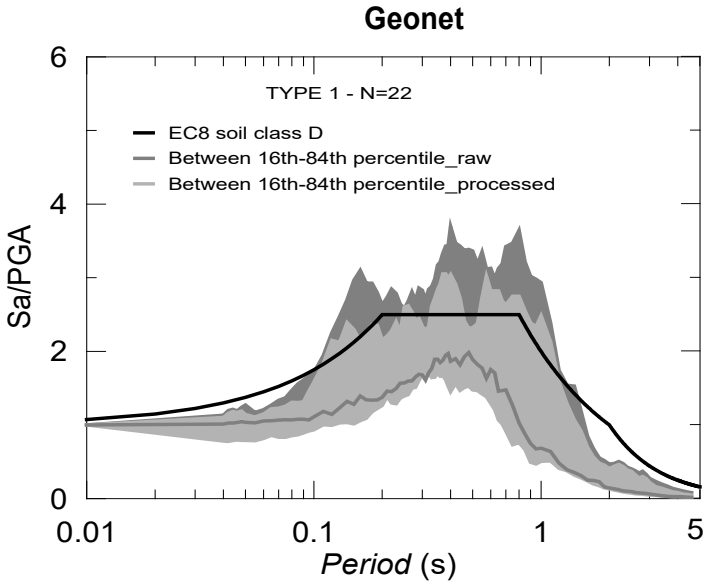

Figure 2.18 Comparison of the spectral shapes of processed versus unprocessed earthquake data.

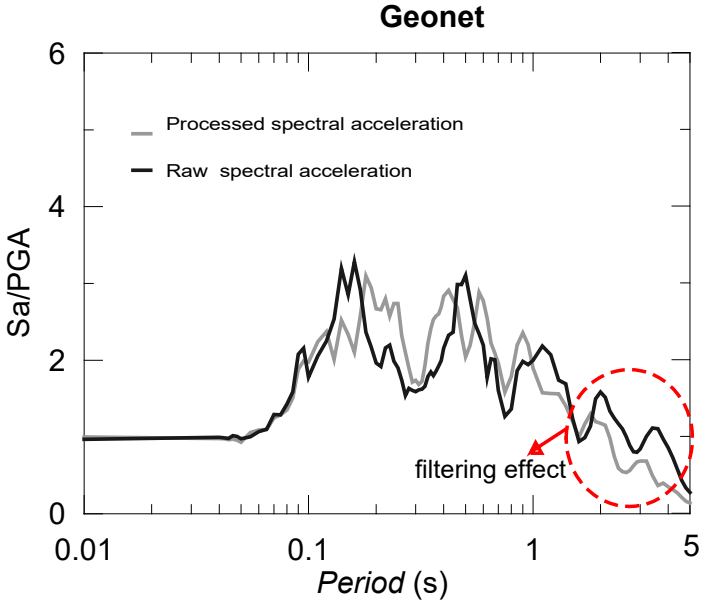

Figure 2.19 Comparison between spectral accelerations of processed and unprocessed data from two individual earthquake records, with respect to the filtering effect at longer periods.

2.6.7 KiK-net

K-NET and KiK-net are two nationwide strong-motion seismograph networks that are operated by the National Research Institute for Earth Science and Disaster Prevention in Japan. K-NET stations do not have information on soil profiles, such as V_S, compression-wave velocity (V_P), N_{SPT}-values, through 30 m from the ground surface, which is the threshold depth to which a soil class can be assigned, based on EC8. In contrast, KiK-net stations provide V_S and V_P values for soil strata below 30 m deep.

In light of this information, KiK-net stations on class D soils are determined by means of average V_S values in the top 30 m of soil, while the K-NET database is excluded. However, KiK-net does not have a proper search engine that can be used to select earthquake events, and it only includes raw earthquake data. On account of that, a web-based search tool, has been developed by Dawood *et al.* (2014) processing 157,000 KiK-net strong ground motions, by applying an automated processing protocol. KiK-net does provide two data search engines, available on the NEEShub website, with desired earthquake parameters—one for metadata and the other for pseudo-spectral accelerations.

At total of 552 and 1,227 earthquake records, measured by stations on class D soil, were found for seismicity Types 1 and 2, respectively. Based on the 16th percentile, median and 84th percentile normalised spectral acceleration shapes of the records, as presented in Figure 2.20, the smoothed design response spectrum in EC8 seems to be a good representation of future earthquake events, as it lies between the median and the 84th percentile shapes of the Type 1 earthquake records. It is, however, closer to the median spectral shape at short and medium periods. The EC8 Type 2 design response spectrum shows a good match with the 84th percentile of the earthquake events at periods above 1 s; however, it only exhibits good agreement with the median of the earthquake events at periods of between 0.1 s and 1 s.

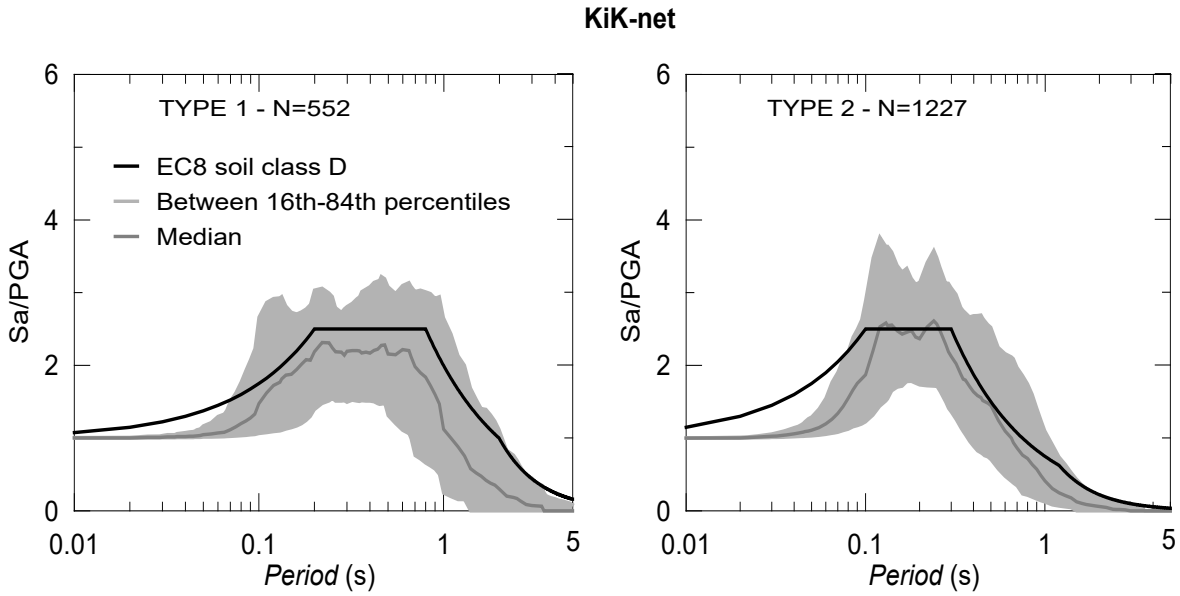

Figure 2.20 Probabilistic empirical earthquake spectral data results from KiK-net database, and corresponding spectral acceleration shapes from EC8.

2.7 EC8 Design Response Spectrum with Respect to ESD

Although some of the investigated earthquake databases contain a considerable amount of data related to soil class D (e.g. Geonet and KiK-net), it might not be rational to draw conclusions on the proxy of the EC8 design response spectrum based on their spectral acceleration results. This is because EC8 is the seismic design provision for tectonic activity in Europe. Hence, the use of earthquake events recorded in this region might give better option to check the suitability of the design response spectrum.

From this perspective, the results from the ESD earthquake database are more related to the EC8 design response spectrum, even though it includes only a small number of earthquake records, compared to Geonet and KiK-net. The conclusion to be drawn, based on the real spectral accelerations in ESD, is that the overall shape of the EC8 design response spectrum for soil class D, in both seismicity types, seems acceptable, but peaks, especially at medium period ranges, are not well represented.

The peaks at medium, long (for seismicity Type 1) and short (for seismicity Type 2) periods can be clearly observed in some individual cases, as shown in Figure 2.21. These results may be due to local site effects on the characteristics of the seismic input motions (e.g. filtering the energy content, and affecting the fundamental frequency and spectral amplification of the seismic motion). The individual spectral accelerations demonstrate that

the actual spectral peaks cannot be represented by the smooth design response spectrum given by EC8 for a soft soil deposit and, thus, justify, at least in this respect, the necessity of site response analysis.

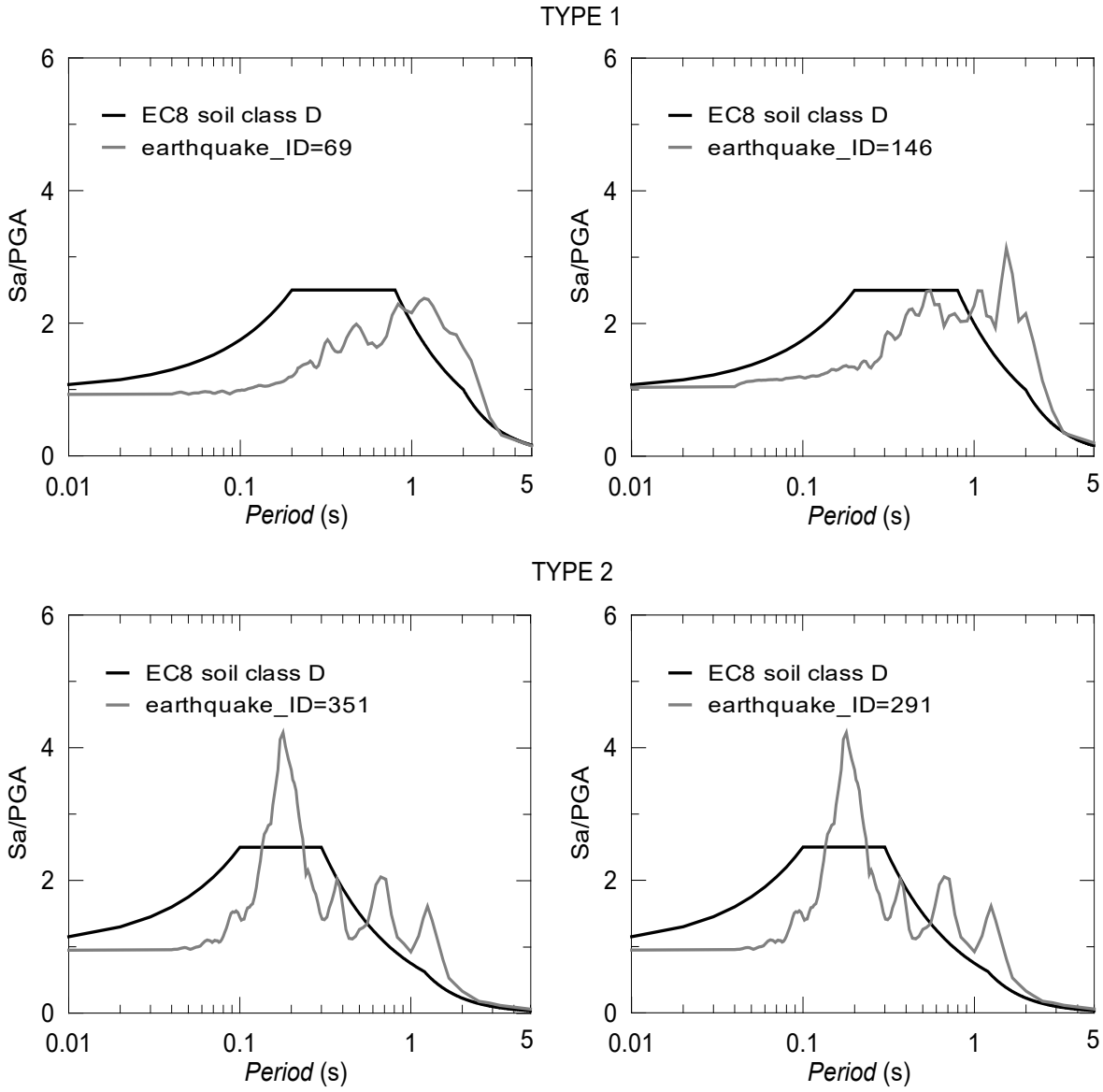

Figure 2.21 Spectral accelerations of two individual earthquake events from ESD not fully captured by the EC8 design response spectra for both Types 1 and 2 seismic intensity levels.

2.8 Concluding Remarks

In this chapter, the early approaches to defining spectral shapes for the design of earth structures was firstly outlined. Secondly, the DSHA and PSHA that are thought to be the foundation of modern design response spectra were demonstrated. Subsequently, investigation of the well-known earthquake databases, with respect to the earthquake motions recorded in class D soils, were conducted. The median, 16th and 84th percentiles of the spectral accelerations were plotted, in order to test the suitability of EC8 design response spectra for a class D soft soil deposit. A considerable number of records were found in the KiK-net and Geonet databases, in comparison to records found in the ITACA, ESD, PEER, USGS and COSMOS earthquake databases. The main conclusions are summarised below.

- Based on the results from the KiK-net and Geonet earthquake databases, the EC8 design response spectrum for class D soils might be revisited so as to incorporate a good representation of probable major earthquake events.

- For the other databases, including ESD, the EC8 Type 1 design response spectrum is, in general, a good proxy, but this is not quite valid for the Type 2 seismicity level.

- Specifically, based on earthquake records from ESD, probable major earthquake events with high earthquake energy cannot be well represented at longer periods by the EC8 design response spectrum, while the low and moderate seismic activities are captured well.

- The peaks at the medium period ranges, especially in some individual events, clearly indicate deficiency in the smooth spectral shape in representing the seismic spectral response.

In general, the results of this initial study highlight some concerns about the suitability of the smooth spectral shape proposed by EC8 for soft soils. They also point out the influence of the characteristics of soft soil deposits on seismic input motions and, hence, justify the importance of site response analysis for soft soil deposits, and the need for the further investigation that constitutes the remaining part of this study.

Chapter 3. Concept of Input Motion Selection and Modification in Structural and Geotechnical Engineering Disciplines

3.1 Introduction

One of the natural hazards that a site can severely experience during the event and its aftermaths, can be seen as an earthquake that might cause extreme damage to the urban areas leading to numerous casualties as well as social and economic impacts. While some regions around the world are not threatened by earthquake events, some have been devastatingly affected through the history of mankind. It is inevitable for the regions near to the seismically active zones, such as North America, New Zealand, Japan, Italy and Turkey, to experience an earthquake within periodic time sequences. Hence, it has been given utmost importance in those regions to the development of performance-based seismic design provisions.

Performance-based seismic design provisions give guidance to the engineering practitioners in the seismic resistant design of the earth structures (buildings, bridges, dams, etc.). The input motion selection in this regard has been a crucial step influencing the seismic response and, ultimately the design. Broadly speaking, a structure can deterministically be designed by considering a maximum credible earthquake event at the site under consideration within a projected lifetime. Or, probabilistic based design can be possible with consideration of a number of seismic input motions. Different seismic design codes provide different conditions in the consideration of the input motions but they all agree on the performance analysis of the structures to be designed in a deterministic or probabilistic way such that they can resist a possible earthquake force within desired limit states.

The reasonable detailing of the input motion selection given within the context of the seismic design codes has been appreciated by the engineering communities as it results in better performance evaluation of the structures leading to cost-saving and most importantly life-saving. It is still in the interest of the researchers to come up with new input motion selection methods such that they are efficient and sufficient in accounting for all possible scenarios in the structural design (Marasco and Cimellaro, 2017). However, the need of

selection for site response analysis has only recently been pronounced as it is not clearly guided by the seismic design codes. The site response analysis might seem vitally important when a site specific response spectrum is required. This is, in particular, true for soft soil deposits where seismic input motions may be subjected to great amplification. In this respect, the selection of input motion can be seen a crucial step of site response analysis.

This chapter, in the first part, includes the basics of the input motion selection from the structural engineering perspective. Furthermore, some recent concerns of the input motion selection in the structural engineering discipline will be presented. In the second part, the situation in the geotechnical engineering discipline with respect to the early challenges and current development in the input motion selection will be explained. Finally, the roles of other two key factors in site response analysis (i.e. shear wave velocity and shear modulus reduction and damping curves) are expressed with reference to several past studies.

3.2 Structural Engineering Perspective

Seismic risk assessment of a site, briefly, involves the seismic excitation applied to the structure (seismic hazard), the response of the structure and, ultimately, the imposed structural damage (vulnerability) and the resulting social and economic impacts (exposure) (Galasso, 2010). The input motion selection links the seismic hazard with the structural response, vulnerability, by means of conducting nonlinear dynamic analysis (NLDA) of structures. Therefore, earthquake selections have been intensively investigated for recent decades with the view to probabilistically assess the seismic risk of the site under consideration.

The selection of the input motions has been regarded as important as modelling of the structure itself. The selection can be conducted from three types of earthquake recordings; (1) artificial accelerations, (2) simulated accelerations and (3) natural records (Bommer and Acevedo, 2004). The first earthquake recording type is thought to be not representing the actual form of the seismic waves as well as its cycles and, thus the energy introduced. The input motions from simulations have also issues related to the estimation of parameters for rupture mechanism (e.g. the rise time). The natural records, in contrast, are the most convincing choice in the seismic performance analysis of structures and in the probabilistic seismic hazard analysis (PSHA). Because, they are, in general, available online, gathered in

well documented databases, improved with digital recording technology in line with the increasing data with time (Iervolino and Manfredi, 2008).

However, the challenge with the natural earthquake records is the considerable record-to-record variability in a specific site for a structure to be designed or retrofitted. Clearly, it is the difference in the magnitude (M) and distance (R) pairs of the earthquake events that makes the description of seismic hazard level of one site, with only one dominant earthquake event, less likely within a specific return period. Hence, it is necessary to, probabilistically, conduct seismic risk analysis that enables to consider all the earthquake events and determine major contributors to the seismic hazard of the site and conduct, accordingly, the input motion selections and modifications. As a result, it is aimed to evaluate, more accurately, the seismic performance of structures with a manageable number of earthquake records that requires less budget and time (Iervolino and Manfredi, 2008). In the next section, detailed information regarding probabilistic seismic hazard analysis relating to input motion selection will be given, while general frameworks of deterministic and probabilistic seismic hazard analysis can be found in Chapter 2.

3.2.1 Probabilistic seismic hazard analysis

Incorporating the pair of M, R, and often epsilon (ε), of each individual event into the seismic hazard estimation of a site is called probabilistic seismic hazard analysis (PSHA) (Bazzurro and Cornell, 1999). The combination of hazard contribution of each fault into the seismic risk level of the region is regarded as the disaggregation or, in the broad literature, deaggregation of the PSHA. (ε, is a distant measurement between the spectral acceleration of an input motion and the mean spectral value from the ground motion prediction equation (GMPE) at a given period (Baker and Allin Cornell, 2006)).

The ultimate goal of the PSHA is to express the mean annual frequency rates of a considered intensity measure (IMs) expecting to exceed at various levels. In the structural engineering discipline, the peak values of the ground motions, (i.e. peak ground acceleration (PGA), velocity (PGV) and displacement (PGD)) and the spectral acceleration at the fundamental period of the structure ($S_a(T_1)$) are common chosen IMs (More details about the term of IM will be provided in the further sections) (Iervolino and Manfredi, 2008). Depending on the desired annual exceeding frequency rate of the chosen IM, a design response spectrum that represents contributions of all the earthquake motions to the seismic hazard of the site at

different period levels can be obtained. Based on that curve, input motion selections can be done with respect to the interested selection criterion and, accordingly, NLDA of the structures can be conducted. Ultimately, the estimated Engineering Demand Parameters (EDPs), which are the seismic performance indicators of a system considered in building designs (Bradley, 2013), will be probabilistically assessed based on the desired design limit state.

In terms of spectral acceleration, Uniform Hazard Spectrum (UHS) is the ultimate engineering interest from PSHA. The first step to compute UHS is to perform PSHA in relation to the spectral accelerations at different periods ((McGuire, 1995; Bazzurro and Cornell, 1999)). Subsequently, the spectral acceleration at each period can be read with regard to the considered annual exceedance frequency rate, the limit state. As a result, the spectral accelerations with the corresponding periods will be plotted. Since the exceedance rate is uniform for each spectral value through the interested period ranges, the ultimate curve is called UHS. An example of plotting UHS from PSHA is demonstrated in Figure 3.1.

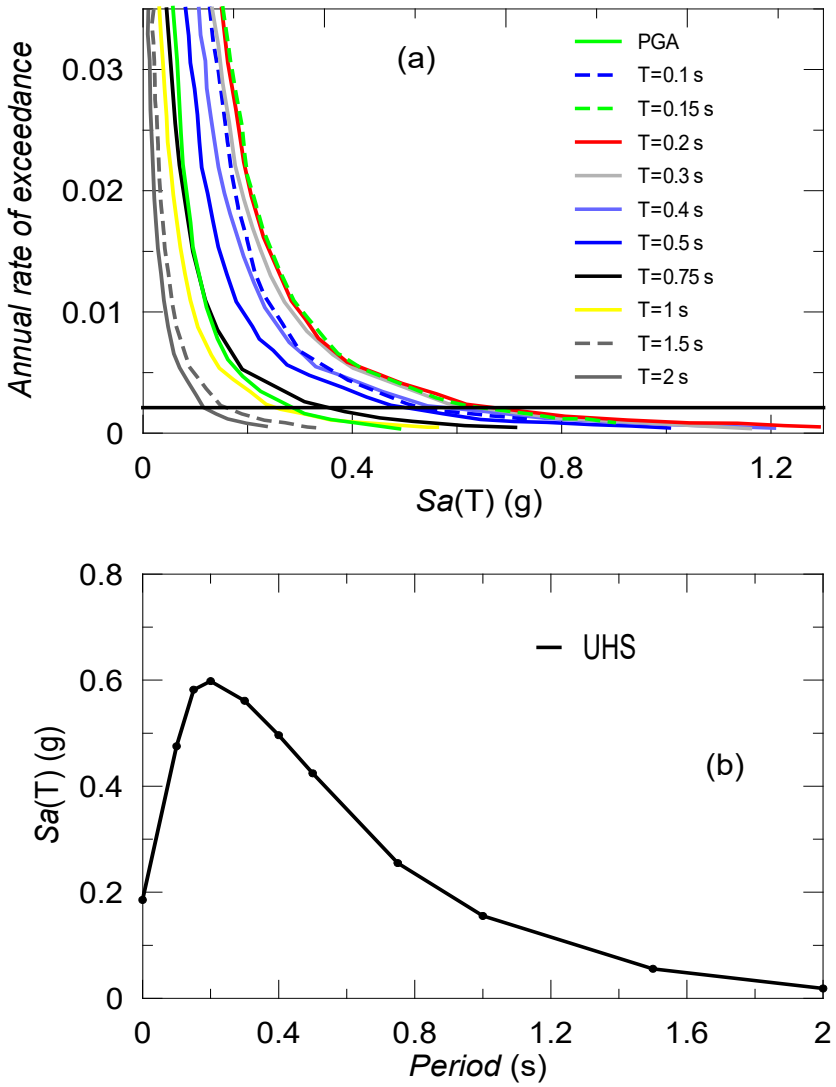

Figure 3.1 (a) PSHA curves for different period interests at the site in southern Italy（a site in Sant'Angelo dei Lombardi）, showing an example of reading spectral acceleration for, in that case, 10% probability of exceedance in 50 years, which is equal to 0.0021 annual rate of exceedance, (b) UHS based on specified annual frequency exceedance rate for the site considered, adapted from Iervolino and Manfredi (2008).

It is well-known that the spectral accelerations at short period ranges are controlled by small to moderate earthquake intensities taking place at short distances, while the far distant earthquake events shape the spectral values at the longer periods in the UHS curve (Bommer and Acevedo, 2004). Hence, a single seismic input motion cannot be represented by the UHS curve at all periods. In spite of this limitation, UHS has become the basis of modern seismic codes, where the smooth design response spectrum curves are standardised with inclusion of soil factors and other standard parameters (e.g. ground acceleration at bedrock, ductility factor and period ranges with respect to acceleration, velocity and displacement dominant regions). This is so that in the absence of PSHA of a site, a target response spectrum for the

engineering practitioners can be produced to select input motions for the seismic performance analysis of structures.

Earthquakes to be selected for the probabilistic seismic performance analysis of structures are expected to reflect the characteristics of the earthquake events that contribute to the seismic hazard level of the site. As mentioned above, the main characteristics of an earthquake event are, in general, regarded as M, R and ε. From PSHA, hazard contribution graph of a site with regard to M and R, even ε, can be plotted and the dominant distance and magnitude ranges or ε at T_1, $\varepsilon(T_1)$, will be assigned. Based on those values, earthquakes can be selected and modified to match precisely with the spectral acceleration of the target response spectrum at T_1, as seen in Figure 3.2.

Alternatively, they can be modified in such a way that their mean spectral values fit well with the target response spectrum giving tolerance level of matching at certain period ranges (e.g. between $0.2T_1$ and $2T_1$ with lower tolerance of 10% given in EC8). This is to allow consideration of higher seismic modes and the elongation of structural periods due to the extreme system nonlinearity, as shown in Figure 3.3.

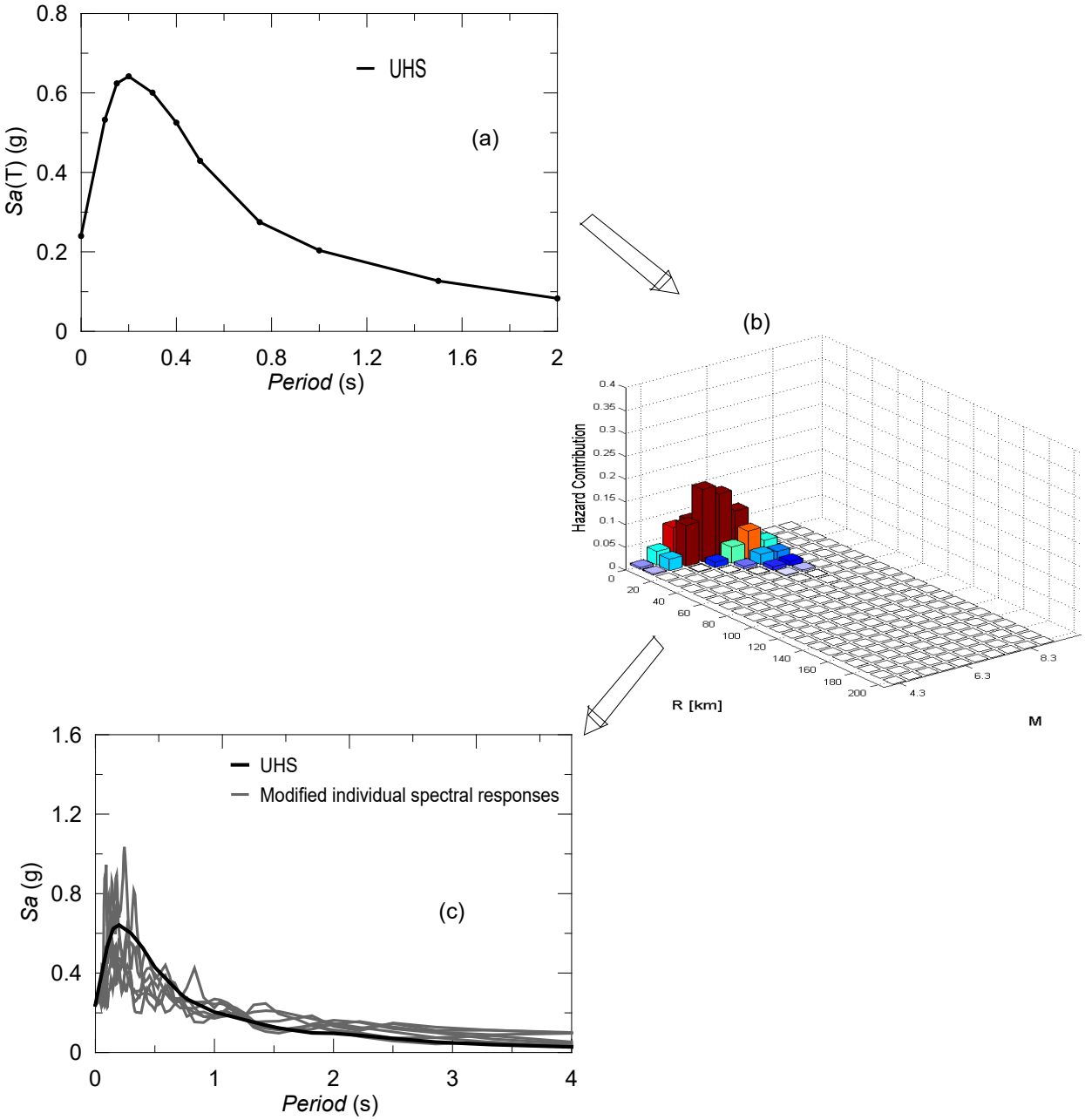

Figure 3.2 Brief process of selecting and scaling earthquake records for a site, a) defining target response spectrum from PSHA for a limit state of interest, b) disaggregation of the seismic site hazard contributions of the events, and c) Scaling of earthquake records to Sa at T_1, adapted from Iervolino *et al.* (2010).

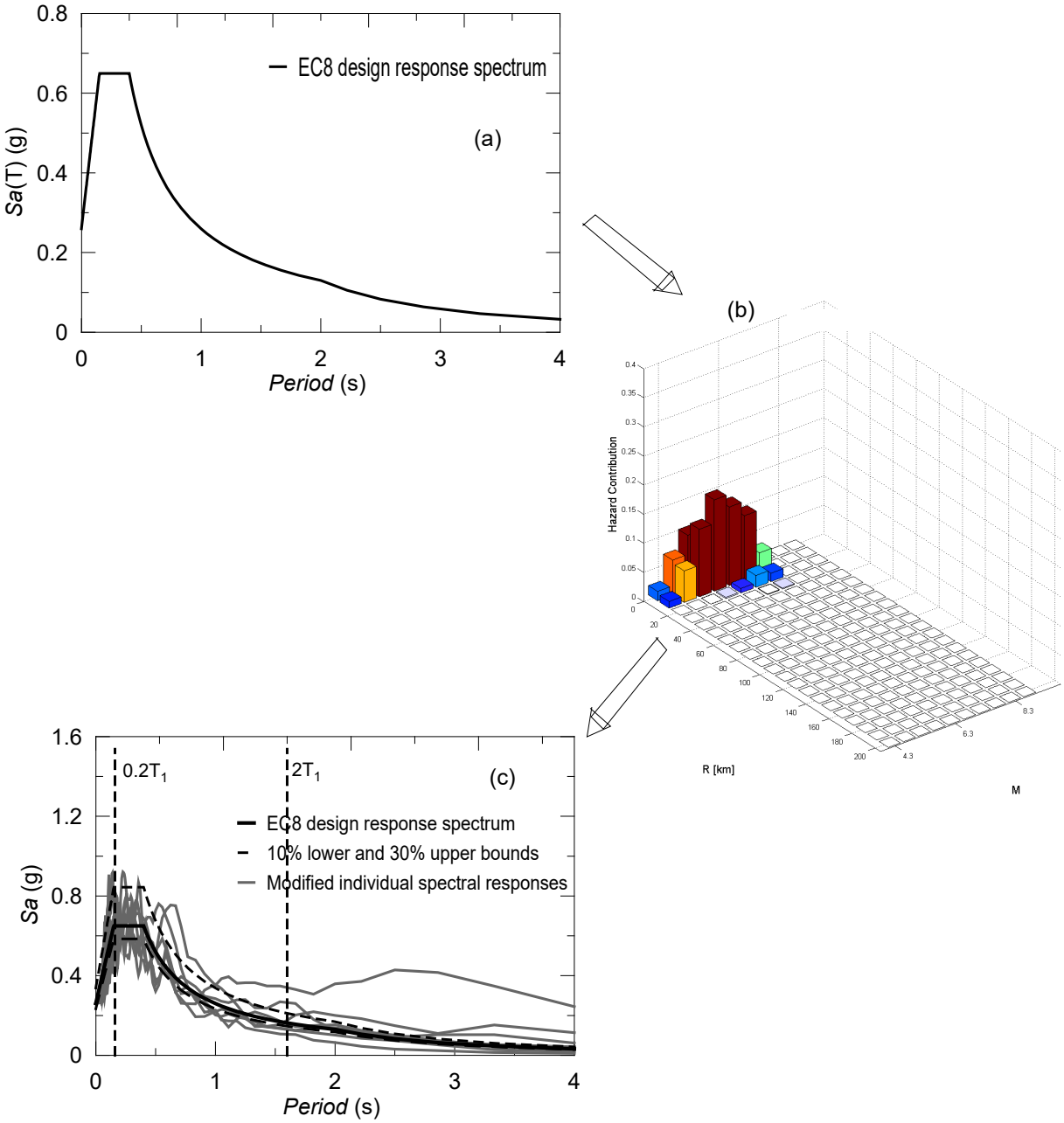

Figure 3.3 An alternative method (e.g. EC8 based) in earthquake selections for NLDA of a structure in a specific site, a) smooth target response spectrum, b) disaggregation of seismic site hazards, and c) scaling of set of earthquake events matching target spectrum within a range of periods limited with related to T_1, adapted from Iervolino *et al.* (2010).

3.2.2 Concepts of earthquake record selection

1. Intensity measures (IMs)

An intensity measure, IM, is a ground motion parameter that strongly reflects the structural response (Baker and Cornell, 2006a). Efficiency and sufficiency are the two important properties of an IM. When the structural response is characterized by an IM without considering the properties of a seismic input motion, such as magnitude and distance, the selected IM is sufficient. Meanwhile, an IM can be described as efficient once the dispersion from the mean structural response within a set of input motions is relatively inconsiderable (Iervolino *et al.*, 2008).

In the early stage of earthquake selection, PGA were commonly applied ground motion parameter as an IM. However, $Sa(T_1)$ is proven to be more sufficient and efficient IM in the consideration of inter-story drift response as an EDP than the PGA since hazard curves for Sa are available at periods of interest and it indirectly implies the structural response. Furthermore, $Sa(T_1)$ is found to be sufficient to represent the influence of duration on structural responses when a single degree of structure is analysed (Iervolino *et al.*, 2006). Additionally, seismic performance of structures is proved to be, in a statistical framework, independent of the duration of the event when the considered EDP is displacement related parameter (e.g. inter-story drift ratio, roof drift ratio). On the contrary, EDPs in relation with cyclic loading (hysteretic ductility or equivalent number of cycles) are strongly influenced by duration.

By considering an IM that is recognized as sufficient and efficient, this can also render a small number of input motions as well as small record-to-record variability of structural response. This is the ultimate desire from NLDA as it reduces the necessary time- and cost-spending. In this regard, the work of Shome *et al.* (1998) shows that, when the input motions are modified to a specific Sa value, the dispersion in the structural response can be significantly reduced and the number of analyses required can eventually be decreased. However, in some cases, Sa cannot be sufficient and efficient, for example, if the oscillation periods of the structure rest at the high periods driven by the larger earthquake events (Iervolino *et al.*, 2008).

Furthermore, $Sa(T_1)$ is not a strong IM candidate when the seismic waves propagate through the soft soil strata. This is because of the fact that soft soil deposits tend to be extremely

nonlinear under strong seismic shakings leading to period elongations. This ultimately causes spectral amplifications at periods greater than T_1. In addition, if non-structural elements are taken into account in the structural design, PGA is regarded as better IM. To overcome these deficiencies of scalar Sa(T_1) scaling along with the M and R pairs, some other scalar IM (i.e. ε) and vector-valued IM (i.e. Sa(T_1) and ε combination) can be used (Baker and Cornell,2005).

2. Sa consideration

Sa is a current widely known IM in the probabilistic assessments of structures which correlates probability of earthquake occurrences in a site (hazard) with the structural responses (response). Generally speaking, the seismic hazard analysis of a site is conducted by earth scientists (e.g. seismologists and geotechnical engineers) as the response analyses are undertaken by structural practitioners. While the Sa values corresponding to the probability of annual exceedance rate are calculated by earth scientists, with configuration of the hazard maps or graphing of the seismic hazard analysis, structural engineers take those values into consideration to predict the structural responses (Baker and Cornell, 2006).

The consistency in the Sa consideration is vital with respect to the structural response predictions. When the seismologists consider the geometric mean of the spectral accelerations in two horizontal directions for GMPEs, structural engineers only consider one single horizontal component of an event for structural analysis (Iervolino *et al.*, 2008). It has been demonstrated by Baker and Cornell (2006) that the probabilistic ground motion hazard analysis for a single fault performed with respect to Sa_{arb} (arbitrary single horizontal components of events), incorporated with the attenuation model (Boore and Bommer, 2005), gives higher annual rate of exceedance, especially at long return periods, than the value computed by using geometric mean spectral accelerations, $Sa_{g.m}$ (i.e. geometric mean of two horizontal components of events). This is because, although Sa_{arb} and $Sa_{g.m}$ are the production of events that give the same median magnitude and distance values, Sa values above averages for Sa_{arb} are greater than those for $Sa_{g.m}$.

Furthermore, two types of response spectra (e.g. Sa_{arb} and $Sa_{g.m}$) are considered in the performance analysis of a two-dimensional one bay frame structure to investigate their effects on the structural response in terms of maximum inter-story drift. Based on linear regression analyses conducted, as it can be seen in Figure 3.5, using Sa_{arb} in the estimation

of structural response leads to less scatter within the results, implying less uncertainty. However, the results based on $Sa_{g.m.}$ show higher dispersion, hence higher uncertainty. To achieve same confidence, more structural analyses with $Sa_{g.m.}$ is required. Because of this, in the current practise, only one arbitrary component of the spectral accelerations (Sa_{arb}) is preferred as an IM in the probabilistic assessment of 2D structural analysis.

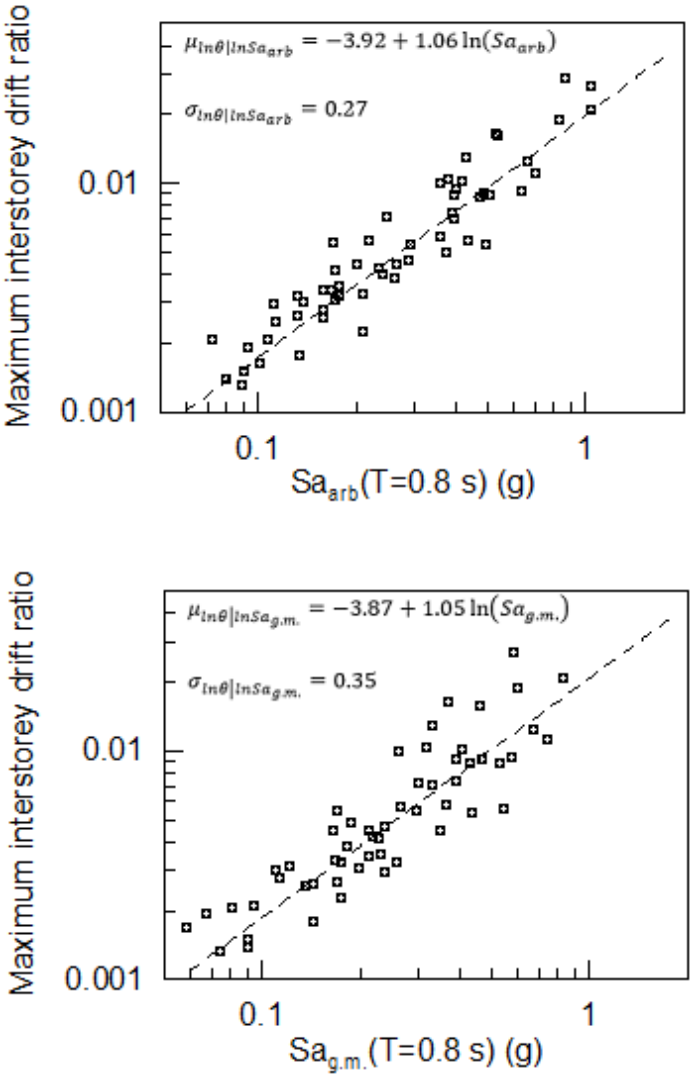

Figure 3.4 Performance estimation of a single frame structure based on (top) the spectral acceleration from one arbitrary component of ground motion (Sa_{arb}), (bottom) the spectral acceleration from geometric mean of the two horizontal components of the ground motion ($Sa_{g.m.}$) (adapted from Baker and Cornell, 2006b).

To overcome the inconsistency in the use of Sa for the seismic hazard and response analyses, three different methods are proposed by Baker and Cornell (2006), which are applicable for two-dimensional structural models:

a. **Computing ground motion hazard based on Sa_{arb}**: the structural response analysis is performed based on Sa_{arb}. This method can provide reduction in variability within the structural responses, but one of the limitations is that the current attenuation laws cannot directly be used with Sa_{arb} in the hazard analysis.
b. **Performing response analysis with respect to $Sa_{g.m.}$:** this method causes increase in the dispersion and leads to less probabilistic confidence for the structural response, (see Figure 3.5b).
c. **Using current practice ($Sa_{g.m.}$ for analysis and Sa_{arb} for response analysis) but expand the response dispersion:** once the hazard analysis and response analysis are conducted with $Sa_{g.m.}$ and Sa_{arb}, respectively. To achieve consistency in Sa, the obtained structural responses will be increased to some extent that they become equivalent to those values calculated based on $Sa_{g.m.}$ involved in structural response analysis (Iervolino *et al.*, 2008).

On the other hand, for three dimensional (3D) structural analysis, $Sa_{g.m.}$ seems to be stronger IM candidate because it is the simplest way of representing the model response. Further, it is commonly used in the structural engineering practices for seismic performance analysis (Stewart *et al.*, 2002).

3.2.3 Code-conformed earthquake selection criteria, EC8 prescription

In order to conduct NLDA of structures, it is, first of all, necessary to obtain a target response spectrum called, also, a design response spectrum. This target response spectrum may be obtained from PSHA (which is called Uniform Hazard Spectrum, UHS) or from seismic design codes (code-conformed response spectrum). As it is highlighted before, seismic hazard analysis of a site (PSHA) provides an elastic design response spectrum depending on chosen IM (e.g. Sa, PGA, PGV etc.) with respect to the annual probability of exceedance level at several oscillation periods. Since, in the current practice, Sa is a convincing IM candidate, elastic spectral acceleration over an engineering interest period range can be obtained from the seismic hazard analysis and be employed in the site response analysis. In order to define the main characteristics of the earthquake events (mainly, M and R) in the response analysis, hazard analyses of all faults in the site should be disaggregated.

It is unlikely, however, to find a site specific PSHA for every region that will give UHS, such as in Europe. Because of that, EC8 describes two types of standard seismic design

response spectra, with respect to their magnitudes to be used in the response analysis. If the surface wave magnitude imposing most of the seismic hazard is equal or less than 5.5, the design response spectrum is defined as Type 2, but if it is greater than 5.5 the target spectrum is Type 1. Depending on the soil class and the a_g (PGA at rock, showing the seismicity level of the site considered), the target response spectrum can be characterised.

In EC8, some prescriptions to be complied with in selecting seismic input motions to conduct NLDA of structures are described. EC8 does not restrict one in the types of the input motion to be selected whether artificial, simulated or recorded accelerograms. However, it puts some criteria on the set of selected motions, showing no reference to its type:

i. At least 3 input motions should be selected;

ii. The average spectral acceleration value of a set of input motions at zero period should not be less than a_gS (S soil factor) for the site considered;

iii. The mean 5% damped response spectrum of a set of events should not be less than 90% of the corresponding spectral acceleration values of the 5% damped design response spectrum between $0.2T_1$ and $2T_1$ (T_1 is the fundamental period of the structure in the direction where the accelerograms applied).

When only three input motions are considered for the seismic performance assessment of structures, the maximum structural response should be considered in design. However, if at least seven earthquake accelerograms are taken into account, it is allowed to consider the average of structural responses. The value of a_g demonstrates the seismicity level of the site in question while S represents the amplification of the motion due to soil characteristics. The matching criterion (i.e. iii) between $0.2T_1$ and $2T_1$ aims to consider, in NLDA, contributions of higher structural modes to the response (lower bound, $0.2T_1$) and elongation of the structural period (upper bound, $2T_1$) attributed to the nonlinearity (Iervolino and Manfredi, 2008).

3.2.4 Reflection of earthquake selection criteria to structural responses

Since this section, it has been shown that earthquake characteristics (mainly, M and R) are thought to be main drivers of PSHA of a site and, ultimately, of earthquake selections to be scaled to $Sa(T_1)$ for nonlinear structural performance analysis. Consideration of M and R in

the seismic hazard and response analyses implies that they are expected to be dominantly influential in the linear and nonlinear behaviour of structures under dynamic motions besides some contributions of the other earthquake features, such as fault mechanism, soil type (Iervolino and Cornell, 2005). Because of that, the seismologists provide rigorous data about earthquake characteristics to be used by structural engineers. In this respect, it gains great interest of structural engineers as to whether M and R consideration is necessary in the input motion selections for NLDA of a structure at a considered site. Furthermore, the question of whether spectral acceleration scaling and scaling magnitude, to the target spectral acceleration at the fundamental period of structure ($Sa(T_1)$), is acceptable in terms of structural responses is raised.

The study of Shome *et al.* (1998), for example, investigates the effects of Sa scaling/scaling intensity and M and R consideration on several post-elastic structural damage measures (e.g. displacement ductility, normalized hysteretic energy, and damage index) by modelling a single five DOF steel structure. Four earthquake bins, each includes 20 earthquake records recorded on stiff soil in California, with different magnitude and distance ranges are utilized and careful attention is paid to not include any pulse-like type or near-source earthquake event so that large dispersion in the results of structural analyses is avoided. It is, firstly, found that scaling of spectral acceleration at $Sa(T_1)$ is a more robust measure of response than PGA. Secondly, proper Sa scaling reduces the number of required nonlinear structural analysis by a factor of 4 as a result of reduction in dispersion. Thirdly, once (M, R) pairs are included in the seismic hazard analysis, there is no need of selecting input motions by considering specific M and R ranges in the response analysis. Lastly, scaling Sa to lower or upper intensities does not introduce any bias into the structural results. The limitation of this study, however, is only one type of structure with the accelerogram recordings at only one type of soil class was tested.

Further on this, Iervolino and Cornell (2005) have analysed three SDOF systems with different periods (short, moderate and long), incorporating with bilinear and trilinear hysteresis, and one MDOF structure with moderate period by selecting/applying two groups of sets of earthquake records (one set is carefully selected and the other is arbitrarily chosen). Again, the records do not include any pulse-like type and do recorded on firm soils. Based on the probabilistic assessments of median drifts of sets, there is no supportive evidence that M and R should be carefully considered in the input motion selection. It was also found that

Sa scaling with up to scale factor of 4 does not introduce any bias into the structural responses (see Figure 3.5). Although the cited study considers several structures with different periods, scaling issue is not deeply investigated because of limitation of the earthquake records such that large scale factors cannot be obtained.

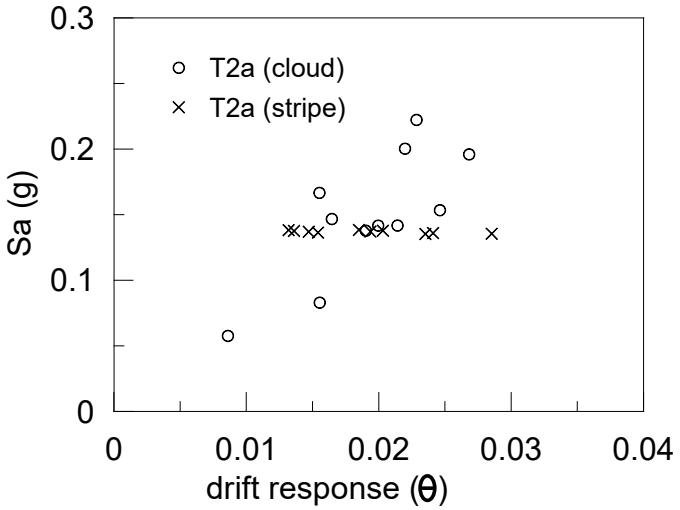

Figure 3.5 Drift responses of a bilinear SDOF system with a 1.5 s fundamental period under a set of input motions without (cloud) and with (stripe) modifications (modified from Iervolino and Cornell, 2005).

The work done by Galasso and Iervolino (2011) investigates the impacts of earthquake input motions on the response estimation of a proper code-confirmed structural model in regard to recordings at same as target/arbitrary soil type, scaling magnitude and a specific M and R scenarios. Selection strategies for all recording sets applied in this study is also complied with the EC8 prescriptions. Maximum inter-story drift ratio, roof ratio and hysteretic energy are considered EDPs. The results are assessed based on the parametric hypothesis tests and concluded that if the spectral accelerations of a set of earthquake event match, individually or on an average, with the target response spectrum, it is not necessary to give attention to M, R and soil condition when input motions are selected. Moreover, linearly scaling of the input motions will reduce the uncertainty in the response values, where scaling magnitude is considered as high as 15 in the study.

Overall, the findings about the influence of Sa scaling in addition to M, R and soil types on the structural response can be summarized as:

- Linear scaling is legitimate and leads to less dispersion in the structural responses and, thus, requires less number of NLDA,

- Scaling magnitude should be carefully taken into consideration since a single event with great scaling factor may cause additional uncertainty into the structural response,
- There is no need for scenario-based earthquake selections; specific range of magnitude and distance, as well as the type of soil where the event is recorded.

3.3 Geotechnical Engineering Perspective

While great attention on input motion selections for NLDA of structures are paid by both research communities and seismic design codes (e.g. EC8, NEHRP etc.), this topic has been studied less in the geotechnical engineering discipline with regard to nonlinear site response analysis of soil deposits. These relatively advanced applications of earthquake selections in the structural engineering discipline can be attributed to the well-established documentation of the topic in modern seismic design codes and clear determination of the structural properties. This is not the case in nonlinear site response analysis, in which poorly instructed parameter choices and unclear code regulations are the main limitations (Kwok *et al.*, 2007).

Over the recent decades, research focus in geotechnical engineering has been more on to the understanding of the propagation of seismic waves, interaction between soil and seismic input motions and, accordingly, simulation of the vertical propagation of seismic waves within horizontally layered soil strata. These necessitate developments of adequate representative soil constitutive models, rigorous determination of soil properties through field and laboratory tests and an appropriate implementation of input motions (Visone *et al.*, 2010). Moreover, different numerical codes solving the wave propagation problem in frequency and time domains are developed in order to simulate the seismic excitation of the soil deposits in conjunction with reasonable boundary conditions. The following section is aimed to give an overview of numerical codes and soil models, with specific description of a finite element code and a soil model employed in this research. Then, the recent implementation of input motion selection strategies in the field is given. Finally, several past studies, dealing with other two major factors that are influential in the site response analysis, namely elastic and nonlinear soil properties are demonstrated.

3.4 Site Response Analysis

Seismic hazard level of an input motion to a specific site is mainly affected by the characteristics of the seismic source and its fault mechanism, deep wave propagation through the rigid bedrock body and local site conditions. While the first two topics are studied in engineering seismology, the geotechnical engineering discipline deals with the last topic (i.e. local site condition).

The local site conditions can influence the amplitude, duration and frequency content of an input motion propagating in the vertical direction through the horizontally layered soil deposits and these effects are termed in geotechnical engineering as local site effects. The damages due to local site effects to the earth structures have been clearly observed in Mexico (Stone *et al.*, 1987), Loma Prieta (Seed, 1990) and recently in Christchurch (Kaiser *et al.*, 2012) earthquake events. The site response amplification and liquefaction are the two major local site effects observed during and aftermath of those earthquake events: the former leads to resonance of structures with a certain range of fundamental periods and the later results in foundation failures due to excessive settlements.

Site response analysis is a great tool to simulate the possible consequences of the local site effects (e.g. the degree of liquefaction, site amplification as well as settlement). One dimensional site response analysis is the most commonly utilised method by geotechnical practitioners. When seismic waves propagate through the soil layers, refracted and reflected waves are produced. Since, in general, shear wave velocities of the soil materials at a layer are higher than those at the above layers, reflected waves are inclined to the vertical direction. This vertical normalisation of the reflected waves leads to almost vertical refraction of the waves when they reach to the ground surface. Hence, one dimensional solution is reasonable with the assumptions that the seismic wave propagation from bedrock to surface is in vertical direction and soil and bedrock surface has infinite horizontal surface (Kramer, 2014).

Widely known numerical analysis applied by geotechnical practitioners is a one-dimensional (1D) equivalent linear visco-elastic approach (Kramer, 2014). It solves the wave propagation problem in frequency domain. Even though this numerical scheme is relatively easy to use and is time- and cost-effective, it has also well-known deficiencies. Specifically, the accumulation of pore water pressures cannot be taken into account as the formulation is based on total stress approach. Furthermore, the approach is not capable of representing

dynamic soil behaviour under intense seismic oscillations, where soil nonlinearity, thus accumulation of displacements and stiffness degradation, is highly likely to take place.

To better simulate the soil behaviour under seismic excitation, numerical schemes solving the problem based on time histories are developed. These numerical solutions can also consider the interaction between the solid phase and the fluid phase, where the excess pore water pressure is involved in dynamic equations. They are, in general, incorporated with a simple or more advanced soil models depending on the complexity of the analyses, and are embedded into the finite element codes. Finite element codes enable to conduct a site response analysis in two-dimensions (2D) or in three-dimensions (3D) when the seismic wave propagation cannot be represented by 1D model in cases such as having inclined soil layers, stiff structure on top of the soil, retaining walls or earth embankments.

3.4.1 Equivalent linear site response analyses

Soil nonlinearity is represented by the equivalent linear approximation based on the exact continuum solution of the seismic waves propagating through the visco-elastic soil elements in the vertical direction (Roesset, 1977). There are two important correlated factors in describing the dynamic behaviour of soil that should be accounted for in the equivalent linear approximation: the stiffness degradation and the hysteretic damping. Since the shear modulus (G) and the damping (D) of a layer are assumed to be constant during cyclic loading, simultaneous changes in G and D with time cannot be captured. Thus, it is required to analyse the soil iteratively until the analysis is converged with respect to G and D values at an earthquake induced shear strain. The process of iteration is given as follows (Kramer, 2014):

1. G and D at low strain levels are assumed for each layer.
2. With the initial G and D profiles, frequency domain site response analysis is conducted, where the time histories of the shear strain, acceleration and displacement at a layer are computed.
3. Effective shear strain for each layer is calculated by using the following equation:

$$\gamma_{eff} = R_{\gamma}\gamma_{max} \tag{3.1}$$

where R_γ is dependent on earthquake magnitude (Idriss and Sun, 1992) given by:

$$R_\gamma = \frac{M-1}{10} \tag{3.2}$$

4. New *G* and *D* values, corresponding to the calculated effective shear strain, are selected for the next iteration.

5. Steps from 2 to 4 are repeated until the convergence criterion is achieved.

The time history responses at each layer are calculated by, firstly, representing the acceleration-time history of an earthquake at bedrock with a fast Fourier transform (FFT) series and, secondly, computing the transfer function for a layer. Ultimately, the inverse fast Fourier transform (IFFT) series are adopted to estimate the shear strain, acceleration and displacement response histories (see schematic representation in Figure 3.7).

The philosophy of the equivalent linear approximation of the nonlinear soil response, described above, is embedded into the commonly utilised computer codes such as SHAKE (Schnabel *et al.*, 1972) and its refined version SHAKE91 (Idriss and Sun, 1992) and EERA (Bardet *et al.*, 2000). While these programs can give results showing some indication of actual site responses, they cannot predict the accumulation and the dissipation of pore water pressure. The permanent displacement also cannot be calculated as it is always considered to be zero at the end of the cyclic loading. Nevertheless, they are able to predict site responses reasonably well when the intensity of the input motion simulated is low, so that the soil behaves within the linear regions. Nonlinear site response analysis, however, is preferable when the earthquake intensity causes the soil to experience great nonlinearity, where permanent displacement and stiffness degradation are expected to accumulate (Elia *et al.*, 2017).

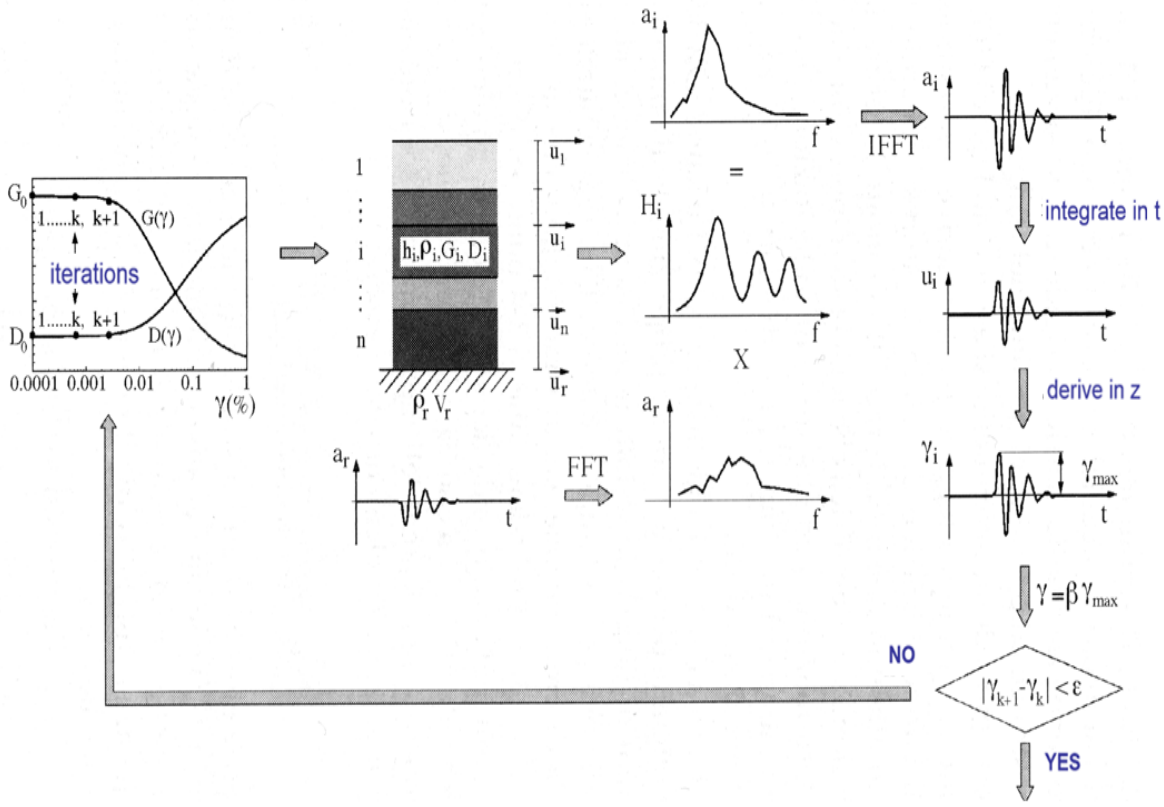

Figure 3.6 Traditional equivalent linear solution of the seismic wave propagation, adapted from Lanzo and Silvestri (1999).

3.4.2 Nonlinear site response analysis

Although equivalent linear site response analyses are easy to apply and computationally efficient, the approach is not sufficient to capture the actual soil behaviour under cyclic loading. To represent the real response of the soil deposit, including soil nonlinearity (irrecoverable deformation, stiffness degradation, energy dissipation, pore water pressure accumulation), an approach that employs direct numerical integration in time domain can be utilised. In a such approach, the dynamic equation of the motion is solved in small time steps with linear or nonlinear stress-strain models (e.g. hyperbolic model, modified hyperbolic model) or with advanced soil constitutive models.

The time integration scheme is, most commonly, explicitly or implicitly implemented in the finite element codes. When the code uses explicit time integration scheme, where the historical information of displacements and their time derivatives used to compute the next step displacement, dynamic solutions become conditionally stable. It is unconditionally stable, however, if the implicit time integration scheme is adopted which relies on time

derivatives of displacement at the end of step, which are unknown, to calculate the displacement. The trade-off between these two schemes depends on the expected accuracy in the response predictions and computational efforts (Kramer, 2014).

Free-field soil deposits with uniformly horizontal layers can be analysed in finite element codes with 1D model. Moreover, finite element codes enable to conduct 2D nonlinear site response analyses, which are required once the soil layers are inclined or the structure responses (such as permanent displacements of slopes or retaining walls) on top of the soil deposits are in the engineering interest. If the soil deposit and its boundary conditions vary in three dimensions or the three dimensional responses of the structures are of great importance (e.g. tunnels, earth dams and bridges), 3D dynamic site response analyses can be adopted, as well (Kramer, 2014).

Table 3.1 shows the available computer programs solving the seismic wave propagation problem with equivalent linear or nonlinear methods based on total stress or effective stress approaches, in 1D and 2D spaces.

TS total stress, ES effective stress, EL equivalent linear, NL nonlinear

Geometry	Program	Source	Type of analysis	
1D	SHAKE	(Schnabel *et al.*, 1972)	TS	EL
	SHAKE91	(Idriss and Sun, 1992)		
	PROSHAKE	(www.proshake.com)		
	SHAKE2000	(Ordóñez, 2000)		
	EERA	(Bardet *et al.*, 2000)		
	TESS	(Pyke, 1992)	TS	NL
	NERA	(Bardet and Tobita, 2001)		
	DEEPSOIL	(Hashash *et al.*, 2012)		
	DESRA_2	(Lee and Finn, 1978)	ES	
	DESRAMOD	(Vucetic, 1986)		
	D-MOD_2	(Matasovic, 2006)		
	D-MOD2000	(Matasovic and Ordonez, 2012)		
	SUMDES	(Li *et al.*, 1992)		
	CYCLIC 1D	(Elgamal *et al.*, 2001)(Elgamal *et al.*, 2001)		
2D	QUAD4	(Idriss, 1973)	TS	EL
	QUAD4M	(Hudson *et al.*, 1994)		
	FLUSH	(Lysmer *et al.*, 1975)		
	QUAKE/W	(Krahn, 2004)	TS	NL

	SPECTRA	(Borja and Wu, 1994)	ES	NL
	DYNAFLOW	(Prevost, 1981)		
	GEFDYN	(Aubry and Modaressi, 1996)		
	TARA-3	(Finn *et al.*, 1986)		
	FLAC 2D	(Itasca, 2002)		
	PLAXIS 2D	(Brinkgreve *et al.*, 2011)		
	SWANDYNE II	(Chan, 1995)		
	OpenSees	(McKenna and Fenves, 2001)		

Table 3.1 Programs for ground response analysis (modified from Italiana (2005)).

3.5 A Finite Element Code, SWANDYNE II

SWANDYNE II is a finite element code developed by Chan (1995). It solves the wave propagation problem in time domain based on fully-coupled effective stress approach: in which solid and fluid phase interactions are simultaneously considered in the following dynamic equations (Zienkiewicz *et al.*, 1999).

$$[M]\ddot{u} + [C]\dot{u} + [K]u - [Q]p = f^s \tag{3.3}$$

$$[Q]^T\dot{u} + [S]\dot{p} + [H]p = f^p \tag{3.4}$$

$[M], [C], [K]$ and $[Q]$ in Equations 3.3 and 3.4 are mass, damping, stiffness and coupling matrices of the system, respectively. $[S]$ is compressibility matrix and $[H]$ is permeability matrix. The f^s and f^p are force matrices for solid and fluid phases, respectively. The u and p are global displacement and pore pressure matrices.

The generalized Newmark (GNjp) scheme is implemented to compute the dynamic responses at each time step (Katona and Zienkiewicz, 1985). When the displacements, pore

water pressures and their time derivatives $\{u_n, \dot{u}_n, \ddot{u}_n, p_n, \dot{p}_n\}$ are known at a time step t_n, their values at the next time step, t_{n+1}, $\{u_{n+1}, \dot{u}_{n+1}, \ddot{u}_{n+1}, p_{n+1}, \dot{p}_{n+1}\}$, can be obtained. The convergence of dynamic solution is achieved with an iterative process employing the Newton Raphson procedure.

$$\ddot{u}_{n+1} = \ddot{u}_n + \Delta\ddot{u}_n$$

$$\dot{u}_{n+1} = \dot{u}_n + [(1-\beta_1)\ddot{u}_n + \beta_1\ddot{u}_{n+1}]\Delta t$$

$$u_{n+1} = u_n + \dot{u}_n\Delta t + \left[\frac{1}{2}(1-\beta_2)\ddot{u}_n + \frac{1}{2}\beta_2\ddot{u}_{n+1}\right]\Delta t^2 \tag{3.5}$$

$$\dot{p}_{n+1} = \dot{p}_n + \Delta\dot{p}_n$$

$$p_{n+1} = p_n + \dot{u}_n\Delta t + \left[\frac{1}{2}\left(1-\bar{\beta}_1\right)\dot{p}_n + \frac{1}{2}\bar{\beta}_1\dot{p}_{n+1}\right]\Delta t$$

In computing the displacement, pore pressure and their time derivatives in each time step, Newton Raphson parameters should satisfy the below conditions so that the iteration algorithm expressed in Equation 3.5 is unconditionally stable:

$$\beta_1 \geq \frac{1}{2} \qquad \text{(for solid phase)}$$

$$\beta_2 \geq \frac{1}{2}\left(\frac{1}{2} + \beta_1\right)^2 \qquad \text{(for solid phase)} \tag{3.6}$$

$$\bar{\beta}_2 \geq \frac{1}{2} \qquad \text{(for fluid phase)}$$

As it is clear from the above expressions that the minimum values for the Newton Raphson parameters are 0.5. However, in the absence of any material damping during the loading, the value of 0.5 for the above parameters may cause numerical problems (e.g. unrealistic spikes in case of simulating seismic waves). Hence, in this case, more numerical damping should be introduced by increasing the values of the Newton Raphson parameters. If the

system has a physical damping (viscous or hysteretic), the minimum conditions will be adequate for the reasonable accuracy of the numerical predictions.

The soil systems, in general, produce damping (e.g. hysteretic damping) based on its plasticity level and the intensity of loading during the dynamic excitation. Once the soil behaviour is assumed as totally elastic at small strain levels (which is mostly the case in the advanced soil constitutive models (Hashash and Park, 2002)), no hysteretic damping will be in place, which may lead to unrealistic resonance behaviour. Hence, it is required to assign a system damping, named Rayleigh damping $[C]$, to dissipate the earthquake energy at low strain levels. In general, Rayleigh damping is computed by the following Equations 3.6 and 3.7 (Clough and Penzien, 2003).

$$[C] = \alpha_R[M] + \beta_R[K] \tag{3.7}$$

$$\begin{pmatrix} \alpha_R \\ \beta_R \end{pmatrix} = \frac{2D}{\omega_m + \omega_n} \begin{pmatrix} \omega_m \omega_n \\ 1 \end{pmatrix} \tag{3.8}$$

where, α_R and β_R parameters are associated indirectly with the f_m and f_n frequencies (hereby ω_m and ω_n are angular frequencies of f_m and f_n, respectively) within which viscous damping is lower than or equal to the target damping (D) ratio.

There are three different descriptions of Rayleigh damping: (1) simplified Rayleigh damping, (2) full Rayleigh damping and (3) extended Rayleigh damping (Figure 3.8). The first one considers only $[K]$ and hence requires the computation of β_R. The second one is proper consideration of $[M]$ and $[K]$, in which two Rayleigh damping parameters should be calculated based on f_m and f_n frequencies. The last one is the extension of the full Rayleigh damping. In addition to the two frequencies mentioned above, it requires two more frequencies of the higher modes of the soil deposit.

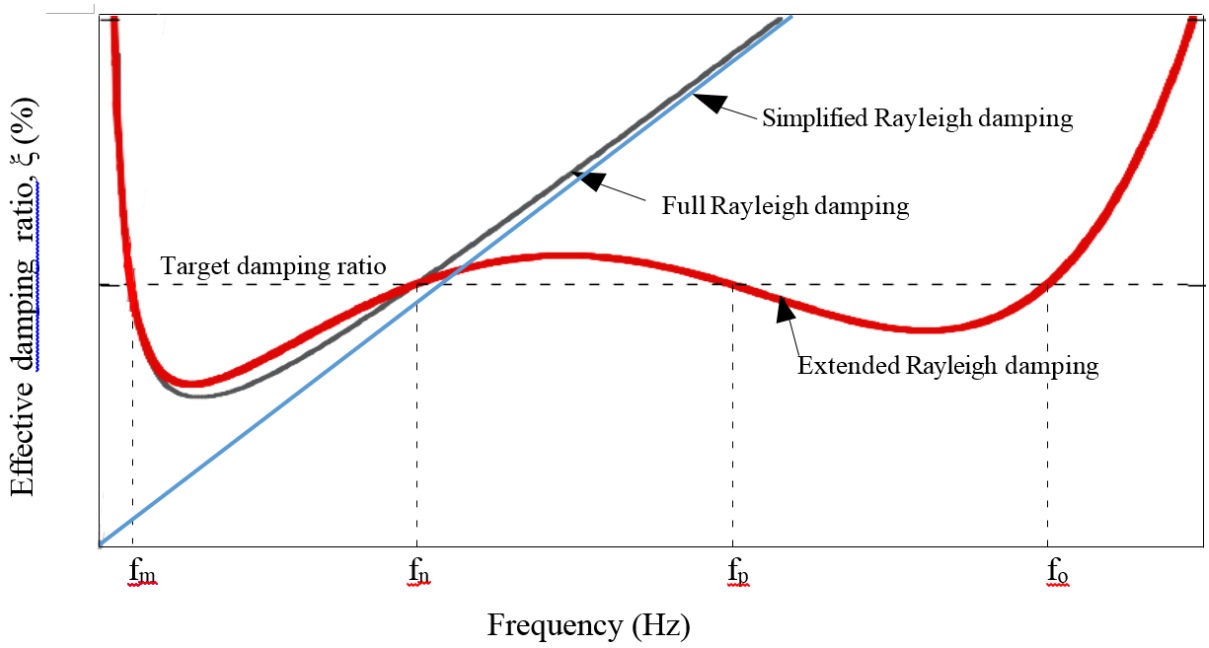

Figure 3.7 Effective damping curves from Simplified, Full and Extended Rayleigh damping formulations, after Park and Hashash (2004).

There are different approaches in defining the f_m and f_n frequencies. One approach suggests to use the fundamental period of the soil column (f_s) for f_m and for f_n to use the fundamental period of the input motion (Hudson *et al.*, 1994). Another approach suggests to take the frequencies of several modes of the soil deposit that lead to a site response from a linear time domain analysis showing good match with a response from a frequency domain analysis (Park and Hashash, 2004). In this approach, it is necessary to iterate linear time domain site response analysis to determine the modes of the soil deposit giving a reasonable response. Alternatively, if one does not want to perform an iterative process to define f_n, 5 times of f_m (which is regarded as equal to f_s) can be adequate to represent the full Rayleigh damping of the soil system in the linear phase (Stewart and Kwok, 2008).

3.6 Developments of Soil Models

The early critical state soil models (Cam Clay model by Roscoe (1963) and subsequently the Modified Cam Clay model by Roscoe and Burland (1968)) are based on the assumption that the soil behaves an elastic manner inside the bounding surface and starts yielding when the stress path touches the surface. The development of soil plasticity and the evolution of the yield surface are described with respect to the flow and hardening rules, respectively. These

functions allow the models to predict the actual response of the soil under different loading conditions.

These early soil models have some obvious limitations. For instance, defining the soil behaviour inside the bounding surface as an elastic response becomes a subject of much research. The sharp decrease of the soil stiffness, when the yield surface is reached, a sudden introduction of plasticity is recognised to be not a reasonable approximation. Moreover, in loading-unloading cases, such as in seismic loading, the soil exhibits only elastic strains, within the bounding surface, and constant excess pore water pressure is predicted. This does not reflect the real soil behaviour under such condition, since the soil is expected to exhibit early irreversibility and continuous change of pore water pressure.

The soil behaviour is often assumed isotropic in the soil models mentioned above since the soil at different initial stress conditions develops the same shapes with proportional extensions in the mean effective stress and deviatoric stress (p'-q) space when it is yielded. However, real soil behaviour shows that the soil loses its strength gradually when the stress moves from the elastic region to the plastic region. Moreover, irrecoverable deformations begin inside the yield surface that produce hysteretic damping, dissipating the energy in the cyclic loading. Natural soils are also shown to be anisotropic, due to loading history and different consolidation in three-dimensional space, as the yield loci are centred on the failure line with elliptical shapes (Panayides, 2014). Because of these deficiencies in the early developed soil models in predicting the real soil behaviour under such loading conditions, new soil models are developed.

In order to consider the early stiffness degradation, accumulation of the pore water pressure and the development of hysteretic damping within the yield surface, new soil models are formulated with the introduction of a small inner yield surface (also called "bubble"). The bubble yield surface separates the elastic region from plastic region within the outer surface so that early irreversibility is taken into account, expressing the stiffness reduction with respect to irrecoverable deformation. Furthermore, the soil mechanism that dissipates the energy in the cyclic loading is also activated by the introduction of the bubble producing hysteretic loops. These are called kinematic hardening models due to the movement of the inner yield surface towards the outer surface during loading. Two surface models (Mroz *et al.*, 1979), kinematic hardening models (Hashiguchi, 1985, 1989) (Hashiguchi, 1989) and

bubble models (Al-Tabbaa and Wood, 1989) are, among others, extension of Cam Clay model.

Besides these developments in predicting soil behaviour under different loading conditions, it is observed that the natural clays exhibit different behaviour from their reconstituted or structureless forms. Natural clays are in structured states due to the interparticle bonding or cementation, thus, have higher strength compared to the same remoulded clays (Burland, 1990). However, the soil structure collapses during loading and the soil follows the reconstituted response pattern when it loses all its structure. In this respect, the progress of the structure loss during loading (or the soil destructuration towards the intact form) is also accounted for in the advanced soil constitutive models such as *S3-SKH* model (Baudet and Stallebrass, 2004), *MSS* model (Kavvadas and Amorosi, 2000) and *RMW* model (Rouainia and Muir Wood, 2000).

3.6.1 An advanced kinematic hardening model (RMW)

The mathematical formulation of the *RMW* model (Rouainia and Muir Wood, 2000) in the general stress space is summarised here. The explanations for the notations are given at the end of the current chapter. Since the model describes the response of the soil skeleton, all stresses are effective stresses (the primes have been dropped for simplicity). The expression of the reference surface is:

$$f_r = \frac{3}{2M_\theta^2}\boldsymbol{s}:\boldsymbol{s} + \left(p - p_c\right)^2 - \left(p_c\right)^2 = 0 \tag{3.9}$$

The bubble surface is written as:

$$f_b = \frac{3}{2M_\theta^2}\left(\boldsymbol{s} - \boldsymbol{s}_{\bar{\alpha}}\right):\left(\boldsymbol{s} - \boldsymbol{s}_{\bar{\alpha}}\right) + \left(p - p_{\bar{\alpha}}\right)^2 - \left(Rp_c\right)^2 = 0 \tag{3.10}$$

The structure surface is given by:

$$F = \frac{3}{2M_\theta^2}\left[\boldsymbol{s} - \left(r-1\right)\boldsymbol{\eta}_0 p_c\right]:\left[\boldsymbol{s} - \left(r-1\right)\boldsymbol{\eta}_0 p_c\right] + \left(p - rp_c\right)^2 - \left(rp_c\right)^2 = 0 \tag{3.11}$$

where p_c is the effective stress defining the size of the reference surface, R is the size of the bubble. M_θ is a dimensionless scaling function for deviatoric variation of the critical state stress ratio, $\boldsymbol{\eta}_0$ a deviatoric tensor controlling the structure, r is the ratio of the sizes of the structure and the reference surfaces, p and $\boldsymbol{s}$ are the mean pressure and deviatoric stress tensor and the symbol ':' indicates a summation of products. The dots over symbols indicate an infinitesimal increment of the corresponding quantity, whereas bold-face symbols indicate tensors.

The scalar variable r, which is a monotonically decreasing function of both plastic volumetric and shear strain, represents the progressive degradation of the material as follows:

$$\dot{r} = -\frac{k}{(\lambda^* - \kappa^*)}(r-1)\dot{\varepsilon}_d \tag{3.12}$$

where λ^* and κ^* are the slopes of normal compression and swelling lines in the ln$v$: ln$p$ compression plane (v being the soil specific volume) and k is a parameter which controls the structure degradation with strain. The rate of the destructuration strain $\dot{\varepsilon}_d$ is assumed to have the following form:

$$\dot{\varepsilon}_d = \left[(1-A^*)\left(\dot{\varepsilon}_v^p\right)^2 + A\left(\dot{\varepsilon}_q^p\right)^2\right]^{1/2} \tag{3.13}$$

where A^* is a non-dimensional scaling parameter and $\dot{\varepsilon}_q^p$ and $\dot{\varepsilon}_v^p$ are the plastic shear and volumetric strain rate, respectively.

Volumetric hardening rule is adopted in the model, where the change in size of the reference surface, p_c, is controlled only by plastic volumetric strain rate, $\dot{\varepsilon}_v^p$, given by:

$$\frac{\dot{p}}{p_c} = -\frac{\dot{\varepsilon}_v^p}{(\lambda^* - \kappa^*)} \tag{3.14}$$

If a stress increment requires movement of the bubble relative to the structure surface, the following kinematic hardening is invoked:

$$\overline{\boldsymbol{a}} = \dot{\hat{\boldsymbol{a}}} + \frac{\dot{p}}{p_c}(\overline{\boldsymbol{a}} - \hat{\boldsymbol{a}}) + \dot{\mu}(\boldsymbol{\sigma}_c - \boldsymbol{\sigma}) \tag{3.15}$$

where $\overline{\boldsymbol{a}}$ and $\hat{\boldsymbol{a}} = p_c[r\boldsymbol{I} + (r-1)\eta_0]$ denote the locations of the centre of the bubble and structure surface respectively, $\boldsymbol{\sigma}_c$ is the conjugate stress and μ is a positive scalar of proportionality. It should be noted that the centre of the structure surface and the deviator of $\hat{\boldsymbol{a}}$ represents the anisotropy of the soil due to structure. The deviator of $\hat{\boldsymbol{a}}$ therefore degrades to zero as r degrades to unity.

The plastic modulus *H* is assumed to depend on the distance between the current stress and the conjugate stress and is given by:

$$H = H_c + \frac{Bp_c^3}{(\lambda^* - \kappa^*)R}\left(\frac{b}{b_{max}}\right)^{\psi} \tag{3.16}$$

where H_c is the plastic modulus at the conjugate stress, *B* and ψ are two additional material properties, $b = \overline{\boldsymbol{n}}:(\boldsymbol{\sigma}_c - \boldsymbol{\sigma})$ is the normalised distance between the bubble and the structure surface and $b_{max} = 2(r/R - 1)\overline{\boldsymbol{n}}:(\boldsymbol{\sigma} - \overline{\boldsymbol{a}})$ is its maximum value.

Finally, the bulk and shear moduli, *K* and *G*, are assumed to depend linearly on the mean effective pressure *p*:

$$K = \frac{p}{\kappa^*}$$
$$G = \frac{3(1-2v)}{2(1+v)}K \tag{3.17}$$

where v is a constant Poisson's ratio.

RMW model is a kinematic hardening model for structured soils which introduces three yield surfaces with the same elliptical shape in the p-q plane and is an extension of the bubble model. The model describes the soil behaviours with the bubble, the structure and the reference yield surfaces. The bubble yield surface enables the smooth transition of the soil

from elastic phase to plastic phase and acts within the structure surface with the current stress with respect to the kinematic hardening rule. The structure surface is the representation of the degree of the soil structure and its anisotropy. The reference surface shows the original yield surface before the soil is structured. When the soil yields, the structure surface starts contracting towards the reference surface as the soil structure gradually collapses.

The size of the reference surface (p_c), the position of the current stress (centre of the bubble surface), the degree of the initial structure (r_o) and the soil anisotropy (η_o) should be known to define the initial yield surfaces. The model uses two elastic parameters (as used in the original Cam Clay model): κ^*, the slope of the swelling line in the lnv : lnp plane (logarithmic volume – logarithmic mean stress compression plane) and υ, Poisson's ratio. The plastic behaviour of the soil is described by λ^*, the slope of the compression line in the lnv : lnp plane, M, the slope of the critical state line and m, governing the ratio of radii of the surfaces in the deviatoric plane.

The size of the bubble is assigned with a parameter R being a ratio between the bubble and the reference surfaces. Two more parameters associated with bubble that play an important role in the hardening behaviour of the soil are stiffness interpolation parameter, B, and stiffness interpolation exponent, ψ. Increasing B, or reducing ψ, results in increase in the plastic hardening modulus and reduction in the plastic strains. The collapse of the structure surface towards the reference surface is governed by a rate of destructuration with strain, k, and distribution of volumetric and distortional destructuration represented by A. The bigger the k, the faster the destructuration happens. When the destructuration is totally volumetric, A equals to 0 and it equals to 1 if the destructuration is fully distortional.

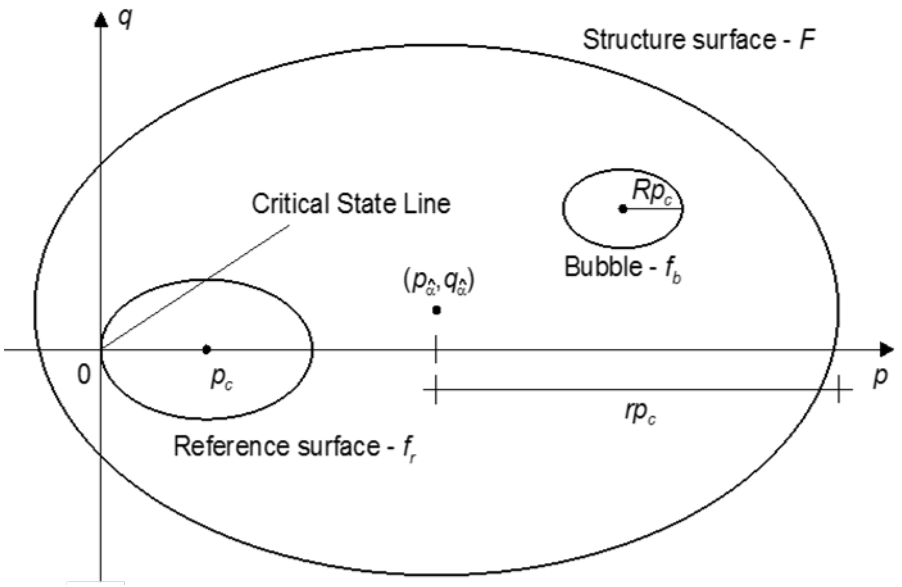

Figure 3.8 Three yield surfaces and the associated parameters described by the *RMW* model.

3.7 Earthquake Selection Strategies Applied in Geotechnical Research

The propagation of seismic waves through soil layers may be exposed to the change in the engineering characteristics of the soil that may lead to some alteration in the characteristics of a ground motion, such as energy contents, peaks and fundamental frequency. Site response analysis is an efficient tool to simulate such interaction between the soil and seismic motions, and requires a series of input motions to consider the uncertainty of a potential earthquake event. The first step in selecting input motions is to define a target response spectrum that may be from design response spectrum or from DSHA or PSHA of a site (which is explained in the first part of this chapter). Accordingly, the bedrock input motions are selected and modified with respect to a specific selection strategy. In this respect, earthquake selection/scaling strategies to be considered is crucial since different selection strategies may result in different site responses at the ground surface.

An earthquake selection strategy developed by Kottke and Rathje (2008) has recently been studied by Rathje *et al.* (2010) by simulating equivalent linear site response analysis in a time domain program called Strata (Kottke and Rathje, 2009). The strategy relies on selecting and scaling of a set of input motions such that the root-mean-square error (RMSE) between the target response spectrum. The median of the scaled input motions is kept at minimum level in the log space. The method does not only minimize RMSE but also it considers the level of standard deviation of the set of input motions. Five groups of 5, 10 and

20 input motions are formed to study the influence of the number of selected and scaled input motions in RMSE and in the level of standard deviation of spectral responses between groups. It is observed that increasing the number of input motions reduces the value of RMSE and the standard deviation of spectral values between groups of input motions. Therefore, it is suggested to select at least 10, or more, input motions in order to obtain stable response at the ground surface from the site response analyses.

The effects of the earthquake selection and scaling strategies on the free-field site response analysis has been studied by Tönük *et al.* (2014). The parametric study uses two numerical codes; Shake91 (Idriss and Sun, 1992) and DeepSoil (Hashash, 2012). It is believed that the quantity of earthquake records can be as many as possible when the seismic hazard condition of a site, as fault mechanism, earthquake magnitude range and source-to-site distance, is carefully taken into consideration in the earthquake selection. 18 input motions recorded on stiff site conditions having shear wave velocity greater than 660 m/s are selected and are subjected to following scaling strategies: (1) PGA scaling, (2) mean spectrum fitting and (3) spectrum scaling. The results indicate that site response spectrum can significantly be influenced by scaling strategies within which mean spectrum fitting is found to give the greatest spectral responses while the PGA scaling causes very similar response spectrum. The spectrum scaling leads to the lowest spectral values comparing with the responses from other selection strategies. Finally, it is recommended to use the scaling strategy that gives the mean spectrum showing the best agreement with the target response spectrum without modifying the frequency content of input motions.

More scaling strategies are implemented in the performance assessment of the soil-structure interacting system of a basement wall (Amirzehni *et al.*, 2015). A number of nonlinear two-dimensional finite difference analyses of basement wall is modelled in FLAC2D (Itasca, 2012). In addition to the spectrally matching method modifying frequency content of the input motions, five linearly scaling methods are studied. These are:

1. PGA Scaling
2. Sa(T_1) Scaling
3. ASCE Scaling
4. Sla Scaling

5. MSE (Mean Squared Error) Scaling.

The performance evaluation of the basement wall is done based on the maximum drift ratio over the wall. The less scatter in the results is observed within the set of earthquake motions when spectral scaling is implemented but extreme scatter and high drift response are observed when PGA scaling is considered. This implies that the spectral scaling is a better scaling option although some doubts over its suitability are raised, since the frequency content of the motion is modified.

While different earthquake selection strategies from the literature are presented in this section, the intention of all is to recognise the best one that leads to a stable response prediction with a minimum number of site response analyses. Considering a set of input motions allows to take into account the uncertainty of a probable earthquake event (i.e. input motion) in the site response analyses. Other two important inputs of site response analyses, which can introduce uncertainty into the response prediction, are shear wave velocity and modulus reduction and damping curves of the soil. In the following section, the findings of past studies dealing with these soil variables in the site response analyses are presented.

3.8 Variability of Soil Properties

A site response analysis can be subjected to three main sources of uncertainty: (1) input motions, (2) shear wave velocity (V_s) and (3) modulus reduction (G/G_o) and damping (D) curves. In the previous section, the methods of dealing with the uncertainty induced by input motions are explained by giving specific attention to the earthquake selection strategies. In this section, four studies, which aim to quantify the uncertainties of V_s and G/G_o and D curves and their impact on the site responses (i.e. spectral response and site amplification predictions), are demonstrated.

3.8.1 Study of Kwok et al. (2008)

The study of Kwok et al. (2008) investigates the influence of variability of V_s profile and G/G_o and D curves. Different programs are employed to study the effect of model-to-model variability. A series of equivalent linear and nonlinear site response analyses are conducted. They consider the site response of the 28 September 2004 Parkfield earthquake with magnitude 6 recorded at the Turkey Flat vertical array site in California.

There are variety of measured V_s profiles at the site with a coefficient of variation of 0.2. The variability of V_s profile is generated in site response analyses by using the first order second moment (FOSM) method (Robert, 1999) which uses profiles of mean and mean +/- $\sqrt{3}$ standard deviations. The statistical model of Darendeli (2001) is implemented to compute the mean and variation of G/G_o and D curves for the site. FOSM method is used to vary the G/G_o and D curves in the site response analyses. Model-to-model variability is studied by using six different programs with mean V_s profile and G/G_o and D curves: SHAKE04 (Youngs, 2004), D_MOD_2 (Matasovic, 2006), DEEPSOIL (Hashash and Park 2001;2002; Park and Hashash, 2004), TESS (Pyke, 2000), OpenSees (McKenna and Fences, 2001) and SUMDES (Li et al., 1992).

The results indicate that the variability of V_s profile appears to be causing a great uncertainty to the site amplification leading to the greatest standard deviations, especially at periods less than the fundamental period of the site. Model-to-model variability is a second source of variability followed by the variability of G/G_o and D curves controlling the uncertainty in the site responses at the surface.

3.8.2 Study of Li and Assimaki (2010)

Li and Assimaki (2010) investigate the influence of variability of V_s profile and G/G_o and D curves on the site response predictions at the ground surface. One-dimensional nonlinear site response analyses are conducted by modelling three downhole array sites in the Los Angeles Basin; La Cienega, Meloland and Obregon Park. The analyses are operated by using "in-house" nonlinear code, which is only available within the university where the code is developed. The code uses a hysteretic scheme developed by the same authors based on the model suggested by Muravskii (2005). It has a capacity to achieve simultaneous convergence of modulus reduction and damping curves in the medium and high strain levels ($> 10^{-3}$). V_s profile and G/G_o and D curves are randomized by using statistical models developed by Toro (1995) and Darendeli (2001), respectively.

Firstly, one weak and one strong synthetic input motion from the earthquake dataset produced by Assimaki *et al*. (2008) are adopted to investigate the sensitivity of impact of variability of soil properties on the site response predictions to the seismic intensity level. Only one soil property is randomized (e.g. V_s profile or G/G_o and D curves) through the MCSs. The mean value of the other soil property is used for the purpose of distinguishing

the influence of the individual soil properties on the site response predictions. Both soil properties are also varied simultaneously. Then, a large number of synthetic input motions are used to study the effect of the variability to the soil conditions (e.g. softer and stiffer soil conditions) and seismic intensity.

The results, represented in terms of spectral accelerations and its logarithmic standard deviations over an engineering period of interest, indicate that a scatter in the response predictions at the surface can be dependent on the variability of both elastic and nonlinear soil properties (i.e. V_s profile and G/G_o and D curves, respectively) when the strong input motion is applied. In case of simulating the weak input motion, only the variability of V_s profile controls the variability in the response prediction. The results also demonstrate that the effect of variability of nonlinear soil properties is more pronounced in the softer soil sites (La Cienega and Meloland). Moreover, the findings from the stiffer site (Obregon Park), where the influence of variability of V_s profile is relatively greater comparing with the other sites, point out the impact of the stiffness contrast at the top 20 m influencing the amount of seismic energy refracted and reflected.

3.8.3 Study of Rathje et al. *(2010)*

Rathje *et al.* (2010) studies the influence of variability of V_s profile and G/G_o and D curves on the median site response, site amplification and its standard deviation. The uncertainty sourcing from input motions is also studied by selecting and scaling 5, 10 and 20 input motions (as explained in Section 3.3.5). One-dimensional equivalent linear site response analyses are simulated using the program STRATA (Kottke and Rathje, 2009) and modelling a deep alluvium site characterized when studying the Sylmar Country Hospital (SCH) in Southern California (Chang, 1996). The program has built-in function of varying the V_s profile and G/G_o and D curves. The statistical models given by Toro (1995) and Darendeli (2001) for randomizing the elastic and nonlinear soil properties are embedded into the program. This feature allows conducting equivalent linear MCSs. It is also capable of using input motions in time series or a response spectrum. If a response spectrum is a form of input, random vibration theory (Rathje and Ozbey, 2006) is utilized.

From initial results, it is recognised that 10 input motions scaled by RMSE method can be sufficient to obtain a stable median response at ground surface. Along with this finding, 60 realisations for each soil property is generated. The input motions are scaled to the peak

ground acceleration of 0.35g aiming to expose more soil nonlinearity. In total, 600 equivalent linear analyses are conducted for each median response presented. It is found that inclusion of variability of V_s profile or G/G_o and D curves or both at the same time leads to predictions of less spectral responses and amplification factors comparing with the baseline responses (which is obtained by using baseline V_s profile and G/G_o and D curves). However, the level of standard deviation reduces for spectral response and increases with amplification factors. Increasing the level of truncation (e.g. +/- two or three standard deviations) around the baseline V_s profile causes further reduction and further scatter in the response predictions. Increasing the interlayer correlation (i.e. the spatial variability statistics) has similar effects. Although it is believed that inclusion of variability of soil property should produce higher spectral responses, the results do not clearly manifest that. Hence, it is suggested to reconsider the procedures used to include the variability of soil property in site response analyses.

3.8.4 Study of Barani et al. *(2013)*

Barani *et al.* (2013) study the influence of variability (or uncertainties) of seismic input motions, soil modelling (i.e. soil depth to model), unit weight, V_s profile and G/G_o and D curves on site responses. Specific site responses investigated are frequency-independent site amplification factor and site amplification function, fundamental frequency of site and spectral accelerations. Two sites located over the alluvial terrace of the Serchio River in northern Tuscany, Italy, are studied. One site sits over a shallow bedrock with depth of 23 m. For the second site, bedrock level is below the top 30 m according to the geophysical and geotechnical investigations.

The study deals with the above uncertainties based on the Monte Carlo approach using Shake91 (Schnabel et al., 1972; Idriss and Sun, 1992) that relies on an equivalent linear approximation of soil nonlinearity. 20 bedrock input motions representing the seismic hazard level of the sites are used in scaled and unscaled forms to investigate their influences on the site responses. RMSE method is used to scale the input motions to the 0.19g 5% damped target design response spectrum with the mean return period of 475 years. Two main soil models are employed to investigate the model-to-model variability. Geometric uncertainty is also studied by varying the thickness of the soil models based on normal distribution. Finally, unit weight, V_s profile and G/G_o and D curves of soil properties are randomized.

Unit weight and V_S are assumed to be lognormally distributed based on their means and standard deviations from the field and laboratory tests. G/G_o and D curves are varied with respect to randomizing the value of shear strain at 64% of the shear modulus ratio (G/G_o), $\varepsilon_{64\%}$ (Bazzurro and Cornell, 2004). This randomization is also carried out based on lognormal distribution.

The results based on the record-to-record variability and the model-to-model variability indicate that the uncertainty in the amplification functions is caused, to a great extent, by the uncertainty in the soil models and, to a less extent, by the uncertainty in the input motions. However, this is not valid for the spectral responses at the surface which are greatly influenced by the intensity of input motions. The results based on the randomization of the remaining soil parameters (each randomized separately by using a single soil model) reflect that the variability of V_S profile is a dominant factor affecting the variability of soil amplification parameters and spectral responses. It is followed by the variability of soil thickness influencing the site responses. On the contrary, variability of unit weight or G/G_o and D curves has inconsiderable impact on the uncertainty in the results. This is assumed to be the result of the seismic intensity level, not leading to extreme soil nonlinearity, especially in case of G/G_o and D curves. It is, therefore, anticipated that the variability of G/G_o and D curves will be one of the major factors controlling the uncertainty in the site responses under strong input motions.

3.9 Conclusions

The key component that links the seismic hazard with structural damage in a seismic risk assessment of a site is known to be the input motion selection. The crucial step in the input motion selection is the determination of the target response spectrum, which can be based on PSHA or code compliant response spectrum and an IM that reflects the structural response as well as seismic intensity. In the absence of PSHA (in other word, UHS), a standard design response spectrum given by the seismic design codes can be employed in the input motion selection.

This chapter shows the different methods that can be used to determine a target response spectrum and an IM in advance of selecting input motions and the inclusions of some earthquake characteristics (M, R and ε) in the input motion selection studied by structural communities. Moreover, the legitimacy of down and up scaling with respect to the target

response spectrum, consideration of two IMs and the consistency with the use of Sa in seismic hazard analysis and performance analysis has been clearly demonstrated. Seismic design provisions also provide relatively clear input selection criteria to be followed for performance-based structural designs.

On the other hand, the focus in geotechnical engineering in the past decades is showed to be more on the modelling of soil behaviour under seismic oscillations. In this respect, suitable platforms with a simple frequency domain programs and time domain finite element codes are provided to simulate soil deposits under seismic motions with reasonable boundary conditions. Depending on the complexity of numerical code adopted, the actual site response can reasonably be predicted.

This chapter also specifically explains the philosophy of the fully-coupled finite element procedure, implemented in SWANDYNE II, emphasizing the dynamic equilibrium, boundary conditions and the damping considerations. Moreover, the features of the early developed soil models along with their drawbacks in representing soil behaviour and, thus, the need for more sophisticated soil model are briefly explained. Then, the development of the bubble models for clay soils, capturing early soil irreversibility, stiffness degradation and producing hysteretic damping is pointed out. Lastly, a kinematic hardening soil model (*RMW*), is described including its advanced characteristics such as introducing a reference surface for the remoulded state of the clay, a structure surface and a bubble surface with the associated model parameters.

Finally, several studies focusing on the input motion selection strategies for site response analyses are briefly presented. Moreover, two important factors or soil properties (i.e. shear wave velocity profile and shear modulus reduction and damping curves) influencing the site responses are discussed with reference to past studies. Based on these reviews, this research will further bring the input motion selection strategies into context of the free-field nonlinear analyses of soft soil deposits causing great amplification. It will also provide further insight into the influence of variability of soil properties on site responses at ground surface.

Chapter 4. Nonlinear Analyses of Lotung Down-hole Array Site

4.1 Introduction

Seismic waves can be subjected to modifications in their predominant acceleration, velocity and displacement, as well as frequency and energy contents during their propagation from the fault line to the earth surface. These shifts are mainly governed by the seismic waves produced at the fault point (fault effects), travelling process through the earth crust structures (path effects), and the vertical propagation within the horizontally layered soil deposits (local site effects) (Kramer, 2014). While the first two effects are in the interest of geologists, the last one is mainly dealt with by the geotechnical engineers.

The impact of local site conditions on the characteristics of seismic waves (usually called bedrock motions) depends on the elastic and dynamic soil properties. If the local site is described by firm material properties, bedrock motions can preserve most of their properties at surface. However, when the site consists of soft soil material, the surface motion will be totally different from the bedrock motion and will be characterised by the higher energy at lower frequencies. This phenomenon was observed in the 1985 Mexico City (Hall and Beck, 1986), 1989 Loma Prieta (Seed, 1990) and the recent Christchurch 2011 (Kaiser *et al.*, 2012) earthquake events.

To simulate the local site problems, site response analysis is generally used. The key factor in site response analysis is the approach used to represent the soil behaviour under dynamic conditions and, in particular, the numerical method (i.e. equivalent linear or nonlinear) coupled with the soil constitutive model employed for the analysis. In this regard, it is necessary to test the performance of the numerical approach adopted against real experimental data. While laboratory and in-situ tests can provide reliable and consistent information about the soil behaviour under different loading conditions, they can sometimes be doubtful because of well-known testing procedure limitations (e.g. soil sample extraction, representativeness of loading condition, etc.). However, down-hole array instruments can correctly measure the site response since the recording process is totally unmanned (Zeghal and Elgamal, 1994). Hence, the recorded earthquake data at array sites can readily be used by the researchers to evaluate the performance of the numerical approaches adopted for site response predictions.

In recent years, seismic array sites have gained great attention, in particular, in seismically active regions, as USA, Mexico, Taiwan and Japan (Elgamal *et al.*, 1995). In 1985, the Electric Power Research Institute (EPRI), Palo Alto, California, and the Taiwan Power Company (TPC), Taipei, Taiwan, have set up a Large-Scale Seismic Test (LSST) site in the Lotung (Taiwan) area, including two nuclear power plant containment structure models with 1/4 and 1/12 scales for soil structure interaction studies (Borja *et al.*, 1999a). The Lotung site was particularly chosen for the high-quality multidisciplinary earthquake data collection since it is located within a seismically active region and the soil deposit over the bedrock comprises of thick alluvial strata with varied depth from 200-600 meters, including recent alluvium layers at the top 40 to 50 meters (Glaser and Leeds, 1996). Within two years after the down-hole array installation, 18 earthquake events have been recorded, including moderate and strong input motions (Shen *et al.*, 1989).

The earthquake data recorded at Lotung at different depths have been used by many researchers to verify the capabilities and limits of the methods developed to define the dynamic characteristic of the soil layers and to predict the site response. In this respect, Elgamal *et al.* (1995) and (Zeghal *et al.*, 1995) developed a method able to predict the stiffness degradation and damping ratio values with respect to the shear stress-strain histories. The method also considered the influence of the accumulation of pore water pressures on the shear stiffness degradation and corresponding damping ratio curves during seismic excitations. It has been proved that the predicted shear moduli and damping ratio values were in reasonable good agreement with the resonant column and cyclic torsional shear test results conducted by EPRI, 1993, at the University of Texas, Austin.

One dimensional seismic wave propagation at the Lotung site have been studied by a number of researches since its instrumentation in 1985. As an example, Li *et al.* (1998) studied the seismic propagation at the site by using a fully-coupled finite element (FE) code, SUMDES (Li *et al.*, 1992), employing a bounding surface plasticity soil model. The code solves the problem in one dimension and considers the motion in three dimensions (vectored motion). Two input motions characterised by discrete shaking duration and waveform were simulated. Good predictions of the horizontal site response were achieved when the vertical response was underestimated by the code. Similarly, Borja *et al.* (2002) tested the performances of two numerical codes; well-known equivalent linear code, SHAKE (Schnabel *et al.*, 1972) and a nonlinear FE code, SPECTRA (Borja *et al.*, 1999a), enabling to apply the motion in three dimensions. The FE code still relies on total stresses and uses a bounding surface plastic

soil model. Again, two earthquake events with different characteristics were used. Both numerical codes predicted the horizontal and vertical site responses reasonably well.

Very recently, Amorosi *et al.* (2016) studied the multi-directionality effects on the site response at Lotung. They performed 3D nonlinear site response analysis using a full-coupled effective stress FE code, PLAXIS (Brinkgreve *et al.*, 2013) and employing an advanced kinematic hardening soil model. They simulated two earthquake events having different characteristics. The horizontal input motions were applied individually and simultaneously. Fairly good agreement with the actual data was obtained when a single horizontal input motion was simulated. In case of applying two horizontal input motions, the site response is overestimated and unrealistic spurious spikes were produced. Overall, when these works with the above mentioned numerical codes and soil models predicted the free-field site response reasonably well, especially with the nonlinear codes, the need of more sophisticated numerical codes coupling with advanced soil models are evidently emphasised and the benefit of the array site data in the performance evaluation of such numerical schemes is greatly appreciated.

In this study a fully-coupled finite element code, SWANDYNE II, with an advanced soil constitutive model (Rouainia and Muir Wood, 2000) is employed and its capability to predict the free-field ground response at Lotung is examined. One weak and one strong input motion recorded on site will be considered. The site will also be analysed using a simple frequency domain visco-elastic code (EERA) for comparison purposes. Firstly, the general information about the site and its instrumentations will be presented. Following that, the characteristics of the seismic input motions applied at the bottom of the soil models will be given. Furthermore, the linear and nonlinear numerical models will be described, including the soil model calibration. Subsequently, the numerical predictions will be presented in terms of acceleration-time histories and site response spectra and compared with the corresponding array data. Finally, some general conclusions will be drawn.

4.2 Description of the Lotung Down-hole Array Site

The Lotung geotechnical array site is located in the north-east part of Taiwan, as seen in Figure 4.1 (Borja *et al.*, 2002). The two 1/4 and 1/12 scaled nuclear power plant containment structures were constructed by Electric Power Research Institute (EPRI) and Taiwan Power Company (TPC) for soil-structure interaction studies. Around the 1/4 scaled model structure, surface accelerometers were deployed over three armed shapes together with two down-hole array instrumentations (shown as DHA and DHB in Figure 4.2).

The three components down-hole accelerometers recording the earthquake data in the east-west (E-W), north-south (N-S) and up-down (U-D) directions were located in the DHA and DHB down-hole arrays at surface and 6 m, 11 m, 17 m and 47 m depths below the ground level. Since the DHA down-hole array was instrumented at a distance of 3.2 m from the edge of the 1/4 scaled structure model, it is likely that the earthquake data recorded along this array are influenced by soil-structure interaction (Borja *et al.*, 1999b). For this reason, the earthquake data obtained from the DHB down-hole array are considered here for free-field site response analyses.

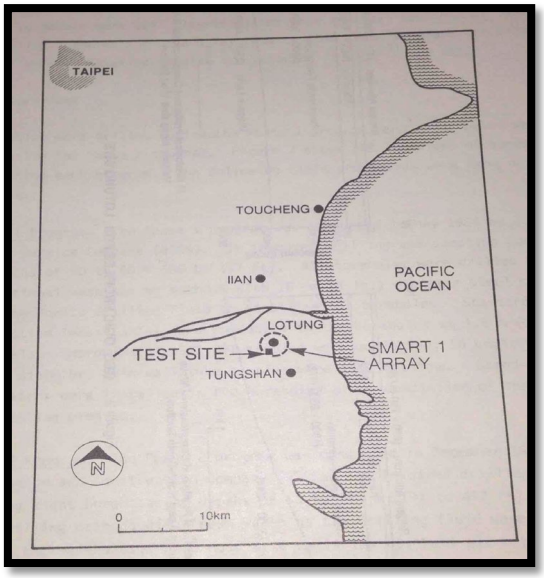

Figure 4.1 Location of the Lotung test site in Taipei, Taiwan (from Anderson and Tang, 1989).

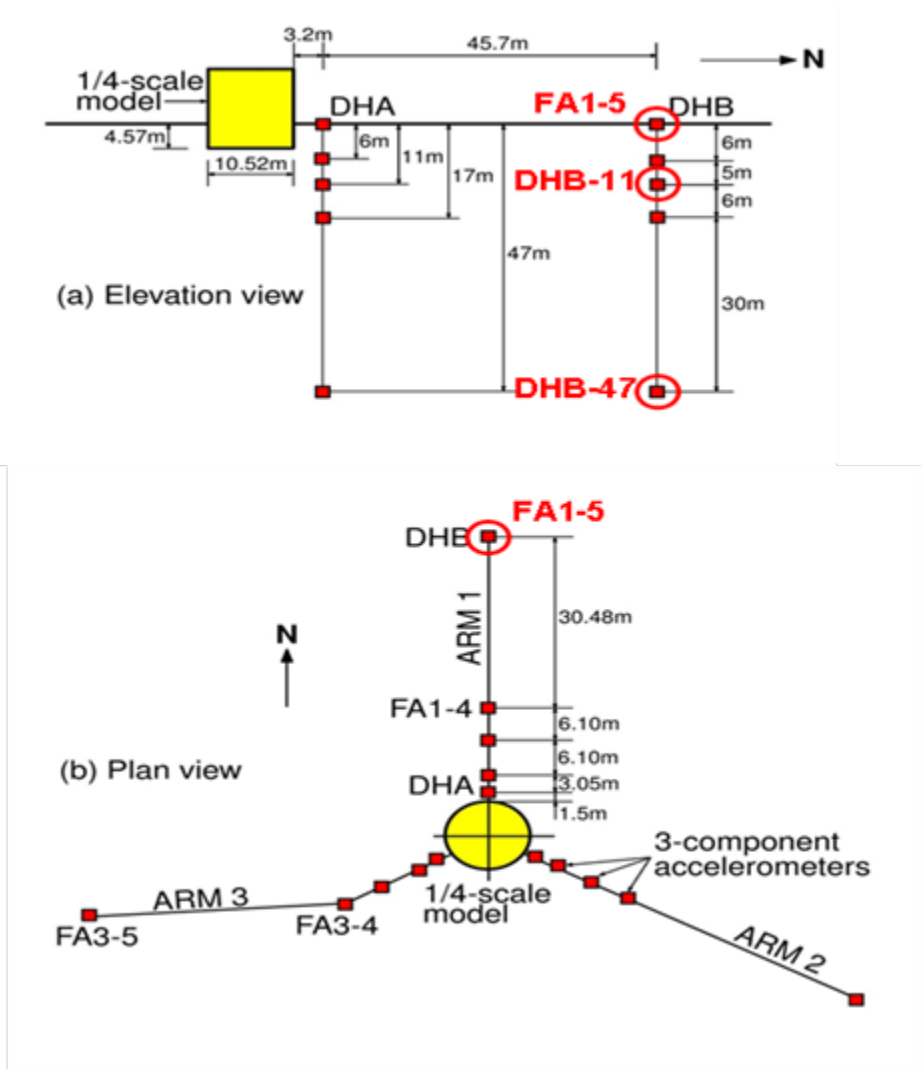

Figure 4.2 (a) Elevation view of the down-hole arrays including the scaled nuclear power plant containment structure and (b) plan view of the overall seismic instrumentations around the same structure model.

In addition to the deployments of surface and down-hole accelerometers, over 20 pore pressure sensors were installed in the late May 1986, within 3 m to 16 m depth, in order to measure pore pressure accumulations during the seismic excitations (Shen *et al.*, 1989). Site conditions and soil properties were determined by in-situ and laboratory tests (EPRI, 1993). Stiffness degradation and damping ratio curves from the laboratory tests conducted by EPRI, 1993, at different depths are shown in Figure 4.3. The laboratory test results clearly indicate that the soil showing a plastic behaviour from 10^{-3} - 10^{-2}% strain level. A small scatter in the test results in terms of stiffness degradation and damping ratio curves can clearly be seen, even though the soil samples were extracted from different depths. While the measured dynamic shear modulus values are positioned over the upper bound curve given for sands by

Seed and Idriss (1970), the measured damping ratio values fit fairly well between the mean and lower bound curves proposed by the same Authors.

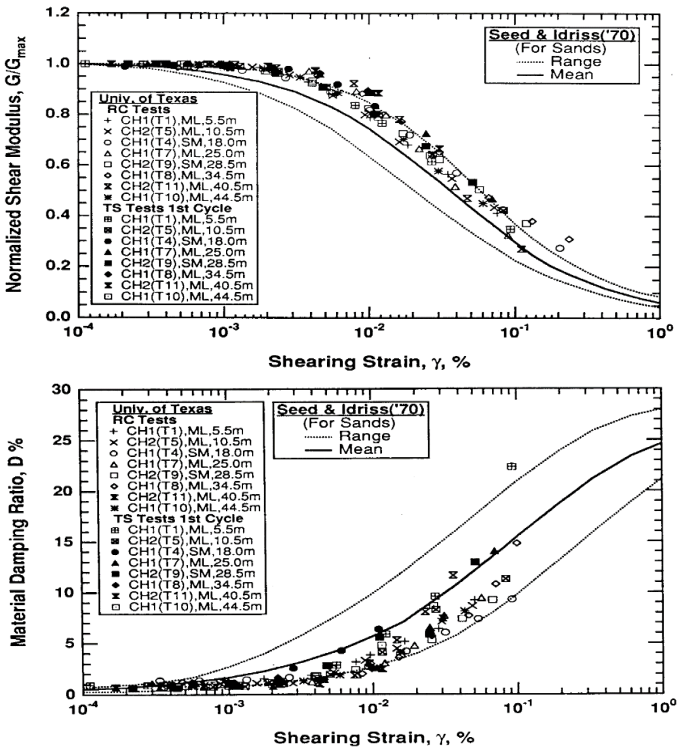

Figure 4.3 Resonant column (RC) and torsional shear tests results for intact silty sand (SM) and sandy silt samples from the LSST site (EPRI, 1993).

Alternatively, Zeghal *et al.* (1995) developed a method to back-calculate the shear modulus reduction and damping ratio curves as a function of shear strain amplitude by using free-field down-hole acceleration histories recorded at the Lotung site. They implemented this method for LSST7, LSST12 and LSST16 earthquake events recorded at the 6 m, 11 m and 17 m depths of the DHB array. The proposed back-figured nonlinear curves match well with those of Seed and Idriss (1970) for sand, too. These back-calculated nonlinear curves are used to calibrate the parameters of the adopted soil constitutive model which will be shown in Section 6 of the present chapter.

4.3 The Soil Properties of the Lotung Down-hole Array Site

The top 47 m of the soil deposit consists of silty clay and gravel with sand layers. The soil layers at the top 17 m were well characterized in terms of elastic and dynamic soil properties (e.g. shear wave velocity (V_s), compression wave velocity (V_p), initial shear stiffness (G_0), Poisson's ratio, stiffness degradation and damping ratio curves) from in-situ and laboratory tests as well as from the empirical approaches (Zeghal *et al.*, 1995). The ground water level was assumed to be within 0.4 m or 0.5 m below the surface(Li *et al.*, 1998) (Schneider, 1993). The total unit weight was assumed to be equal to 19 kN/m^3 for the sandy/silty/clayey layers and 19.5 kN/m^3 for the gravelly layers (Borja *et al.*, 1999a). The average specific gravity of soil was calculated to be around 2.7. The general properties of the soil samples from different depths determined by using the laboratory tests by EPRI, 1993 are shown in Table 4.1.

LL = liquid limit, PI = plasticity index and e = void ratio

Depth (m)	Soil description	LL (%)	PI (%)	Water content	Total unit weight (kN/m^3)	e	Specific gravity	Degree of saturation (%)
5.5	Silt	-	-	31	17.9	0.93	2.65	88
10.5	Silt	-	-	32.5	18.9	0.85	2.65	100
18	Silty fine sand	-	-	33.3	17.5	1.02	2.65	87
28.5	Silty sand	-	-	31.2	19.1	0.82	2.65	100
34.5	Clayey silt	32	7	35.3	18.9	0.92	2.7	100
40.5	Clayey silt	33	8	31.1	18.8	0.89	2.7	95
44.5	silt	-	-	24	20.5	0.56	2.65	100

Table 4.1 General properties of the soil from the LSST site at different depths.

Another important elastic property of the soil is the coefficient of earth pressure at rest, K_0. The value of K_0 has impacts on the ground response of the soil deposit in two different aspects:

1. the initial stress state of the deposit is calculated based on the K_0 value and the maximum past vertical effective overburden pressure,
2. during the earthquake loading, the lateral total stress, σ_h, is subjected to change that also partially depends on the initial K_0 value (Li *et al.*, 1998).

During a cyclic loading condition, the soil is assumed to be subjected to the simple shear stress and zero lateral strains. If the initial K_0 value of the soil is less than 1, under a dynamic motion the K_0 value tends to reach a value of 1 (isotropic normal stress state) (Pyke, 1973; Youd and Croven, 1975). Such an increase in K_0 may result in the reduction of the deviatoric stress, thus increasing the liquefaction resistance. Furthermore, it causes increase of the pore water pressure depending on the increase in the total mean normal stress.

Previous earthquake events striking the site can affects the K_0 value of the soil deposit since in each event the soil elements are subjected to cyclic loadings (Li *et al.*, 1998). For this reason, the K_0 value for the soil in the LSST site can be greater than its original value. The work of Li *et al.* (1998), in this respect, proposes K_0 value for the site by using a trial-error method to obtain results in terms of pore water pressure such that they are in good agreement with the recorded data from the 14 November 1986 earthquake event (LSST16). It was found that considering K_0 close to 1 gives good results in terms of excess pore water pressure with time. They also suggest a value of 0.8 for the top 3 m because of its recent geological formation.

The Poisson's ratios (v) for the soil layers can be calculated from the value of K_0 or using the compression wave velocity and shear wave velocity profiles measured from up-hole seismic tests. By using V_p and V_s profiles, the lower v value calculated for the top 10 meters was found to be around 0.46 while the remaining layers were assumed to have a v value as high as 0.48 (Berger *et al.*, 1989).

4.4 Earthquake Data Recorded at the Lotung Down-hole Array Site

During the 1985 and 1986, the LSST site was subjected to 18 earthquake events including moderate and strong input motions. One weak (LSST11) and one strong (LSST7) earthquake events with magnitude 4.3 and 6.2, respectively, are selected to be applied at the bottom of the numerical soil models. General information regarding the earthquake events is provided in Table 4.2. The recordings of the earthquake events at the DHB down-hole array with record names FA1-5, DHB6, DHB11, DHB17 and DHB47 refer to the accelerations measured at surface, 6 m, 11 m, 17 m and 47 m depth, respectively. PGA values of the recorded input motions at associated depths are presented in Table 4.3.

Event	date	Magnitude, M_w	Epicentral distance (km)	Focal depth (km)
LSST11	17/7/1986	4.3	6.0	2.0
LSTT7	20/5/1986	6.5	66.0	15.8

Table 4.2 General information for the LSST11 and LSST7 earthquake event.

Locations/names of accelerometers		**FA1-5**	**DHB6**	**DHB11**	**DHB17**	**DHB47**
LSST11 PGA(g)	**E-W**	0.065	0.046	0.041	0.043	0.046
	N-S	0.104	0.068	0.064	0.058	0.062
	U-D	0.432	0.259	0.178	0.0.169	0.146
LSST7 PGA(g)	**E-W**	0.16	0.15	0.12	0.1	0.08
	N-S	0.21	0.14	0.11	0.09	0.1
	U-D	0.04	0.04	0.04	0.04	0.03

Table 4.3 Peak accelerations of the weak (LSST11) and strong (LSST7) earthquake events at different depths in East-West (E-W), North-South (N-S) and Vertical (U-D) directions.

Spectral accelerations of the recorded earthquake data at ground surface, 6 m, 11 m, 17 m and 47 m depth are reported in Figure 4.4. The figure shows that the strong input motion, having a higher focal depth and epicentral distance, is characterised by an energy content concentrated in the higher periods. In contrast, the weak input motion, striking the deposit from a shallow fault mechanism and a shorter epicentral distance, is characterised by a seismic energy at relatively low periods.

While the E-W component of the strong input motion is amplified regularly at around the first and second modes of the soil deposit, the N-S component of the same event shows a complex behaviour during its travelling path from the bedrock to the ground surface, which can be probably attributed to the different geological formation of the site in the E-W and N-S directions. The site, in fact, sits over a smooth layered Pleistocene formation in the E-W direction, as shown in Figure 4.5, but the same formation has some inclination in the N-S direction, thus leading to two substantially different seismic excitations in the E-W and N-S directions. In particular, the PGA of the E-W component of the earthquake event increases only 6% from 6 m to the ground surface, while 50% increase in the N-S component is observed at the same range of soil depth.

Figure 4.4 indicates the period shift (or energy shift of the input motion) of the spectral accelerations to the longer periods in both directions from bottom level to the ground surface. This can be attributed to the fact that the soil material characterised by higher shear modulus may not influence the characteristics of input motions, hence the effect of nonlinear soil behaviour cannot be clearly observed. However, when the input motion propagates through the soft soil layers, the spectral responses may show great amplification with a shift to the longer periods as observed in the LSST7 earthquake event. For both components of the weak input motion, several spectral peaks are observed as the motion is characterised by the energy at high frequencies, thus the influence of soil nonlinearity is expected to be very limited.

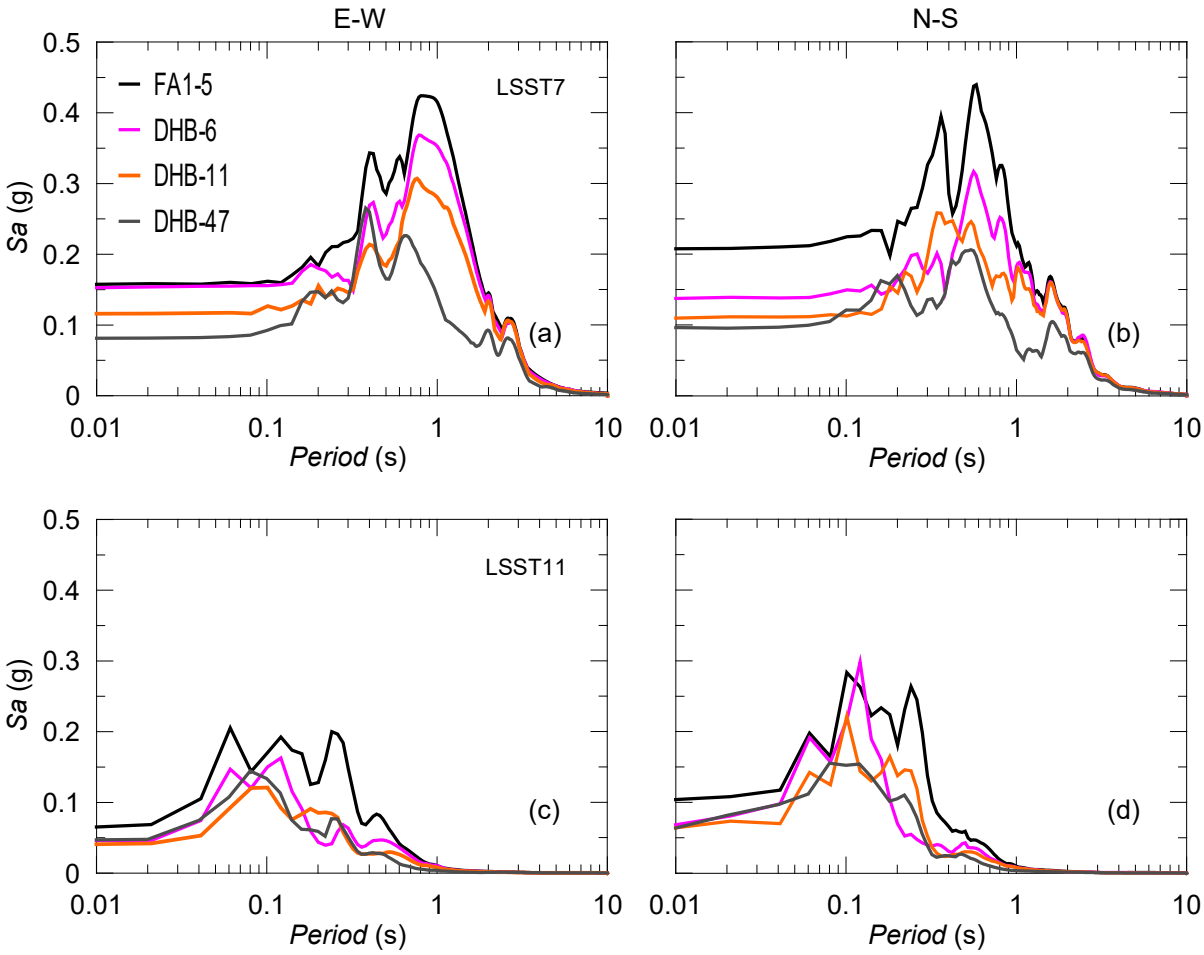

Figure 4.4 Recorded spectral acceleration, *Sa*, at different depths for the E-W and N-S components of the (a, b) LSST7 and (c, d) LSST11 earthquake events.

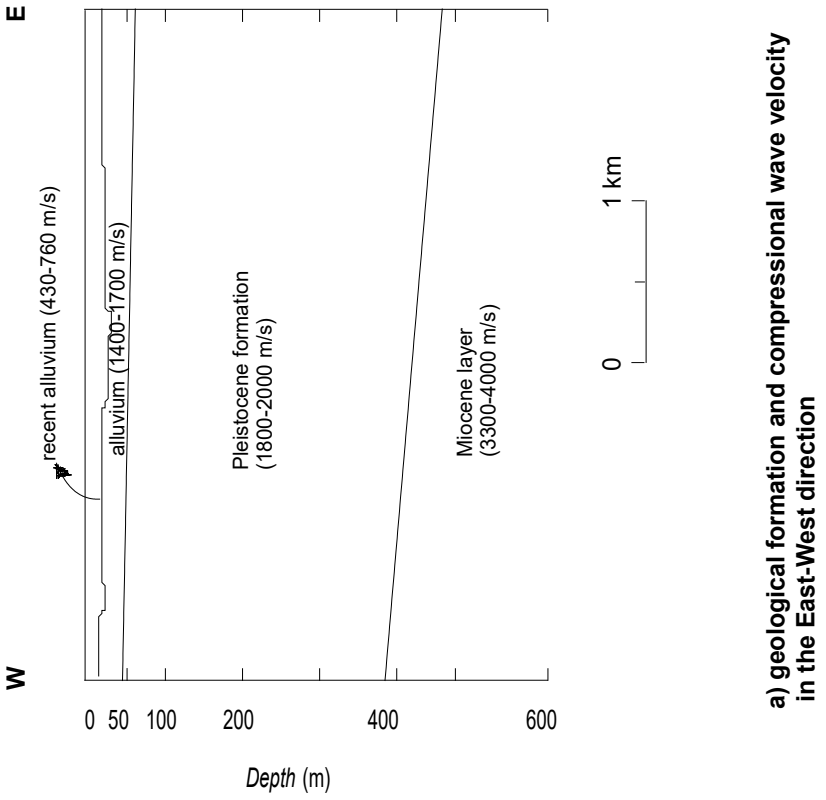

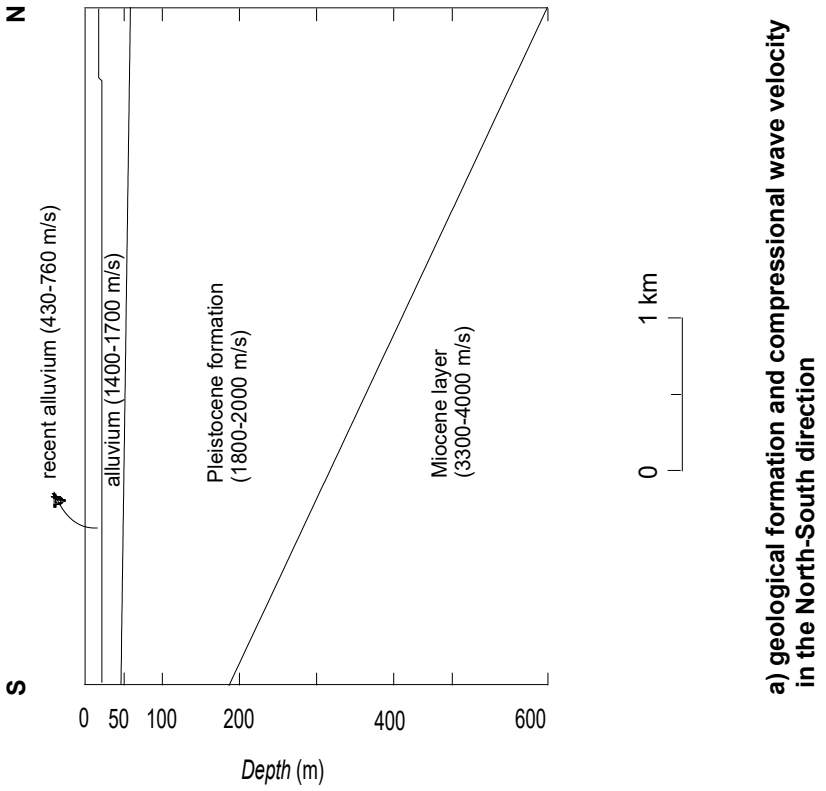

Figure 4.5 Geologic profile of the Lotung site (after Anderson and Tang, 1989)).

4.5 Numerical Modelling of the Lotung Down-hole Array Site

4.5.1 Equivalent linear visco-elastic model

The EERA code (Bardet *et al.*, 2000) represents the nonlinear soil behaviour via an equivalent linear approach. It uses the exact formulation of wave propagation in horizontally layered soil deposits subjected to vertically propagating transient motions (Roesset, 1977) and solves the problem in the frequency domain. The nonlinear shear modulus, G, and corresponding damping ratio, D, at a specific shear strain is obtained by means of an iterative procedure. The code assumes the G and D values are constant during the seismic oscillations within each soil layer. Because of this, it should be guaranteed that the number of iterations is sufficient to achieve a specified convergence at the induced shear strain in each soil layer.

The EERA analyses conducted in this study use the small-strain stiffness profile shown in Figure 4.6c. The profile is discretised into 1 m layers and a constant stiffness within each sub-strata is assigned. To achieve a rational comparison, the same stiffness degradation and damping ratio curves adopted in the nonlinear FE model are used in the EERA simulations.

4.5.2 Nonlinear FE model

To overcome the well-known deficiencies of the equivalent linear approach, nonlinear schemes solving the wave propagation problem by direct numerical integration in the time domain can be implemented. The code SWANDYNE II (Chan, 1995) used in this study is a fully-coupled finite element code solving the problem in the time domain and enabling to model the soil deposit in two or three-dimensional spaces. Linear or nonlinear dynamic analyses can be performed, using the Generalised Newmark method (Katona and Zienkiewicz, 1985) for time integration. In particular, the values of the Newmark parameters selected in all the FE analyses presented in this study are $\beta_1 = 0.600$ and $\beta_2 = 0.605$ for the solid phase and $\beta_1^* = 0.600$ for the fluid phase. These values ensure that the solution is unconditionally stable and the energy is dissipated at the high frequencies so that unrealistic spikes are avoided (Zienkiewicz *et al.*, 1999).

A 5 m wide, 47 m high FE mesh composed by 235 isoparametric quadrilateral finite elements with 8 solid nodes and 4 fluid nodes has been adopted in the FE dynamic simulations. This mesh configuration meets the need of the minimum distance between the element nodes,

Δl_{node}, which should not be greater than one-tenth to one-eighth of the seismic wavelength (Bathe, 1982):

$$\Delta l_{node} \leq \frac{\lambda_{min}}{(8-10)} = \frac{V_{s,min}}{(8-10)f_{max}} \tag{4.1}$$

The base of the model is assumed to be rigid, while equal displacements have been imposed the nodes along the vertical side boundaries (i.e. tied-nodes lateral boundary conditions). This boundary type is also called as repeatable boundary conditions and its efficiency in performing free-field seismic wave propagation problem was demonstrated by Kontoe *et al*. (2007). Fluid flow is not permitted at the base and at the lateral boundaries of the mesh (impervious boundary conditions), while draining is allowed at the top of the FE model. In addition, the adopted soil constitutive model predicts almost a linear behaviour at small strain levels (e.g. shear strain < 10^{-3}%), which can result in unrealistic resonance behaviour. Hence, 3% Rayleigh damping is introduced. The Rayleigh damping is represented in the FE model by means of two coefficients, α_R and β_R, which are 0 and 0.0082 based on the formulation given in Chapter 3 Section 5. In the nonlinear site response analyses presented here, the mass damping matrix is ignored and only the stiffness damping matrix is taken into consideration for the calculation of the Rayleigh damping introduced in the simulations.

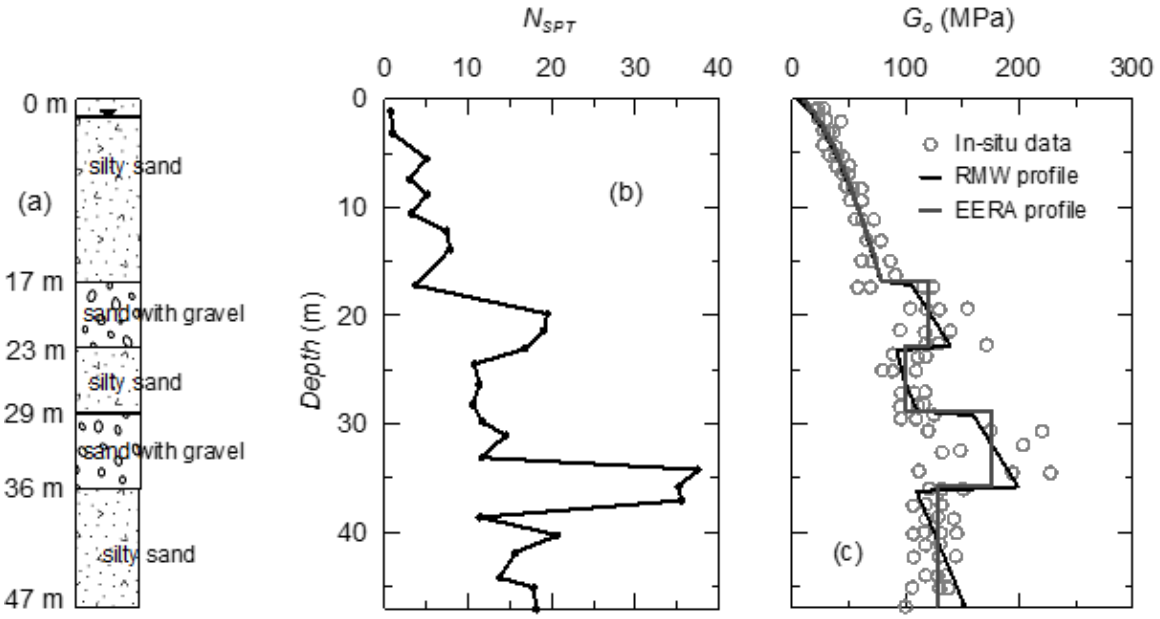

Figure 4.6 Local soil profile at the LSST site: (a) stratigraphy; (b) SPT log; (c) elastic shear modulus.

4.6 The Calibration of the Advanced Soil Constitutive Model Parameters

To include the influence of nonlinear soil behaviour on the seismic wave propagation, the kinematic hardening soil model (*RMW*) developed by Rouainia and Muir Wood (2000) is employed in the fully-coupled finite element analyses. The *RMW* model has the capacity to simulate some of the key features of the dynamic behaviour of natural clay soils such as the shear stiffness degradation with strain amplitude, the corresponding increase of hysteretic damping and the related accumulation of pore water pressure under undrained conditions. The model has been implemented in SWANDYNE II with an explicit stress integration algorithm and a constant strain sub-stepping scheme. *RMW* has been successfully employed in the past to simulate both static (Gonzalez *et al.*, 2012; Panayides, 2014) and dynamic geotechnical problems (Elia and Rouainia, 2012; Elia and Rouainia, 2014). For more details on its formulation and implementation, the reader is referred to Rouainia and Muir Wood (2000) and Zhao *et al.* (2005) (see also Chapter 3). In previous versions of the model, a classical hypo-elastic formulation was implemented to determine the bulk and shear moduli, K and G_0. In this study, however, the well-known equation proposed by Viggiani and Atkinson (Viggiani and Atkinson, 1995) for the small-strain shear modulus has been used to reproduce the dependency of G_0 on the mean effective stress and over-consolidation ratio:

$$\frac{G_o}{p_r} = A\left(\frac{p'}{p_r}\right)^n OCR^m \tag{4.2}$$

where p_r is a reference stress taken as 1 kPa, p' is mean effective stress, OCR is the over-consolidation ratio defined in terms of mean effective stress, A, m and n are the soil plasticity index (PI) dependent stiffness parameters. The best-fit G_0 profile in Figure 4.6c is achieved with A, m and n parameters shown in Table 4.4. In addition, OCR is considered 4 from 0 to 6 m depth and for the remaining soil profile a constant value of 2 is defined.

The parameters of the advanced soil constitutive model, *RMW*, are determined based on the shear modulus and damping ratio curves proposed for the Lotung site by Zeghal *et al.* (1995). They suggested three different nonlinear curves, thus three different materials, for the layers between 0-6 m, 6-11 m, and 11-17 m (as shown in Figure 4.7). These stiffness degradation and damping ratio curves also matched well the different laboratory test results conducted by the National Taiwan University, the University of California, Davis and the University of Texas at Austin. It was assumed that the shear modulus and damping ratio curves of the

soil between 17 and 47 m are equal to those from 11 to 17 m, since more detailed data relevant to the deeper material were not available. Therefore, three different materials can be identified along the soil deposit in terms of dynamic soil properties, although the inclusion of sand with gravel between 17 and 23 m and 29 and 36 m are characterized by higher values of effective friction angles (based on the SPT data shown in Figure 4.6b). It is noted that the lack of a proper characterization of the deeper materials (i.e. below 17 m) in terms of soil dynamic properties at the LSST site can affect the accuracy of the site response simulations and, therefore, its influence on the seismic wave propagation process has been investigated in the last part of the chapter.

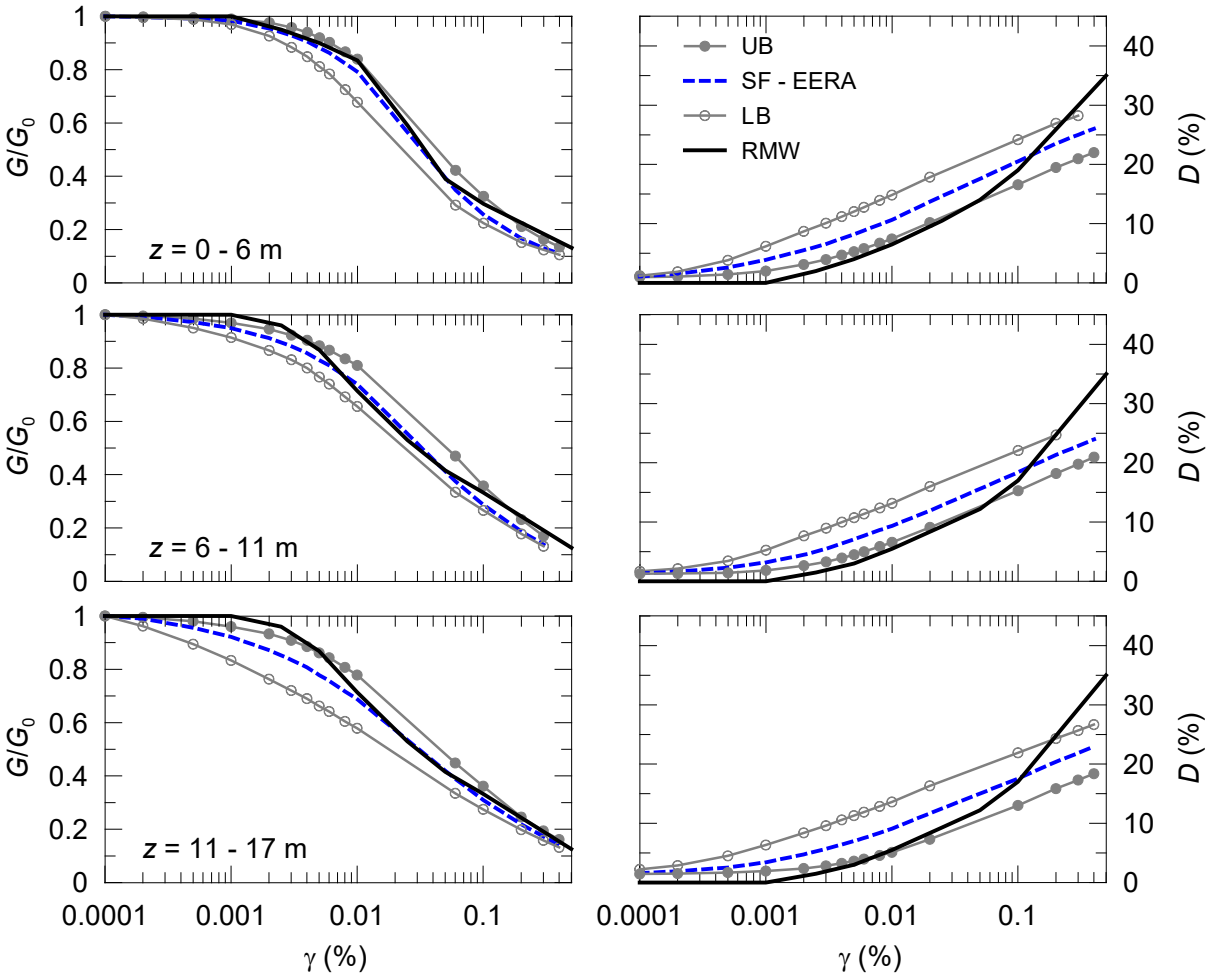

Figure 4.7 Shear modulus degradation and damping ratio curves adopted in this study (RMW) in comparison with Zeghal *et al.* (1995).

The soil model parameters that govern the nonlinear curves of Figure 4.7 are listed in Table 4.4. λ^* and κ^* are calculated based on λ (the slope of the compression line) and κ (slope of the swelling line) values obtained from odometer test results (EPRI, 1993). M, the slope of the critical state line, is calculated from friction angle predictions obtained from measured *SPT-N* values by using the following empirical formulation (Hatanaka and Uchida, 1996):

$$\emptyset_d = (20N)^{0.5} + 18 \tag{4.3}$$

$$M = \frac{6 \sin \emptyset}{3 - \sin \emptyset} \tag{4.4}$$

The size of the bubble (controlled by the parameter R) is kept small for all the three materials, hence a small elastic behaviour of the soil is ensured. This is due to the fact that the soil at the array site shows an irreversible behaviour at small strain levels of around 10^{-2}% (Tang, 1987). The structure surface is considered centred on the isotropic axis, thus $\boldsymbol{\eta}$ equals to 0, with no initial soil structure, i.e. r_0 is equal to 1. The value of Poisson's ratio is taken equal to 0.46 constant with depth, corresponding to the K_0 value of 0.85 proposed by Li *et al.* (1998) and Berger *et al.* (1989).

The remaining soil parameters, B and ψ controlling the plastic shear modulus, are calibrated by producing the stiffness degradation and corresponding damping ratio curves with SM2D (Chan, 1995). Soil element undrained strain controlled cyclic simple shear (CSS) tests are performed. For each strain level, the secant shear modulus and the damping ratio values are predicted at the end of a number of cycles which is adequate to attain a steady-state condition where no more stiffness loss or hysteretic damping can be observed.

Depth	λ^*	κ^*	M	R	B	ψ	r_0	A	m	n
0-17 m	0.03	0.0015	0.922	0.08	0.60	1.0	1.0	1000	0.36	0.82
17-23 m	0.03	0.0015	1.096	0.08	0.60	1.0	1.0	1900	0.36	0.82
23-29 m	0.03	0.0015	0.814	0.08	0.60	1.0	1.0	1350	0.36	0.82
29-36 m	0.03	0.0015	0.941	0.08	0.60	1.0	1.0	1900	0.36	0.82
36-47 m	0.03	0.0015	0.730	0.08	0.60	1.0	1.0	1150	0.36	0.82

Table 4.4 Soil model parameters for different soil layers.

4.7 Results of the Equivalent Linear and Nonlinear Site Response Analyses

In this section, the results of the site response analyses during the weak (LSST11) and strong (LSST7) input motions are presented separately in terms of acceleration-time histories and site response spectra at different depths. Furthermore, maximum acceleration and shear strain profiles along depth obtained with the two numerical approaches are discussed. The performances of both numerical approaches are assessed and their benefits and drawbacks in the site response predictions are discussed. It should be noted that some of the results shown in this section have been published in the work of Elia *et al*. (2017).

4.7.1 Results for the LSST11 earthquake event

The acceleration-time history predictions for the LSST11 earthquake event at three different depths obtained with the equivalent linear and nonlinear numerical approaches are given in Figure 4.8. In the same figure, the accelerations recorded by the instrumented accelerometers at the DHB down-hole array are also shown. Since the event is expected to have the most energy content at the higher frequencies, only the first 10 s of the acceleration-time histories are represented. Figure 4.9 presents the corresponding spectral responses of both the simulated and recorded acceleration-time histories of the LSST11 earthquake event. At depths of 11 and 6 m, the equivalent linear and nonlinear numerical approaches predict the site responses reasonably well, capturing the PGAs almost exactly and following the path of the recorded response spectra, especially at the longer periods (after about 0.3 s). The predictions at ground surface also approach the real site response. The FE code predictions at surface become un-conservative, while EERA gives over-predicted ground surface response spectra, more evident in the N-S direction.

Both numerical approaches perform relatively well in predicting the response spectra at longer periods, as shown in Figure 4.9a and Figure 4.9b. The results are consistent with previous studies by Zalachoris and Rathje (2015) and Kaklamanos *et al.* (2015), who pointed out that at the lower frequencies linear and nonlinear numerical approaches produce identical spectral response, while at the higher frequencies overestimation by the linear approach and under-prediction by the nonlinear approach can be observed when the strain level is less than 0.1%.

In terms of maximum acceleration and maximum shear strain profiles, shown in Figure 4.10, both numerical approaches result in similar responses at the bottom of the soil deposit up

until 20 m depth in both directions. However, especially at the top 5 m, the maximum acceleration and shear strain profiles obtained with the FE and EERA analyses show some discrepancy. EERA predicts greater accelerations and shear strains than the FE code at ground surface.

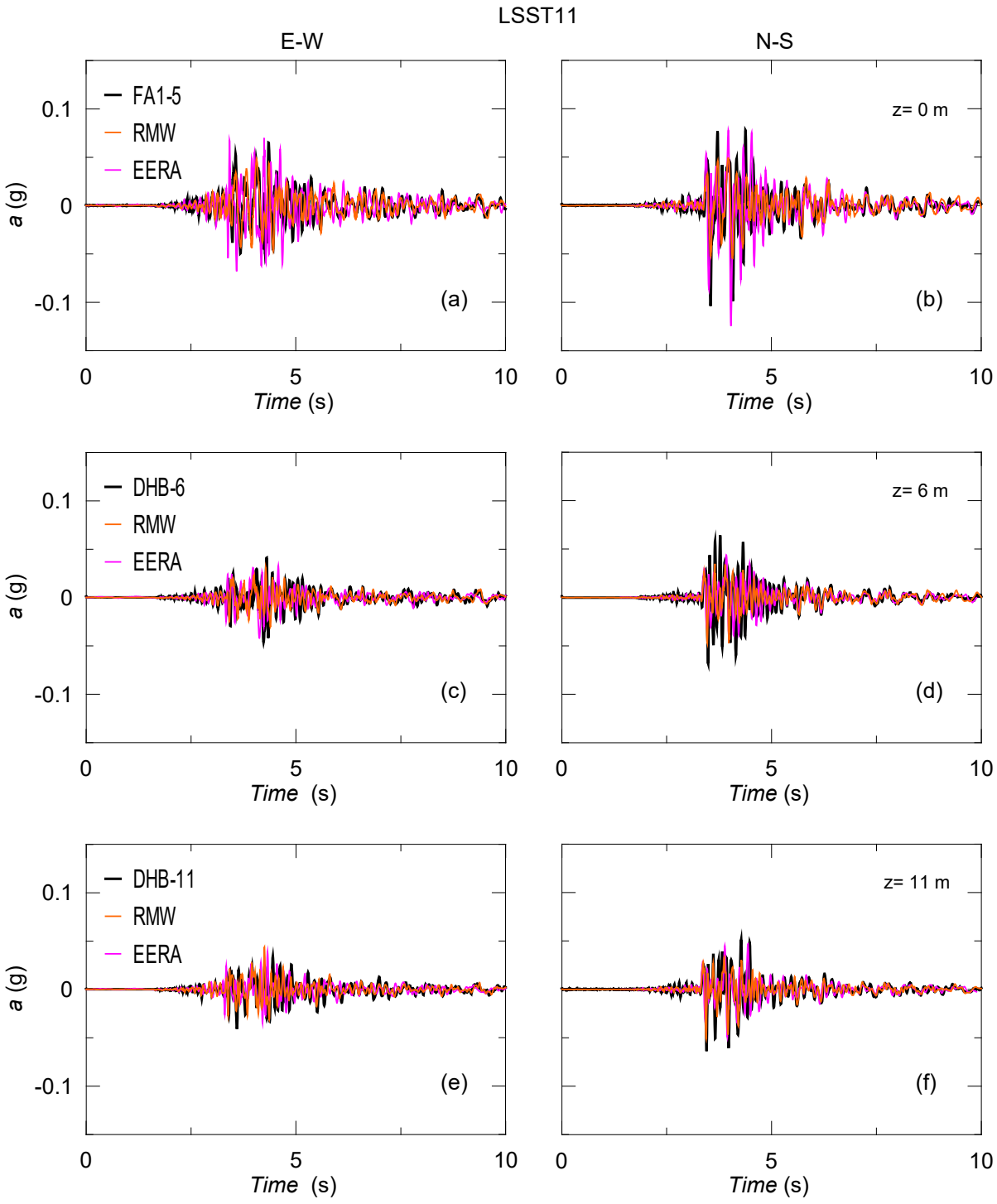

Figure 4.8 Comparisons of the recorded acceleration-time histories for the LSST11 earthquake event with the predictions at three different depths based on equivalent linear (EERA) and nonlinear numerical approaches (SWANDYNE II) in the E-W (left-side) and N-S directions (right-side).

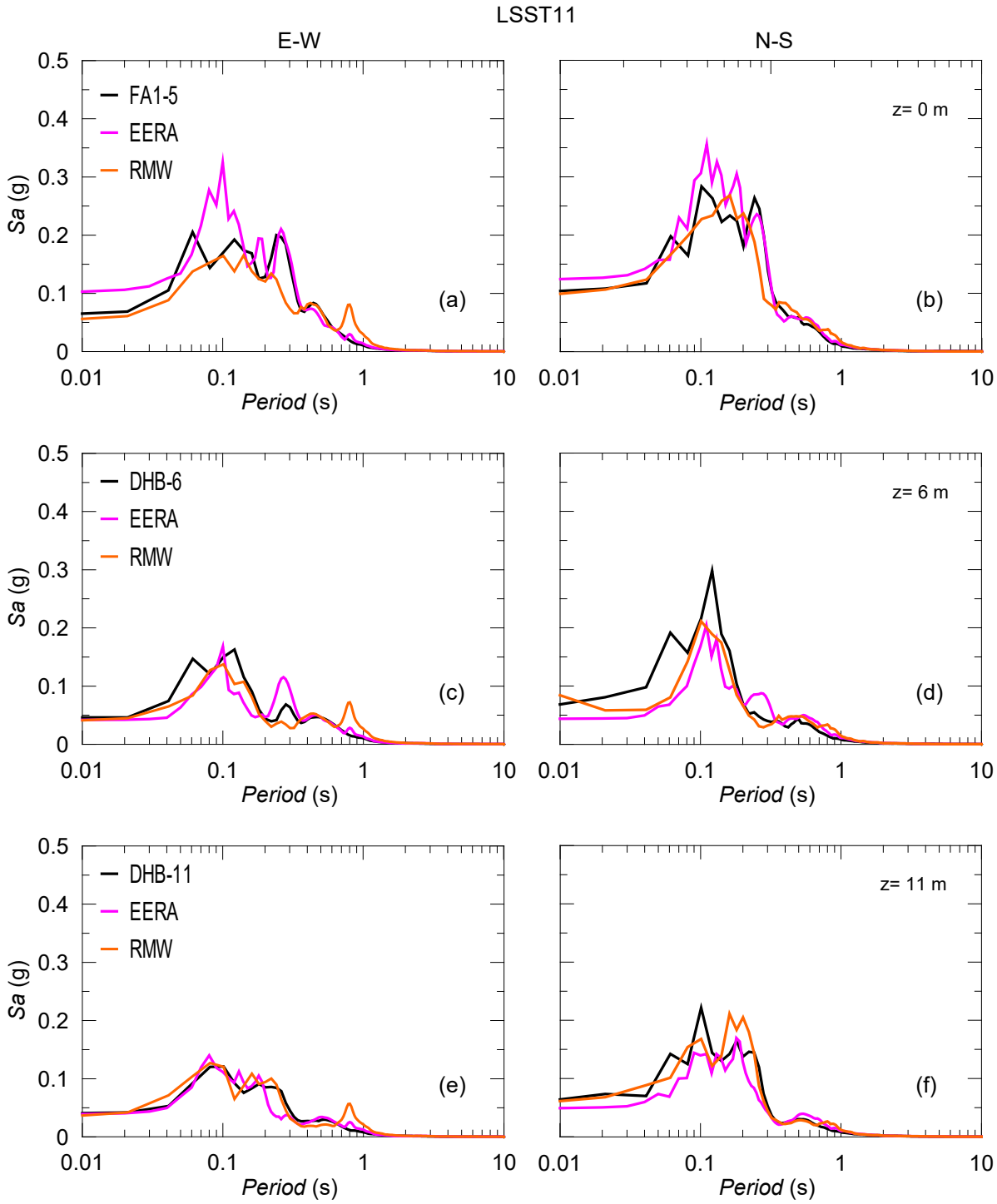

Figure 4.9 Comparisons of the recorded response spectra for the LSST11 earthquake event with the ground response spectrum predictions at three different depths based on equivalent linear (EERA) and nonlinear numerical approaches (SWANDYNE II) in the E-W (left-side) and N-S directions (right-side).

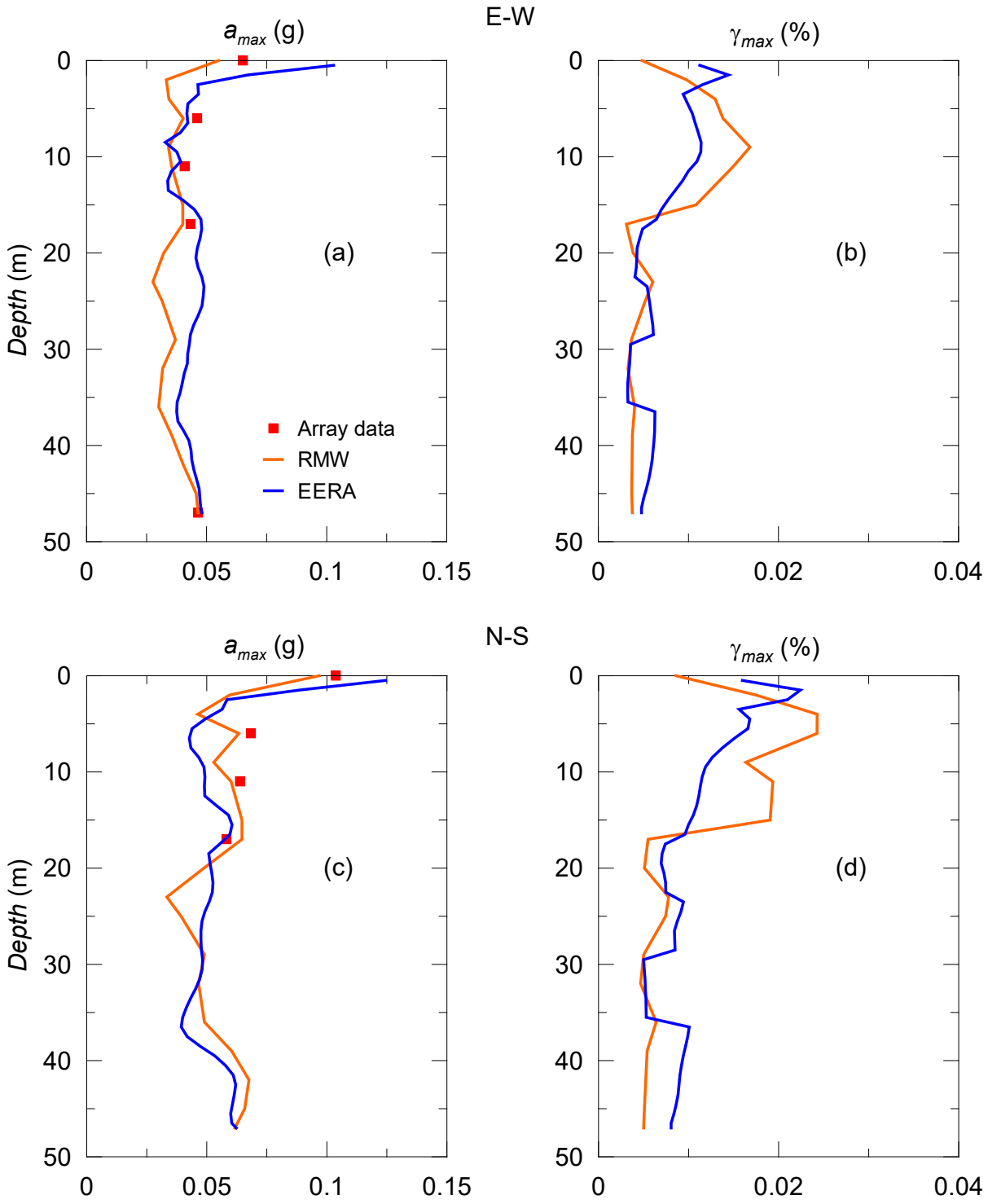

Figure 4.10 Maximum acceleration (a_{max}) and shear strain (γ_{max}) profiles predicted by EERA and FE codes and recorded PGAs at different depths during the LSST11 earthquake event in the E-W and N-S directions.

The LSST11 earthquake event, being characterised by low input energy, induces shear strain levels in the deposit unable to produce soil permanent displacements. Figure 4.11 presents the shear stress versus shear strain curves (i.e. backbone curves) induced by the weak input motion. The maximum predicted shear strain in this case is equal to about 0.02%. It can also be observed that, in parallel with an increase of the strain level towards the ground surface of the soil deposit, the FE analysis predicts a softer stiffness behaviour without any hysteretic loops under both components of the earthquake event. More clearly, a discrete increase of shear strain between 15 m and 5 m depths obtained from the nonlinear FE analyses is observed whereas relatively smooth shear strain increase is achieved by EERA analyses at the same depth ranges. This trend is evidently reflected by the backbone curves showing relatively more and less stiffness degradations for the FE (Figure 4.11c, e) and EERA (Figure 4.11d, f) codes at 6 and 11 m depths. At the top 5 m, both numerical approaches indicate a reduction of shear strain towards the ground surface leading to similar shear stress-strain relation. It is also important to note that, from ground surface to the deeper depths, the amplitude of the shear strain reduces and both numerical approaches predictions become similar in terms of shear stress-strain histories in the E-W and N-S directions.

Overall, the equivalent linear approach seems to offer a reasonable approximation of the soil nonlinearity in the site response prediction of the weak input motion with some over-prediction at the shorter periods. The nonlinear numerical approach also leads to a good prediction of the real site response, even though some under-prediction at the shorter periods is observed. Both numerical approximations, however, perform well in predicting the site response spectra at the longer periods. Nevertheless, the full capabilities of the nonlinear approach are not fully exploited in this case, due to the low energy content of the weak input motion concentrated in the high frequency range.

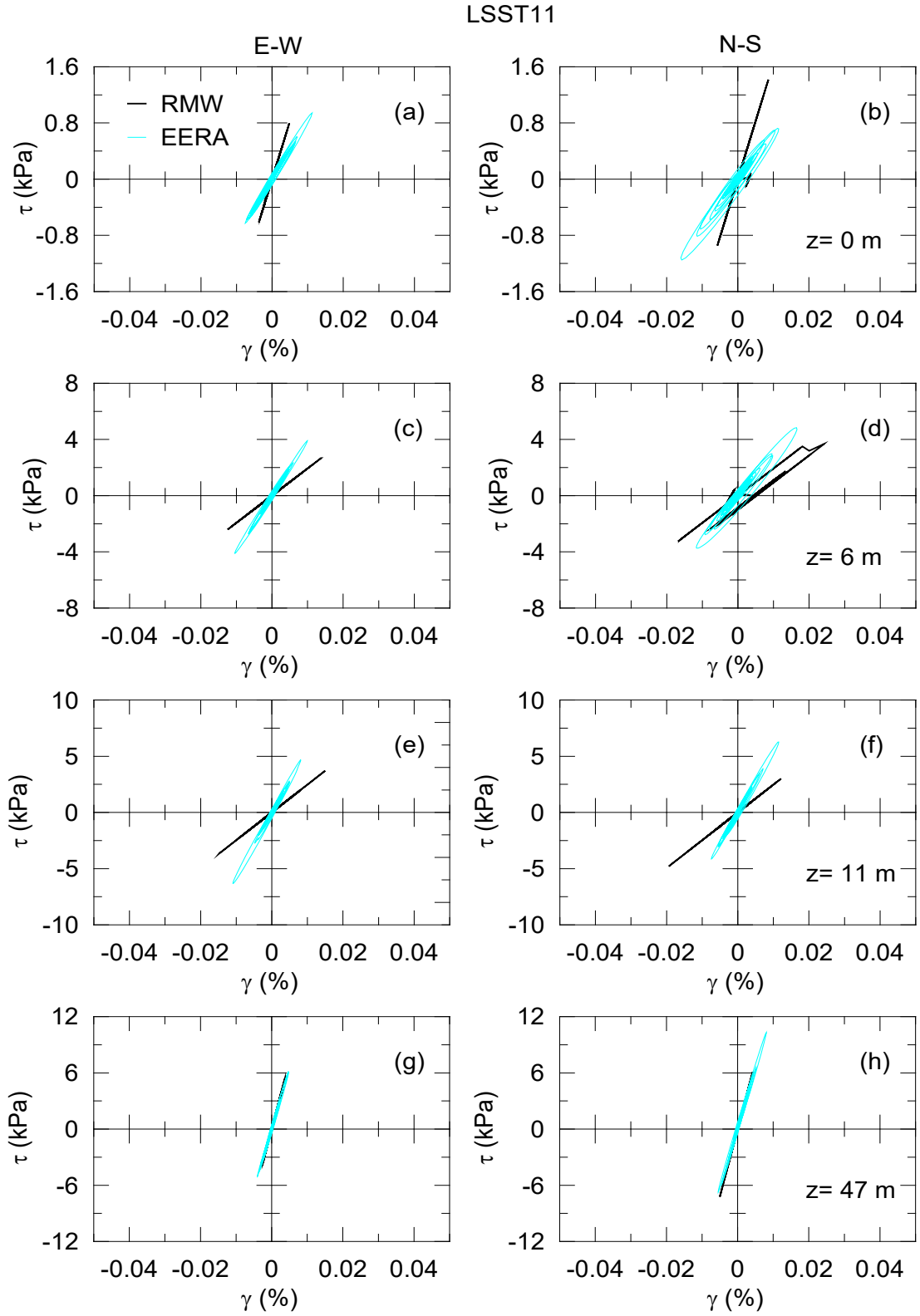

Figure 4.11 Stress-strain curves obtained from the equivalent linear and nonlinear site response analyses at different depths during the E-W (left-side) and N-S (right-side) components of the LSST11 earthquake event.

4.7.2 Results for the LSST7 earthquake event

The results of the LSST7 earthquake event are presented using the same format adopted before. In particular, Figure 4.12 shows the comparison of the acceleration-time history predictions from EERA and SWANDYNE II with the real data at three different depths. The corresponding response spectra at ground surface, 6 and 11 m depth are shown in Figure 4.13. Although the full acceleration-time histories have being used for the determination of the response spectra, only the time histories between 5 and 20 s are presented here. Since the LSST7 earthquake event has a greater energy content than the LSST11 motion, the soil will show more nonlinearity and the capabilities of both numerical approaches are expected to be more clearly highlighted in this case.

EERA is able to predict the site response reasonably well at 6 and 11 m depth under both components of the LSST7 earthquake event, capturing the PGAs and zero crossing. At ground surface, the code under-predicts the site response in the E-W direction and over-predicts it in the N-S direction. Moreover, the time shift in the acceleration-time history of the N-S component at ground surface is evident, as seen in Figure 4.12b. Nevertheless, the EERA predictions are in good agreement with the array data, especially at the higher periods bigger than 1 s (Figure 4.13).

With respect to the results obtained from the nonlinear FE analyses, better predictions can be observed at the considered depths when the E-W component of the earthquake event is applied at the bottom of the soil model (Figure 4.12a, c, e). The nonlinear approach captures almost exactly the PGAs and the spectral acceleration values of the down-hole recordings over the interested period range (Figure 4.13a, c, e). The nonlinear FE analysis of the site during the N-S component of the earthquake event under-predicts the response spectra at ground surface, 11 and 6 m depth (Figure 4.12b, d, f). This is also reflected to the spectral response predictions shown in Figure 4.13b, d, f.

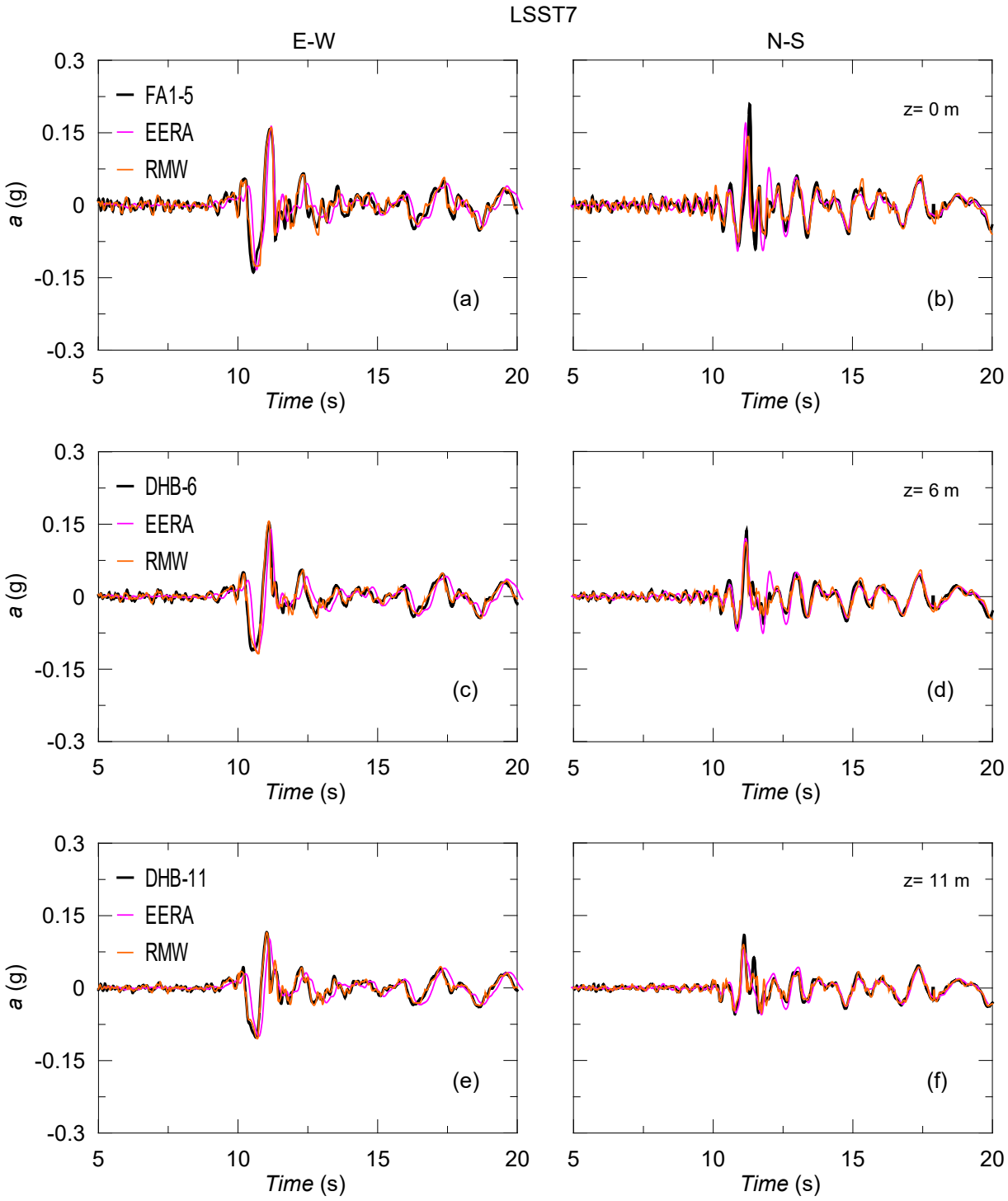

Figure 4.12 Comparisons of the recorded acceleration-time histories for the LSST7 earthquake event with the predictions at three different depths based on the equivalent linear (EERA) and nonlinear numerical approaches (SWANDYNE II) in the E-W (left-side) and N-S directions (right-side).

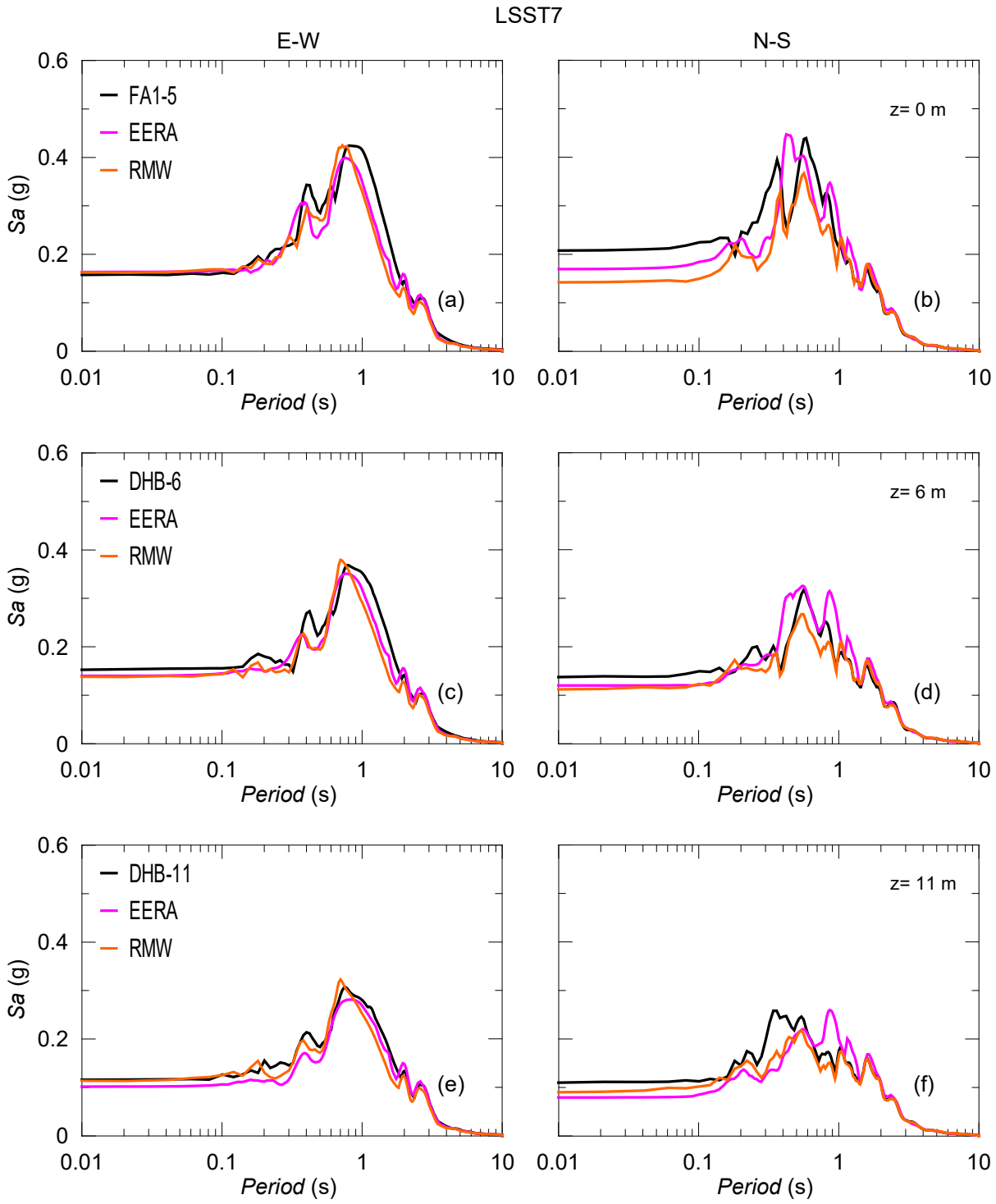

Figure 4.13 Comparisons of the recorded response spectra for the LSST7 earthquake event with the ground response spectrum predictions at three different depths based on the equivalent linear (EERA) and nonlinear numerical approaches (SWANDYNE II) in the E-W (left-side) and N-S directions (right-side).

Figure 4.14 shows the maximum acceleration and shear strain profiles predicted by the equivalent linear and nonlinear numerical approaches under the LSST7 earthquake event in the E-W and N-S directions. The maximum acceleration profiles obtained from both numerical procedures are quite identical in the E-W direction and they capture well the measured PGAs at different depths. In contrast, the PGAs of the N-S component is under-predicted by both analyses. The equivalent linear approach results in better predictions than the nonlinear FE code at ground surface and 6 and 11 m depth, as can be seen in Figure 4.14c. With respect to the maximum shear strain, both approaches lead to the quite similar strain levels below 10 m, giving shear strains at around 0.1% and 0.15% in the E-W direction (Figure 4.14b) and between 0.05% and 0.1% in the N-S direction (Figure 4.14d). This can also be seen from their shear stress-strain histories at associated depths presented in Figure 4.15. However, at the top 10 m, the nonlinear FE code predicts greater shear strains than those of EERA code in the E-W and N-S directions. The FE code also expresses permanent displacement at that range of depth as shown in Figure 4.15a-d. This is the reflection of the soil behaviour under such a strong motion which cannot be presented by the EERA code.

Figure 4.14 indicates that the FE code under-predicts the PGAs of the N-S component of the earthquake event at relatively lower strain amplitude as opposed to achieving good predictions in the E-W direction at higher strain values. Hence, the under-prediction in the N-S direction cannot be attributed to the soil constitutive model employed in the FE code producing a great level of damping at the higher strain level. Further research on the improvement of the N-S site response predictions is given in the last section of the current chapter, Section 4.7.4.

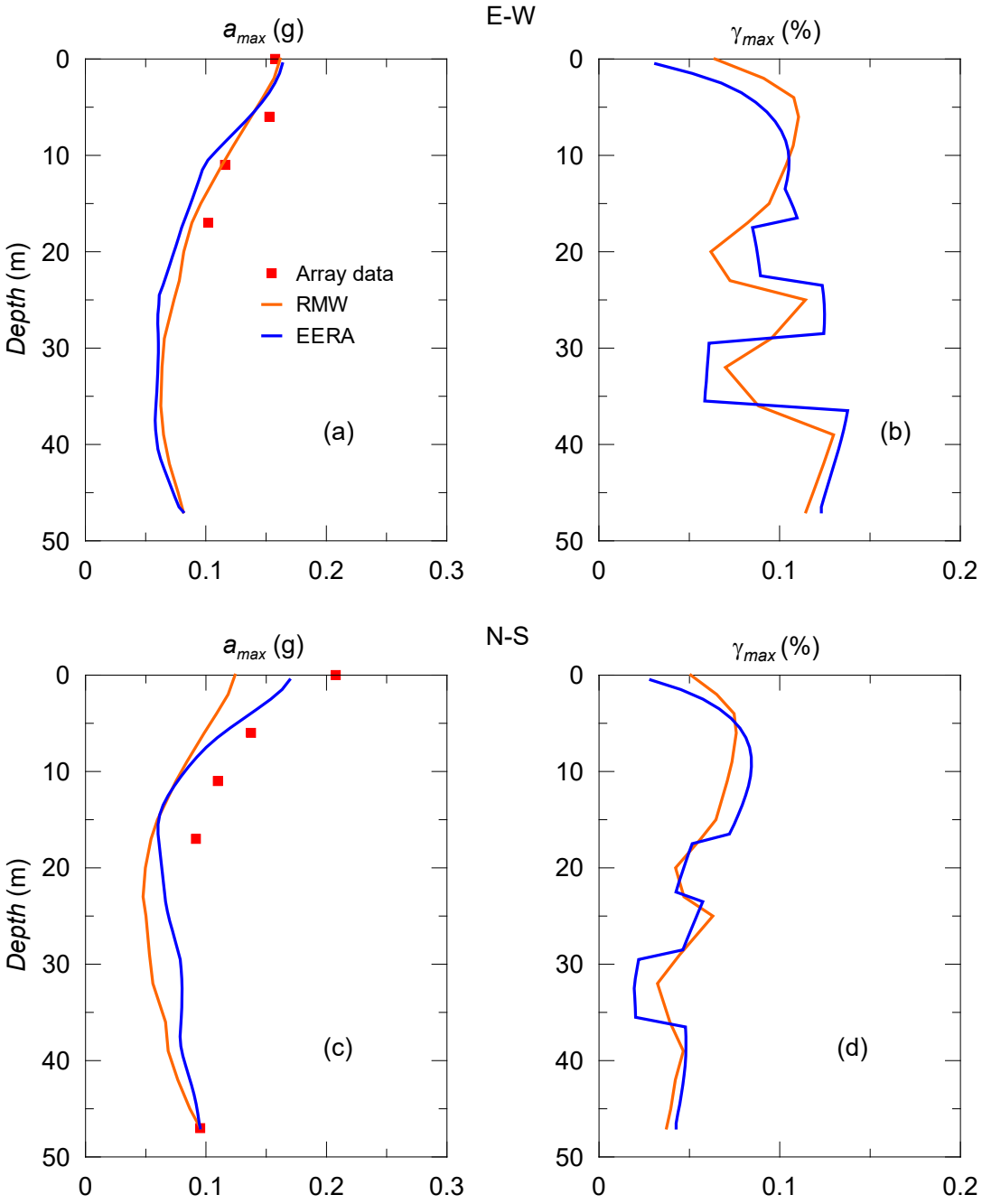

Figure 4.14 Maximum acceleration and shear strain profiles predicted by EERA and FE codes and recorded PGAs at different depths during the LSST7 earthquake event in the E-W and N-S directions.

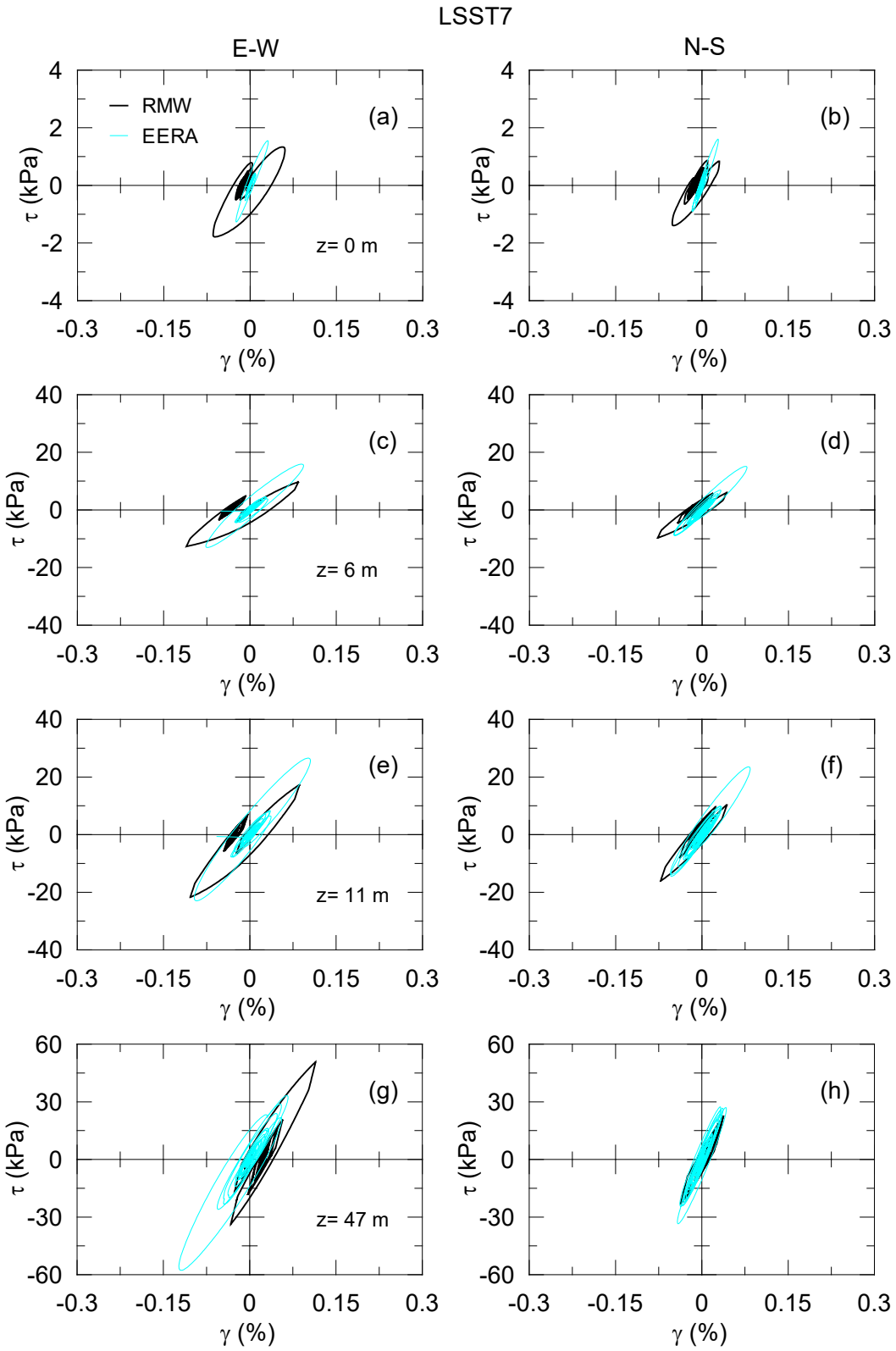

Figure 4.15 Stress-strain curves obtained from the equivalent linear and nonlinear site response analyses at different depths during the E-W (left-side) and N-S (right-side) components of the LSST7 earthquake event.

4.7.3 Pore pressure prediction from the nonlinear site response analyses

One of the advantages of using a fully-coupled nonlinear finite element code in the site response analysis is that the accumulation of the pore water pressure during the seismic excitation can be captured. This is not possible with the equivalent linear visco-elastic or any total stress nonlinear schemes. In the Lotung site, after the LSST7 earthquake event of the 20th of May 1986 pore water pressure transducers were installed at depths between 3 and 16 m, where liquefaction was considered possible, to measure the excess pore water pressure during future seismic activities (Shen *et al.*, 1989).

The excess pore water pressure distribution at the end of FE analyses are shown in Figure 4.16 for both the LSST7 components. The numerical results are compared with a set of data recorded during the LSST16 earthquake event. This event was characterised by similar values of peak ground acceleration, epicentral distance magnitude of those relative to the LSST7 earthquake event. The comparison shows a reasonable agreement between recorded and predicted excess pore pressures.

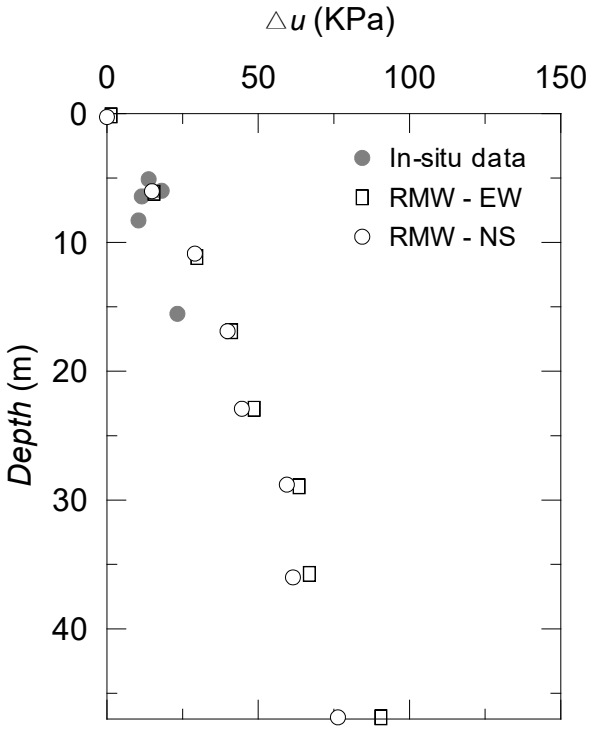

Figure 4.16 Measured and predicted excess pore water pressure during the LSST7 earthquake event in the E-W and N-S directions.

4.7.4 Further research on the LSST7 earthquake event

As highlighted before, while the FE code performs well in predicting the site response of the strong input motion in the E-W direction, it is not able to fully capture the response in the N-S direction, in particular at the top 6 m. This cannot be attributed to the over-damping of the employed soil model, since the E-W motion induces higher shear strains than the N-S component and still good predictions can be achieved for the E-W event.

In order to better analyse the problem of the under-prediction of the accelerations in the N-S direction, it has been decided to simulate only the top 17 m of the soil deposit for a number of reasons:

1. A proper geotechnical characterization of the soil deposit in terms of stiffness degradation and damping ratio curves is not available for the soil below 17 m. Hence, by modelling only the top 17 m of the soil deposit, the uncertainty in the soil dynamic properties below that depth is eliminated.
2. Secondly, the change in the stiffness profile below 17 m does not significantly influence the response predictions at 11 m, 6 m depth and at ground surface.
3. A record of the acceleration-time history of the LSST7 earthquake event is also available at 17 m depth.

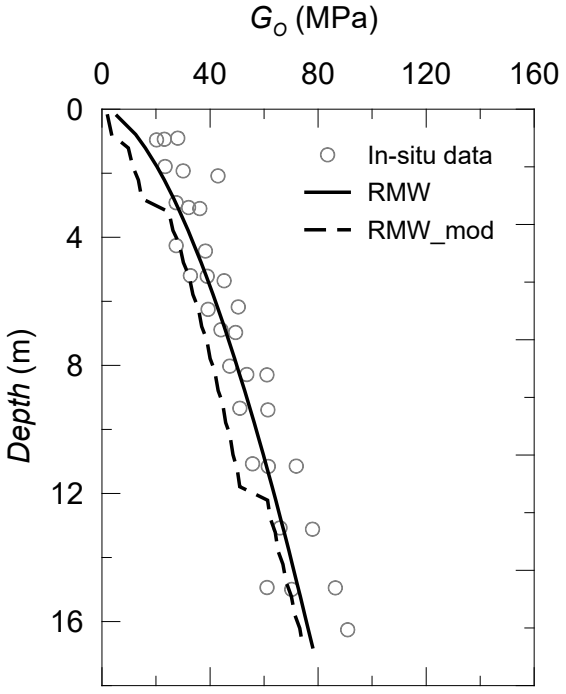

Figure 4.17 In-situ data, original (RMW) and modified (RMW_mod) stiffness profiles used in the shortened soil column analyses.

To improve the site response prediction of the strong input motion in the N-S direction without giving attention to the predictions in the E-W direction, the stiffness profile of the soil deposit has been modified, especially in the top 6 m, as shown in Figure 4.17. The reason to concentrate the attention on the top 6 m of the soil deposit is because around 60% increase in the peak ground acceleration takes place from 6 m to ground surface. It should be noted that the reduced G_0 profile is still within the limits of the in-situ measurements, also presented in Figure 4.17, showing a natural variability with a standard deviation of 10 MPa (Andrade and Borja, 2006).

The reduction in the stiffness profile leads to a better prediction in the N-S direction at 11 and 6 m depth and, particularly, at ground surface as can be seen in Figure 4.18 and Figure 4.19b, d, f. The problem of early acceleration peak time, observed in the N-S acceleration-time history prediction by using stiffer profile, is not seen at the ground surface when the reduced stiffness profile is used. The FE analysis also provides good predictions at 11 and 6 m depth when the E-W input motion is simulated with a reduced initial stiffness profile (Figure 4.18 and Figure 4.19c, e), while it over-predicts accelerations at ground surface (Figure 4.18 and Figure 4.19a). While the reduction in the stiffness profile does not seem to affect dramatically the site response predictions at 11 and 17 m depth in both directions, great spectral amplifications takes place at the top 6 m. The reason for this might be the fact that the soil near to the ground surface is exposed to more nonlinearity in comparison with the deeper layers. Hence, any change (reduction in this case) in the initial stiffness profile at the near surface results in considerably different predictions.

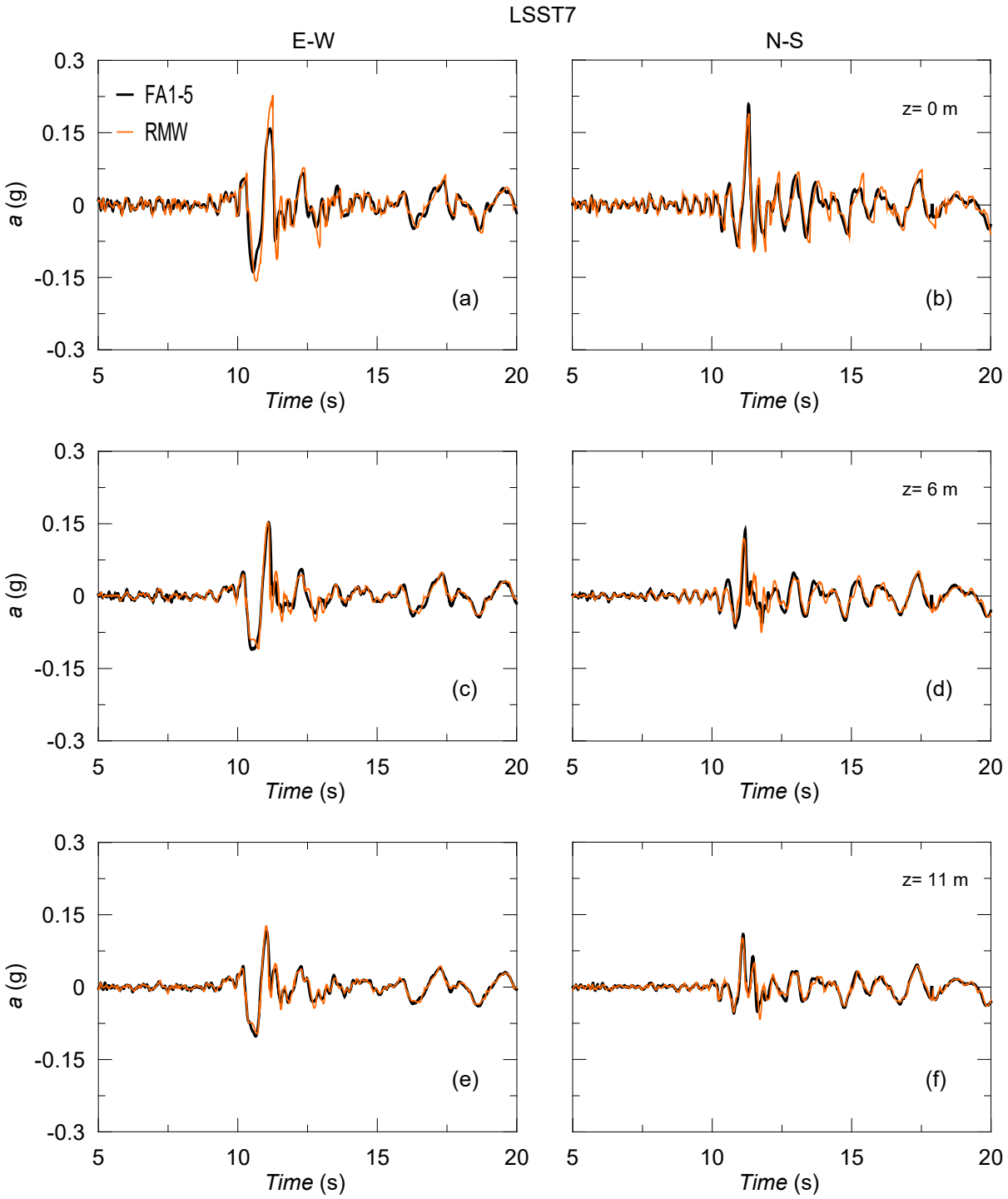

Figure 4.18 Comparisons of the recorded acceleration-time histories for the LSST11 earthquake event with the predictions at three different depths based on the equivalent linear (EERA) and nonlinear (SWANDYNE II) numerical approaches in the E-W (left-side) and N-S directions (right-side) by adopting the reduced stiffness profile.

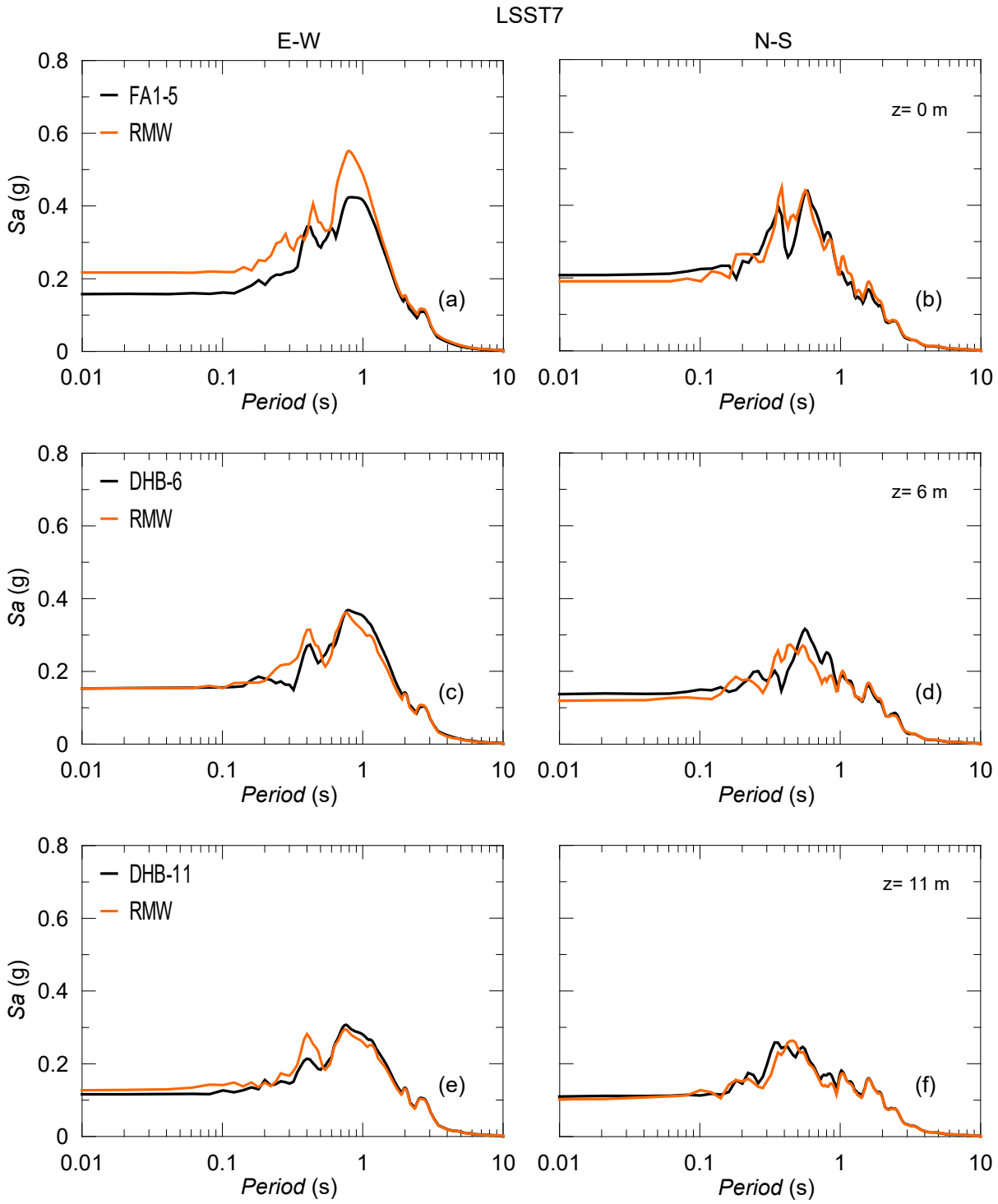

Figure 4.19 Comparisons of the recorded response spectra for the LSST7 earthquake event with the ground response spectrum predictions at three different depths based on the nonlinear numerical approach in the E-W (left-side) and N-S (right-side) directions using the reduced stiffness profile.

The maximum acceleration and maximum shear strain profiles in the E-W and N-S directions are plotted in Figure 4.20 along with the profiles obtained from the full column analyses. The figure clearly indicates the improvement in the PGA predictions of the N-S component of the strong motion and the over-prediction of the PGAs of the same input motion in the E-W direction, especially at ground surface. The predicted maximum shear strains by the shortened soil column analyses are greater than those from the full soil model analyses (seen in Figure 4.21) (it should be noted that the ratcheting behaviour, as clearly shown in Figure 4.22, is considered in computing maximum shear strains) . This can be attributed to the depth of the soil model where the input motion is applied. As it is observed from our full and shortened soil model analyses that when the soil deposit is shaken at relatively lower depth, it causes greater shear strains and also leads to greater spectral acceleration amplifications.

Overall, the improvement in the site response prediction in the N-S direction appears to be possible if the stiffness profile is reduced over a shorter soil column depth. This, however, causes over-prediction of the site response at the ground surface in the E-W direction, but, still good predictions can be obtained at 6 and 11 m depth.

Finally, it should be noted that, in addition to the initial stiffness profile, also the nonlinear curves may affect the site response predictions. Therefore, Monte Carlo simulations could be conducted to consider the influence of both soil properties variability on ground response predictions at Lotung, as discussed later in this dissertation.

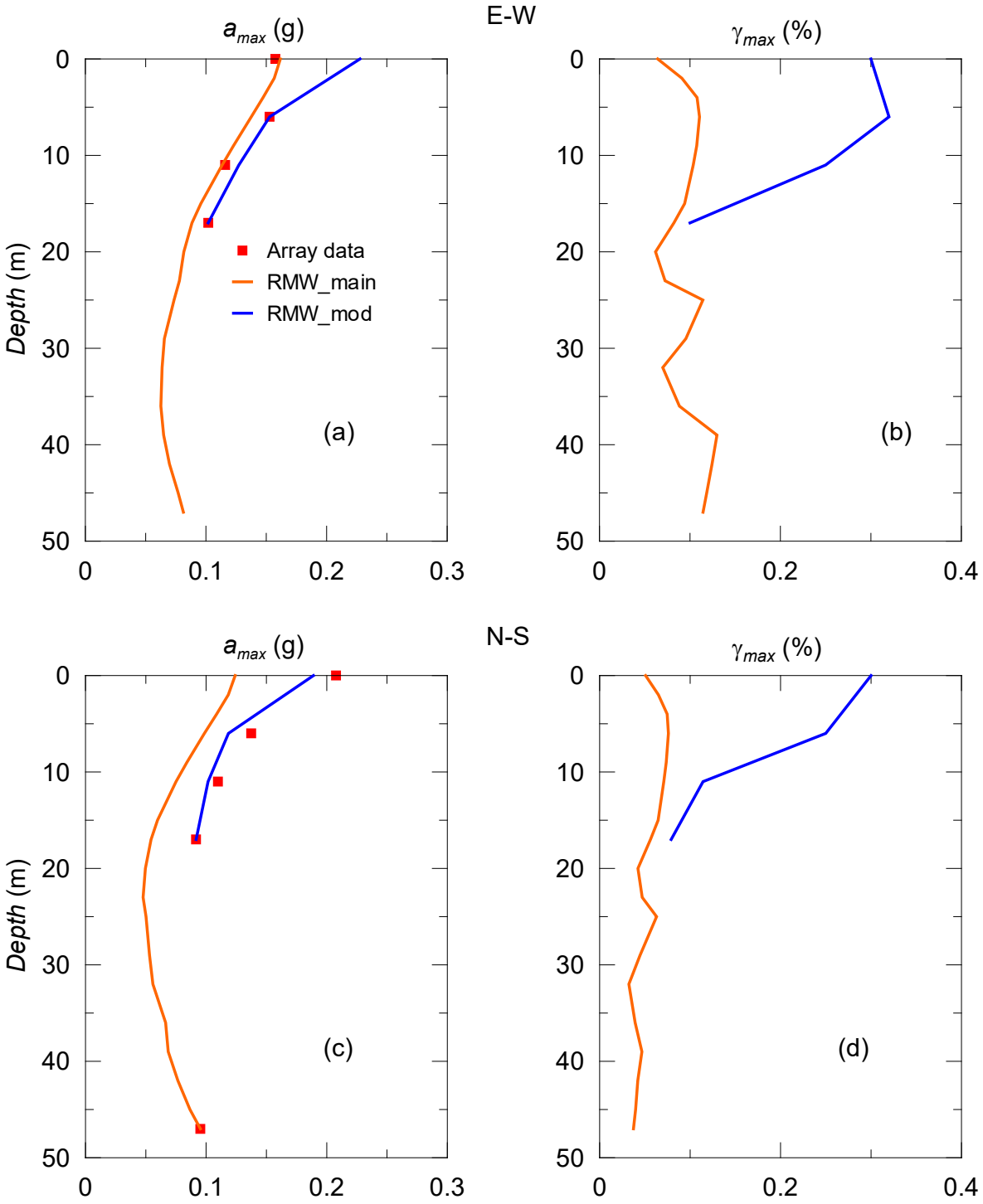

Figure 4.20 Maximum acceleration and shear strain profiles predicted by the FE code adopting the full (RMW_main) and shortened (RMW_mod) stiffness profiles and recorded PGAs at different depths during the LSST7 earthquake event in the E-W and N-S directions.

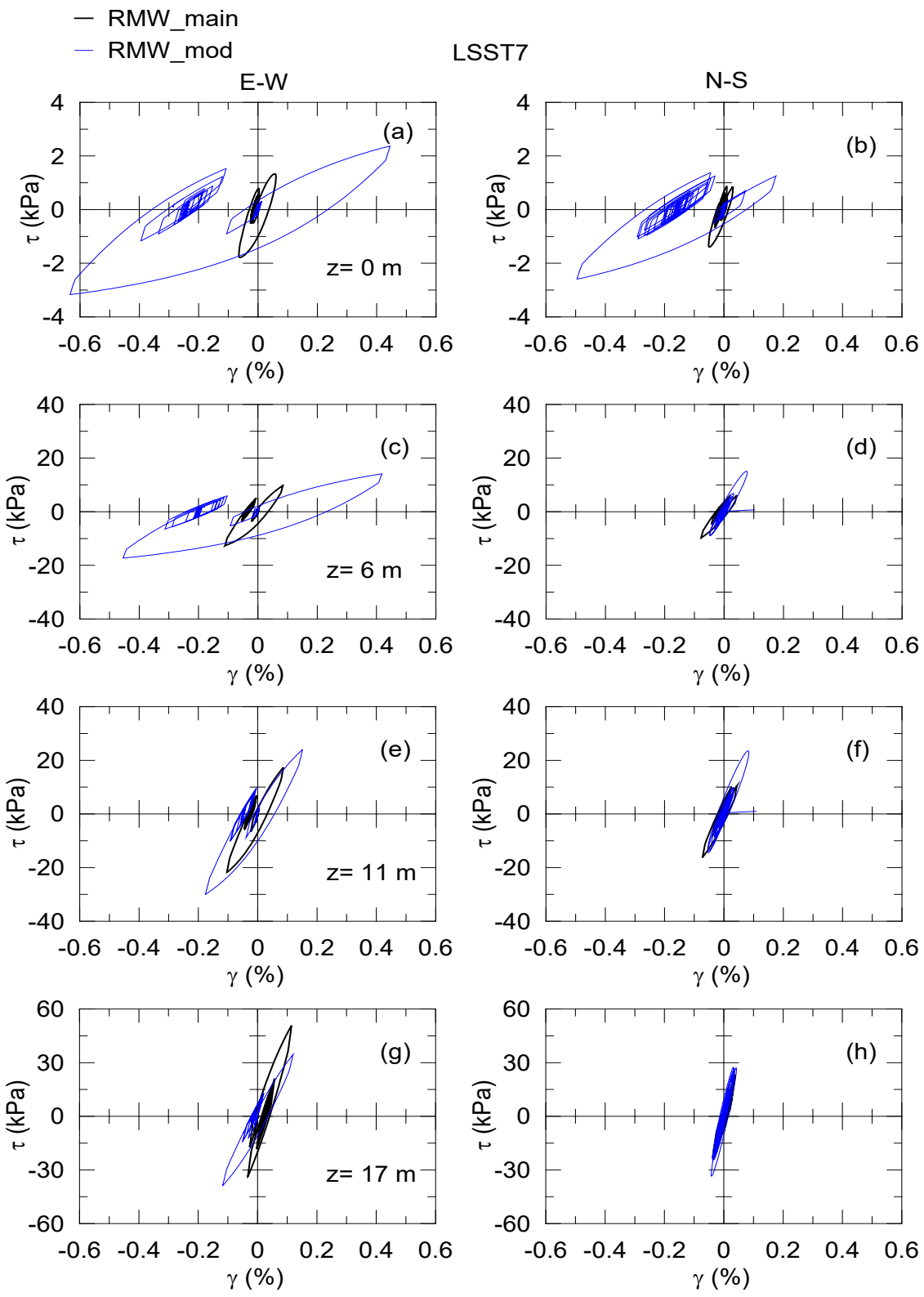

Figure 4.21 Stress-strain curves obtained from the nonlinear site response analyses at different depths during the E-W (left-side) and N-S (right-side) components of the LSST7 earthquake event using the full (RMW_main) and shortened (RMW_mod) stiffness profiles.

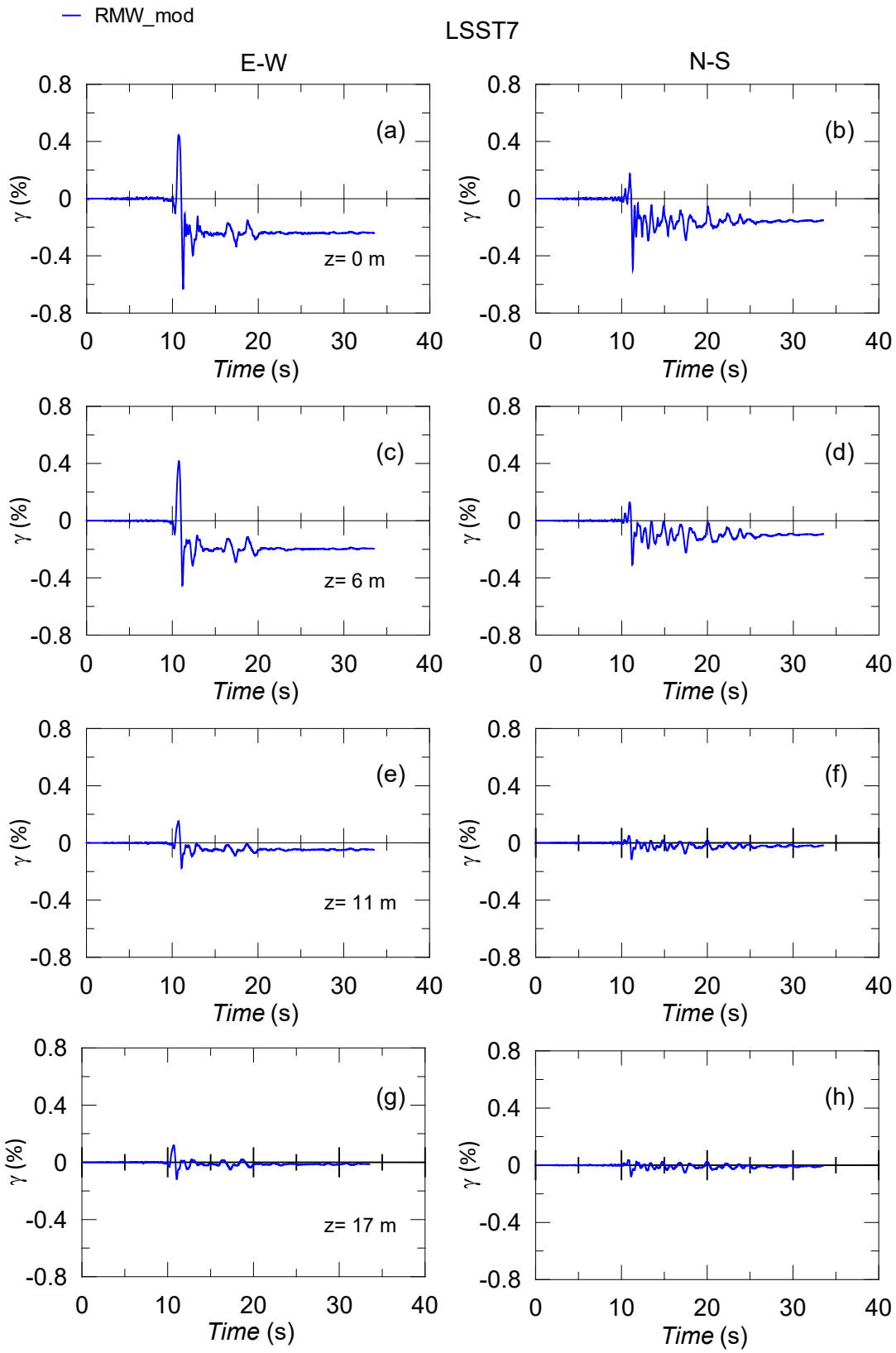

Figure 4.22 Shear strain histories predicted by the FE code in both directions during the LSST7 earthquake event employing the reduced stiffness profile.

4.8 Conclusions

The Large-Scale Seismic Test (LSST) site in Lotung, Taiwan, is analysed by using the frequency domain equivalent-linear visco-elastic program EERA and the time-domain fully-coupled finite element code SWANDYNE II where the advanced soil constitutive model *RMW* is employed to represent the soil nonlinearity. To test the full predictive capabilities of the two approaches, one weak (LSST11) and one strong (LSST7) input motion recorded at the LSST site are considered. Two horizontal components (E-W and N-S) of the earthquake events are separately applied at the bottom of the numerical models. The site response predictions are, then, compared with the array data at three different depths, specifically at 6, 11 m depth and at ground surface.

The FE nonlinear approach performs well with some under-prediction, especially at ground surface, when the weak input motion is applied in both horizontal directions. EERA, conversely, results in over-predicted accelerations, while both approaches give similar results at the longer periods (> 0.3 s). Under the strong input motion, EERA still produces reasonable predictions indicating actual responses in the E-W and N-S directions. The FE code, in this case, performs well in predicting the recorded accelerations as it captures the PGAs at all depths as well as giving almost identical spectral responses to the array data when the E-W component of the strong motion is applied at bedrock. However, if the N-S component of the strong motion is simulated, the FE code under-predicts the accelerations at ground surface, while at 6 and 11 m depth it leads to better site response predictions.

When the stiffness profile of the soil deposit is reduced, in particular at the top 6 m, and a shorter column is considered some improvement in the site response predictions is observed under N-S component of the strong motion. This stiffness reduction, on the other hand, causes over-prediction of the site response at the ground surface in the E-W direction while at 6 and 11 m depth the FE approach still gives good results in terms of acceleration-time histories and spectral acceleration responses. This shows the importance of stiffness change, in particular, at the near surface where the soil is expected to experience more nonlinearity leading to greater spectral amplifications.

In conclusion, this research highlights the importance of using array sites for the verification of different numerical approaches. Particularly, the performances of equivalent linear and nonlinear numerical approaches in predicting seismic site responses have been evaluated and their limitations and benefits have been emphasized. Furthermore, the study highlights the

crucial influence of stiffness variability on the results of site response analyses. This leads to the need of further research to investigate the influence of soil property variability on site response predictions, which has been addressed in Chapter 6 of this thesis.

Chapter 5. Analysis of Input Motion Selection Strategies

5.1 Introduction

The alteration of the earthquake characteristics from bedrock level to the ground surface, due to local site conditions is of great interest to the engineering communities concerned with the seismic design of earth structures, buildings and infrastructure. This phenomenon is less pronounced in stiff soil deposits but more associated with soft soil deposits. In this respect, a reasonable approximation of the site response is specifically important in soft soil deposits. The common method of predicting local site effects is to propagate seismic waves in the vertical direction through the horizontally layered soil deposits by means of simple or sophisticated numerical methods. This enables to assess the surface acceleration-time histories, response spectra, amplification factors (AFs). In parallel, this will also allow to manipulate the soil stiffness degradation and associated hysteretic damping in response to the shear strains induced by a possible earthquake event (Kwok *et al.*, 2007; Amorosi *et al.*, 2010).

The site response analysis is mainly governed by the bedrock motions, the stiffness degradation and damping curves with shear strains and the shear wave velocity profile of the soil deposit. These components sustain some uncertainty attributed to: i) the ambiguity in the selection of a probable earthquake event with specific features from a database (i.e. magnitude, distance, fault mechanism, compatibility with the target response spectrum), ii) the possible variability in the measurement of shear wave velocity owing to the heterogeneous soil deposit and iii) the influence of the soil disturbance during laboratory test procedures to determine the soil nonlinear dynamic characteristics (Phoon and Kulhawy, 1999). These uncertainties may ultimately cause a bias in the site responses at the surface if they are not properly taken into consideration (Li and Assimaki, 2010).

Several researchers have dealt with the above uncertainties to quantify their possible effects on ground response predictions. For this purpose, Monte Carlo simulations have been conducted with linear or nonlinear soil models by varying site properties (Bazzurro and Cornell, 2004; Stewart and Kwok, 2008; Rathje et al., 2010). While these studies explicitly indicate the importance of accounting for the shear wave velocity, stiffness degradation and damping variability in site response analyses, they also recognise the fundamental impact of bedrock motion selection on the accuracy of site response results.

To minimize the bias in the ground response predictions and, thus, the number of simulations, the simulated input motions can be subjected to some modification and scaling.

Different input motion selection and scaling methods, such as peak ground acceleration (PGA) scaling, spectral matching and the mean squared error (MSE) approach, have been proposed mainly in structural engineering literature (Shome *et al.*, 1998; CEN, 2005; Hancock *et al.*, 2006; Ancheta *et al.*, 2013), but their application to geotechnical earthquake engineering problems is limited (Kottke and Rathje, 2008; Mazzoni *et al.*, 2012; Tönük *et al.*, 2014; Amirzehni *et al.*, 2015). Specifically, no clear guidance is provided to the geotechnical engineers by the national or international design codes when dealing with advanced ground response analyses of soft deposits, which account for soil nonlinear properties.

This chapter examines the impact of different earthquake selection and scaling strategies on the free-field ground response of an ideal soft soil deposit (classified as soil class D according to EC8). Five selection approaches of the input motion spectral accelerations are adopted in this study: 1) scaling at PGA only, 2) scaling at the natural period of the soil column (T_1), 3) scaling in a period range of $0.2T_1$–$2T_1$ according to what is proposed in EC8, 4) scaling based on mean squared error, and 5) matching the spectral shape of the input response spectrum to the target demand using the spectral matching method, which alters the frequency content of the earthquake through a wavelet algorithm. Sets of seven bedrock motions are used for each selection strategy, considering two seismic intensity levels of 0.15g and 0.35g representing weak and strong input motions, respectively.

Equivalent linear visco-elastic simulations and advanced time domain nonlinear analyses are conducted to investigate the performance of different numerical approaches in the prediction of site response. The comparison with EC8 in terms of amplification and soil factors is subsequently presented to highlight the inability of the code prescription to fully capture site effects, which occur in soft soil deposits for low seismic intensity levels. The results of the advanced nonlinear simulations are then interpreted in terms of spectral response and Engineering Demand Parameters (EDPs) at ground surface, i.e. relative horizontal displacement, peak acceleration and spectral acceleration at the first natural period of the soil deposit ($Sa(T_1)$). The influence of increasing the number of bedrock input motions from 7 to 14 for each selection strategy on the ground spectral accelerations and EDPs is also investigated. In addition, a statistical analysis aimed at comparing the

differences in the EDPs associated to each set of records is presented. Finally, the level of correlation between Arias intensity (I_a) and Dobry's duration ($D_{5\text{-}95}$) of the input motions and the EDPs is presented.

5.2 FE model

An ideal soft clay soil deposit with 50 m depth and 5 m width is modelled in the fully-coupled finite element code SWANDYNE II. The soil column is discretised by 250, 1×1 m isoparametric quadrilateral finite elements with 8 solid nodes and 4 fluid nodes (Figure 5.1). This mesh generation ensures that the seismic wave transmission is represented accurately through the FE soil model (Bathe and Saunders, 1984). During the dynamic analyses, the bottom of the mesh is assumed to be rigid at the bedrock, while the nodes along the vertical sides are characterized by the same displacements (i.e. tied-nodes lateral boundary conditions). The modified input motions are directly applied to the solid nodes at the base of the mesh as prescribed horizontal displacement time histories. The dynamic simulations are carried out with a time step corresponding to that of the earthquake input signals.

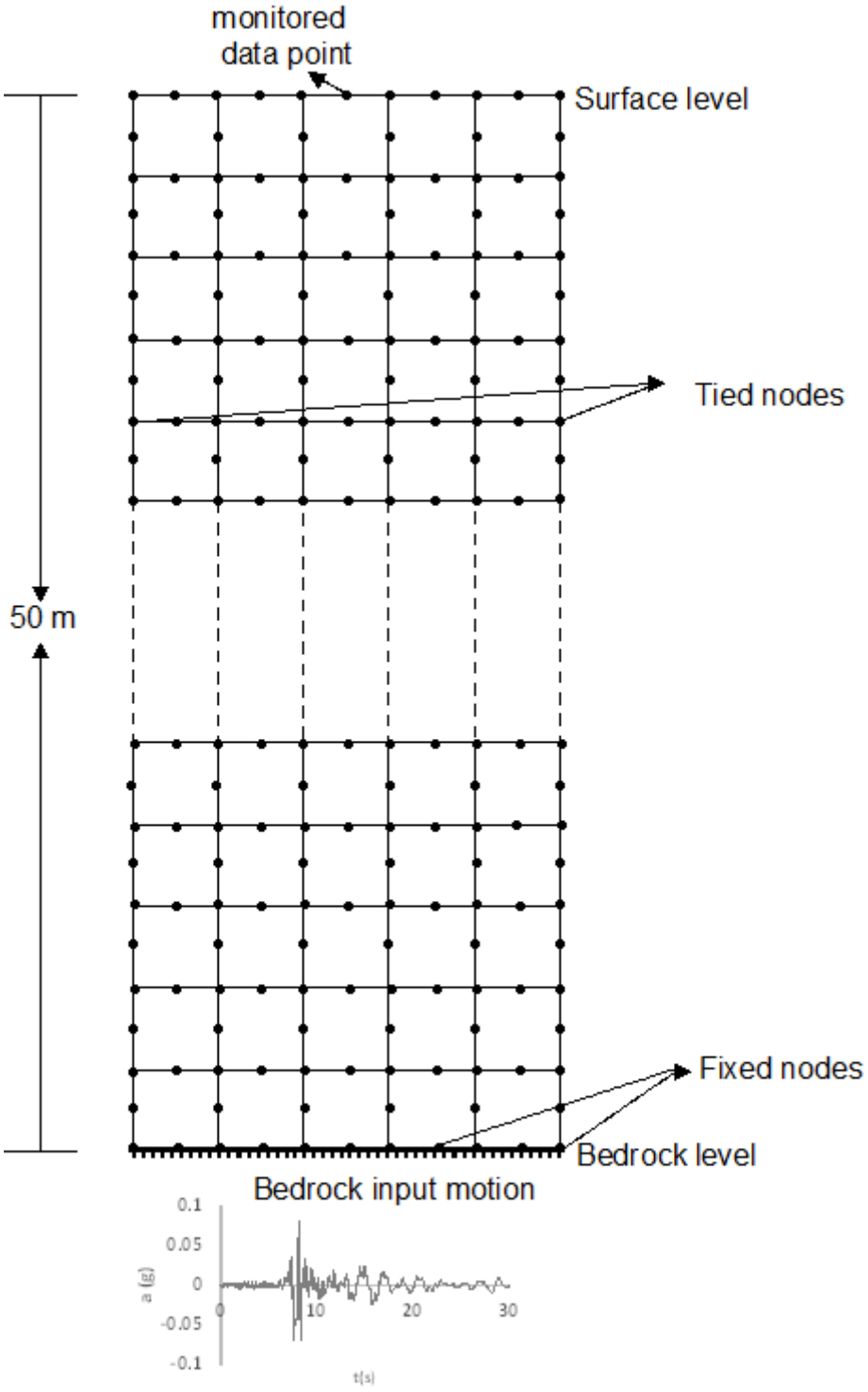

Figure 5.1 An ideal 50 m soft clay soil model discretised with 1×1 m isoparametric quadrilateral finite elements with 8 solid nodes and 4 fluid nodes.

The advanced soil model *RMW* (Rouainia and Muir Wood, 2000) is employed to simulate the dynamic soil behaviour during the nonlinear site response analyses. *RMW* has been successfully employed to predict the dynamic performance of different earth structures (Elia and Rouainia, 2012; Elia and Rouainia, 2014) as it can capture early irreversibility, accumulation of pore pressure, stiffness degradation and damping ratio curves and the destructuration of soil under undrained conditions. In this work, the soil material parameters are determined by conducting a series of undrained cyclic simple shear test simulations under controlled strain levels in order to produce normalised shear modulus and damping curves representative of a soft soil deposit (Vucetic and Dobry, 1991). In the dynamic simulations performed with SWANDYNE II, only 2% Rayleigh damping is introduced, with coefficients of α_R and β_R being equal to 0 and 0.0075, respectively, to avoid the propagation of spurious high frequencies and to compensate for the model underestimation of damping in the small-strain range.

The initial stiffness profile of the soil deposit is obtained using the equation proposed by (Viggiani and Atkinson, 1995) for the dependency of the small-strain shear modulus, G_0, on the mean effective stress and overconsolidation ratio (as its formulation is given in Chapter 4 Section 6). In particular, the dimensionless stiffness parameters *A*, *m* and *n* in the equation, which depend on the plasticity index, are set equal to 1050, 0.27 and 0.84, respectively. In the initialisation phase of the FE model, an overconsolidation ratio of 1.5 is assumed constant with depth. The resulting shear wave velocity profile has an average value in the top 30 m of the column equal to 140 m/s, thus classifying the deposit as a soil class D according to EC8. Accordingly, the first natural period (T_1) of the deposit is equal to 1.17 s.

It should be noted that in the EERA analyses, the same profile of small-strain stiffness implemented in the FE model is discretised by constant stiffness sub-strata of 1 m thickness. Moreover, to perform a consistent comparison between the two different numerical approaches, the same normalised stiffness modulus decay and damping curves obtained with *RMW* (see Figure 5.2) are used as inputs in the EERA simulations.

The model parameter	λ*	κ*	M	ν	R	A	B	η	k	Ψ	r_o
	0.252	0.0297	1.35	0.22	0.1	0.494	8	0.0	0.5	1	1.75

Table 5.1 *RMW* model parameters calibrated against the nonlinear curves given by Vucetic and Dobry (1991).

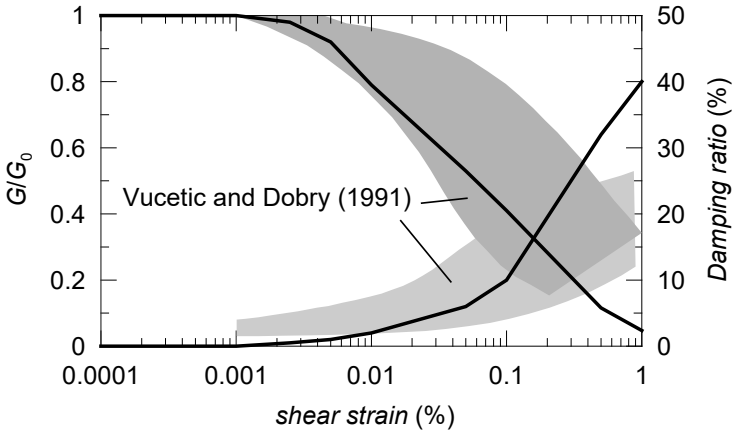

Figure 5.2 Shear stiffness degradation and corresponding damping ratio curves based on plasticity index (PI) values and *RMW* model parameters.

5.3 The Selection Strategies

In this section, the adopted selection strategies to investigate their roles in prediction of less biased site responses are described along with the tools used. Two target response spectra are set according to EC8 prescription with 0.15g and 0.35g seismic intensity levels. These correspond to the EC8 5% damped design response spectrum given for soil class A. The intention in defining a low and high intensity target response spectra is to emphasise the effect of soil nonlinearity in the seismic wave propagation process. Two sets of seven and 14 input motions are selected for each selection strategy. Consideration of at least seven input motions is to take median responses into account, which is in accordance with the EC8 criterion. The number of input motions is increased to investigate its influence on the average site response spectra and EDPs.

The selection strategies studied in this research are;

- PGA scaling
- Sa(T_1) scaling
- $0.2T_1$-$2T_1$ scaling
- Spectral matching

- Mean squared error (MSE) scaling.

The selection of input motions according to the first three of above selection strategies are conducted by using the computer program REXEL (Iervolino *et al.*, 2010). The SEISMOMATCH (Seismosoft, 2016) program applies spectral matching using the wavelets algorithm suggested by Abrahamson (1992) and Hancock *et al*. (2006) while MSE scaling is available online on the Peer Ground Motion Database (PGMD) website (Ancheta *et al.*, 2014). SEISMOMATCH requires inputting the accelerograms to apply full matching procedure with the target response spectrum whereas the REXEL and PGMD programs automatically select and scale, linearly, the input motions.

PGA scaling focuses only on the compatibility of the input motions, on an average, with the target response spectrum at zero period. Because of this, reasonable compatibility of the median response spectrum with the target response spectrum over period ranges cannot be expected, as seen in Figure 5.3-4a. Sa(T_1) scaling seeks for an average compatibility at T_1 of the target response spectrum. Nevertheless, the median response spectra still match well with the targets over all interested period range in both seismic intensity levels (Figure 5.3-4b). $0.2T_1$-$2T_1$ scaling presented in Figure 5.3-4c is proposed by EC8, where; 1) the average compatibility with the target response spectrum is achieved within $0.2T_1$-$2T_1$ period range with lower tolerance of 10%, and 2) the average PGA is not less than that of the target response spectrum (more details about the selection criteria included in EC8 can be found in Chapter 3 Section 3.2.5). The dotted lines in the figures are the representation of the target response spectrum at 10% lower bound conditioned by EC8 and 30% upper bound suggested by Iervolino *et al.* (2010).

MSE scaling is based on total difference between the spectral acceleration of the events and the target response spectrum in the log space, over the entire engineering period range (Equation 5.1). It gives input motions whose average response spectrum is in good agreement with the target response spectrum as shown in Figure 5.3-4d. Figures 5.3-4e present the full matching of the input motions with the target response spectra in both seismic intensity levels. The input motions selected according to $0.2T_1$-$2T_1$ scaling are processed for this selection strategy as SEISMOMATCH does not automatically apply input selections and modifications.

$$\mathrm{MSE} = \frac{\sum_i w(T_i)\{ln[Sa^{target}(T_i] - ln[f \times Sa^{record}(T_i]\}^2}{\sum_i w(T_i)} \tag{5.1}$$

, in which parameter f is a linear scale factor applied to match the target response spectrum over an entire period range. $w(T_i)$ is a weight function that allows users to assign a more precise match of the response spectrum to the target for specific period range.

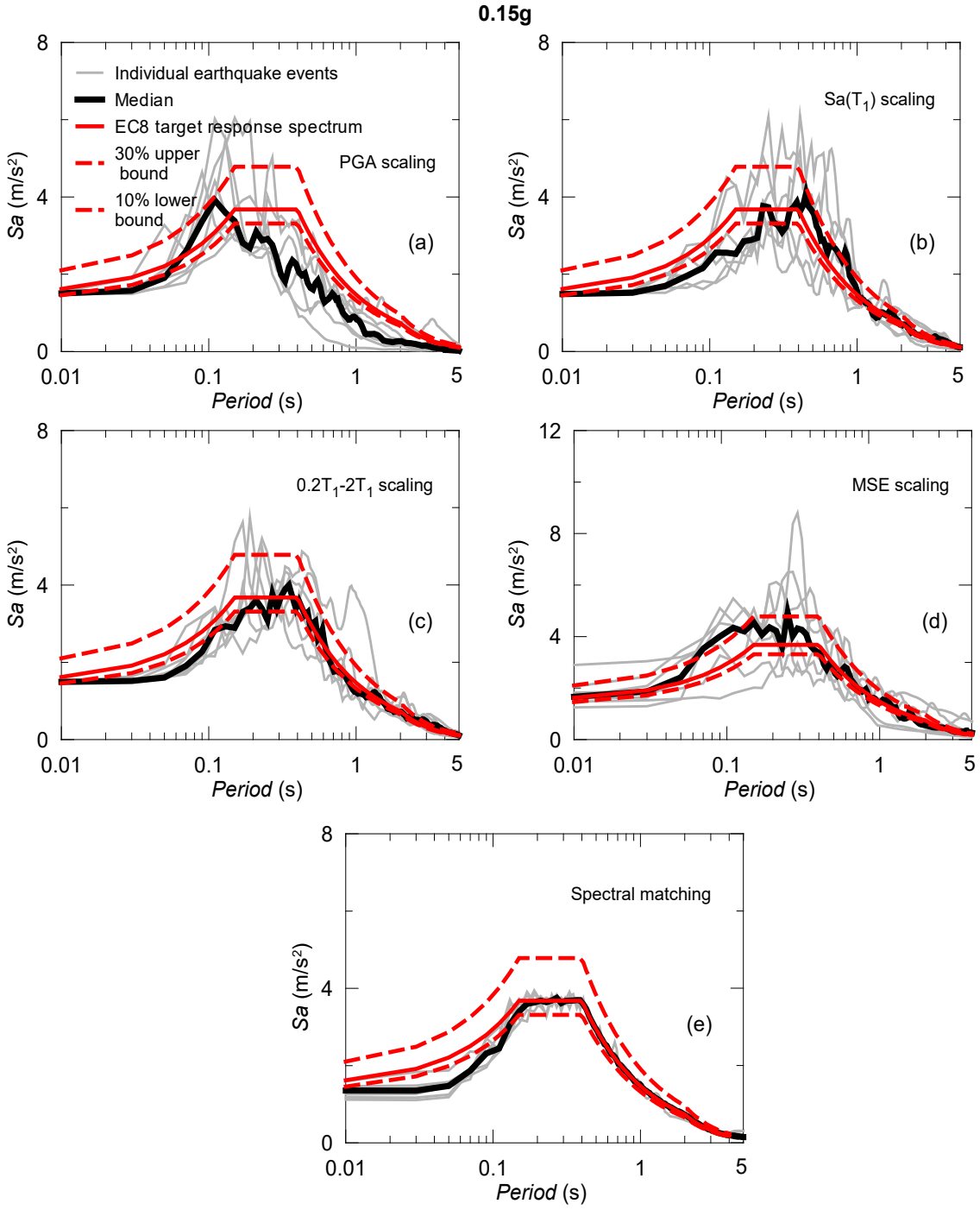

Figure 5.3 Modified input motions to the 5% damped EC8 design response spectrum with their median response spectra for a) PGA scaling, b) Sa(T_1) scaling, c) 0.2T_1-2T_1 scaling, d) MSE scaling and d) spectral matching at 0.15g seismic intensity level along with lower (10%) and upper (30%) limits.

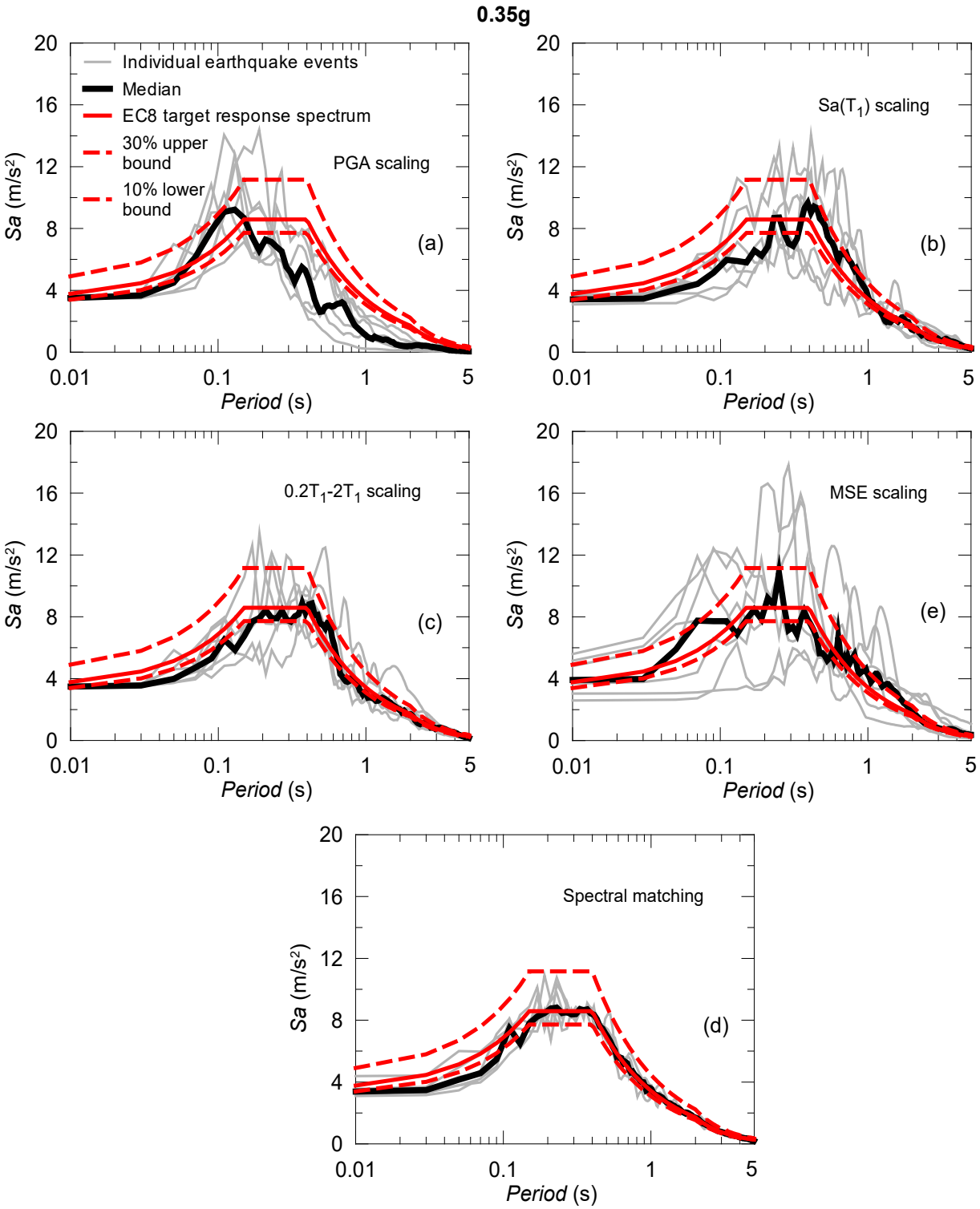

Figure 5.4 Modified input motions to the 5% damped EC8 design response spectrum with their median response spectra for a) PGA scaling, b) Sa(T_1) scaling, c) 0.2T_1-2T_1 scaling, d) MSE scaling and d) spectral matching at 0.35g seismic intensity level along with lower (10%) and upper (30%) limits.

	Waveform ID	Eq. ID	Eq. Name	Date	*M*	Fault Mechanism	*R*
PGA scaling	55	34	Friuli	6/5/1976	6.5	Thrust	23
	59	35	Friuli (aftershock)	7/5/1976	5.2	Thrust	27
	95	52	Friuli (aftershock)	17/6/1976	5.2	Oblique	26
	128	63	Friuli (aftershock)	15/9/1976	6	Thrust	28
	149	65	Friuli (aftershock)	15/9/1976	6	Thrust	12
	169	80	Calabria	11/3/1978	5.2	Normal	10
	182	87	Tabas	16/9/1978	7.3	Oblique	12
Sa(T_1) scaling	296	146	Campano Lucano	23/11/1980	6.9	Normal	80
	5821	1888	Strofades (aftershock)	18/11/1997	6	Strike slip	93
	4675	1635	South Iceland	17/6/2000	6.5	Strike slip	13
	410	189	Golbasi	5/5/1986	6	Oblique	29
	46	34	Fruili	6/5/1976	6.5	Thrust	146
	5807	1885	Kalamata	13/10/1997	6.4	Thrust	93
	6335	2142	South Iceland (aftershock)	21/6/2000	6.4	Strike slip	15
$0.2T_1$-$2T_1$ scaling and Spectral matching	292	146	Campano Lucano	23/11/1980	6.9	Normal	25
	5814	1885	Kalamata	13/10/1997	6.4	Thrust	61
	1243	473	Izmit (aftershock)	13/9/1999	5.8	Oblique	15
	342	307	Cazulas	24/6/1984	4.9	Oblique	24
	286	146	Campano Lucano	23/11/1980	6.9	Normal	78
	1902	659	Anchialos	30/4/1985	5.6	Normal	55
	1255	472	Izmit	17/8/1999	7.6	Strike slip	78
	Record sequence no.						

MSE scaling	765	Loma Prieta	17/10/1989	6.93	Reverse oblique	9.64
	788	Loma Prieta	17/10/1989	6.93	Reverse oblique	73
	1011	Northridge-01	17/1/1994	6.69	Reverse	20.29
	1165	Kocaeli	17/8/1999	7.51	Strike slip	7.21
	1245	Chi-Chi	21/9/1999	7.62	Reverse oblique	37.72
	4083	Parkfield-02	28/9/2004	6	Strike slip	5.29
	5618	Iwate	14/6/2008	6.9	Reverse	16.27

Table 5.2 Basic properties of the input motions with 0.15g seismic intensity levels selected based on the selection strategies (*M* is for magnitude and *R* is for epicentral distance).

	Waveform ID	Eq. ID	Eq. name	Date	*M*	Fault Mechanism	*R*
PGA scaling	55	34	Friuli	6/5/1976	6.5	Thrust	23
	59	35	Friuli (aftershock)	7/5/1976	5.2	Thrust	27
	128	63	Friuli (aftershock)	15/9/1976	6	Thrust	28
	149	65	Friuli (aftershock)	15/9/1976	6	Thrust	12
	169	80	Calabria	11/3/1978	5.2	Normal	10
	182	87	Tabas	16/9/1978	7.3	Oblique	12
	193	91	Montenegro	9/4/1979	5.4	Thrust	15
$Sa(T_1)$ scaling	296	146	Campano Lucano	23/11/1980	6.9	Normal	80
	5821	1888	Strofades (aftershock)	18/11/1997	6	Strike slip	93
	4675	1635	South Iceland	17/6/2000	6.5	Strike slip	13
	410	189	Golbasi	5/5/1986	6	Oblique	29
	46	34	Fruili	6/5/1976	6.5	Thrust	146
	5807	1885	Kalamata	13/10/1997	6.4	Thrust	93
	6335	2142	South Iceland (aftershock)	21/6/2000	6.4	Strike slip	15

$0.2T_1$-$2T_1$ scaling and Spectral matching	292	146	Campano Lucano	23/11/1980	6.9	Normal	25
	5814	1885	Kalamata	13/10/1997	6.4	Thrust	61
	1243	473	Izmit (aftershock)	13/9/1999	5.8	Oblique	15
	286	146	Campano Lucano	23/11/1980	6.9	Normal	78
	182	87	Tabas	16/9/1978	7.3	Oblique	12
	198	93	Montenegro	15/4/1979	6.9	Thrust	21
	198	93	Montenegro	15/4/1979	6.9	Thrust	21
	Record sequence no.						
MSE scaling	77		San Fernando	9/2/1971	6.61	Reverse	1.81
	680		Whittier Narrows-01	1/10/1987	5.99	Reverse oblique	18.12
	765		Loma Prieta	17/10/1989	6.93	Reverse oblique	9.64
	1011		Northridge-01	17/1/1994	6.69	Reverse	20.29
	1108		Kobe	17/1/1995	6.9	Strike slip	0.92
	1165		Kocaeli	17/8/1999	7.51	Strike slip	7.21
	1257		Chi-Chi	21/9/1999	7.62	Reverse oblique	37.72

Table 5.3 Basic properties of the input motions with 0.35g seismic intensity levels selected based on the selection strategies.

5.4 Results and Discussions

The site responses from equivalent linear and nonlinear analyses are presented in this section in terms of median response spectra and EDPs at the ground surface. The performances of the two numerical approaches are assessed based on response spectra and maximum acceleration and maximum strain profiles. The validity of the EC8 design response spectrum for a soft soil is then discussed with reference to the response predictions. Moreover, the median EDP responses from nonlinear FE analyses are analysed for all the selection strategies. Furthermore, the influence of the number of the input motions on the site response predictions is evaluated. Lastly, a statistical test (i.e. t-test) is conducted to check whether the median EDP responses from the selection strategies can be regarded as equal.

5.4.1 Site response spectra from selection strategies

The median site response spectra obtained from seven site response analyses are given in Figure 5.5 at two seismic intensity levels, 0.15g and 0.35g. The responses from EERA analyses are represented in Figure 5.5a-b while those from FE analyses are shown in Figure 5.5c-d. In all cases, the first (T_1=1.17 s) and second (T_2=0.39 s) natural modes of the soil deposit contribute to the site response as the spectral accelerations presented in Figure 5.5 at around the associated modes of periods show discretely greater amplifications.

The spectral accelerations from PGA scaling are totally different from the accelerations based on other selection strategies in both numerical analyses and seismic intensity levels. PGA scaling also results in responses positioned well below the EC8 design response spectrum. This can be attributed to the compatibility criteria of PGA scaling with the target, as it only modifies the PGA of input motions applied at the bottom of the soil deposit. Hence, the selected and modified input motions are not in good agreement with the target response spectrum at periods higher than 0.1 s, Figure 5.3a and Figure 5.4a. Ultimately, the spectral responses obtained at the surface are separate from the design response spectrum and from the other selection strategies. The site responses under input motions modified based on MSE scaling also divert from the other three selection strategies at low and high seismic intensities when EERA code is adopted.

Focusing on the results of nonlinear FE analyses, MSE scaling leads to similar spectral responses with the others at 0.15g seismic intensity level. Although, it also shows similarity at the higher seismic intensity level, it does not cause similar amplification at around second natural period of the soil deposit. This might be owing to the sharp spectral change in each individual response spectrum considered by PGMD program for MSE scaling and great dispersion in the spectral peaks over the engineering period range. This issue is not investigated in this research but the reader can refer to the study of Mazzoni *et al.* (2012) for more information. The spectral responses from other three selection strategies, namely $Sa(T_1)$, $0.2T_1$-$2T_1$ scaling and spectral matching strategies are reasonably similar for both seismic intensity levels and numerical approaches. Although the results of the selection strategies based on equivalent linear and nonlinear approaches are interpreted and analysed within the same context in here, the difference in the spectral responses due to the numerical approaches is discussed in the following section at both seismic intensity levels.

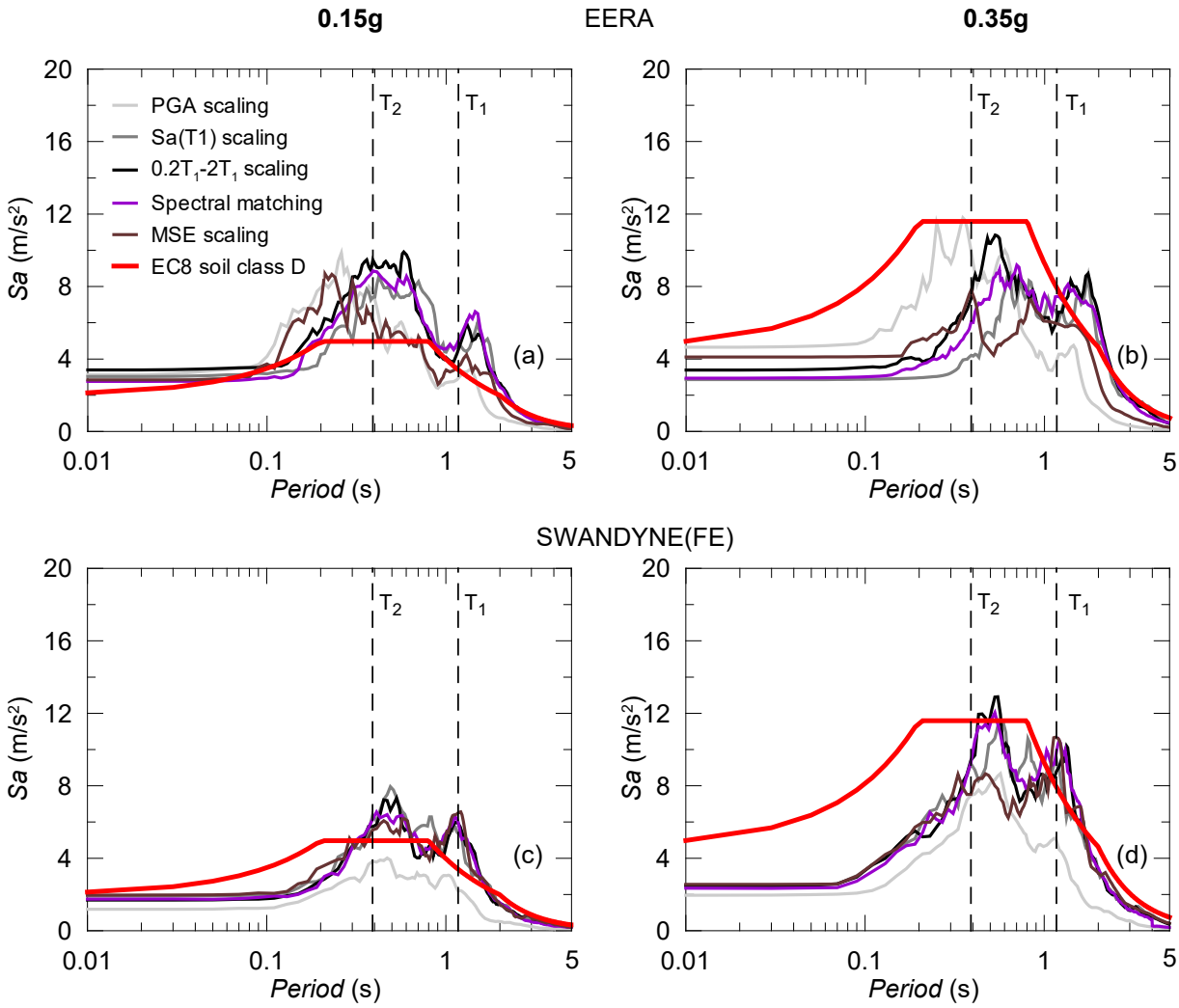

Figure 5.5 Median site response spectra predictions obtained for each selection strategy at the surface by EERA (a, b) and FE codes (c, d) at 0.15g (left) and 0.35g (right) seismic intensity levels.

5.4.2 Performance evaluation of the numerical approaches

As the equivalent linear approach implemented in EERA uses the stiffness degradation and associated damping curves employed in the nonlinear FE analyses, their performances can rationally be compared. The equivalent linear and nonlinear analyses predict indiscrete spectral responses at around T_1. At around second natural period of the soil deposit, the EERA code has a wider period band of spectral peaks than the nonlinear predictions for the three selection strategies, namely Sa(T_1) scaling, $0.2T_1$-$2T_1$ scaling and spectral matching.

At 0.15g seismic intensity level, the spectral accelerations from the EERA analyses show greater amplification than those from the FE analyses at all engineering period of interest. In contrast, at the higher seismic intensity level, the predictions of nonlinear site response

analyses exhibit clear de-amplification at high frequencies. This is not clearly observed when the EERA code is used. However, the EERA code spectral predictions demonstrate more period elongation in both seismic intensity levels implying implicitly greater nonlinearity even though both numerical approaches cause similar shear strain at the surface (can be seen in Figure 5.5a-b and Figure 5.6a-b). The reason for the greater period elongation observed in the equivalent linear site response analyses may be attributed to the consideration of constant dynamic shear modulus (G) and damping (D) values for each soil layer correspondent of the induced shear strain levels during the propagation of input motions. Hence, more stiffness degradation and more damping are taken into consideration by the EERA code, which ultimately leads to large period elongation.

In contrast, the FE analysis represents the nonlinear soil behaviour by predicting continuous change of stiffness and damping properties throughout the motion. These features of the advanced nonlinear approach result in dissipating the earthquake energy during the seismic oscillation and capturing the stiffness degradation and damping levels with a more realistic way at the current stress-strain condition. Ultimately, the period elongation becomes less pronounced in the nonlinear FE analyses and the predicted spectral responses are expected to be a more reasonable approximation of the actual soil behaviour. Thus, from this point onwards, the study uses the results of the FE analyses in the evaluation of the EC8 design response spectrum and further examination of the selection strategies.

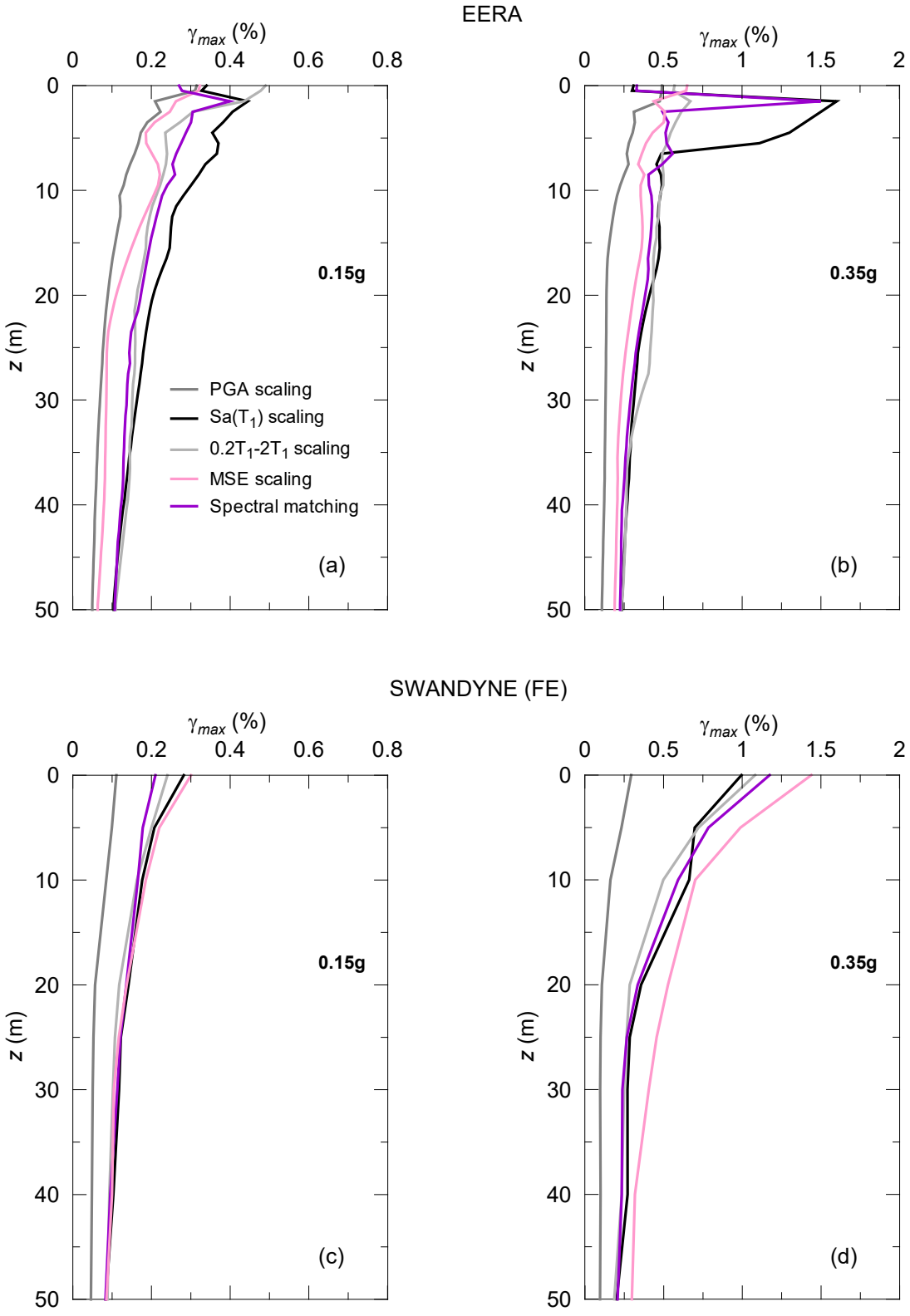

Figure 5.6 Median maximum γ_{max} shear strain profiles of EERA (a, b) and FE (c, d) site response analyses obtained for each selection strategy at 0.15g and 0.35g seismic intensity levels.

While the benefit of using FE analysis in site response prediction is appreciated, the computed maximum shear strain values at the ground surface for all the selection strategies (except from the strain values for PGA scaling), in particular at the 0.35g seismic intensity level shown in Figure 5.6d, seem to be in the range where the advanced soil model (*RMW*) produces a great level of damping as can be depicted from Figure 5.2. The stiffness degradation and damping values against different shear strain levels up to 1% presented in Figure 5.2 are obtained by conducting strain controlled cyclic simple shear tests where the hysteretic loops are perfectly centered around the origin of the stress-strain axes. This means that the permanent strain accumulation is not accounted for in the stiffness and damping calculations at the end of the dynamic cycles and as a result, leads to the computation of larger damping value. On the contrary, the soil is expected to express permanent deformation under especially moderate and strong earthquake events. Hence, consideration of the absolute maximum strain amplitude in defining the maximum damping level of the soil during seismic excitation may mislead one in the performance evaluation of the soil model.

To make this standpoint more obvious, the shear strain-time histories and shear stress-strain curves of the input motions are closely investigated through the soil profile for each selection strategy. The method used in the determination of the strain level leading to maximum hysteretic loop is not to take the maximum absolute strain value but rather to compute the maximum difference between two adjacent peaks and half of this value so that the hysteretic loop is centred at a point other than the origin of the strain axis. By doing so, the centring of the hysteretic loops at the origin of the strain axis is eliminated and, hence, the ratcheting soil behaviour is taken into consideration. In this way, the maximum hysteretic loop may better be approximated and matched well with the corresponding induced shear strains.

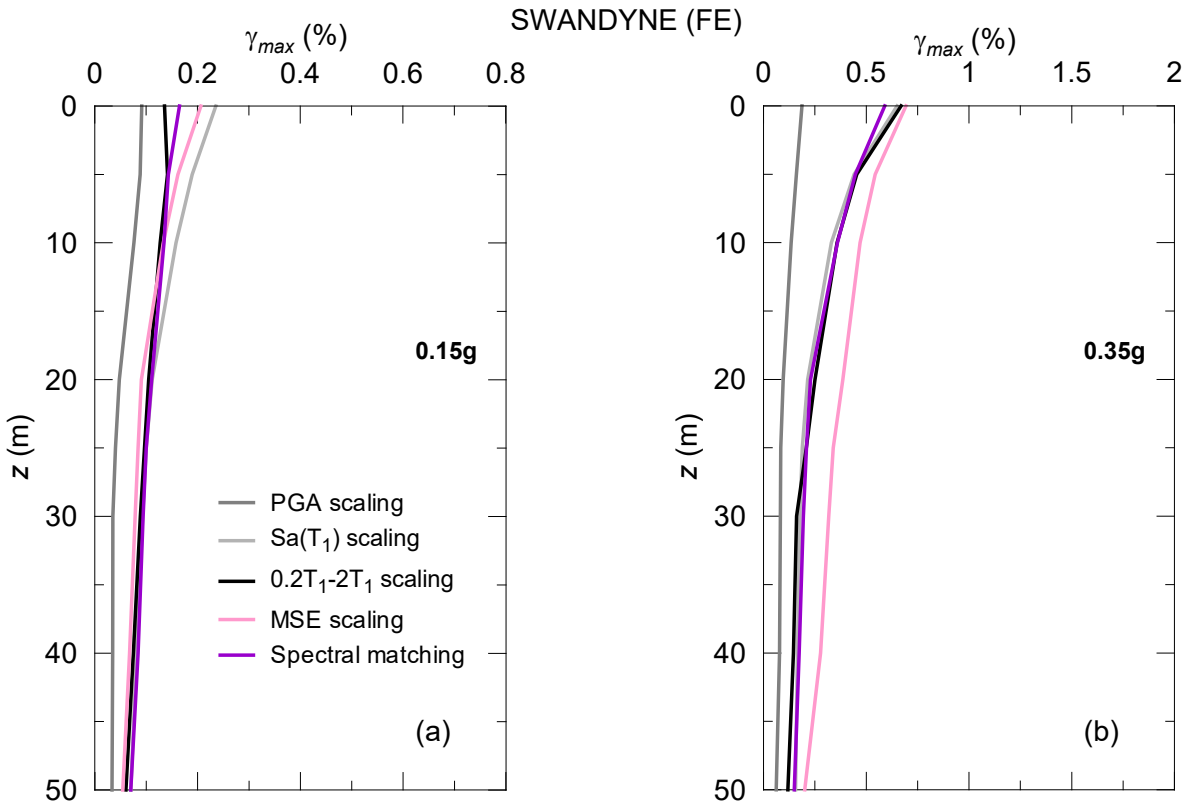

Figure 5.7 Replotting the shear strain profiles for each selection strategy based on maximum difference between two adjacent strain peaks in the shear strain-time histories (i.e. consideration of ratcheting behaviour).

By using this method, the median shear strain profiles for each selection strategy at lower and higher seismic intensity levels are recalculated and plotted in Figure 5.7a-b, respectively. At the lower seismic intensity, the recalculated strain profiles do not diverge considerably from the previous plots given in Figure 5.6c as opposed to the obvious decline, particularly at the ground surface, in the maximum strain levels (Figure 5.6d against Figure 5.7b) at the higher seismic intensity level. This is due to the fact that the higher the seismic intensity level of the input motion, the greater nonlinear behaviour and, thus greater permanent shear strain is expected to be accumulated. On account of that, the difference between the two approaches in the calculation of the maximum shear strain producing maximum hysteretic loop becomes even more obvious when the seismic intensity level of the input motion is relatively greater.

The shear strain-time histories and shear stress-strain curves of two individual earthquake events with lower and higher seismic intensity levels are represented in Figure 5.8 and Figure 5.9, respectively. The backbone curves for the low intense input motions exhibit less nonlinear behaviour as it can also be clearly seen in their shear strain-time histories with a

comparably small amount of permanent strains. However, the ratcheting soil behaviour under the 0.35g seismic input motions is more than evident from the shear strain histories as well as from the backbone curves. Hence, the method used in the calculation of the maximum strain level giving the highest damping seems to be more accurate approximation than considering the absolute maximum strain value.

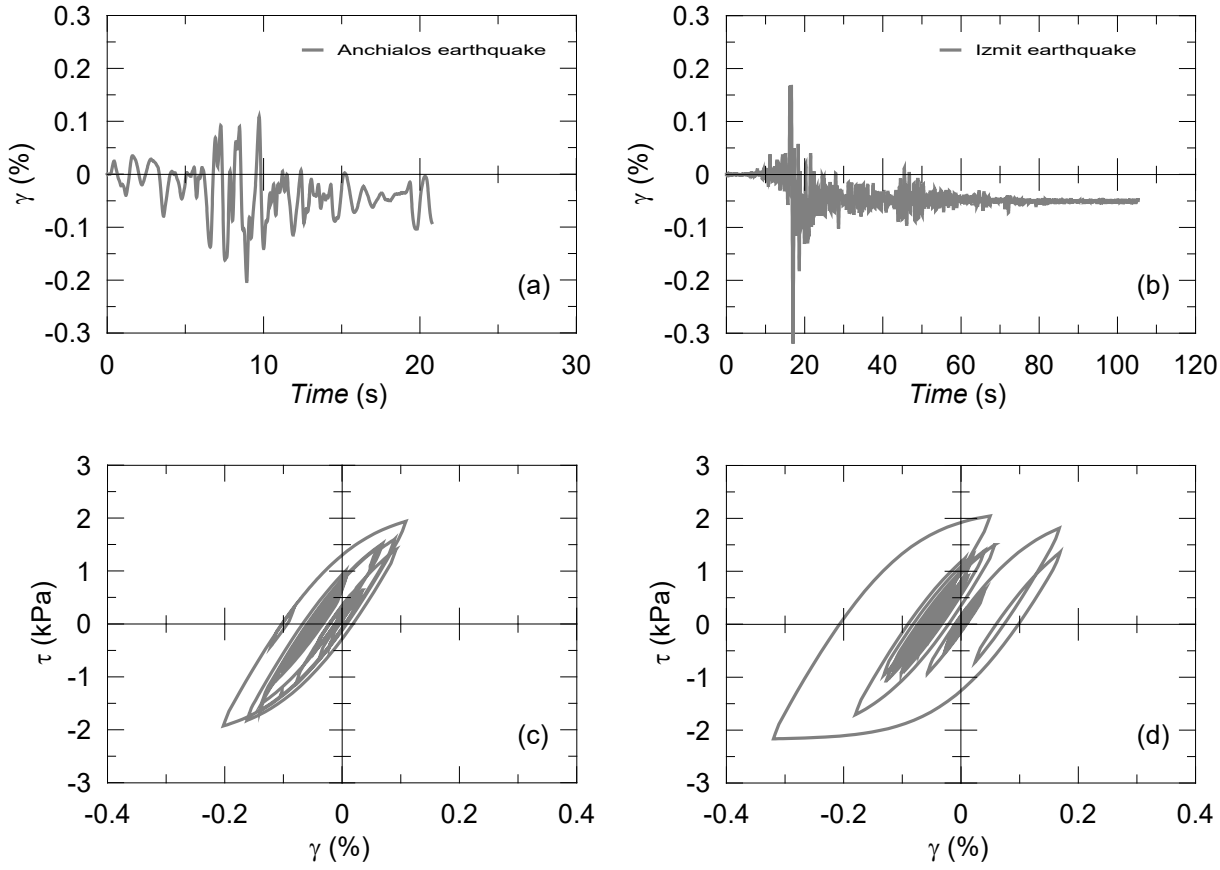

Figure 5.8 Shear strain-time histories (a-b) and backbone curves (c-d) for Anchialos (30/4/1985) and Izmit (17/8/1999) earthquake events from nonlinear site response analyses at 0.15g seismic intensity level.

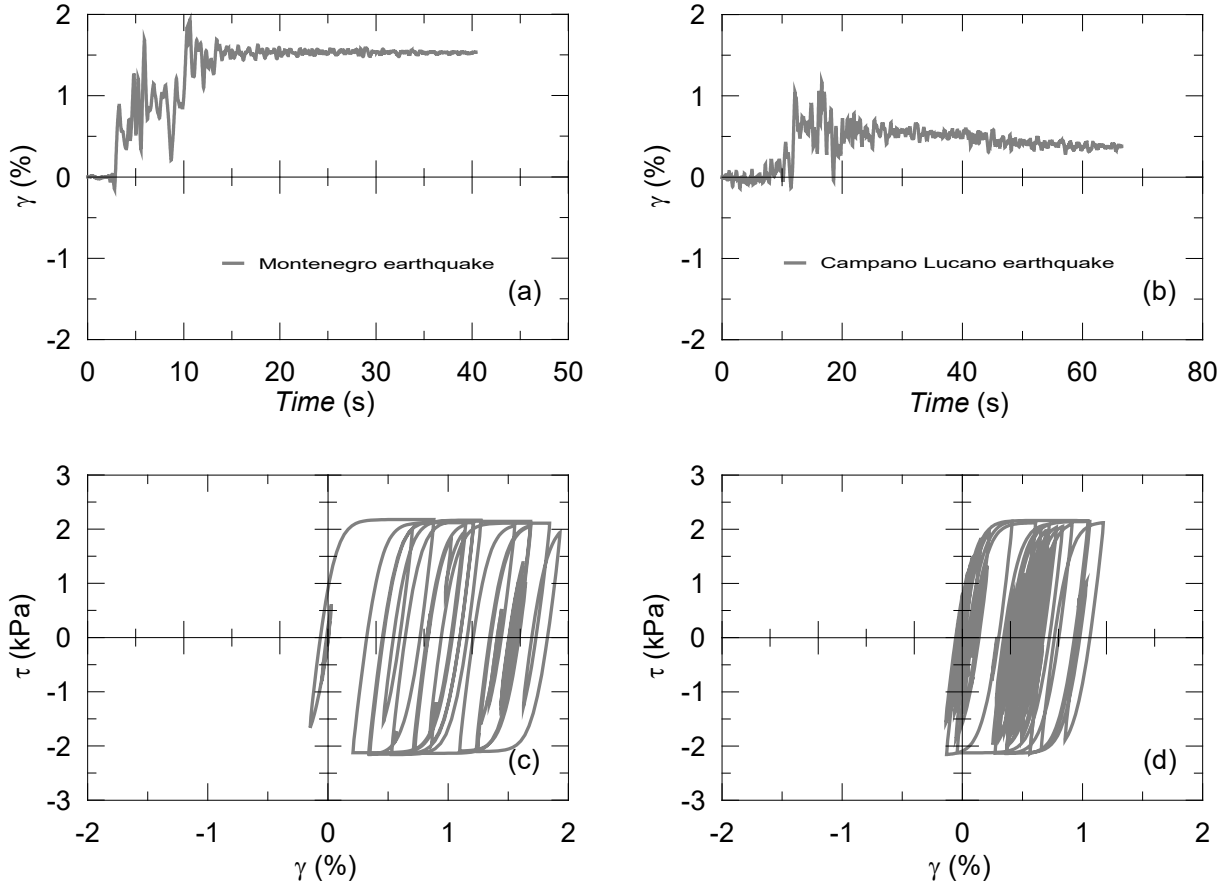

Figure 5.9 Shear strain-time histories (a-b) and backbone curves (c-d) for Montenegro (15/4/1979) and Campano Lucano (23/11/1980) earthquake events from nonlinear site response analyses at 0.35g seismic intensity level.

To show the limitation of the equivalent linear method in the site response prediction, the shear strain-time histories and shear stress-strain curves of the same earthquake events are plotted in Figure 5.9 and Figure 5.10. The permanent shear strain is not well captured as it always converges to zero at the end of the analyses. Although the method produces viscous damping at both seismic intensities, it does not represent the ratcheting soil behaviour, especially at the higher seismic intensity. While the EERA is still acceptable when the low intense input motion is simulated, it is better to adopt, as it is always suggested, a nonlinear effective stress approach to simulate high intense input motions.

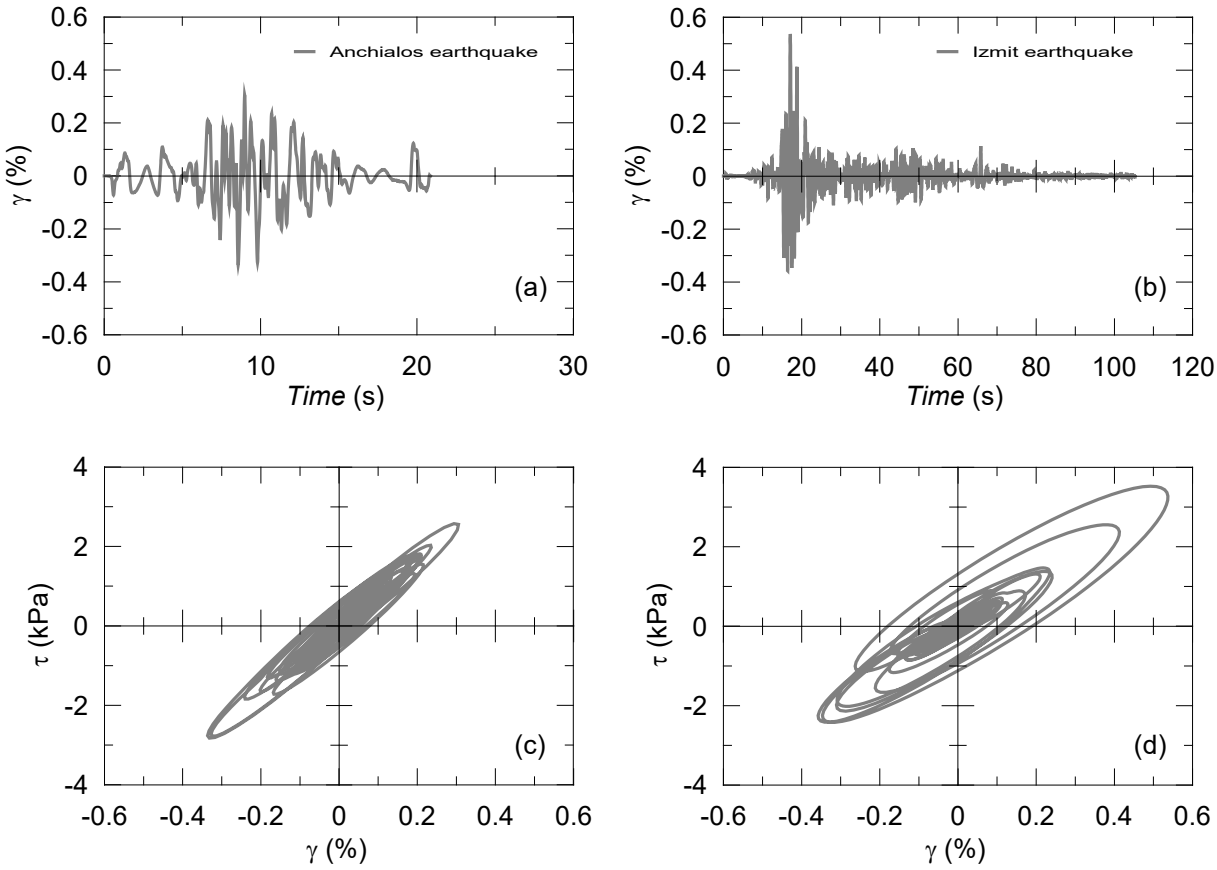

Figure 5.10 Shear strain-time histories (a, b) and backbone curves (c, d) for two individual earthquake events from equivalent linear site response analyses at 0.15g seismic intensity level.

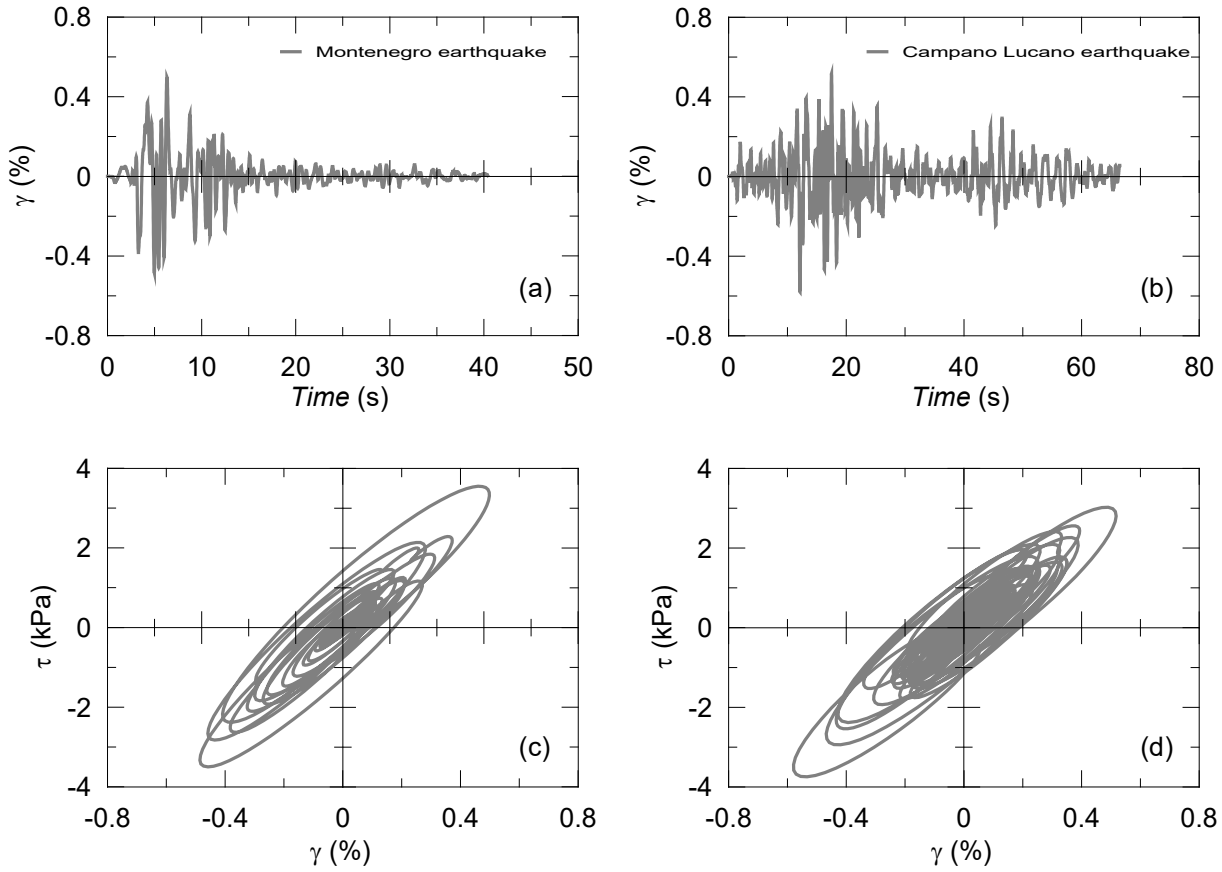

Figure 5.11 Shear strain-time histories (a, b) and backbone curves (c, d) for two individual earthquake events from equivalent linear site response analyses at 0.35g seismic intensity level.

5.4.3 Proxy of the EC8 design response spectrum

EC8 design response spectrum for a class D soft soil does not seem to be a good representation of a probable future earthquake event since the spectral peaks are not captured at the lower seismic intensity level (Figure 5.5c). Nevertheless, for an earthquake event with the 0.35g seismic intensity level, it captures well the predicted surface response spectra, even though the amplification at around T_1 is still not fully represented as demonstrated in Figure 5.5d. This case of EC8 design response spectrum becoming a better proxy for an earthquake event with the higher seismic intensity level is also highlighted in the study of Pitilakis *et al.* (2012) . They have used real input motions recorded on soil class C and categorized them into three groups; one includes all the records, the second group is records with PGA greater than 2 m/s^2 and the last one contains records having PGA greater than 15 m/s^2. They found that with the increase in the intensity level of the input motion, EC8 design response spectrum for soil class C becomes more conservative.

EC8 design response spectrum for soil class D also tends to be more conservative at higher seismic intensity levels, based on the predicted response spectra of the selection strategies. This trend is also demonstrated in Figure 5.12 with respect to the amplification factors (AF) in which higher amplification is obtained by analysing the input motions with 0.15g seismic intensity levels in comparison with those from 0.35g seismic intensity levels. It should be noted that AF is the ratio at the same ordinates between spectral accelerations at the ground surface and those at the bedrock level.

The selection strategies give similar amplification over the engineering period range at the higher intensity level while only the amplification factors from PGA and MSE scalings differ from the other three selection strategies. The reason of attaining relatively less amplification with MSE scaling strategy is due to considerable dispersion between spectral peaks as expressed in Section 5. The case with PGA scaling, however, is that the selected input motions based on this strategy include energy concentrated more in the shorter periods (between 0 and 0.5 seconds, as seen in Figure 5.2 and Figure 5.3). When they are propagated through the layers of a soft clay deposit, the earthquake energy shifts to the longer periods with some amplification. On account of that, the ratio between the spectral values at a single period above 0.5 s becomes far greater than those from the other selection strategies. Importantly, this diversion of spectral amplification of PGA scaling from those of the other selection strategies is not taken place at the lower seismic intensity levels attributing, probably, to the less nonlinearity and, thus no energy shift.

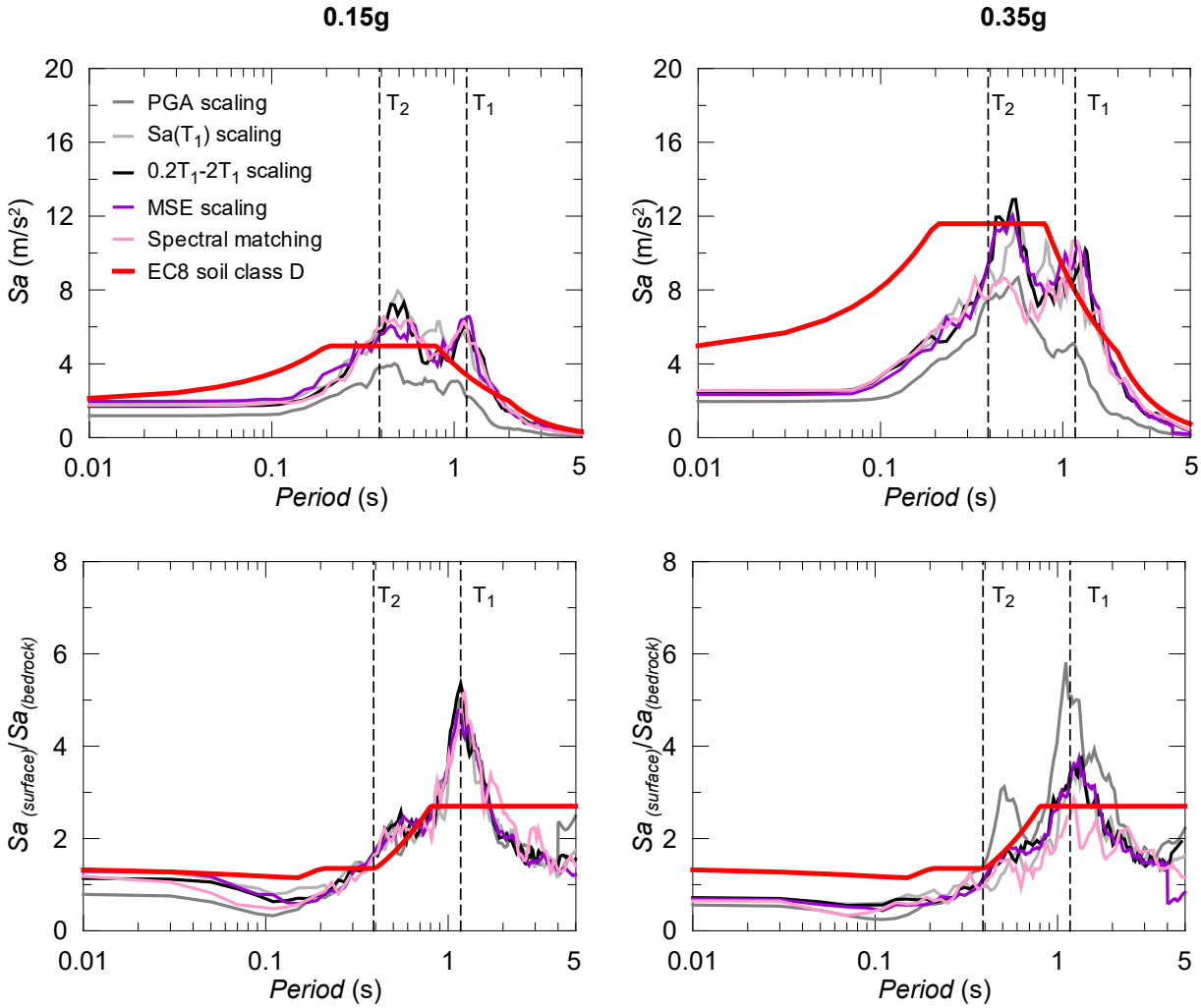

Figure 5.12 Amplification factors obtained from each selection strategy at 0.15g and 0.35g seismic intensity levels.

Maximum amplification factors in Figure 5.12 can be used to identify the soil factor (S) for each selection strategy. However, these values cannot truly describe the soil factor since the spectral accelerations do not only exhibit amplification from bedrock motion to the motion of softer soils but also show alteration in the period ordinates of the plateau, (i.e. the motion at the softer soil has wider plateau over longer periods when the bedrock motion has narrower plateau over shorter periods) (Rey *et al.*, 2002). In order to consider this change in the S calculation, spectral shape ratio (SR) is determined. SR is the ratio of the areas under the response spectrum normalised with the distance (R) (which is the distance between station and fault point, otherwise it is epicentral distance) between 0.05 s to 2.5 s at the ground surface and at the bedrock level, seen in Equation 5.3. This formulation of SR is originally given by Housner (1952) for spectral velocities. Soil factor is computed by dividing the amplification factor to the SR value, shown in Equation 5.4 (Pitilakis *et al.*, 2012).

$$AF = \frac{Sa\ at\ the\ surface}{Sa\ at\ the\ bedrock} \tag{5.2}$$

$$SR = \frac{\int_{0.05}^{2.5} R.Sa(t)dt\ at\ the\ surface}{\int_{0.05}^{2.5} R.Sa(t)dt\ at\ the\ bedrock} \tag{5.3}$$

$$soil\ factor\ (S) = \frac{amplification\ factor\ (AF)}{spectral\ shape\ factor\ (SR)} \tag{5.4}$$

Table 5.5 demonstrates the calculated SR and S values for each selection strategy at 0.15g and 0.35g seismic intensity levels with the EC8 recommendation. Although, two different seismic intensities are considered for the input motions of the selection strategies, the type of the target response spectra and the soil type are the same; Type 1 and soil class D, respectively. Hence, it is anticipated to obtain roughly same values of S factors in both seismicity levels at least within each selection strategy. This consistency is achieved when $0.2T_1$-$2T_1$ scaling and spectral matching strategies are applied. Additionally, their S values are similar comparing with those obtained from the other selection strategies. This similarity is also retained when different levels of seismic intensities are taken into consideration with $0.2T_1$-$2T_1$ scaling and spectral matching strategies as shown in Table 5.5 giving S values around 2.2 and 2.1, respectively. Nonetheless, neither of the S values from the selection strategies acknowledges the value recommended by EC8 for a soft class D soil confirming the study of Pitilakis *et al.* (2012) who found S value greater than EC8 suggested.

Selection strategy	Spectral shape ratio (SR)		Soil factor (S)	
	0.15g	0.35g	0.15g	0.35g
PGA scaling	1.9	1.6	2.7	3.6
Sa(T_1) scaling	2.20	2.0	2.1	1.7
$0.2T_1$-$2T_1$ scaling	2.1	1.7	2.4*	2.2*
MSE scaling	2.2	1.5	2.4	1.9
Spectral matching	2.3	1.8	2.1*	2.1*
EC8 suggestion	2.05 (calculated)		1.35	

Table 5.4 SR and S values for each selection strategy along with EC8 recommendation.

Seismic intensity	SR		S	
	$0.2T_1$-$2T_1$ scaling	Spectral matching	$0.2T_1$-$2T_1$ scaling	Spectral matching
0.15g	2.1	2.3	2.4	2.1
0.2g	2.1	2.1	2.3	2.1
0.25g	1.9	1.9	2.2	2.1
0.3g	1.9	1.9	2.4	2.1
0.35g	1.7	1.8	2.2	2.1

Table 5.5 SF and S values at different seismic intensity levels based on $0.2T_1$-$2T_1$ and spectral matching strategies.

Figure 5.13 indicates the spectral responses of the 50 m soft soil deposit under input motions with different seismic intensity levels. Input motions are modified according to $0.2T_1$-$2T_1$ scaling and spectral matching strategies. It is clear that the EC8 design response spectrum may not be able to capture the spectral responses at around T_1 at all seismic intensity levels. This is, in particular, true for 0.15g and 0.2g seismic intensity levels. The spectral peaks at around T_2 are also not represented by the code design spectrum at these two seismic intensities. However, at the higher seismic intensity levels (rather than these two) the spectral peaks are well captured by the design response spectrum.

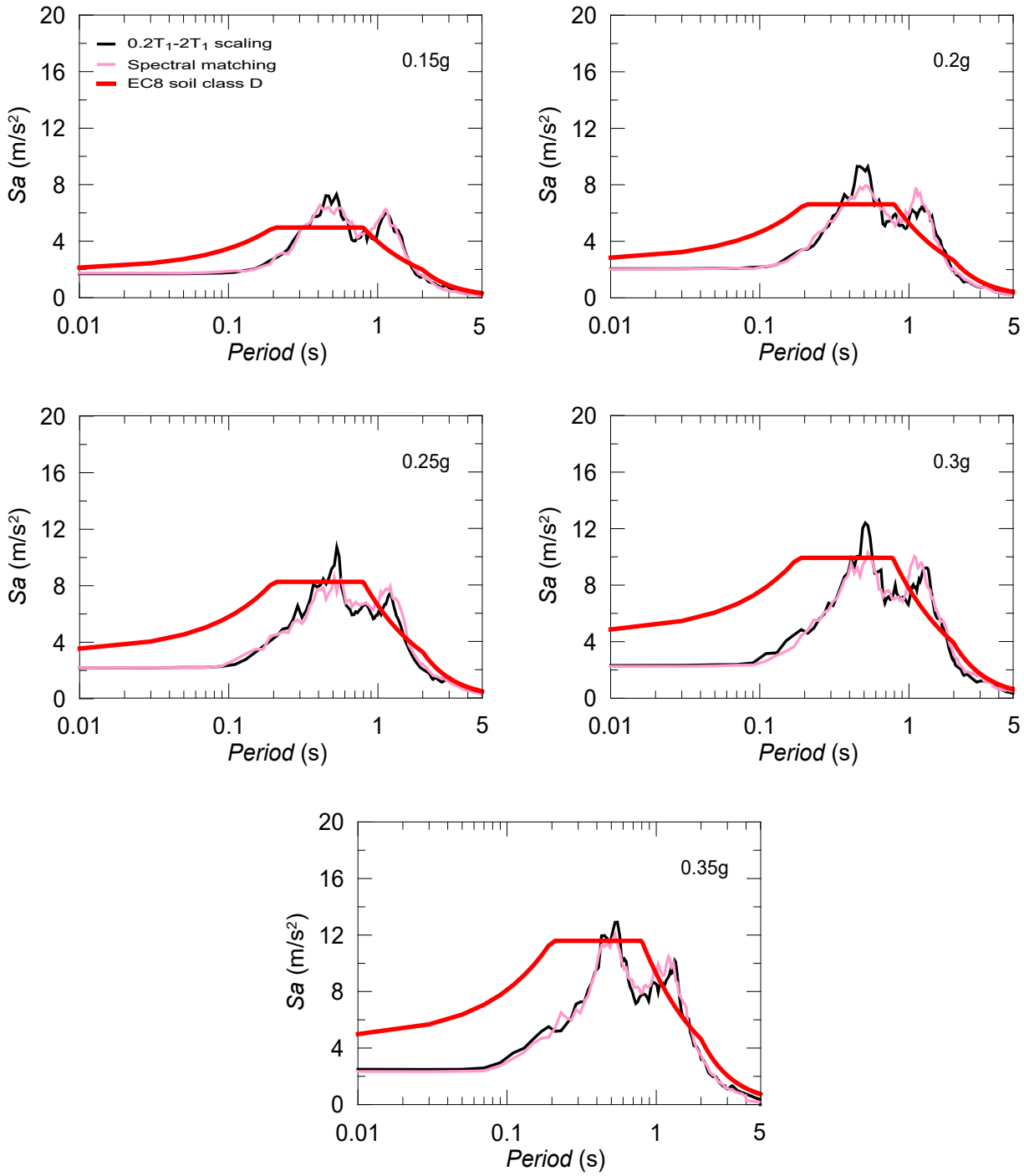

Figure 5.13 Representativeness of EC8 Type 1 design response spectrum for a soil class D at different seismic intensity levels.

In addition to the testing of the soil factor given by EC8 for class D soil deposit at two different Type 1 seismic intensity levels, soil deposits with different depths are also simulated to further examine the design response spectrum. As spectral matching modifies the frequency content of the input motions, only $0.2T_1$-$2T_1$ scaling is utilised. From the interpretations noted above in this section, this selection strategy is the best alternative to spectral matching amongst the remaining earthquake selection strategies.

25 m, 30 m, 40 m, 50 m, 60 m, 80 m and 100 m soil deposits are simulated using 0.15g and 0.35g input motions, selected according to $0.2T_1$-$2T_1$ scaling. At the lower intensity level, the surface spectral responses from the nonlinear analyses of 25 m and 30 m soil deposits show amplifications over the plateau of design response spectrum. As highlighted before, even though the natural periods of these two soil deposits lie below the plateau, the design response spectrum does not capture the spectral peaks. When the soil depth is increased, the natural period becomes greater. This implies that the spectral peak may no longer be observed at the plateau of the design response spectrum, where the maximum spectral acceleration is considered. This can be seen in Figure 5.14 for soil deposits with 40 m or more depths that the spectral peaks at the first two natural periods cannot be represented for the low intense input motions.

The spectral predictions from the nonlinear analyses of soil deposits at the higher seismic intensity level are given in Figure 5.15. The EC8 design response spectrum seems to be a good proxy for the 0.35g input motions when 25 m, 30 m and 40 m soil deposits are simulated. If the input motions propagated in 50 m and above soil deposits, the EC8 design response spectrum is not able to cover the spectral peaks at around T_1. However, the peaks at the second natural periods are well captured as the earthquake energy is dissipated at high frequencies. In the meantime, spectral values at the longer periods are exposed to greater amplifications due to the characteristics of deep soil deposits.

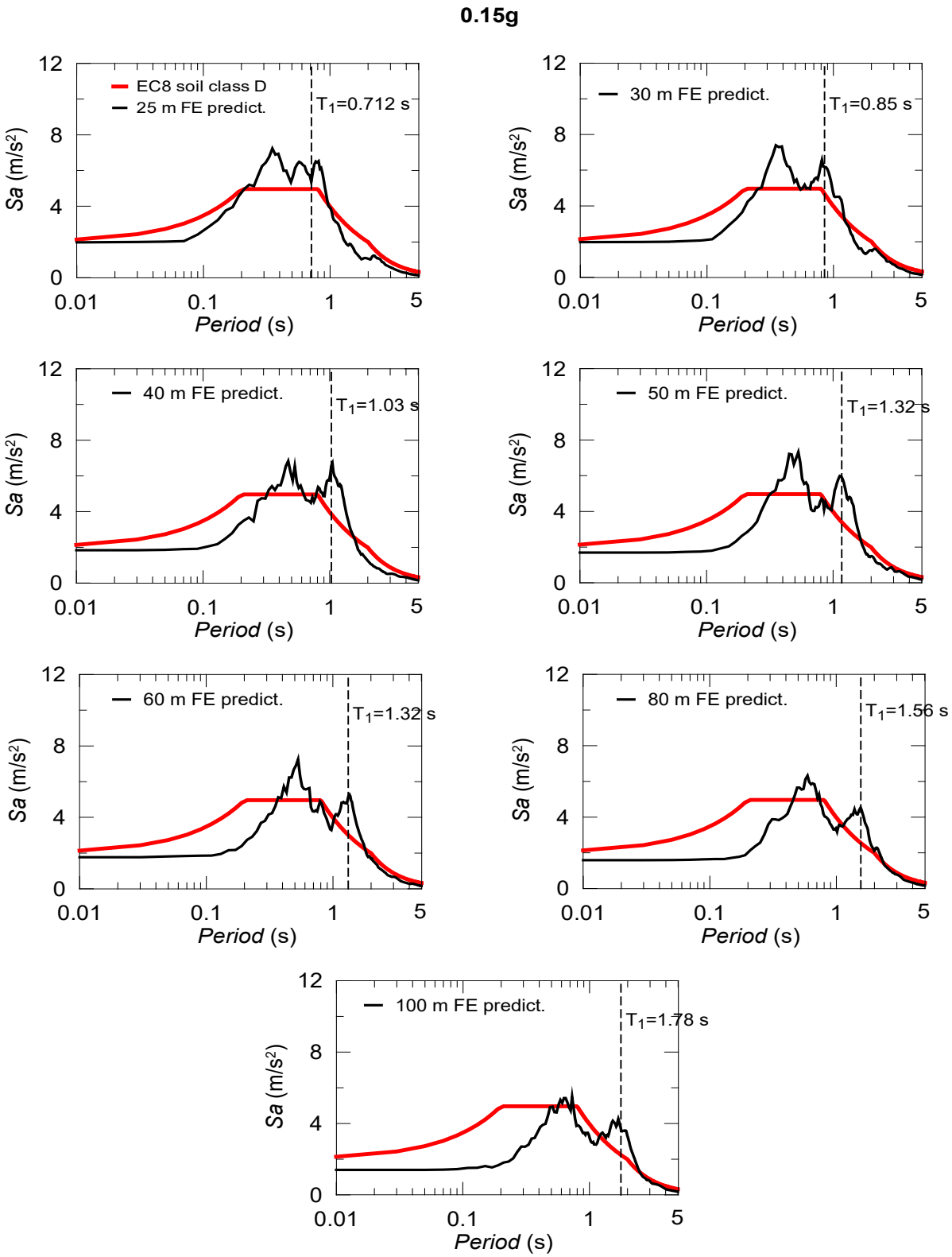

Figure 5.14 Median spectral response predictions from the nonlinear analyses of depth varied soil deposits against EC8 design response spectrum for a soil class D at 0.15g seismic intensity level.

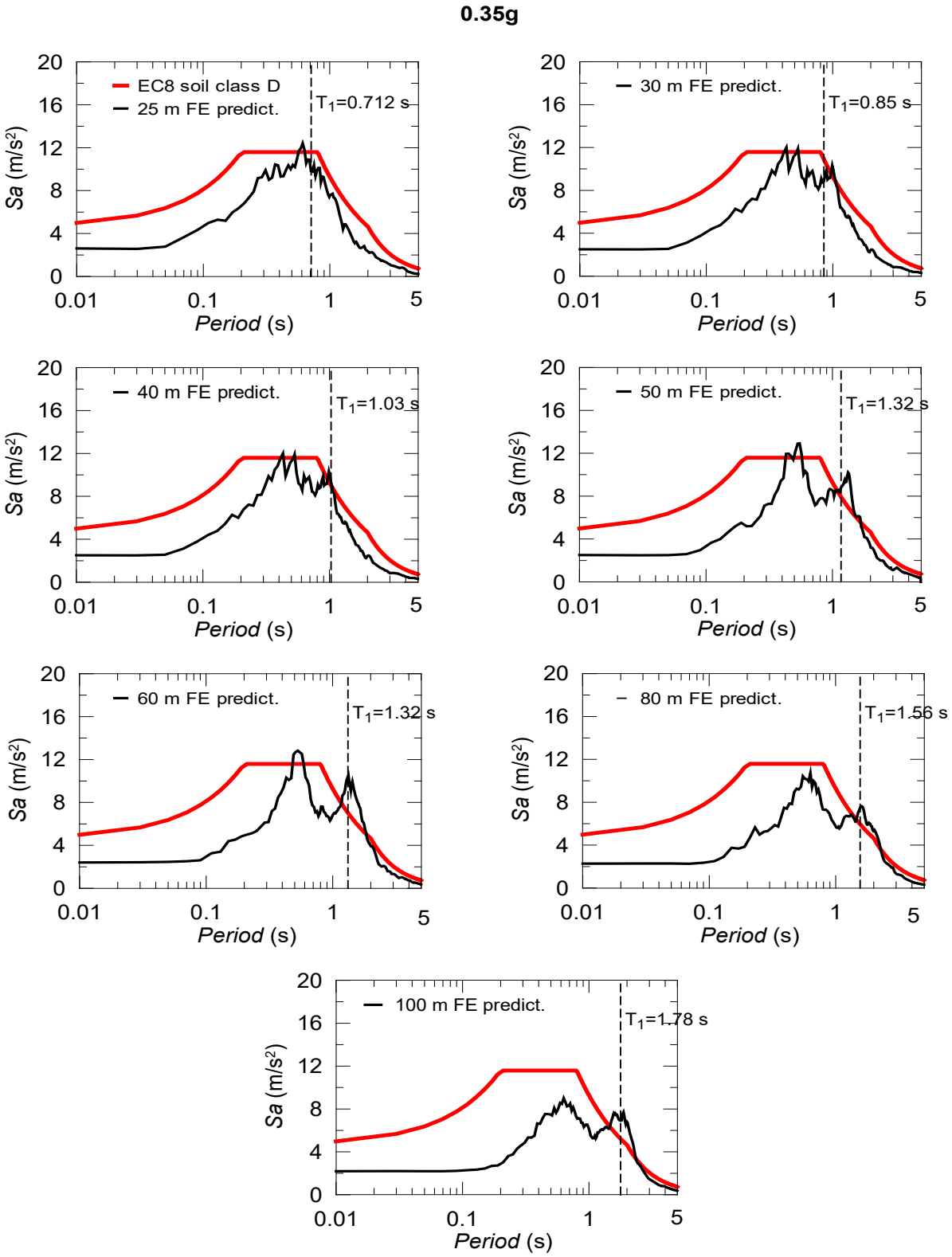

Figure 5.15 Median spectral response predictions from the nonlinear analyses of depth varied soil deposits against EC8 design response spectrum for a soil class D at 0.35g seismic intensity level.

5.4.4 EDPs at ground surface

The earthquake selection strategies are also analysed with respect to the EDPs (relative displacement, PGA and $Sa(T_1)$) at the ground surface at both seismic intensity levels. Relative displacement, PGA and $Sa(T_1)$ responses are presented in Figure 5.16a-b, c-d and e-f, at 0.15g and 0.35g seismic intensities, respectively. The blue circles in Figure 5.16 represent the responses from individual input motions, red circles show the mean value, upper and lower dotted lines exhibit mean plus one and mean minus one standard deviation within each selection strategy. Discussing the selection strategies with respect to EDPs enables to show the dispersions introduced by each strategy. This contributes to, in addition to the previous evaluations (e.g. in terms of median spectral responses and soil factors), the determination of the best selection strategy.

The nonlinear site response analyses under input motions selected based on PGA scaling produce EDPs considerably less than those from remaining selection strategies. However, the scaling strategy gives median PGA, one of the three EDPs, relatively similar to those predicted by the remaining selection strategies (Figure 5.16), especially at the higher seismic intensity level. This is due to the fact that PGA scaling focuses on the compatibility with the target response spectrum at only zero period, where the other selection strategies have similar PGA values, on an average basis.

The site response analyses obtained by using the remaining selection strategies give similar mean EDP responses at both seismic intensity levels. But, the EDPs represent distinguishably higher dispersion within a set of modified input motions according to MSE scaling as can be shown in Figure 5.16. This is more pronounced at the higher seismic intensity due to the soil nonlinearity effect causing more uncertainty into the site response prediction. The cause of this discrete level of dispersion, as expressed earlier in Section 5.4.1, can be attributed to the great scatter in the spectral peaks of the bedrock motions applied at the bottom of the soil deposit.

Noticeably, the EDPs associated with spectral matching are the least scattered responses at both seismic intensity levels. This is owing to the fact that it includes bedrock motions which are fully matched with the target response spectrum producing relatively more stable responses at the ground surface. Interestingly, $Sa(T_1)$ scaling introduces similar (or even less) variability in the EDP responses than that caused by $0.2T_1$-$2T_1$ scaling. This is more obvious in the responses of relative displacement and $Sa(T_1)$ at both seismic intensity levels. In this

respect, Sa(T_1) scaling seems to be as much convincing candidate in selection and modification of input motions as $0.2T_1$-$2T_1$ scaling in the site response analyses while the first preference can be spectral matching even though the alteration of the frequency content of the input motions is still questionable. The results presented in this study are consistent with the findings of Shome *et al.* (1998) and Iervolino and Cornell (2005), who investigated the variability of the EDP response during structural dynamic analyses. It is also known (e.g. Seifried and Baker (2016)) that the spectral matching procedure reduces the variance of the structural response due to variability of the earthquake records, thus providing a platform to estimate the mean response with fewer numbers of analyses. Nevertheless, the modification of the frequency content of the input motions through the spectral matching method does not produce ground motions representative of actual earthquake records.

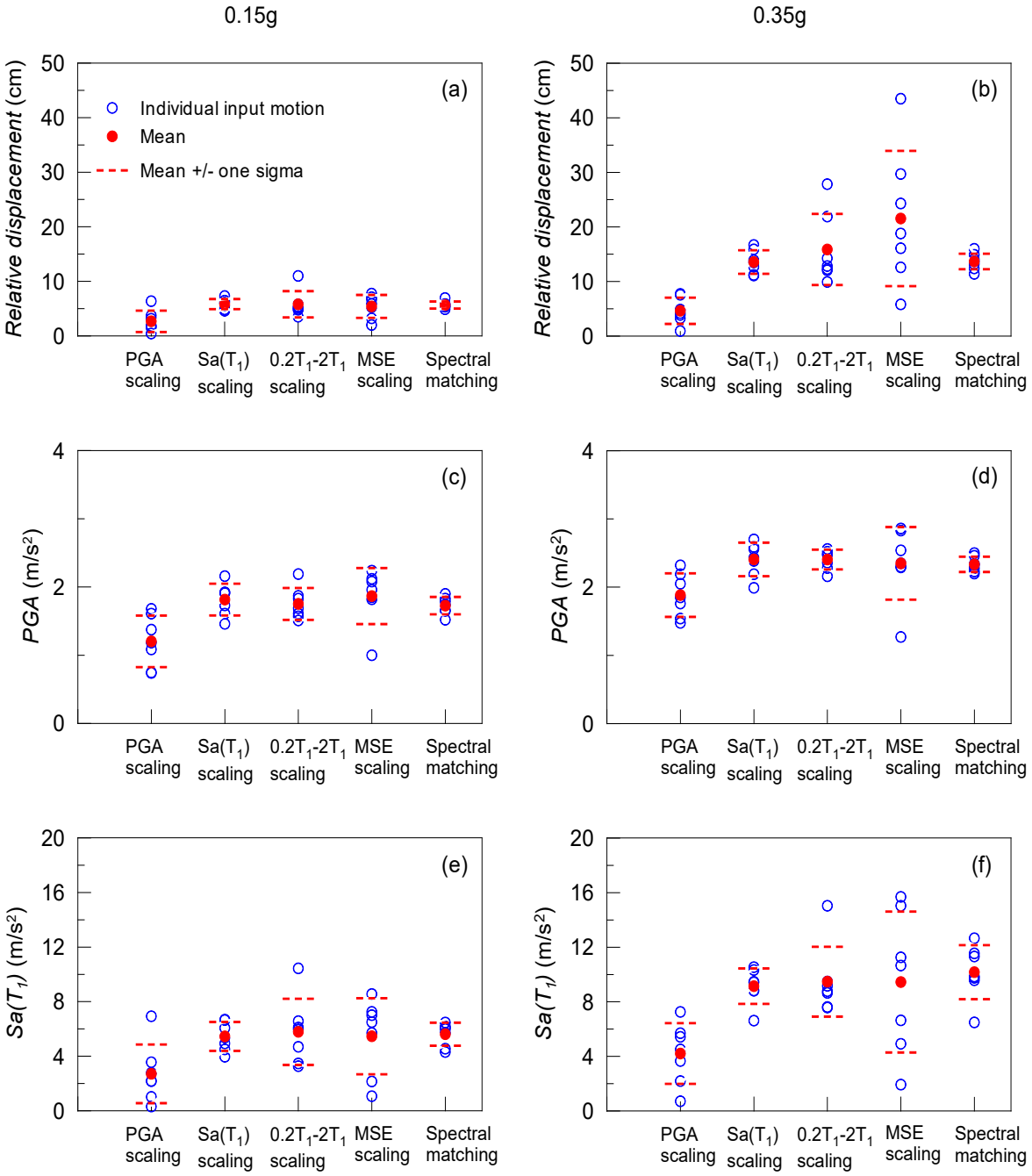

Figure 5.16 EDPs of the earthquake selection strategies at 0.15g (left) and 0.35g (right) seismic intensity levels obtained by using seven input motions, including mean and mean plus/minus one standard deviation.

5.4.5 Effects of number of bedrock motions

EC8 provides a lower limit for the number of input motions to be considered when one wants to consider average responses from the dynamic performance analyses. Based on this recommendation by EC8, in this research, seven input motions for each selection strategy are selected and modified to consider the mean responses from the nonlinear site response

analyses for comparison purposes. The assumption behind the consideration of seven input motions is that a stable mean response can be achieved and more than seven dynamic analyses may lead to an approximately identical mean response. In order to test this assumption in the site response analyses, 14 input motions modified according to each selection strategy are simulated.

As can be seen in Figure 5.17 and Figure 5.18, increasing the number of input motions to 14 does not provide considerably different spectral response predictions at the ground surface for all the selection strategies in both seismic intensity levels. 14 number of analyses gives similar response spectra, especially for $0.2T_1$-$2T_1$ scaling, MSE scaling and spectral matching strategies. The similarity becomes more obvious for these selection strategies at the higher seismic intensity level with relatively well-matched spectral peaks. However, it is less likely to catch same similarity by adopting PGA scaling and $Sa(T_1)$ scaling strategies since the average compatibility with the target response spectrum is only achieved at a single period. Hence, there is no control mechanism that will lead to selection and modification of the input motions with similar spectral values at the other periods. In contrast, the other three selection strategies seek compatibility with the target response spectrum at a certain or entire period range, which, ultimately leads to similar responses with consideration of seven and 14 number of input motions.

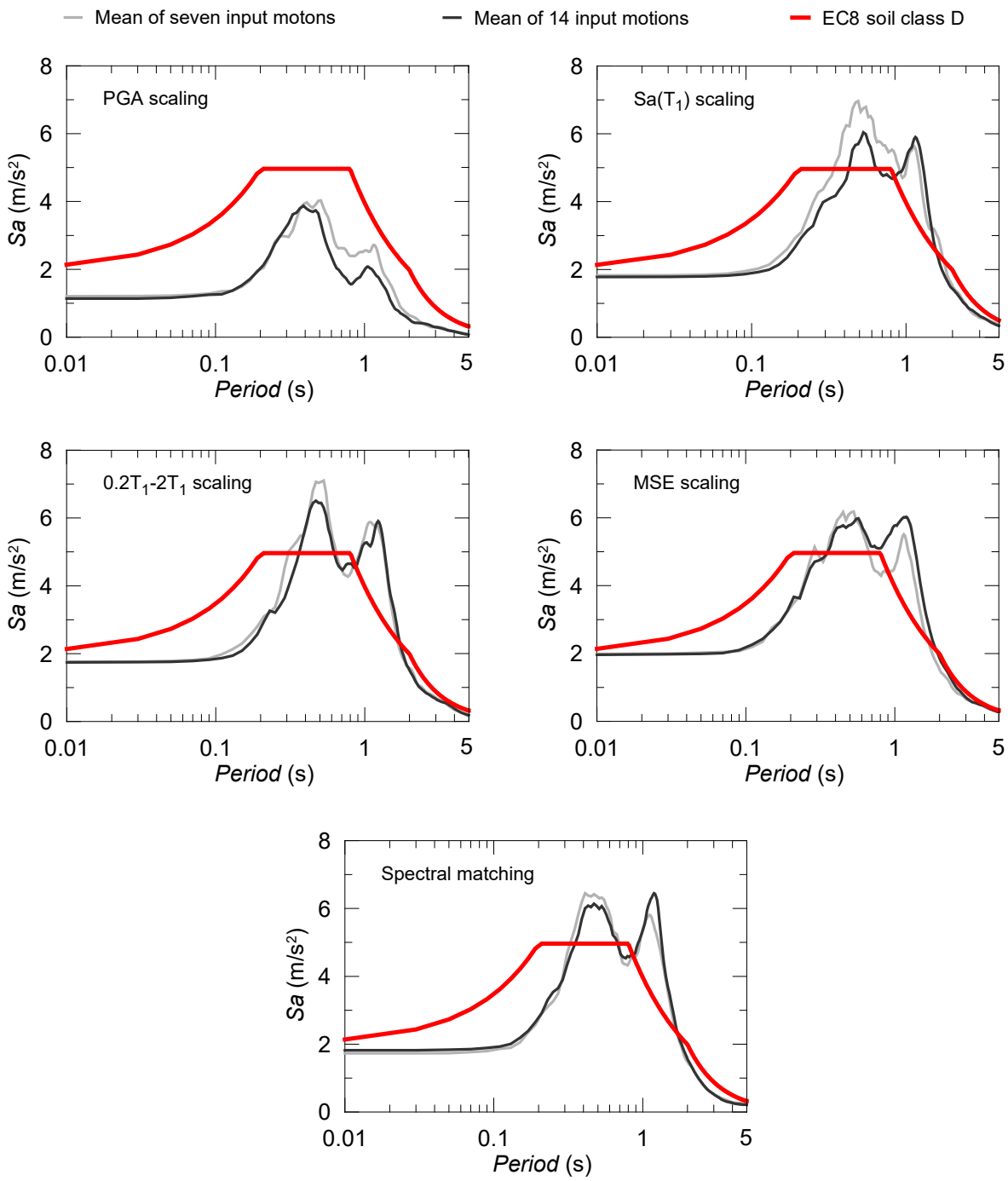

Figure 5.17 Effect of increasing the number of bedrock motions on the ground surface response spectra with 0.15g seismic intensity level.

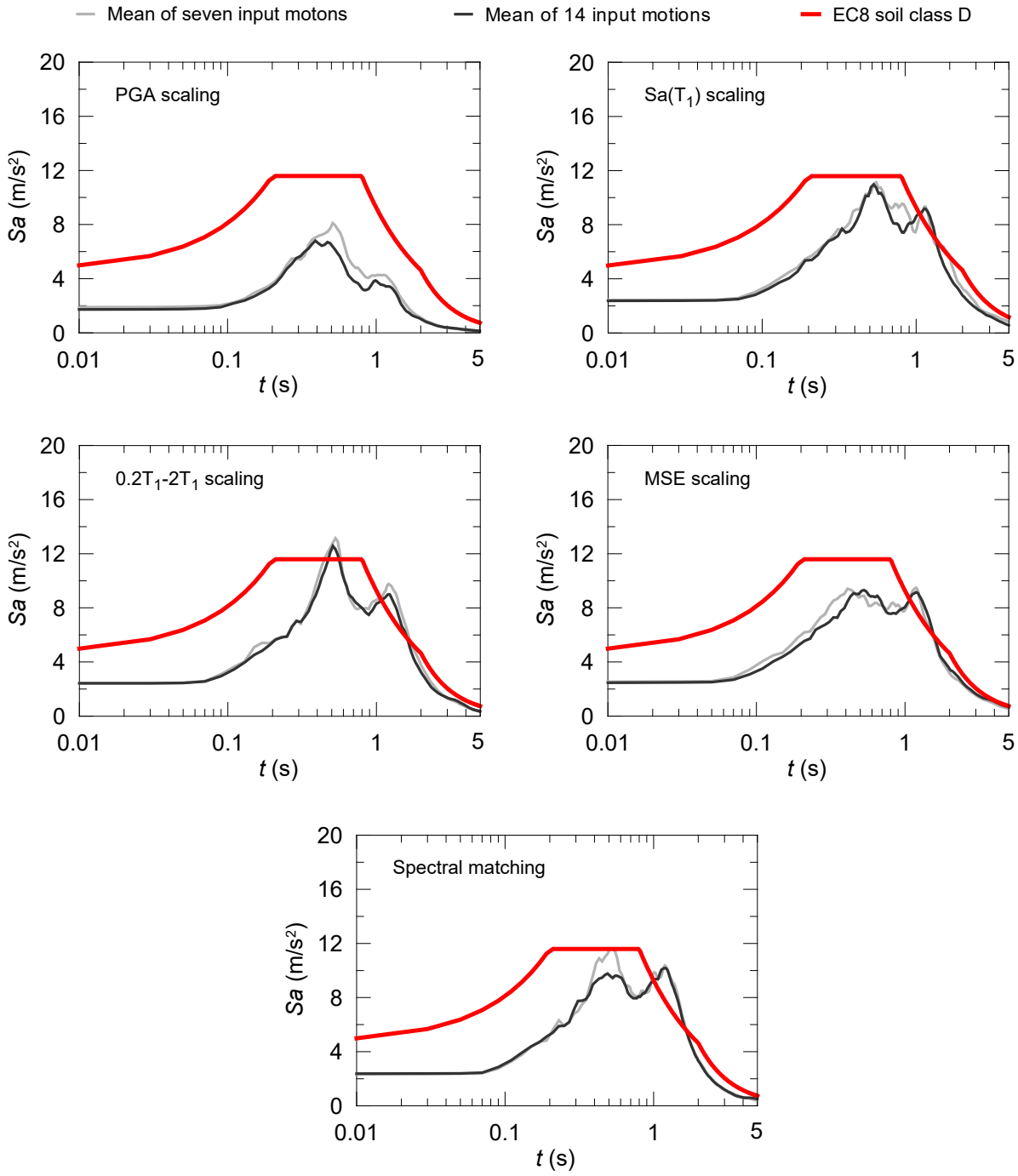

Figure 5.18 Effect of increasing the number of bedrock motions with 0.35g seismic intensity level on the ground surface response spectra with 0.35g seismic intensity level.

In terms of EDPs, Figure 5.19 represents the individual responses of 14 input motions for each selection strategy along with mean and mean plus/minus one standard deviation. Furthermore, Figure 5.20 is plotted to make the changes in standard deviations more apparent. It indicates the level of dispersion between the standard deviation of EDPs from seven and 14 input motions and calculated based on following formula:

$$\Delta\sigma(\%) = \frac{\sigma_7 - \sigma_{14}}{\sigma_7} \times 100$$

The figures at first, second and third rows of Figure 5.20 show the results for relative displacement, PGA and Sa(T_1), respectively. Also, the figures at first and second columns are indications of results for 0.15g and 0.35g seismic intensities. The plots below the zero axis points out that the standard deviation of seven input motions is less than that of 14 input motions (Case 1). When the plots are above the zero axis it is otherwise (Case 2).

For the results in terms of relative displacement, only Sa(T_1) scaling and MSE scaling leads to the Case 1 at 0.15g seismic intensity. In addition, PGA scaling, Sa(T_1) scaling and spectral matching suits to that case at 0.35g seismic intensity. For the two remaining EDPs, MSE scaling always cause the Case 2 in both seismic intensities and it is followed by PGA scaling and $0.2T_1$-$2T_1$ scaling for Sa(T_1) only at 0.15g seismic intensity. From these observations, it can be interpreted that increasing the number of input motions to 14 can reduce the standard deviation when MSE scaling is applied. Otherwise, this cannot be valid for the remaining selection strategies, especially when PGA and Sa(T_1) is considered as EDPs.

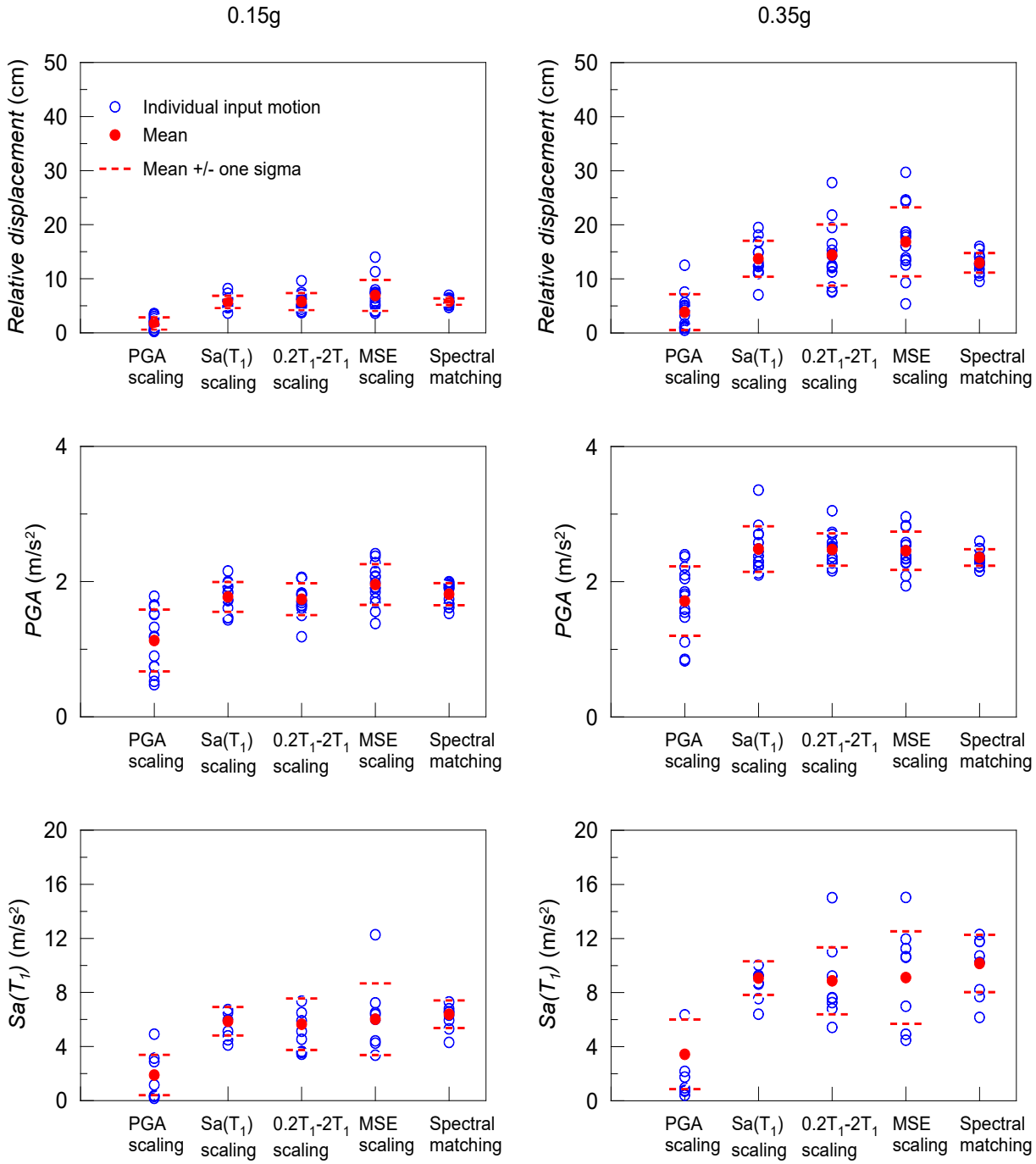

Figure 5.19 EDPs of the earthquake selection strategies at 0.15g (left) and 0.35g (right) seismic intensity levels obtained by using 14 input motions, including mean and mean plus/minus one standard deviation.

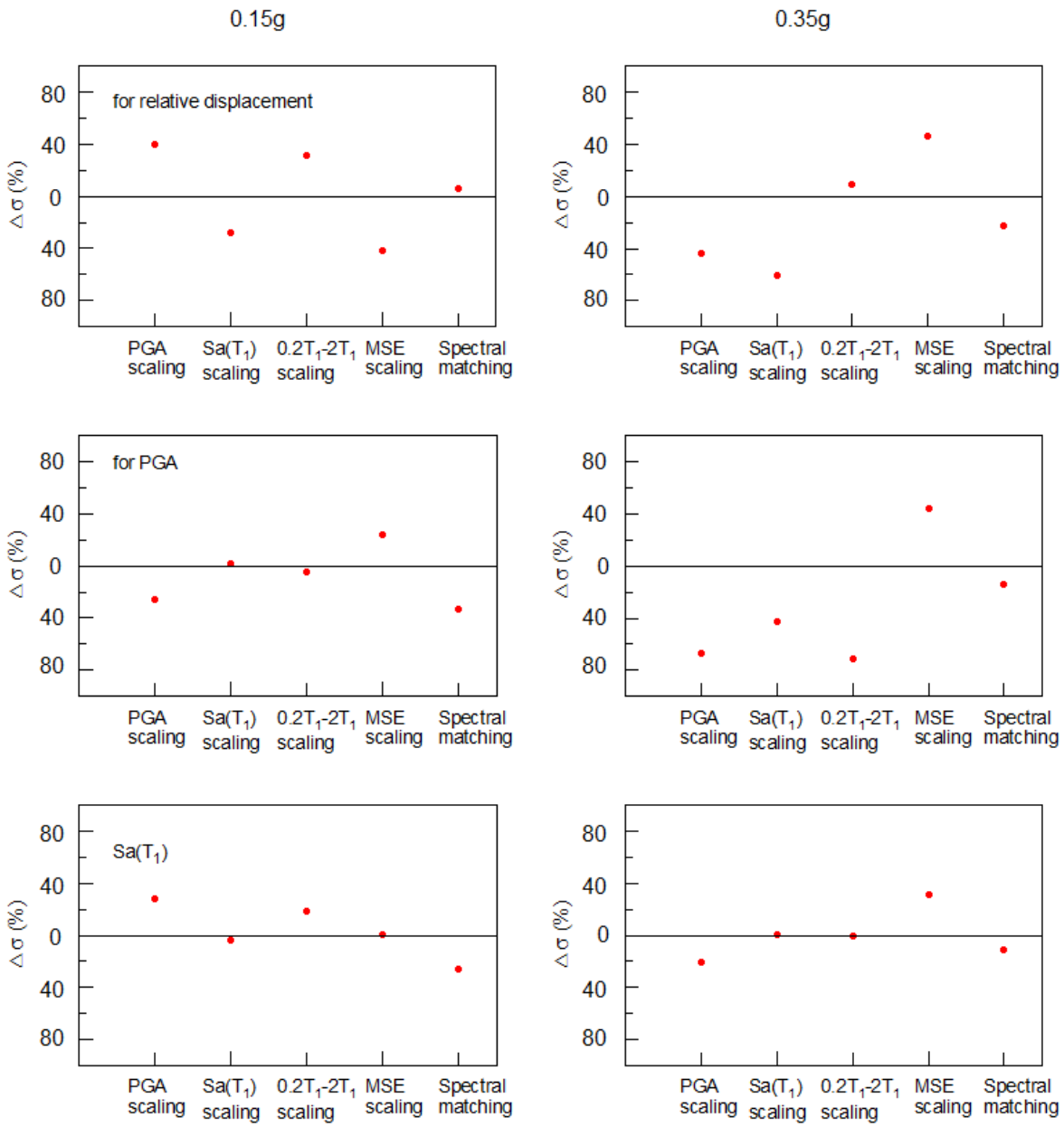

Figure 5.20 Standard deviations (σ) of seven and 14 response analyses conducted by applying different selection strategies.

Overall, seven input motions can be adequate to get stable site response spectra at the ground surface, when $0.2T_1$-$2T_1$ scaling, MSE scaling and spectral matching strategies are applied. For the other selection strategies, in particular, PGA and $Sa(T_1)$ scaling strategies, it might not be possible to obtain similar response spectra due to spectral compatibility conditions. It also seems that, based on EDPs, there is no need of increasing the number of input motions more than seven, when spectral matching, $0.2T_1$-$2T_1$ scaling or $Sa(T_1)$ scaling strategies are considered, since this does not clearly reduce the variability in the responses at the ground surface.

5.5 Hypothesis Test

In order to assess site response predictions according to the earthquake selection strategies in terms of the extent of the median EDP responses can be seen as equal, hypothesis tests are conducted. The median EDPs are checked with Shapiro and Wilk (1965) test for log-normal distributions and confirmed that it cannot be rejected at 95% significance level.

A two-tail Aspin-Welch (Welch, 1938) test is utilised to check the null hypothesis that the median EDP of one selection strategy is equal to that of the any other one at the same seismic intensity level, an alternative hypothesis is they are not equal. The test is preferred to the Standard t-test since the variances in the populations are assumed not equal. The p-value is computed by using the below Equation 5.4, in which y_1 and y_2 are the sample means, s_1 and s_2 are the sample standard deviations and n_1 and n_2 are the sample sizes. With the null hypothesis, the n-1 degrees of freedom with t-distribution is considered in the test.

$$t = \frac{y_1 - y_2}{\sqrt{\frac{s_1}{n_1} + \frac{s_2}{n_2}}} \tag{5.4}$$

Table 5.6 and Table 5.7 represent the computed p–values for pairs of selection strategies. Since 95% significance level is considered, the p-values less than 0.05 in the tables reject the null hypothesis and those higher than that do not reject it.

1, 2, 3, 4 and 5 represent sets of input motions from PGA scaling, Sa(T_1) scaling, 0.2T_1-2T_1 scaling, MSE scaling and spectral matching, respectively.

		0.15g							0.35g						
		1	2	3	4	5			1	2	3	4	5		
for relative displacement	1	1.00						1	1.00						
	2	**0.00**	1.00					2	**0.00**	1.00					
	3	**0.02**	0.98	1.00				3	**0.00**	0.40	1.00				
	4	**0.03**	0.64	0.75	1.00			4	**0.01**	0.14	0.31	1.00			
	5	**0.01**	0.71	0.89	0.77	1.00		5	**0.00**	0.47	0.83	0.24	1.00		
for PGA	1	1.00						1	1.00						
	2	**0.00**	1.00					2	**0.01**	1.00					
	3	**0.01**	0.62	1.00				3	**0.00**	1.00	1.00				
	4	**0.01**	0.78	0.54	1.00			4	0.08	0.80	0.79	1.00			
	5	**0.01**	0.40	0.80	0.42	1.00		5	**0.01**	0.50	0.32	0.95	1.00		
For Sa(T_1)	1	1.00						1	1.00						
	2	**0.01**	1.00					2	**0.00**	1.00					
	3	**0.03**	0.75	1.00				3	**0.00**	0.77	1.00				
	4	0.06	0.99	0.82	1.00			4	**0.04**	0.88	0.99	1.00			
	5	0.01	0.76	0.86	0.89	1.00		5	**0.00**	0.28	0.58	0.74	1.00		

Table 5.6 Aspin-Welch test results for the EDPs of the earthquake selection strategies, each having seven rock input motions, at two seismic intensity levels, the p-values lower than 0.05 is in bold.

1, 2, 3, 4 and 5 represent sets of input motions from PGA scaling, Sa(T_1) scaling, 0.2T_1-2T_1 scaling, MSE scaling and spectral matching, respectively.

			0.15g							0.35g					
			1	2	3	4	5			1	2	3	4	5	
for relative displacement		1	1.00						1	1.00					1
		2	**0.00**	1.00					2	**0.00**	1.00				2
		3	**0.00**	0.92	1.00				3	**0.00**	0.70	1.00			3
		4	**0.00**	0.17	0.20	1.00			4	**0.00**	0.12	0.29	1.00		4
		5	**0.00**	0.85	0.97	0.17	1.00		5	**0.00**	0.46	0.38	**0.04**	1.00	5
for PGA		1	1.00						1	1.00					1
		2	**0.00**	1.00					2	**0.00**	1.00				2
		3	**0.00**	0.70	1.00				3	**0.00**	0.94	1.00			3
		4	**0.00**	0.08	**0.04**	1.00			4	**0.00**	0.21	0.12	1.00		4
		5	**0.00**	0.59	0.34	0.13	1.00		5	**0.00**	0.83	0.85	0.25	1.00	5
for Sa(T_1)		1	1.00						1	1.00					1
		2	**0.00**	1.00					2	**0.00**	1.00				2
		3	**0.00**	0.71	1.00				3	**0.00**	0.79	1.00			3
		4	**0.00**	0.20	0.22	1.00			4	**0.00**	0.11	0.15	1.00		4
		5	**0.00**	0.84	0.67	0.64	1.00		5	**0.00**	0.97	0.83	0.34	1.00	5

Table 5.7 Aspin-Welch test results for the EDPs of the earthquake selection strategies, each having 14 rock input motions, at two seismic intensity levels, the p-values lower than 0.05 is in bold.

As it is clearly shown in Table 5.6, the involvement of PGA scaling in a pair (seen in the first rows) causes rejection of the null hypothesis in all three EDP responses, giving p-values, mostly, less than 0.05. On the contrary, the median responses of the pairs from the other selection strategies do not reject the null hypothesis in any combination, indicating p-values distinctively higher than 0.05 in both seismic intensity levels.

The t-test is also conducted for the site responses from 14 input motions of earthquake selection strategies, keeping the null and alternative hypotheses same. The test results imply the same interpretations depicted above that the median responses from PGA scaling are not accepted as equal to those of the other selection strategies whose pairs do not refuse the null hypothesis, as shown in Table 5.7. However, one pair (Spectral Matching – MSE scaling) in relative displacement at the 0.35g seismic intensity level and one ($0.2T_1$-$2T_1$ scaling – MSE scaling) in PGA results at the 0.15g seismic intensity level also reject the null hypothesis. This is the result of introducing more bias into the site responses at the ground surface when the number of input motions is increased, as highlighted in Section 5.4.5.

While so far the influence of the selection strategies on the site responses (spectral acceleration, relative displacement, PGA and $Sa(T_1)$) is investigated, it is worth to look at the effect of the main characteristics of the bedrock input motions on the site responses at surface. For this aim, Arias intensity (I_A, m/s) and Dobry's duration ($D_{5\text{-}95}$) are considered as two of the main features of an input motion. While the former is a measure of an input motion showing the shaking intensity (Arias, 1970), the latter is a time interval within which 5% and 95% of the Arias intensity is obtained (Dobry *et al*., 1978). All the sets of seven and 14 bedrock motions for the earthquake selection strategies (105 input motions, in total for each selection strategy) are combined within the same seismic intensity level, ultimately the correlation test is conducted. The test relies on:

$$r = \frac{S_{xy}}{\sqrt{S_{yy}S_{xx}}} \tag{5.5}$$

$$S_{xy} = \sum_{i=1}^{n}(x_i - \bar{x})(y_i - \bar{y}) \tag{5.6}$$

$$S_{xx} = \sum_{i=1}^{n} (x_i - \bar{x})^2 \tag{5.7}$$

Once the sample correlation coefficient (r-value) is calculated, then, the test statistic considers Equation 5.8 to compute the population correlation coefficient:

$$\frac{r}{\sqrt{(1-r^2)/(n-2)}} \tag{5.8}$$

where n is the sample size, n-2 is degrees of freedom. The null hypothesis of the test is that there is not a significant correlation between I_A or $D_{5\text{-}95}$ of the input motions and the relative displacements (or PGA, or Sa(T_1)).

The p-values and the r-values of the tests are shown in Table 5.8. Again, the p-values less than 0.05 express that the null hypothesis is rejected, otherwise it is not rejected. The null hypothesis is only not rejected at the lower seismic intensity level when I_a correlation with the EDPs are checked. On the other hand, $D_{5\text{-}95}$ correlation tests with only the relative displacement at the lower seismic intensity level and Sa(T_1) at the higher seismic intensity level reject the null hypothesis.

In terms of correlation significance, the correlation coefficients of I_A with relative displacement and PGA are higher than those of $D_{5\text{-}95}$ with the same EDPs in both seismic intensity cases (see Figure 5.21-22). This clearly indicates that I_A of an input motion is associated more strongly with the relative displacement and the PGA at the ground surface than $D_{5\text{-}95}$. In terms of Sa (T_1) ground response, both properties of an input motion show similar correlation significance.

Property of input motion	0.15g					
	Relative displacement		PGA		$Sa(T_1)$	
	r value	p-value	r value	p-value	r value	p-value
I_a	0.257	**0.008**	0.3	**0.002**	0.189	0.0523
D_{5-95}	0.119	**0.021**	0.12	0.227	0.186	0.058
	0.35g					
	Relative displacement		PGA		$Sa(T_1)$	
	r value	p-value	r value	p-value	r value	p-value
I_a	0.307	**0.001**	0.314	**0.001**	0.244	**0.0123**
D_{5-95}	0.14	0.149	0.156	0.11	0.238	**0.014**

Table 5.8 Correlation test results between I_A and D_{5-95} of the rock input motions and the EDPs at the ground surface, rejection of null hypothesis (p-values) given in bold.

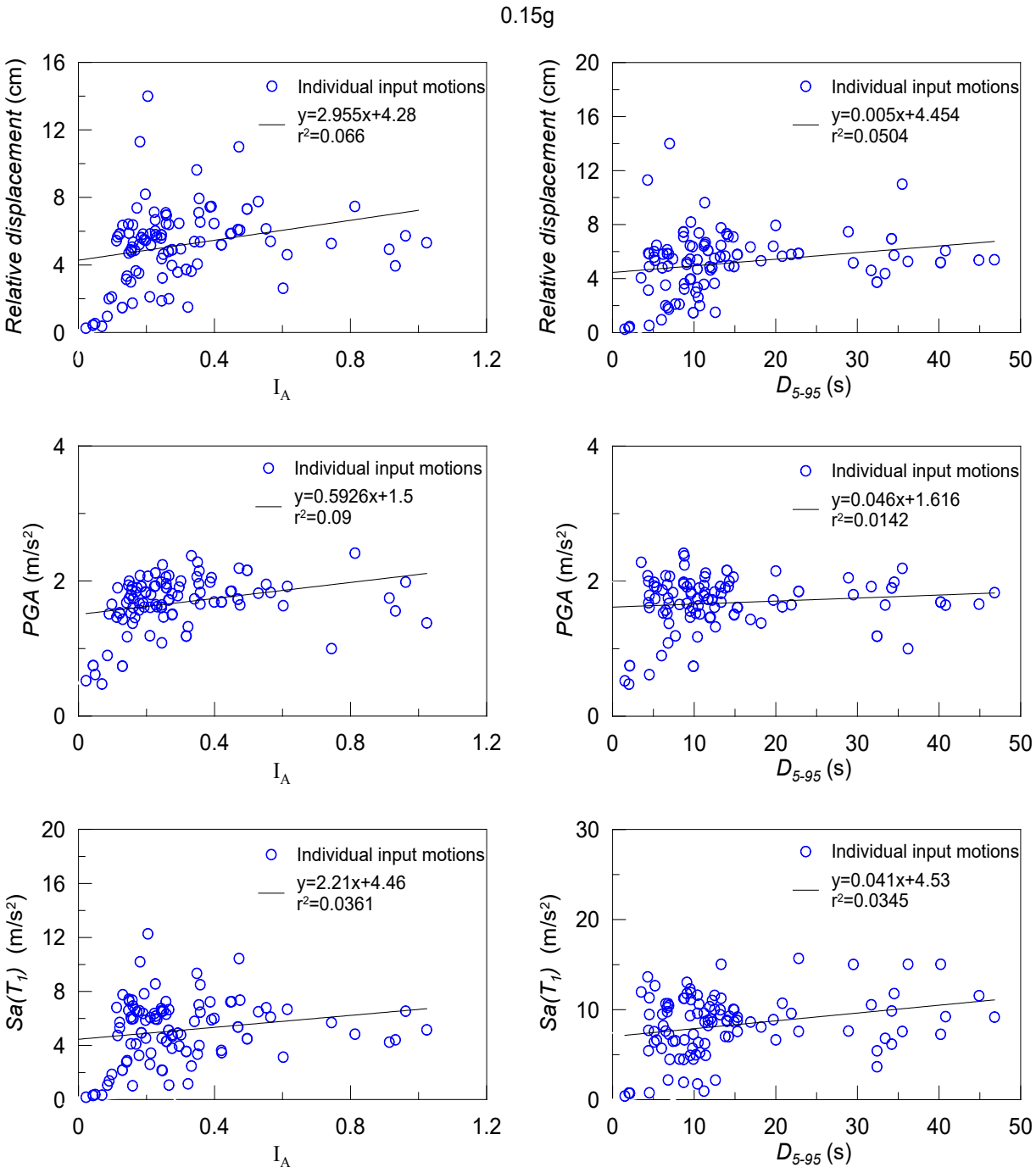

Figure 5.21 Representation of the correlation level between I_A (left-sided) or $D_{5\text{-}95}$ (right-sided) of input motions -having 0.15g seismic intensity level- and EDPs.

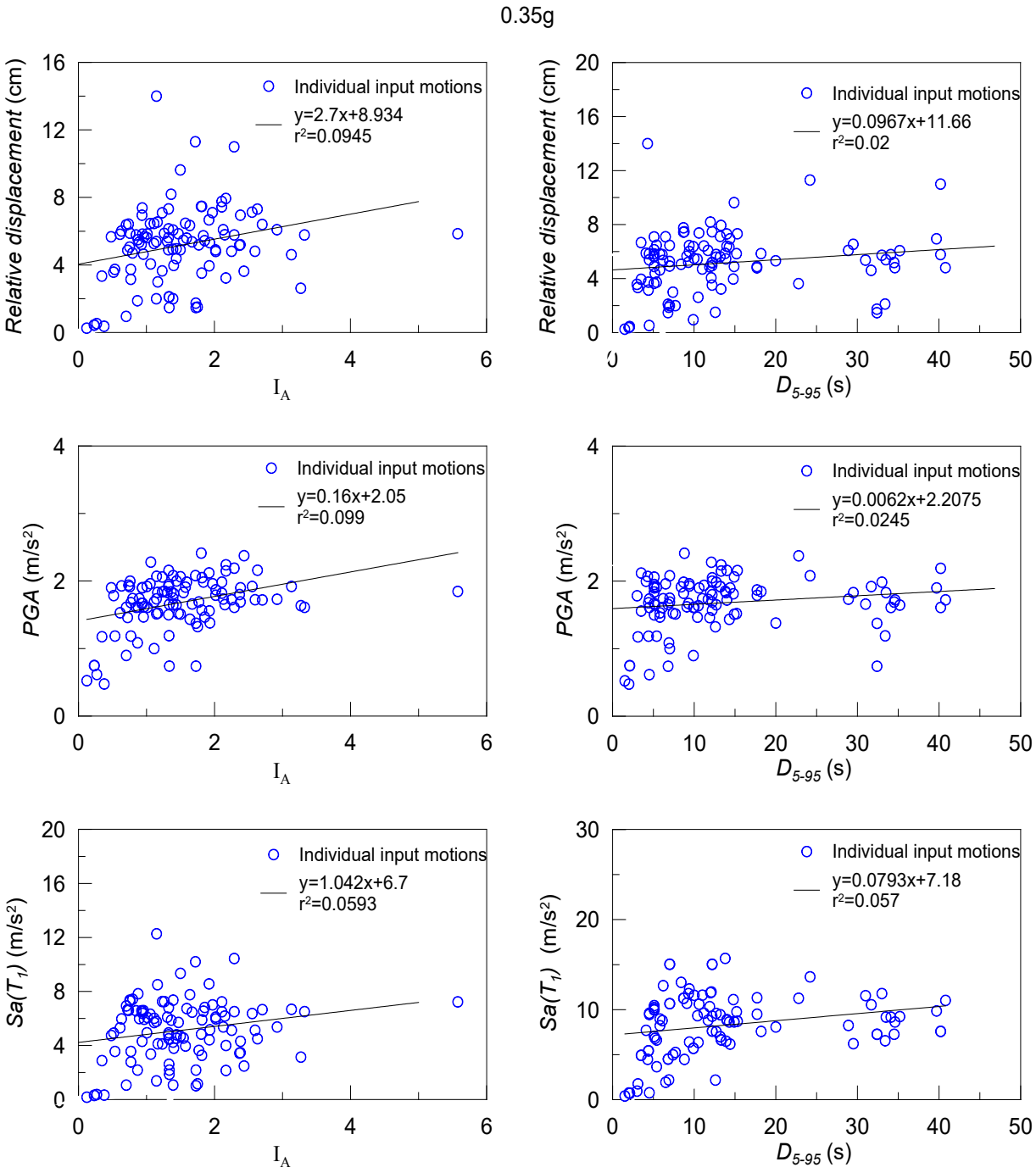

Figure 5.22 representation of the correlation level between I_A (left-sided) or $D_{5\text{-}95}$ (right-sided) of input motions -having 0.35g seismic intensity level- and EDPs.

5.6 Conclusions

This study analyse the effects of input motion selection strategies on the responses of an ideal soft clay soil deposit in terms of site response spectra, relative displacement, PGA and $S_a(T_1)$. The work presented in this chapter diverts from the previous studies as to considering five different selection strategies and testing EC8 design response spectrum for soft clay soil deposits by using a nonlinear FE code. An equivalent linear frequency domain approach implemented in EERA code and a fully-coupled effective stress based FE approach implemented in SWANDYNE II, are employed in the dynamic analyses. The FE code adopts the advanced soil constitutive model *RMW*, which is capable of capturing soil early nonlinearity, hysteretic damping, accumulation of pore water pressure and the soil structure degradation.

Two different computer programs, namely REXEL and SEISMOMATCH, and one website-based program (PEER Ground Motion Database) are used in forming sets of bedrock motions (according to the two target response spectra indicating low and high seismic intensity levels) with respect to each selection strategy. As the proxy of the EC8 design response spectrum for a soft soil (with soil class D) has recently being questioned in representing a possible earthquake event, the median spectral response predictions at the ground surface are also compared with the code spectrum.

From the results of both numerical approaches, PGA scaling provides considerably different median response spectra at 0.15g and 0.35g seismic intensity levels. MSE scaling also gives site response spectra relatively less amplified in the shorter periods at the higher seismic intensity level owing to the large dispersion in the spectral peaks but leads to similar response to the remaining selection strategies at the lower seismic intensity level. Amongst the remaining three selection strategies, $0.2T_1$-$2T_1$ scaling and spectral matching strategies result in almost identical response spectra, giving more conservative spectral acceleration at the shorter periods, and similar result to that from $Sa(T_1)$ scaling at the longer periods. In this respect, one can prefer selecting input motions in site response analysis based on $0.2T_1$-$2T_1$ scaling or spectral matching strategies. However, $0.2T_1$-$2T_1$ scaling may seem to be a more convincing candidate between the two as spectral scaling modifies the frequency content of the input motions as opposed to linear scaling used in $0.2T_1$-$2T_1$ scaling which long been proved to be legitimate.

The benefit of using FE code instead of equivalent linear code in site response analysis is revealed as the FE code with the adopted advanced soil model is capable of representing stiffness degradation and producing hysteretic damping at the exact induced shear strain amplitude during seismic excitation. These features implemented in the code lead to more realistic representation of the soil behaviour and prediction of the site responses. Meanwhile, an approach is used to proximate the maximum induced shear strain level in the nonlinear approach taking the ratcheting soil behaviour into account and, hence providing better approximate maximum strain value that produces maximum hysteretic damping.

The EDP results from the nonlinear FE analyses indicate that spectral matching causes the least scattered responses within a set of seven input motions amongst the other selection strategies. The EDPs from Sa(T_1) scaling also exhibit such dispersions that may favour this selection strategy over or be an alternative of $0.2T_1$-$2T_1$ scaling. Hence, if the preference for the input motion selection is not spectral matching, one of these two strategies can be a second choice to get a reasonably stable EDPs at the ground surface, although the median EDPs of all the selection strategies can be regarded as equal based on t-test results except those from PGA scaling. This is also valid when the median EDPs for sets of 14 input motions are considered.

Increasing the number of input motions from seven to 14 in case of applying $0.2T_1$-$2T_1$ scaling and spectral matching strategies does not affect the median responses. For the remaining selection strategies, it seems not possible to obtain identical response spectra as their compatibility conditions (i.e. scaling at PGA and scaling at T_1) and large dispersion in the spectral peaks (i.e. MSE scaling). The increase in the number of input motions seems also not favourable because it does not bring more stability into the EDP responses for the selection strategies, except from MSE scaling (where the increase leads to reduction in the variability of EDPs). Therefore, it might not be in the engineering interest to consider 14 input motions rather than seven with presented selection strategies for site response analysis.

Based on the predicted response spectra for the selection strategies from FE analyses, the EC8 design response spectrum for a soft soil does not seem to be a good representative of a probable earthquake event at the lower intensity level while it is a relatively better proxy for the higher intensity level. Moreover, the soil factor suggested by EC8 for a soft soil under seismicity Type 1 input motion is found less than those obtained from the dynamic analyses. Although the extent of this research is not to such degree that a new soil factor or spectral

shape will be recommended, it highlights the necessity of revisiting the EC8 design response spectrum for a soft soil. Alternatively, and may be the best choice is to conduct site specific response analysis under a set of bedrock motions when the site is located over the soft soil deposit.

Chapter 6. Influence of Soil Properties Variability on Nonlinear Site Response Predictions: Application to the Lotung Site

6.1 Introduction

Ground response analysis is a key tool in the seismic design of earth structures. To predict local site effects, seismic input motions are propagated through the deposit approximating the dynamic characteristics of the soil by means of equivalent linear or nonlinear approaches. The results of the simulations are, then, interpreted mostly in terms of response spectra and amplification factors obtained at surface (Kramer, 2014). Nonlinear soil behaviour can be approximated by an equivalent linear characterisation of soil dynamic properties. As it is explained in Chapter 3 Section 3.3.1, the method makes use of the exact continuum solution of wave propagation in horizontally layered visco-elastic materials subjected to vertically propagating transient motions (Roesset, 1977). It models the nonlinear variation of soil shear modulus (G) and damping (D) with shear strain through a sequence of linear analyses with iterative update of stiffness and damping parameters. For a given soil layer, G and D are assumed to be constant with time during the shaking. Therefore, an iterative procedure is needed to ensure that the properties used in the linear dynamic analyses are consistent with the level of strain induced in each layer by the input motion (Kramer, 2014). The analysis is performed adopting a total stress approach.

In contrast, nonlinear approaches used in conjunction with a numerical time integration scheme and an effective stress approach are capable of fully capturing soil nonlinearity, pore water pressure build-up and consolidation settlements induced by the earthquake. Although the equivalent linear approximation is simpler and time effective, the nonlinear approach may yield more accurate results. In particular, the benefit of time domain nonlinear schemes can be fully appreciated when the site is shaken by a strong seismic motion (e.g. Elia (2014)).

The free-field seismic response prediction under a single bedrock motion is controlled by the elastic and nonlinear soil properties (i.e. the initial shear wave velocity (V_s) profile, the normalized shear modulus (G/G_0) reduction and damping curves). The V_s profile of a soil deposit is commonly measured by means of in-situ tests, such as cross-hole, down-hole,

seismic cone, SASW, suspension logging methods (e.g. EPRI (1993); Kramer (2014)) The shear modulus degradation and associated hysteretic damping can be determined over a

range of shear strains through laboratory testing of undisturbed soil samples (e.g. resonant column/torsional shear, cyclic triaxial and cyclic simple shear tests).

Although site response analysis usually adopts the deterministic values of the elastic and nonlinear soil properties, their uncertainty and variability in space, even within a single soil layer, should be taken into account (e.g. Phoon and Kulhawy (1999)). In this respect, the effect of soil properties variability on site response predictions is nowadays of great interest for researchers in the geotechnical earthquake engineering field (e.g. Field *et al*. (2003); Bazzurro and Cornell (2004a); Bazzurro and Cornell (2004b); Idriss (2004) Andrade and Borja (2006); Sarma and Irakleidis (2007); Rota *et al*. (2011).

The most common way of including the variability of the soil properties in site response analyses is through Monte Carlo Simulations (MCSs). As an example, Roblee *et al*. (1996) investigated the influence of the variability of soil properties on the site response prediction through MCSs. They employed a stochastic finite-fault model able to produce a seismic motion with a specific magnitude and distance from the fault. The model was also capable of accounting for soil properties variability within an equivalent linear formulation. The results indicated that i) site effects variability is clearly a function of the distance (and, therefore, of the seismic intensity level); ii) path effects have little impact on response variability near fault, but become more pronounced as source-to-site distance increases; iii) source effects contribute most to parametric variability at longer periods and are relatively insensitive to both site type and distance.

Li and Assimaki (2010) also conducted MCSs of the site response of three well-investigated down-hole array sites located in the Los Angeles Basin, using the earthquake dataset developed by Assimaki *et al.* (2008) based on synthetic records. It was demonstrated that the impact of nonlinear soil properties variability depends strongly on the seismic intensity of the applied input motion, particularly for soft soil profiles. On the contrary, the effects of velocity profile uncertainties are less intensity dependent and more sensitive to the velocity impedance in the near surface that governs the maximum site amplification. Similarly, Rathje *et al.* (2010) performed MCSs for equivalent linear site response analysis by including variability coming from the elastic and nonlinear soil properties. The results pointed out that modelling shear wave velocity variability generally reduces the predicted median surface motions and amplification factors, most significantly at periods less than the site period, while accounting for the variability in nonlinear properties has a slightly smaller

effect. Moreover, including the variability in soil properties significantly increases the standard deviation of the amplification factors but has a lesser effect on the standard deviation of the surface motions.

This chapter investigates the influence of variability in elastic and nonlinear soil properties on the site response prediction of the Large Scale Seismic Test (LSST) site in Lotung, Taiwan. The fully-coupled finite element (FE) code SWANDYNE II (Chan, 1995) is adopted and plasticity is introduced in the FE simulations through the advanced elasto-plastic model (*RMW*) developed by Rouainia and Muir Wood (2000). The performance of the *RMW* model in fully-coupled dynamic analysis of earth structures has been demonstrated in previous works (e.g. Elia and Rouainia (2012); Elia and Rouainia (2014)). In particular, the LSST site has already been studied in Chapter 4, but using a deterministic approach, i.e. adopting a single shear wave velocity profile and one set of G/G_0 and D curves predicted by the *RMW* model. In this work, the variability of elastic and nonlinear soil properties in Lotung is accounted for through a Monte Carlo approach. One weak and one strong input motions recorded at the site are considered to test the sensitivity of the ground response prediction to the seismic intensity level.

6.2 Lotung Site and Earthquake Records

Since the detailed information about the site is given in Chapter 4, this section only intends to briefly summarise them. The Lotung accelerometer array is located in the north-east part of Taiwan (Tang *et al.*, 1990). The site geology consists of recent alluvium and Pleistocene materials over a Miocene basement. The upper alluvial layer, 30-40 m thick, consists mainly of clayey-silts and silty-clays (Anderson, 1993). The water table is located approximately at a depth of 1 m. The local geological profile shows a 17 m thick silty sand layer above a 6 m thick layer of sand with gravel resting on a stratum of silty clay interlayered by an inclusion of sand with gravel between 29 m and 36 m.

The site was instrumented in 1985 with down-hole accelerometers located at different depths. Of particular interest here is the vertical array named DHB, which can be considered representative of the free-field response at Lotung. The bedrock formation is assumed to be at a depth of 47 m, where the recordings of the corresponding accelerometer have been used in the numerical simulations as input motions. Within two years from the instrumentation, 18 earthquake events were recorded with low, moderate and high seismic intensity levels at

the LSST site. Two input motions, one strong (LSST07) and one weak (LSST11), have been considered in this work. For the sake of simplicity, only the E-W component of the earthquake events has been adopted in the FE simulations (the case of adopting the N-S component of the earthquake events is presented in Appendix B). Table 6.1 gives general information about the two earthquakes and Figure 6.1 shows their acceleration-time histories.

Event	**Date**	**Magnitude, M_L**	**Epicentral distance (km)**	**Focal depth (km)**
LSST07	20/5/1986	6.2	66.0	15.8
LSST11	17/7/1986	4.3	6.0	2.0

Table 6.1 Earthquakes recorded by the LSST array and used in the analyses.

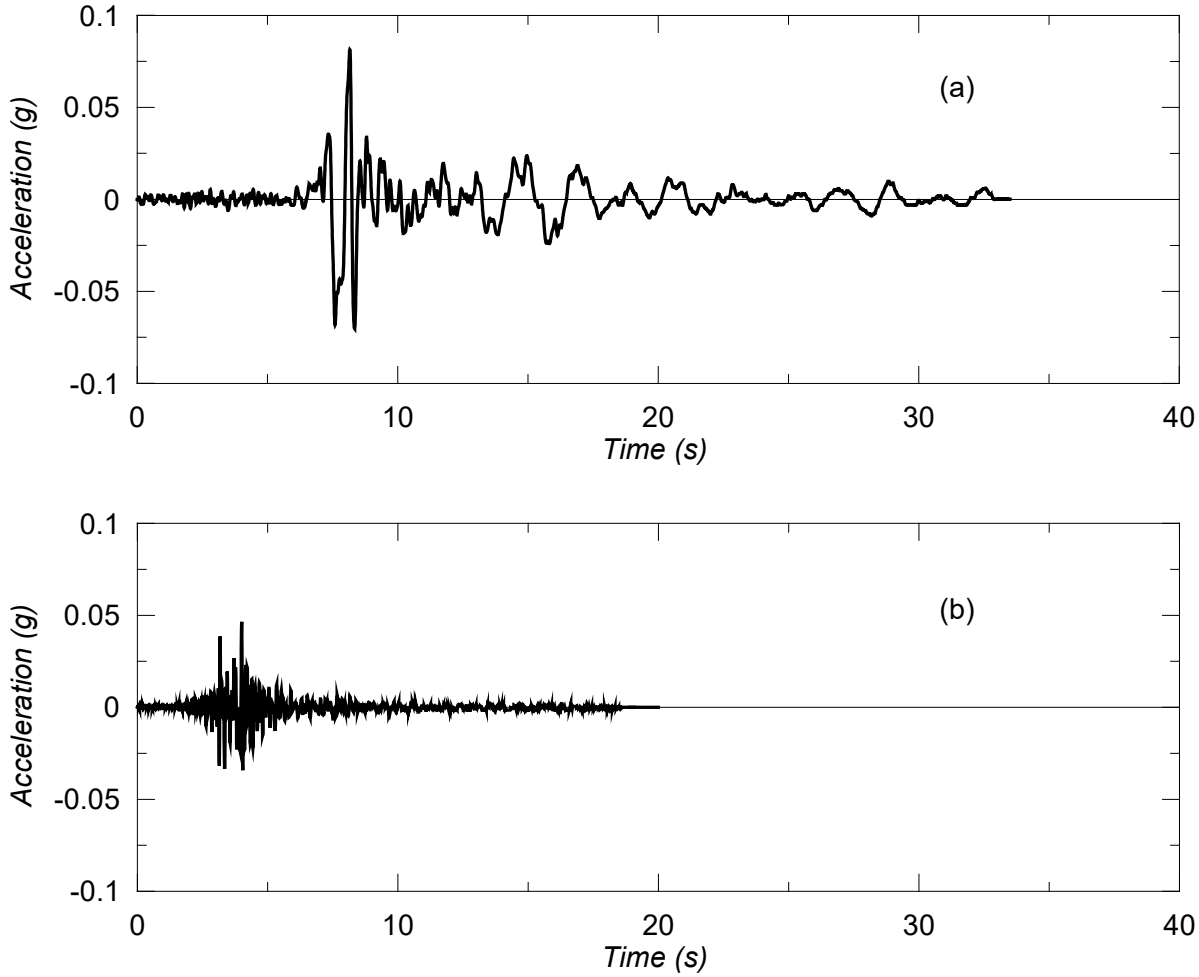

Figure 6.1 Recorded input motions at the Lotung site in the East-West (E-W) direction: (a) strong earthquake event (LSST7) and (b) weak earthquake event (LSST11).

6.3 Variability of Soil Properties

The shear wave velocity profile along with shear modulus reduction and damping curves are the main soil dynamic properties which have significant impact on the response of a site subjected to a specific earthquake event. These properties can vary spatially due to aleatory or epistemic uncertainties. The aleatory uncertainty (or randomness) depends strongly on the site geology and cannot be reduced by collection of additional information (Roblee et al., 1996). On the other hand, epistemic uncertainty can be caused by man-made errors during laboratory soil testing or deficiencies of current methods in determining the soil properties and can be minimised, for example, by gathering good quality data and developing more rigorous field and laboratory measurement techniques (e.g. Roblee et al. (1996); Rathje et al. (2010)).

Most of the soil properties are known to exhibit a high coefficient of variance (*COV*) that can be represented appropriately using a Monte Carlo method (e.g. Li and Assimaki (2010)). In order to randomise the soil properties in each MCS, a specific probabilistic distribution for each property is required. However, since the availability of soil data to constrain the selected probabilistic distribution is usually very limited, it is more practical to formulate such distribution based on data from several well-monitored and investigated sites.

In this respect, Toro (1995) has developed a statistical model - based on generic soil profiles retrieved from EPRI database (EPRI, 1993)- to randomise low-strain shear wave velocity profiles. The model is able to predict random soil stiffness profiles by considering a baseline V_s profile, the data distribution and the interlayer correlation. Once the average value of V_s at the top 30 m of the deposit is known, the stiffness profile can be randomised using the logarithmic standard deviation and the interlayer correlation parameters given by the statistical model.

Darendeli and Stokoe (2001) developed an empirical method based on extensive data of G/G_0 and D curves obtained from resonant column and cyclic torsional shear tests on soil samples retrieved from different geotechnical array sites. The dynamic characteristics of these soils were interpreted in terms of confining pressure, overconsolidation ratio, number of loading cycles, loading frequency and site class. The model is based on a first order second-moment Bayesian statistical method and is able to generate correlated G/G_0 and D curves.

In this work, the amount of data from the Lotung site in terms of high quality shear wave velocity measurements and G/G_0 and D laboratory data allows to undertake MCSs with well-constrained probabilistic distributions. The generation of stiffness variability with depth and G/G_0 and D curves for the LSST site is described in the following sections.

6.3.1 Point variability of the initial stiffness profile

The shear wave velocity values obtained at different depths from the results of seismic cross-hole and up-hole tests performed at the LSST site are illustrated in Figure 6.2. To represent the small-strain shear modulus (G_0) profile of the Lotung site, the equation proposed by Viggiani and Atkinson (1995) is adopted in the FE procedure:

$$\frac{G_o}{p_r} = A\left(\frac{p'}{p_r}\right)^n OCR^m \tag{6.1}$$

where p_r is a reference pressure, p' is mean effective stress, OCR is overconsolidation ratio and A, m and n are dimensionless stiffness parameters. The details of the FE model and its boundary conditions are presented in Chapter 4. In the initialisation of the FE model, a higher overconsolidation ratio has been assumed for the upper part of the column (from 0 to a depth of 6 m), with an average R equal to 4, while a constant overconsolidation ratio of 2 has been imposed for the remaining part of the model. Therefore, the G_0 profile is completely controlled by the parameters A, m and n of Equation 6.1 and to randomise the small-strain shear modulus profile it is necessary to transfer the variability of G_0 to these parameters.

Considering that m and n have relatively less effect on the elastic formulation (due to their small range of values) than the parameter A, they are regarded as deterministic input with values of 0.36 and 0.82, respectively. Hence, only the parameter A is subjected to variability when the initial stiffness profile is randomised for the MCSs. In particular, a point variability is considered here, i.e. the initial stiffness profile is varied with a certain standard deviation with respect to a baseline profile. A lognormal distribution of A (and consequently of G_0) can be reasonably fitted through the data points for the different layers, as presented in Figure 6.2a. In addition, this assumption provides realistic stiffness profiles as it only generates positive values of G_0 (Andrade and Borja, 2006). The mean variation of G_0 with depth shown in the figure corresponds to the baseline profile used to obtain baseline responses.

If the only random parameter in the above equation is A, the mean and standard deviation of G_0 are:

$$\left.\begin{aligned} \mu_{G_o} &= \mu_A\left(\frac{p'}{p_r}\right)^n OCR^m \\ \sigma_{G_o} &= \mu_A COV_A\left(\frac{p'}{p_r}\right)^n OCR^m \end{aligned}\right\} \tag{6.2}$$

Since the stress and overconsolidation ratio dependency of G_0 is preserved in the calculation of the mean and standard deviation, the coefficient of variance (COV) of G_0 can be computed as:

$$COV_{G_o} = \frac{\sigma_{G_o}}{\mu_{G_o}} = COV_A \tag{6.3}$$

which implies that the *COV* is kept constant in the transformation of A into G_0.

After ensuring the consistency in the *COV*, it is necessary to calculate the statistical parameters of the lognormal distribution, e.g. the mean and standard deviation. The calculation of these parameters, along with the probability density function (PDF) of A, is given as:

$$A: \ln(\mu_{lnA}, \sigma_{lnA}) = exp(\mu_{lnA} + \sigma_{lnA} \times \xi) \tag{6.4}$$

where $\xi \sim N(0,1)$ is a normally distributed random variable.

$$\left.\begin{aligned} \mu_{lnA} &= ln\left(\frac{\mu_A}{\sqrt{1 + COV_A^2}}\right) \\ \sigma_{lnA} &= \sqrt{ln(1 + COV_A^2)} \end{aligned}\right\} \tag{6.5}$$

Once the PDF expression of A (i.e. Equation 6.4) is substituted into Equation 6.1, G_0 can be written as follows:

$$G_o = exp(\mu_{lnA} + \sigma_{lnA}\xi)p'\left(\frac{p'}{p_r}\right)^n OCR^m \tag{6.6}$$

Rearranging the above expression leads to:

$$G_o = \exp(\mu_{lnA} + (1-n)p_r + nln(p') + mln(OCR) + \sigma_{lnA}\xi) \tag{6.7}$$

From this formulation, the transformation of variability from A to G_0 only affects the mean of $\ln G_0$ when a certain desired variability is given by the standard deviation (Depina *et al.*, 2015). Then, the log-normally distributed G_0 can be given as:

$$G_o : \ln\left(\mu_{lnG_o}, \sigma_{lnG_o}\right) \tag{6.8}$$

and:

$$\left.\begin{aligned} \mu_{lnG_o} &= \mu_{lnA} + (1-n)p_r + nln(p') + mln(OCR) \\ \sigma_{lnG_o} &= \sigma_{lnA} \end{aligned}\right\} \tag{6.9}$$

Once the G_0 profile has been randomised, the corresponding V_s variation with depth is obtained for each realisation assuming a total unit weight of the soil equal to 20 kN/m^3 (as proposed by Borja *et al.* (1999a)). Figure 6.2b displays examples of randomised shear wave velocity profiles used in this study.

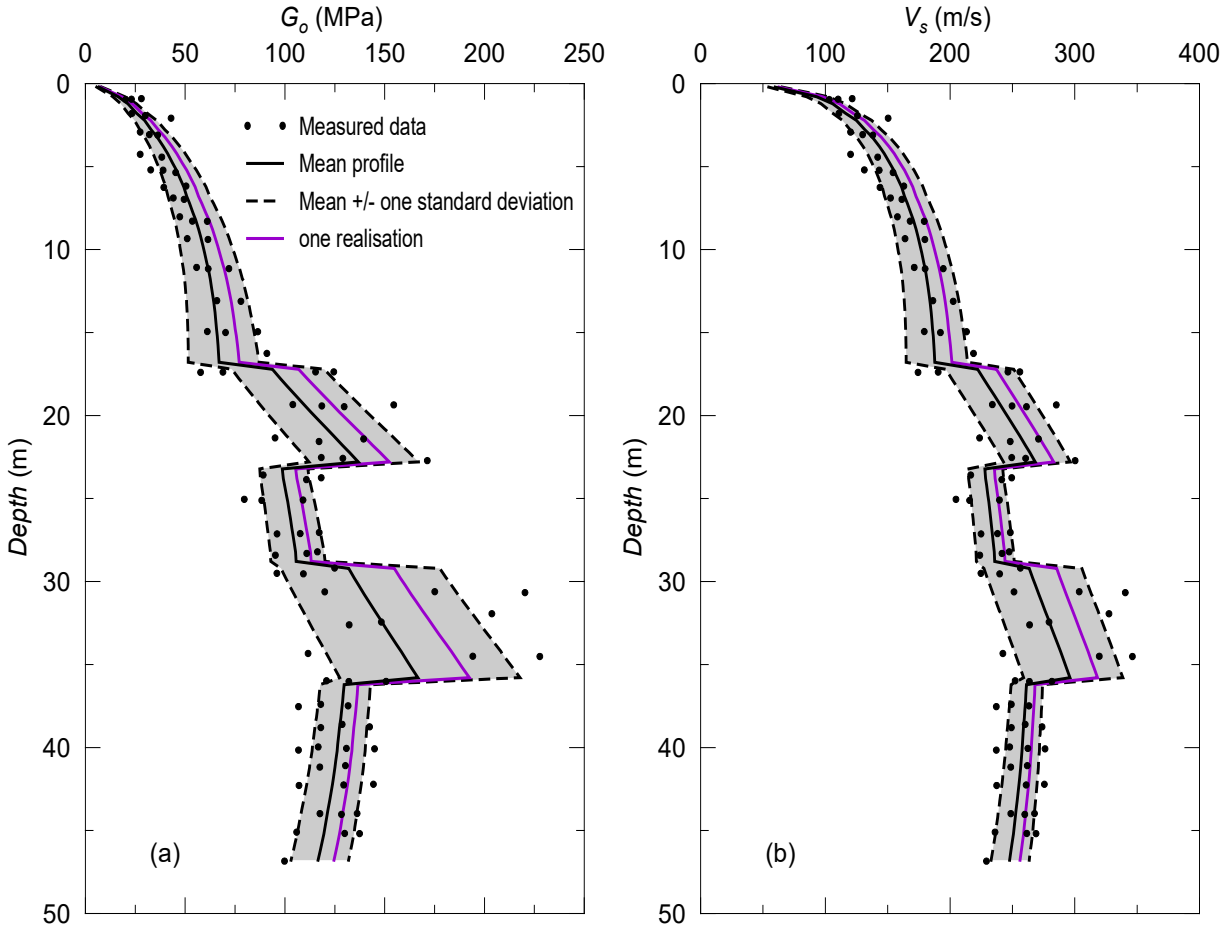

Figure 6.2 Point variability of stiffness: (a) shear modulus (G_0) profile and (b) shear wave velocity (V_s) profile.

6.3.2 Spatial variability of the initial stiffness profile

In addition to the point variability of the initial stiffness profile discussed in the previous section, the V_s profile can also be varied spatially (e.g. Phoon and Kulhawy (1999)). The spatial variation of a soil property is generally modelled by random fields generating a series of values to be used in MCSs. In this study, a one-dimensional random field is implemented in the vertical direction, assuming homogeneity in the horizontal direction, to investigate the influence of spatial variability of the elastic soil property (i.e. shear wave velocity) on the site response prediction. The matrix decomposition technique is adopted to generate the random field (El-Kadi and Williams, 2000). The covariance function Σ_{ij} is defined with respect to the covariance of the parameter lnG_0 and the distance between data points d_{ij} as follows:

$$\Sigma_{ij} = \sigma^2_{lnG_0} e^{-\frac{1}{L}|d_{ij}|} \tag{6.10}$$

where the correlation length, L, is taken equal to 2 m (Depina *et al.*, 2015).

The covariance matrix is decomposed based on the Choleski method (Nash, 1990) as follows:

$$\Sigma_{lnG_0} = CC^T \tag{6.11}$$

$$C_{mm}C_{im} = \Sigma_{im} - \sum_{k=1}^{m-1} C_{ik}C_{mk} \tag{6.12}$$

$$G_0 = \exp(C\xi + \mu_{lnG_o}) \tag{6.13}$$

where C is a lower triangular matrix, ξ is the vector of Gaussian random variables with zero mean and unit standard deviation. An example of a random field generation is illustrated in Figure 6.3 along with mean +/- one standard deviation.

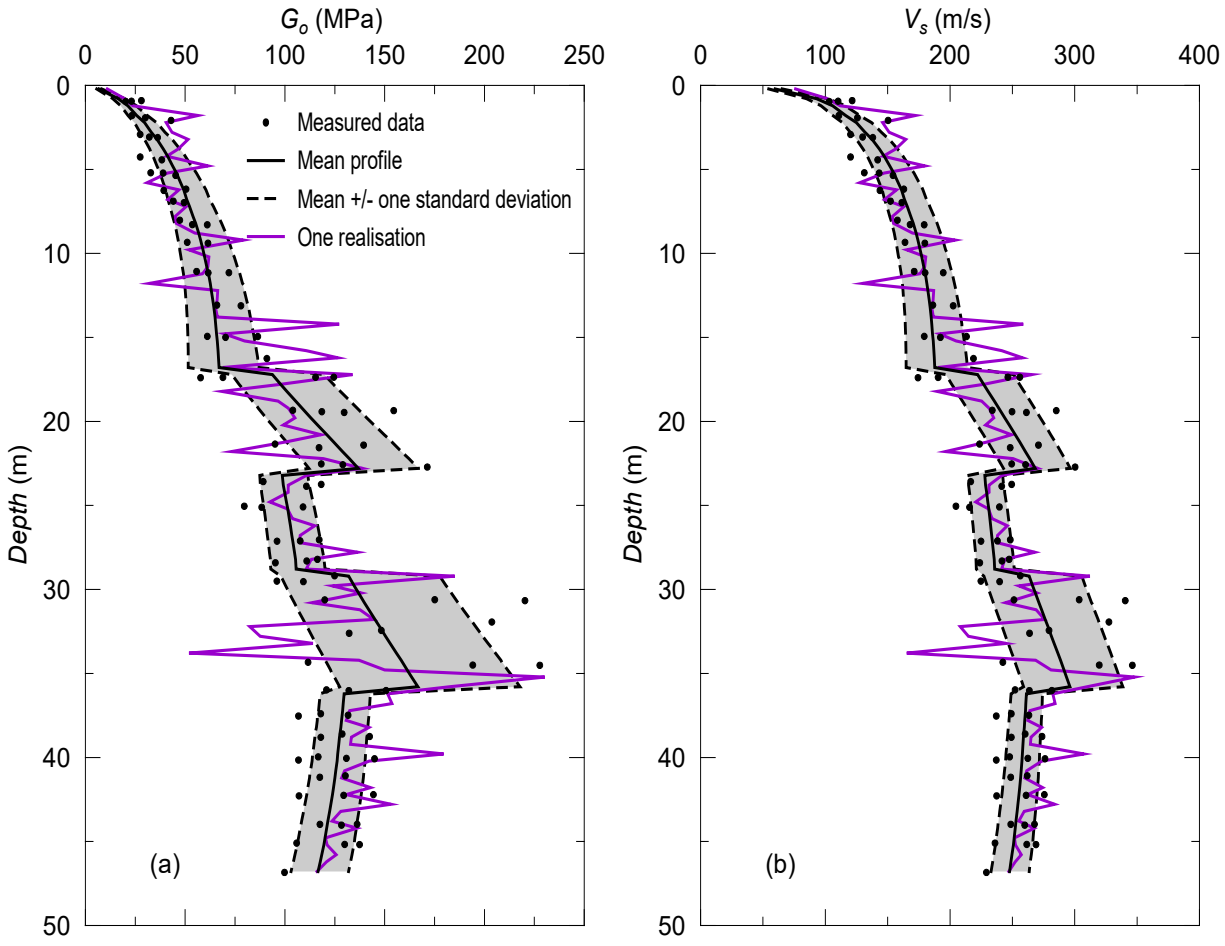

Figure 6.3 Spatial variability of stiffness: (a) shear modulus (G_0) profile and (b) shear wave velocity (V_s) profile.

6.3.3 Variability in nonlinear soil properties

The randomisation of the stiffness degradation and corresponding damping curve is, in most cases, based on empirical expressions developed considering different soil types and stress conditions (e.g. Darendeli and Stokoe (2001), Zhang *et al.* (2005)). To randomly generate the nonlinear soil parameters, it is necessary to describe their statistical distribution and define any correlation between them.

In this work, the G/G_0 and D curves are the output of the *RMW* model adopted in the simulations. The constitutive law allows to reproduce some of the key features of the cyclic behaviour of natural soils, such as the destructuration induced by the loading, the decay of the shear stiffness with strain amplitude, the corresponding increase of hysteretic damping and the accumulation of excess pore water pressure under undrained conditions. A kinematic-hardening translation rule is used to model the movement of the centre of bubble

in a direction parallel to the line joining the current stress, $\boldsymbol{\sigma}$, and the conjugate stress, $\boldsymbol{\sigma}_c$, as follows:

$$\dot{\bar{\boldsymbol{\alpha}}} = \dot{\hat{\boldsymbol{\alpha}}} + \frac{\dot{p}_c}{p_c}(\bar{\boldsymbol{\alpha}} + \hat{\boldsymbol{\alpha}}) + \dot{\mu}(\boldsymbol{\sigma}_c - \boldsymbol{\sigma}) \tag{6.14}$$

where $\bar{\boldsymbol{\alpha}}$ and $\hat{\boldsymbol{\alpha}} = p_c\left[r\boldsymbol{I} + (r-1)\boldsymbol{\eta}_0\right]$ denote the locations of the centre of the bubble and structure surface respectively, μ is a positive scalar of proportionality and r is the degree of structure, which is a monotonically decreasing function of the plastic strain. It should be noted that the centre of the structure surface and the deviator of $\bar{\boldsymbol{\alpha}}$ represents the anisotropy of the soil due to structure. The deviator of $\bar{\boldsymbol{\alpha}}$ therefore degrades to zero as r degrades to unity. The plastic modulus H is assumed to depend on the distance between the current stress and the conjugate stress and is given by:

$$H = H_c + \frac{1}{\|\bar{n}\|}\frac{Bp_c^3}{(\lambda^* - \kappa^*)R}\left(\frac{b}{b_{max}}\right)^{\psi} \tag{6.15}$$

where λ^* and κ^* are the slopes of normal compression and swelling lines in the ln$v$: ln$p$ compression plane (v being the soil specific volume), $b = \bar{\boldsymbol{n}}:(\boldsymbol{\sigma}_c - \boldsymbol{\sigma})$ is a measure of the distance between the bubble and the structure surface and $b_{\max}$ is the nominal maximal value of b. The additional soil parameters ψ and B control the rate of decay of stiffness with strain and the magnitude of the contribution of the interpolation term, respectively. The hardening modulus H_c is derived from the consistency condition on the structure surface when the bubble and the structure surface are in contact.

The randomisation of the soil nonlinear parameters can be achieved by varying the *RMW* parameters which mostly affect the predicted stiffness degradation and damping curves. To identify these parameters, a series of single element simulations of strain-controlled undrained cyclic simple shear (CSS) tests are conducted by applying different shear strain amplitudes. After 500 cycles for each strain level, which is considered to be sufficient to achieve a steady-state condition (Elia *et al.*, 2011), the secant shear modulus and damping values are obtained. From an extensive parametric study, it is observed that the G/G_0 and D curves are greatly affected by the interpolation exponent ψ in Equation 6.15.

The remaining *RMW* parameters are assumed equal to those used in Chapter 4, which were calibrated against the dynamic laboratory tests performed on soil samples retrieved from the Lotung site. The soil parameter ψ is considered as log-normally distributed between a lower value of 0.1 and an upper value of 4. The range of ψ values is determined in order to reasonably capture the empirical data by Zeghal *et al.* (1995) showing good agreement with the laboratory results (EPRI, 1993), presented in Figure 6.4. The mean value of the parameter ψ is set equal to 1.1. The *COV* of ψ is assumed equal to 0.4, in accordance with the guidance given in the literature (e.g. Phoon and Kulhawy (1999); Chen *et al.* (2008)).

Random ψ values are generated such that they are within the lower and upper limit. The corresponding G/G_o and D curves obtained through CSS simulations with the *RMW* model are shown in Figure 6.4. The smaller ψ value gives the upper bound G/G_o curve and thus leads to the lower bound damping curve. In contrast, for the bigger value of ψ the *RMW* model predicts a more rapid stiffness degradation (lower bound G/G_o curve), resulting in higher hysteretic damping (upper bound damping curve). This inverse trend of the predicted G/G_o and D curves indicates how the *RMW* model is able to automatically capture the well-known negative correlation between the two curves.

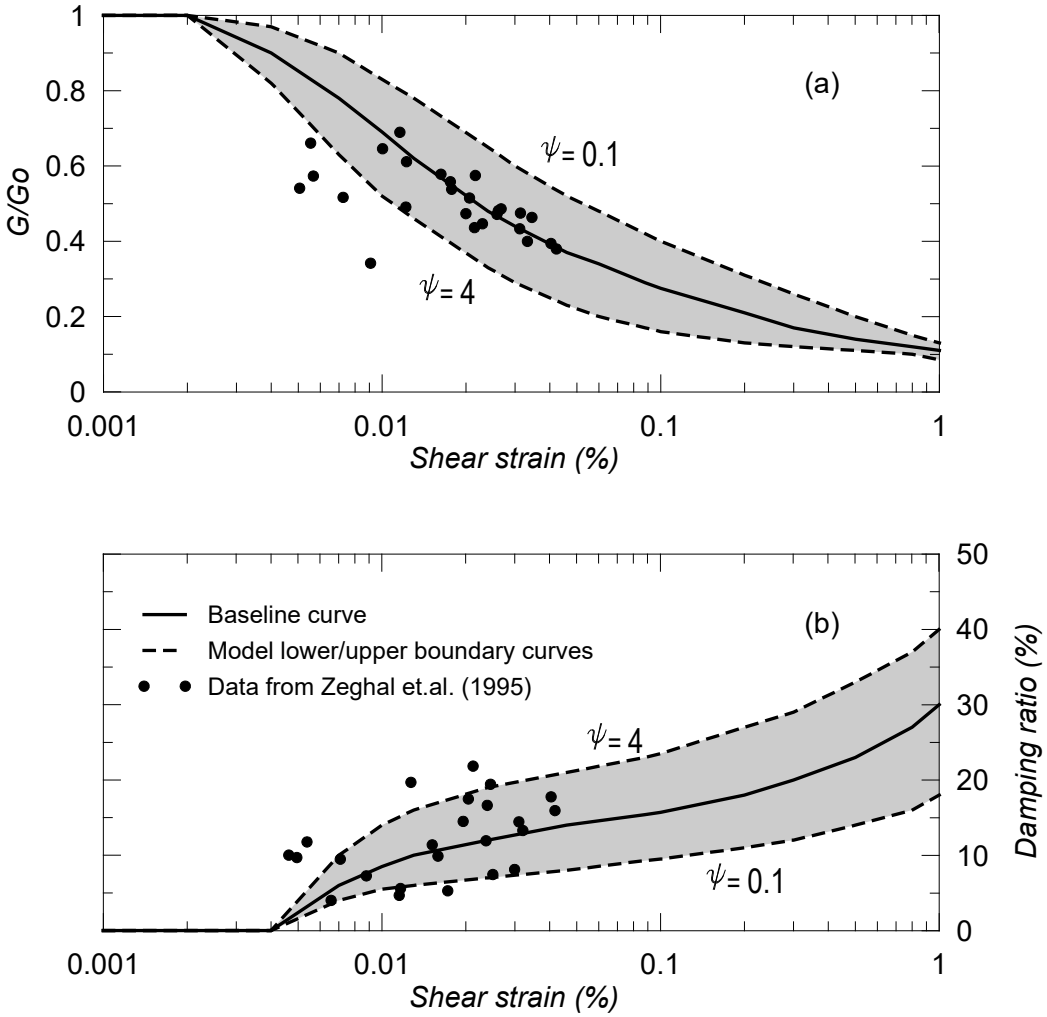

Figure 6.4 Influence of effect of soil model parameter (ψ, psi) limiting: (a) shear stiffness reduction (G/G_o) and (b) damping (D) curves along with analytical data from Zeghal *et al.* (1995).

6.4 Results and Discussion

In this section, the results of MCSs of Lotung nonlinear site response are presented in terms of median response spectrum predicted at ground surface and compared with the actual LSST recorded data and the response spectra computed by using the best-estimate soil properties (baseline response) using a deterministic approach. The influence of variability of point stiffness, spatial stiffness and nonlinear soil properties is investigated for both the strong and the weak input motion. All figures show the results obtained using 200 stiffness or 200 nonlinear curves realisations, unless mentioned otherwise. To accurately assess the site response predictions, the standard deviation of the logarithmic spectral accelerations, σ_{lnSa}, is also plotted, as suggested by Li and Assimaki (2010) and Rathje *et al.* (2010).

6.4.1 Effects of soil properties variability on site response under the strong input motion

The surface response spectra of the nonlinear site response analyses when the strong input motion (LSST07) is applied at bedrock are shown in Figure 6.5. The results are obtained with the V_s profile and G/G_o and D curves being randomised around the baseline within plus and minus one standard deviation. Point variability of the initial stiffness profile is considered first. By statistically changing the V_s profile, the MCSs exhibit only a modest variation in the response spectra at surface over the engineering period of interest (Figure 6.5a). Moreover, the median is remarkably similar to the baseline response prediction. In contrast, a significant variation in the response spectra can be observed by randomising the G/G_o and D curves (Figure 6.5b). The median, in this case, also closely matches the baseline response, thus indicating that the variation of nonlinear soil properties does not necessarily lead to a different or improved surface response prediction with respect to a deterministic approach. By simultaneously varying the V_s profile and the G/G_o and D curves, still similar median response is observed as it closely matches with the baseline response spectrum (Figure 6.5c). However, simultaneous variation of the soil properties causes the increase in the standard deviation of the surface response spectra (σ_{lnSa}), especially at periods lower than 0.2 s and periods higher than 0.3 s, which can be seen in Figure 6.5d.

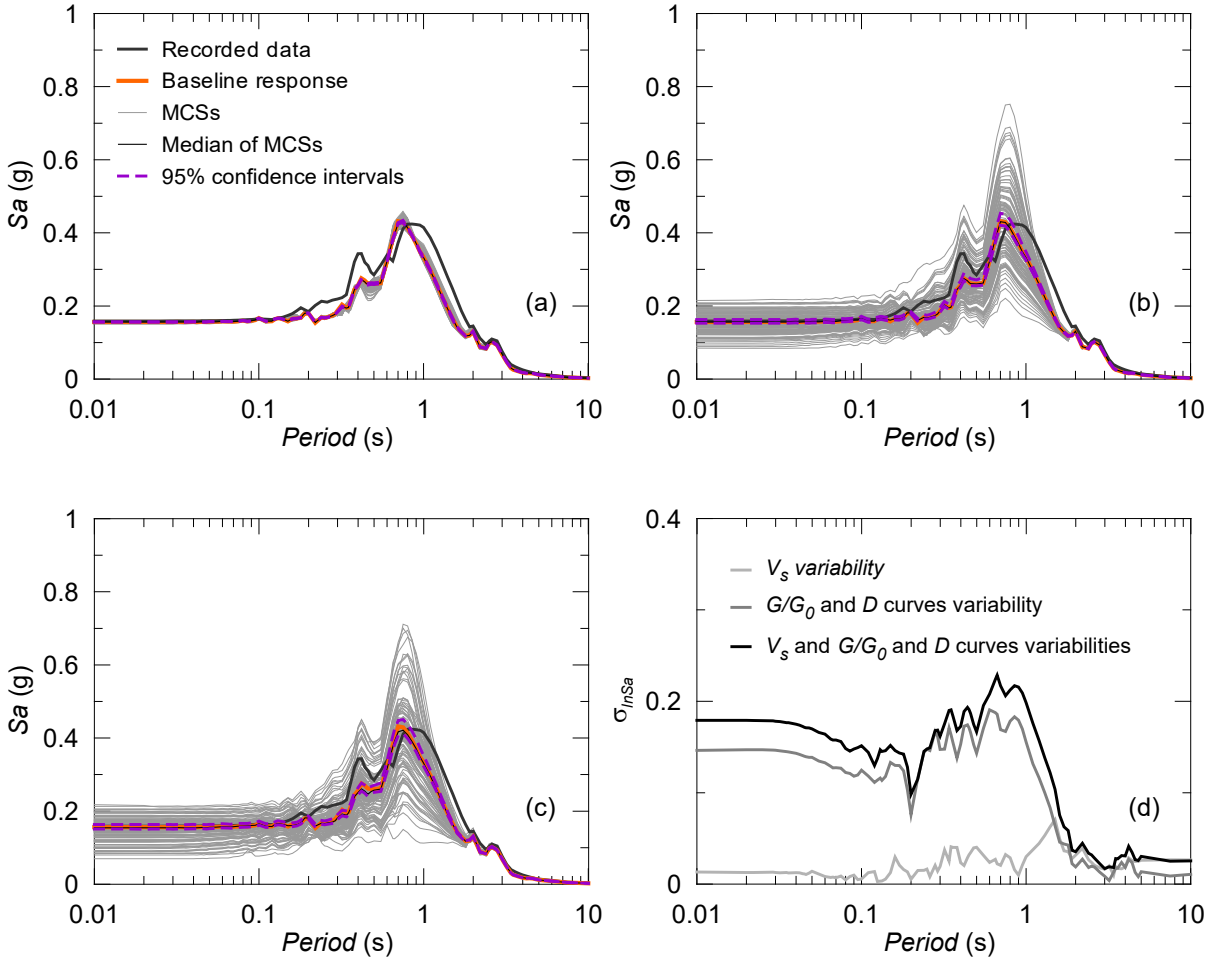

Figure 6.5 Site response prediction under the strong input motion (LSST7): (a) variability of V_S profile, (b) variability of G/G_o and D curves, (c) simultaneous variability of V_S profile and of G/G_o and D curves and (d) logarithmic standard deviations, σ_{lnSa}, in each case.

The confidence intervals for spectral accelerations over the interested period range are computed based on Cox method (Land, 1972). This method is shown to be effective in representing intervals for lognormally distributed data (Zhou and Gao, 1997). The spectral curves showing 95% confidence intervals do not exhibit any band of spectral ranges at any periods when the V_s profile is varied (Figure 6.5a). In the cases of varying G/G_o and D curves or simultaneous changes of the soil properties, marginal spectral intervals at around T_1 can be observed while the intervals are mostly overlapped at other periods (Figure 6.5b of Figure 6.5c). This interval curves imply that it is 95% true that the median responses from any 200 MCSs with the V_s profile and/or G/G_o and D curves will be within those intervals covering reasonably well the baseline responses as well as recorded data.

To estimate the number of MCSs required to achieve a stable site response prediction when the G/G_o and D curves are varied, five suites of 10, 20 and 50 realisations are considered. Each suite represents a reasonable realisation of nonlinear curves, such that comparing the

results from different suites provides an evaluation of the statistical stability of the computed response. This analysis is not performed for the shear wave velocity profile, as the results of MCSs presented in Figure 6.5a show that the spectral response at surface of 200 different realisations of V_s exhibit inconsiderable level of dispersion around the baseline prediction. The median surface response spectrum and σ_{lnSa} at each period are computed for each suite of G/G_o and D curves and plotted in Figure 6.6.

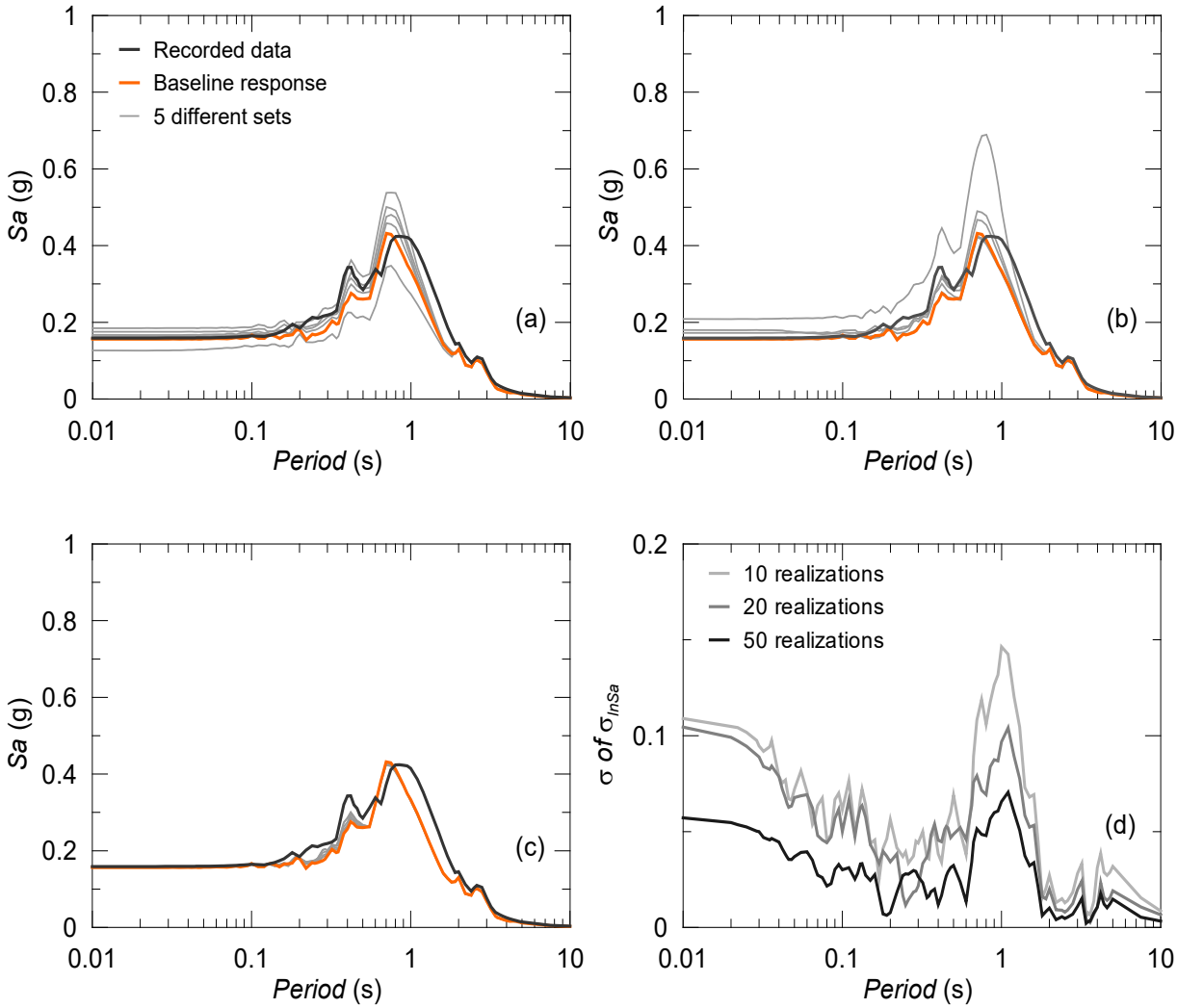

Figure 6.6 Median responses of 5 sets: (a) 10 realisations of G/G_o and D curves, (b) 20 realisations, (c) 50 realisations and (d) standard deviations of σ_{lnSa} within each set.

It is clear how 10 and 20 realisations do not produce a consistent median response at surface. In contrast, using 50 (or more) realisations allows to predict a stable response, very close to the baseline prediction (Figure 6.6c). This is also evident in Figure 6.6d, where the reduction of the standard deviation as the number of realisations increases from 10 to 50 is presented. At the lower periods, sets of 10 and 20 realisations have similar but higher values of standard deviation with respect to the suite composed by 50 realisations, while the difference become

evident at around 0.85 s, representing the first natural period of the soil deposit, T_1. This can be explained by the tendency of the system to oscillate around its fundamental period, leading to substantial spectral amplifications at this period. Therefore, the spectral response predictions become more sensitive to the variability of the soil properties at around T_1, causing great deviations in the results. At the higher periods (greater than 2 s), the standard deviations of the suites composed by 20 and 50 realisations are very similar and approaching zero.

The median surface response obtained for one, two and three standard deviation level of truncation around the V_s baseline profile is presented in Figure 6.7, while the effect of changing the truncation level of the G/G_o and D curve distributions is shown in Figure 6.8. As the standard deviation around the V_s profile is increased from one to three, no appreciable effect on the median response spectra at the surface can be observed, resulting in an identical degree of uncertainty in terms of σ_{lnSa} (Figure 6.7d). On the contrary, increasing the level of truncation of the G/G_o and D distributions causes high variability in the response prediction. For one standard deviation (corresponding to the results presented in Figure 6.5b), the maximum σ_{lnSa} is less than 0.2, while it reaches a value of 0.4 at around T_1 with a truncation of two standard deviations as the amount of G/G_o and D data captured increases from 68% to 95% (Figure 6.8d).

The increase in the truncation level of the G/G_o and D curve distributions also increases the spectral distances between 95% confidence intervals, which is more apparent, again, at around T_1. However, this increase of interval widths with the truncation levels (i.e. from one to two and three standard deviations) leads to better coverage of the recorded data as can be seen in Figure 6.8b and Figure 6.8c. Hence, it can be interpreted that median responses from any 200 MCSs with two or three standard deviations of the G/G_o and D curves can reflect the actual responses better than that of one standard deviation.

Considering a truncation level of three standard deviations, thus implying that almost all G/G_o and D data are included in the analysis, a slight decrease in the σ_{lnSa} is observed. In general, accounting for a wide variability of the G/G_o and D curves produces higher standard deviations of the logarithmic spectral accelerations at surface, but the median response remains almost unchanged. Moreover, the level of shear strain induced by the strong motion is sufficient to induce nonlinear effects in the soil behaviour, thus making the site response very sensitive to the variability of the G/G_o and D curves. This is confirmed by Figure 6.9,

where the influence of stiffness profile and nonlinear curves variability on the maximum horizontal acceleration (a_{max}) and maximum shear strain (γ_{max}) profiles is presented.

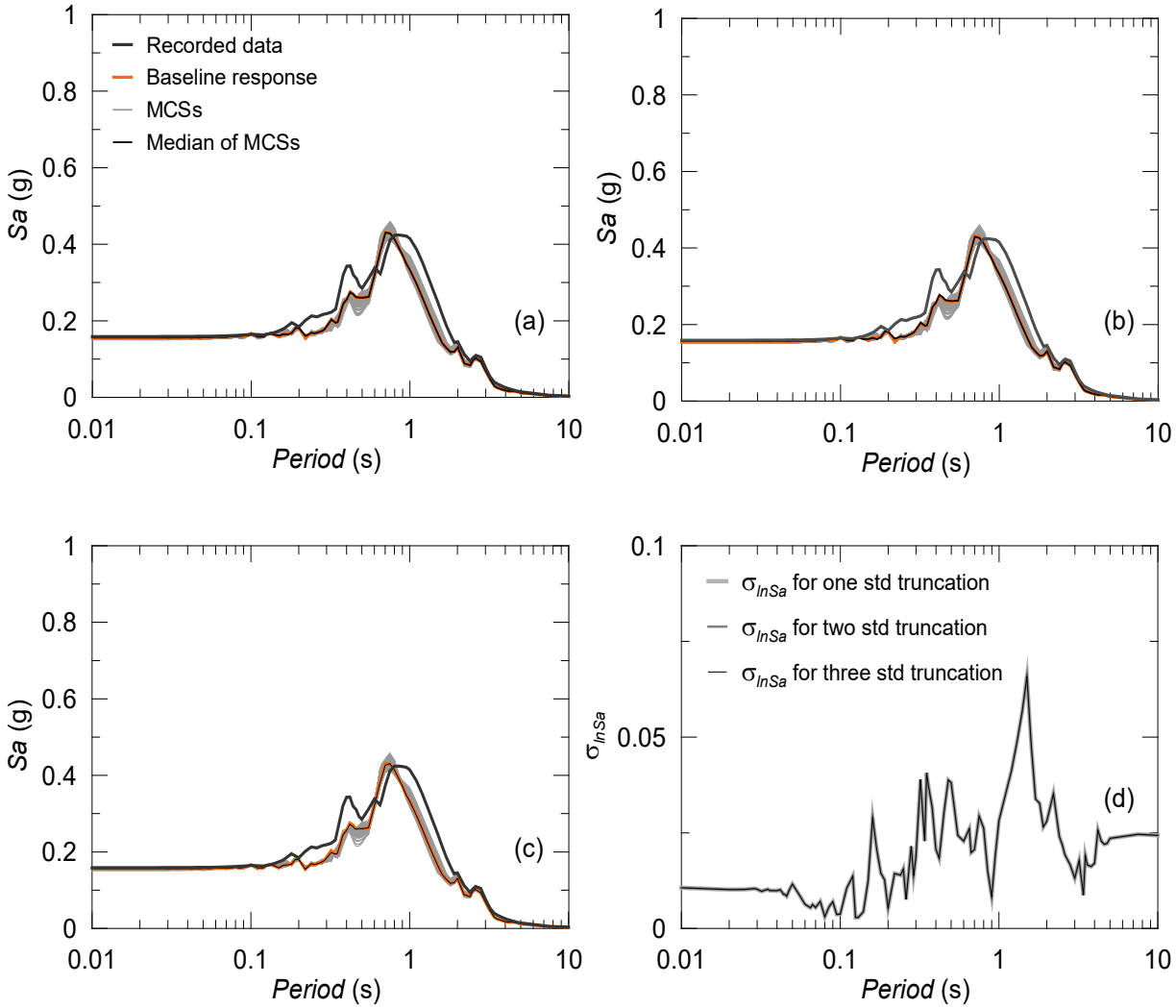

Figure 6.7 Influence of the level of truncation around the baseline V_s profile on site response prediction using the strong input motion: (a) with one std, (b) with two std, (c) with three std and (d) σ_{lnSa} at the ground surface.

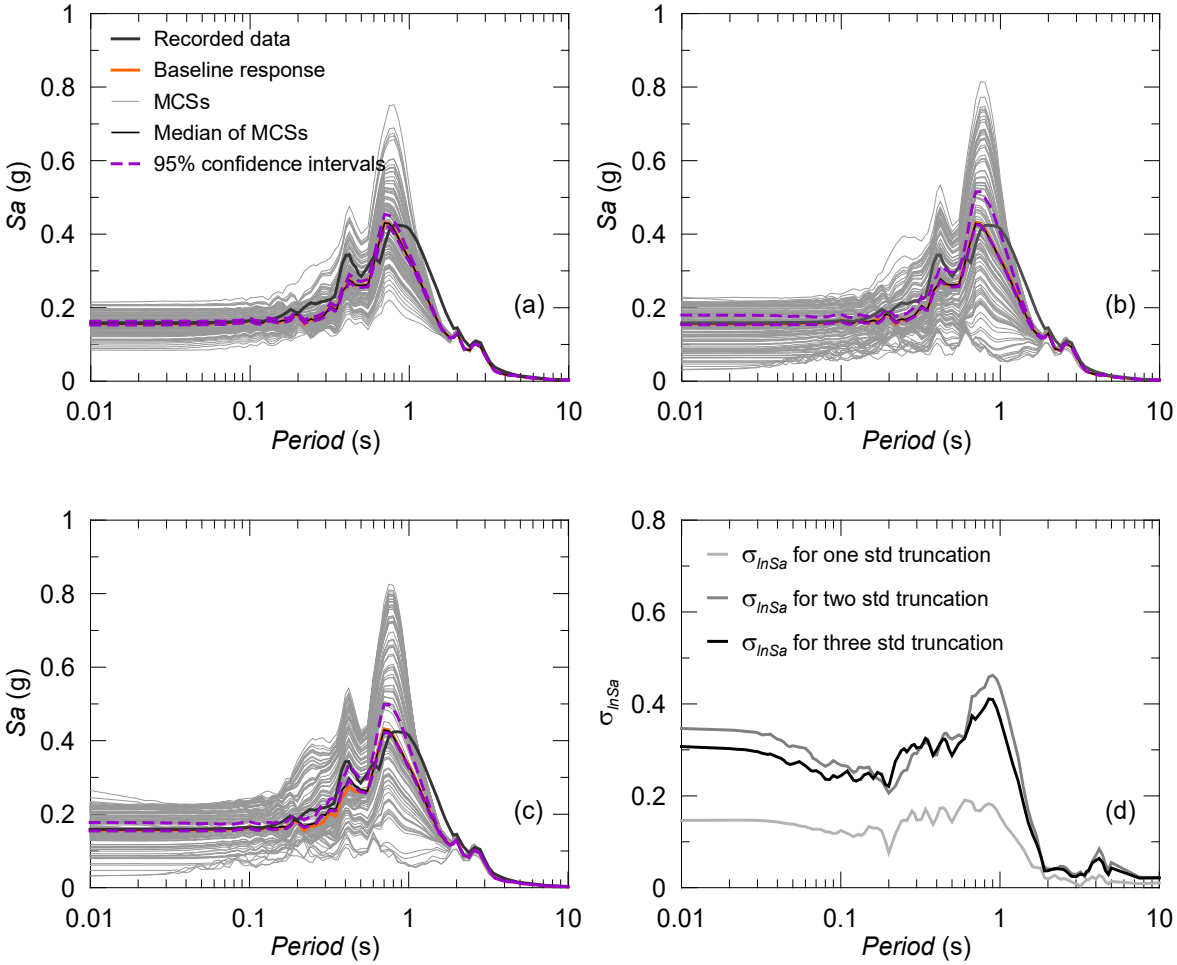

Figure 6.8 Influence of the level of truncation around the baseline G/G_o and D curves on site response prediction using the strong input motion: (a) with one std, (b) with two std, (c) with three std and (d) σ_{lnSa} at the ground surface.

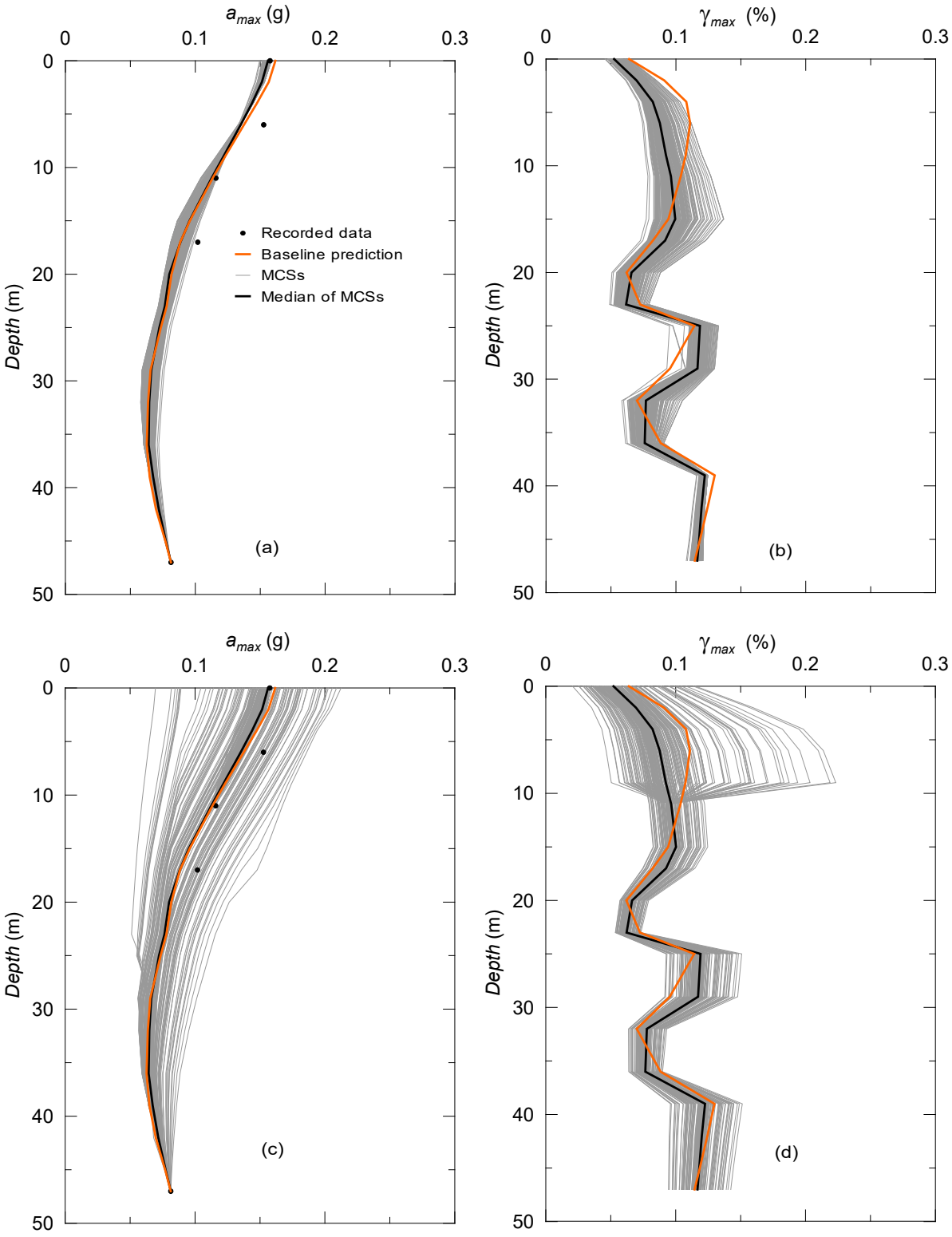

Figure 6.9 Maximum horizontal acceleration (a_{max}, in unit g) and maximum shear strain (γ_{max}, %) profiles when V_s profile (a, b) and G/G_o and D curves (c, d) are varied.

Finally, Figure 6.10 shows the results of the MCSs when the stiffness profile is spatially varied as described in Section 6.3.2. It seems that the spatial stiffness variability does not affect the median prediction under the strong input motion, although the standard deviation

of the logarithmic spectral accelerations increases when the level of truncation rises (Figure 6.10d).

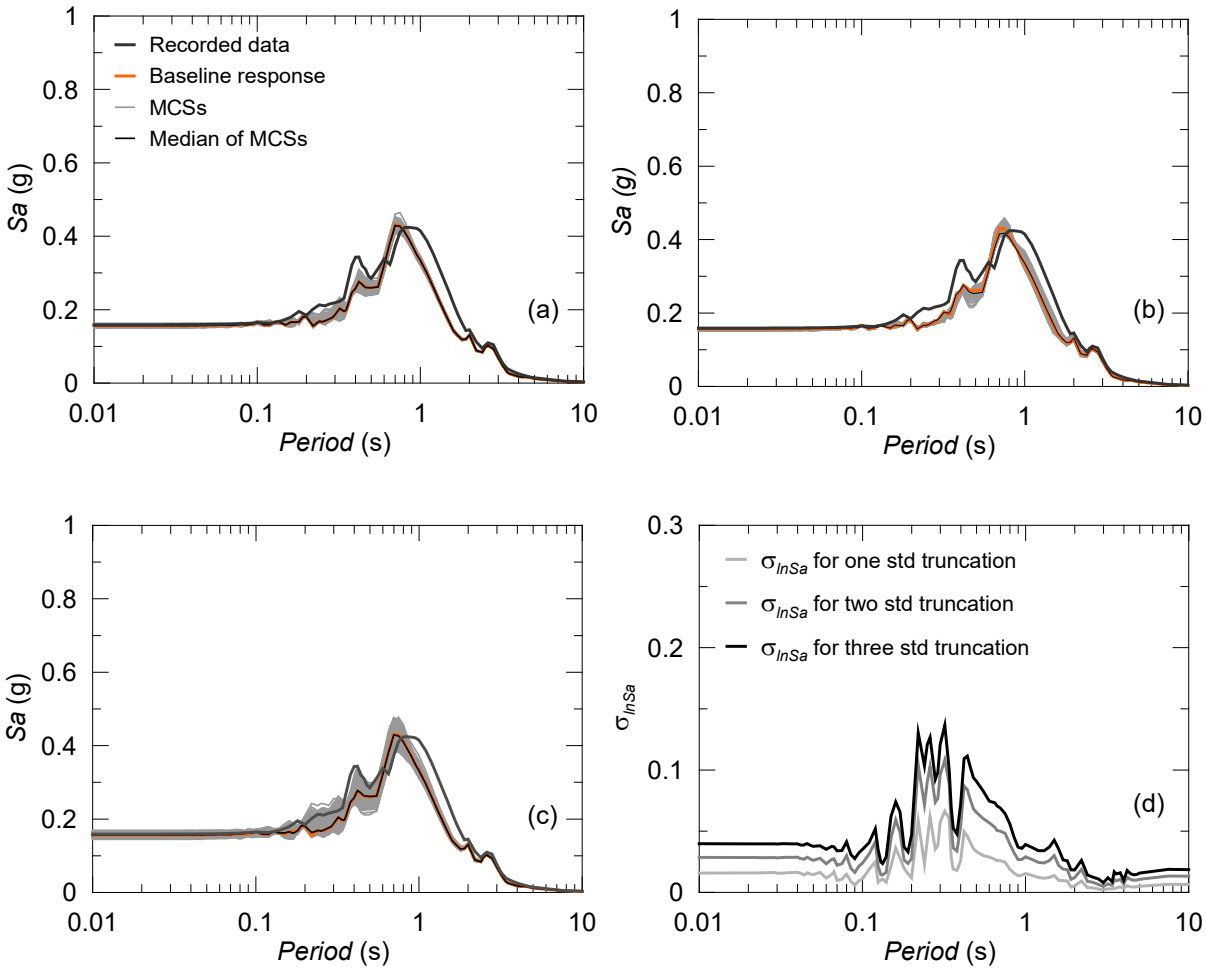

Figure 6.10 Median responses of 5 sets: (a) 10 realisations of V_s profile, (b) 20 realisations, (c) 50 realisations and (d) standard deviations of σ_{lnSa} within each set.

6.4.2 Effects of soil properties variability on site response under the weak input motion

An analogous statistical analysis is conducted applying the weak motion LSST11 at bedrock. Figure 6.11 describes the influence of stiffness profile and nonlinear curves variability on the site response prediction in this case. Similar to the discussion in the previous section, point variability of the initial stiffness profile is considered first. The variation of the V_s profile has now a significant impact on the site response prediction at the surface (Figure 6.11a). The median response spectrum obtained from MCSs is greater than the baseline result between 0.1 s and 0.35 s and closer to the actual recorded data, thus indicating that an improved prediction can be obtained in the weak motion case if the shear wave velocity profile variability is accounted for. In contrast, there is almost no influence of the variability

of the G/G_o and D curves on the response at surface, as seen in Figure 6.11b showing an exact match between each MCS and the baseline spectral prediction. Simultaneous variation of the V_s profile and the G/G_o and D curves causes similar median response closely matching with the baseline response spectrum (Figure 6.11c). This also does not lead to any significant change of the σ_{lnSa} at all periods (Figure 6.11d). It should be noted that there is an insignificant level of confidence interval coverages, especially when the G/G_o and D curves are varied (Figure 6.11b). This shows that small amounts of spectral changes can be observed in median responses of any possible 200 MCSs with the variation of the V_s profile and/or the G/G_o and D curves, and ultimately spectral predictions can give good indication of the actual response (Figure 6.11a, b and c).

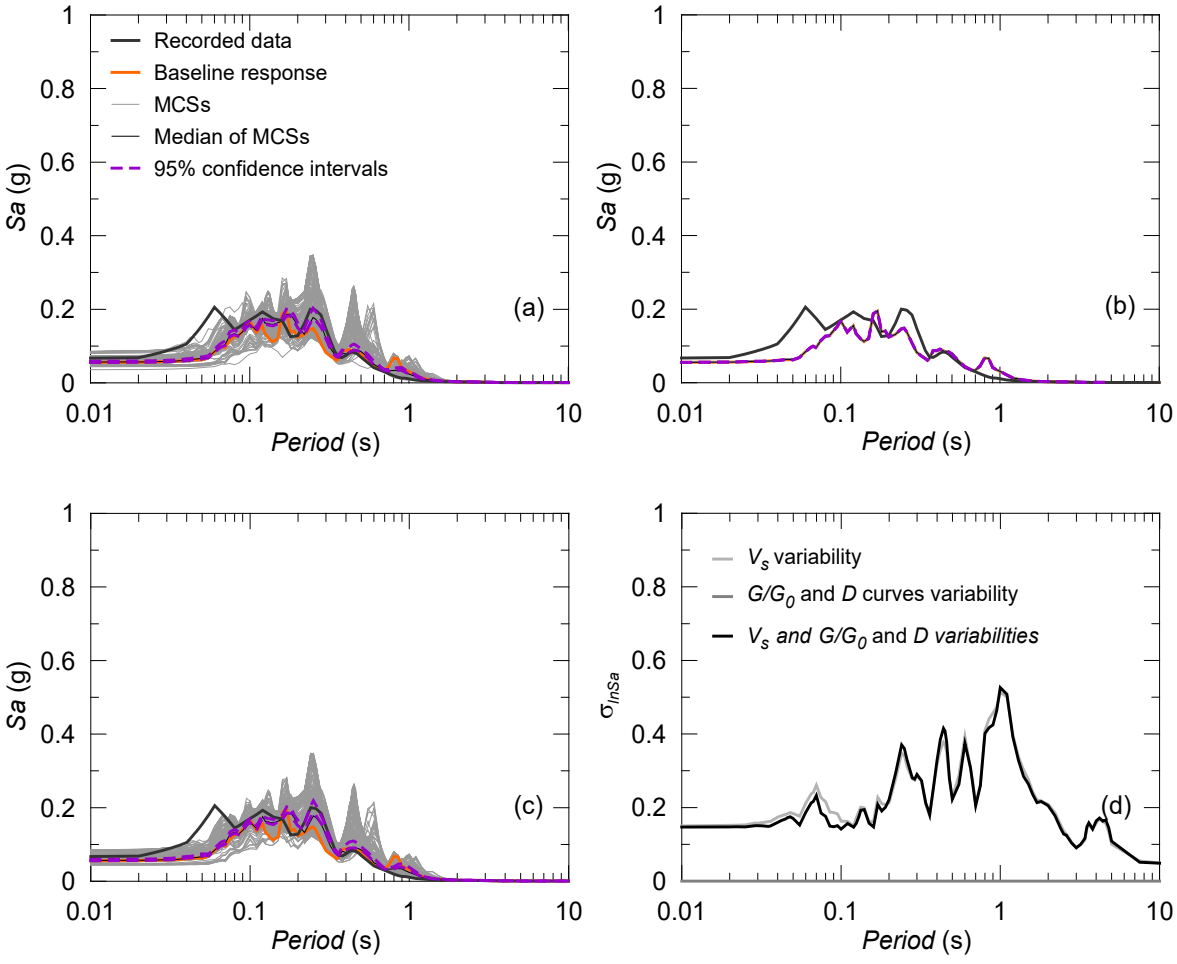

Figure 6.11 Site response prediction under the weak input motion (LSST11): (a) variability of V_s profile, (b) variability of G/G_o and D curves, (c) simultaneous variability of V_s profile and of G/G_o and D curves and (d) logarithmic standard deviations σ_{lnSa} in each case.

Since the V_s profile is the only factor controlling the predicted spectral accelerations when the weak input motion is considered, the adequate number of initial stiffness profile realisations required to get a stable response at the surface is investigated. Figure 6.12 presents the median response spectra for five sets of 10, 20 and 50 realisations of V_s and their standard deviations. The suites of 10 or 20 realisations produce a significant variation in the median responses (Figures 6.12a and 6.12b). Conversely, the sets of 50 realisations reduce the variability of the median responses, particularly in the period range between 0.3 s and 2 s, as shown in Figure 6.12c. This ensures a more stable response at the surface. When suites of 50 realisations are considered, discrepancies between the median spectral values can be still observed, but the level of standard deviation is considerably reduced (Figure 6.12d).

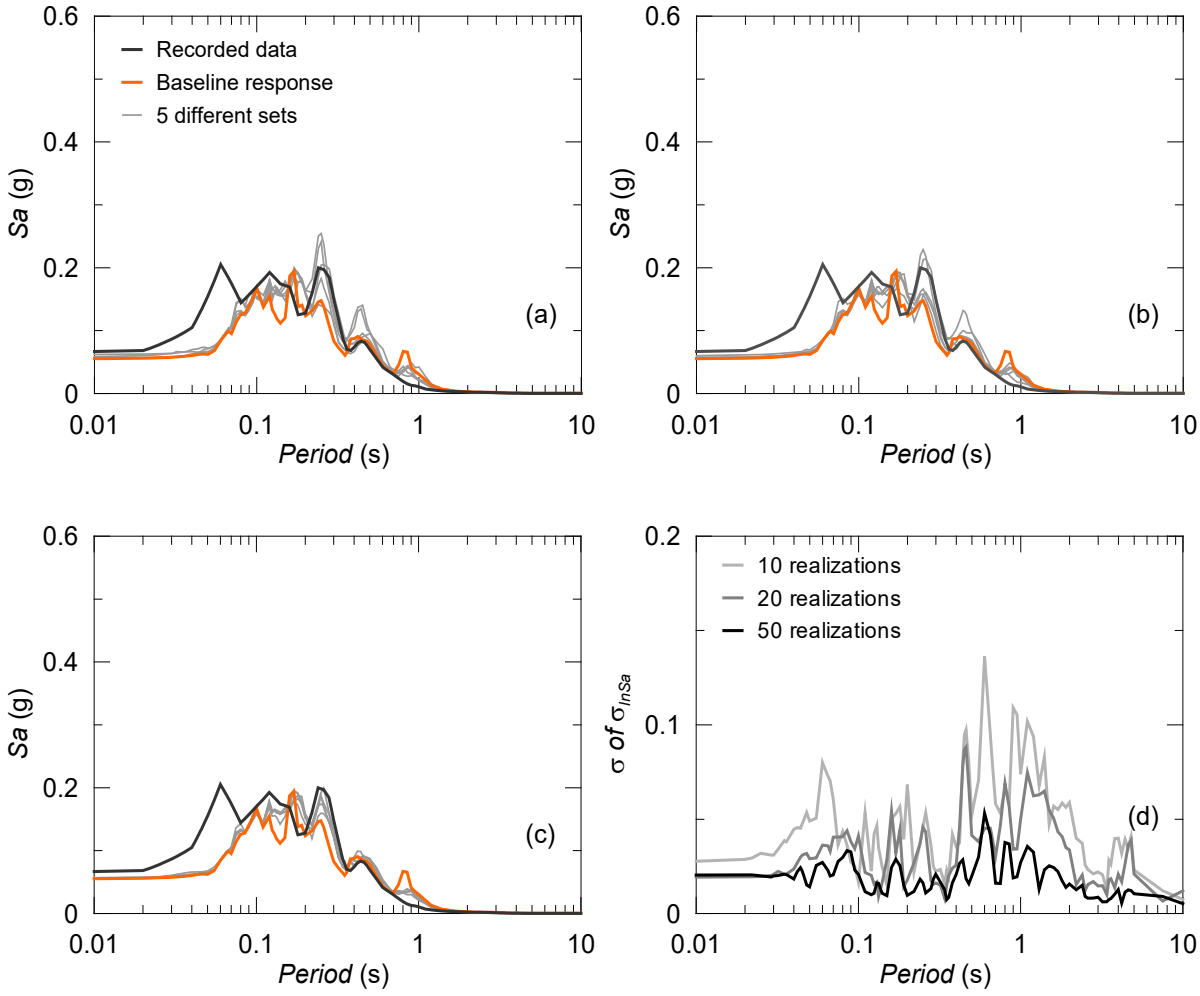

Figure 6.12 Median responses of 5 sets: (a) 10 realisations of V_s profile, (b) 20 realisations, (c) 50 realisations and (d) standard deviations of σ_{lnSa} within each set.

Figure 6.13 presents the median surface response obtained for one, two and three standard deviation level of truncation around the V_s baseline profile. The consideration of a wide range of variability of the V_s profile by increasing the level of truncation leads to an

improvement in the response prediction at the surface. Actually, the predicted median response spectrum becomes almost identical to the recorded data for periods higher than 0.2 s when two standard deviations are considered (Figure 6.13b). No further improvements with respect to the recorded accelerations at the site can be obtained by increasing the truncation level to three standard deviations (Figure 6.13c). At the same time, the logarithmic standard deviation of the spectral accelerations increases with rise of the truncation level (Figure 6.13d). Therefore, considering two or three standard deviation level of truncation around the V_s baseline profile can result in a better prediction at surface, but this requires more site response analyses to obtain the same level of stability in the simulation results. For the spectral curves of 95% confidence intervals, increasing the level of truncation level does not cause any considerable changes in the widths of intervals (Figure 6.13a, b and c) as they are closely matched and cover the recorded data reasonably well in all the cases.

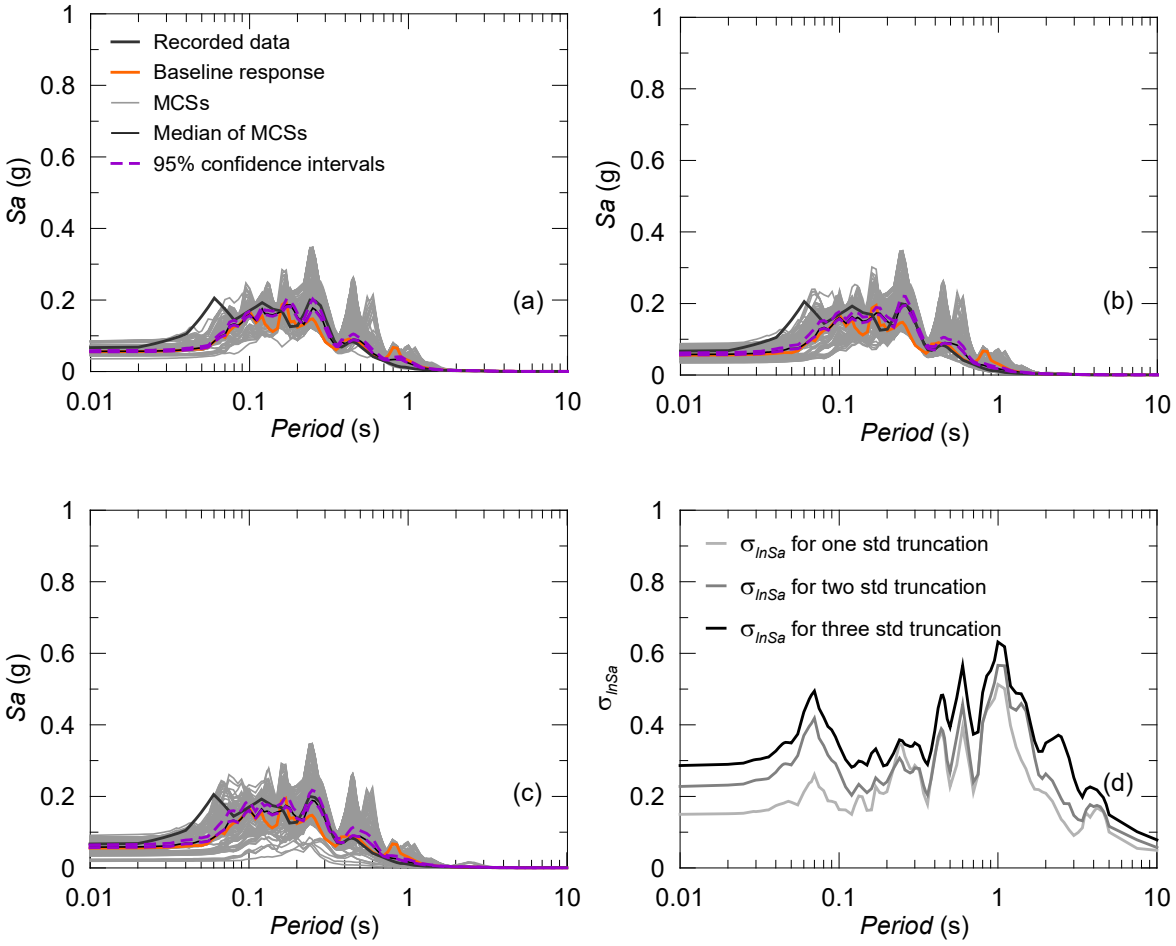

Figure 6.13 Influence of the level of truncation around the baseline V_s profile on site response prediction using the weak input motion: (a) with one std, (b) with two std, (c) with three std and (d) σ_{lnSa} at the ground surface.

On the contrary, the change in the truncation level around the G/G_o and D curve distributions does not introduce appreciable changes or variability in the response prediction, as shown in Figure 6.14, thus confirming the results presented in Figure 6.11b. The site response is, in fact, more sensitive to the initial stiffness profile when the weak motion is applied at bedrock, as the level of shear strain induced by the earthquake in this case is most likely to lie within the elastic region. Figure 6.15 presents the influence of stiffness profile and nonlinear curves variability on the a_{max} and γ_{max} profiles for the LSST11 event. Consistently with the results shown in Figure 6.11a, the median profile of a_{max} is closer to the Lotung data recorded along the depth when the variation of the V_s profile is accounted for, while the variability of the G/G_o and D curves has almost no effect of the MCS results (as indicated by Figure 6.11b).

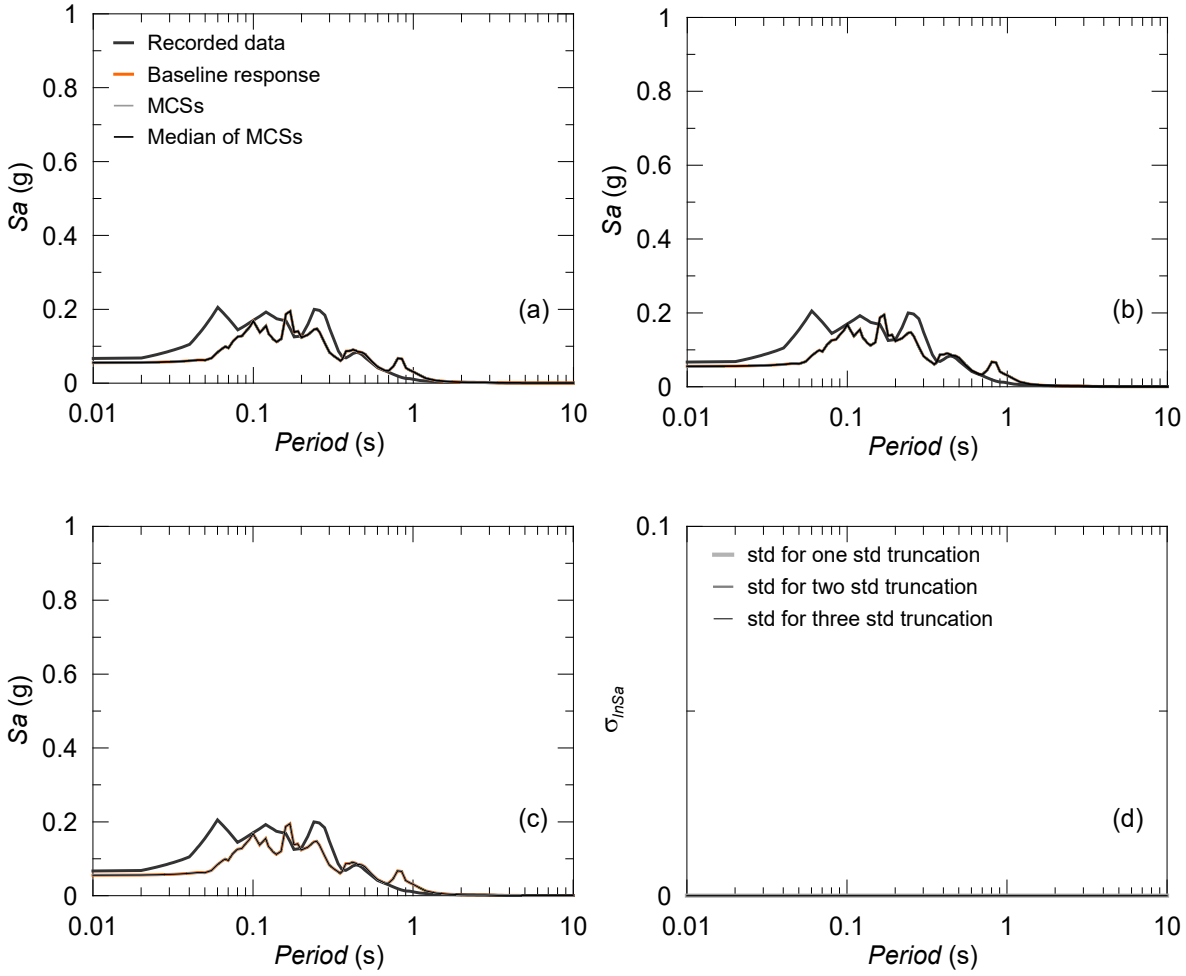

Figure 6.14 Influence of the level of truncation around the baseline G/G_o and D curves on site response prediction using the weak input motion: (a) with one std, (b) with two std, (c) with three std and (d) σ_{lnSa} at the ground surface.

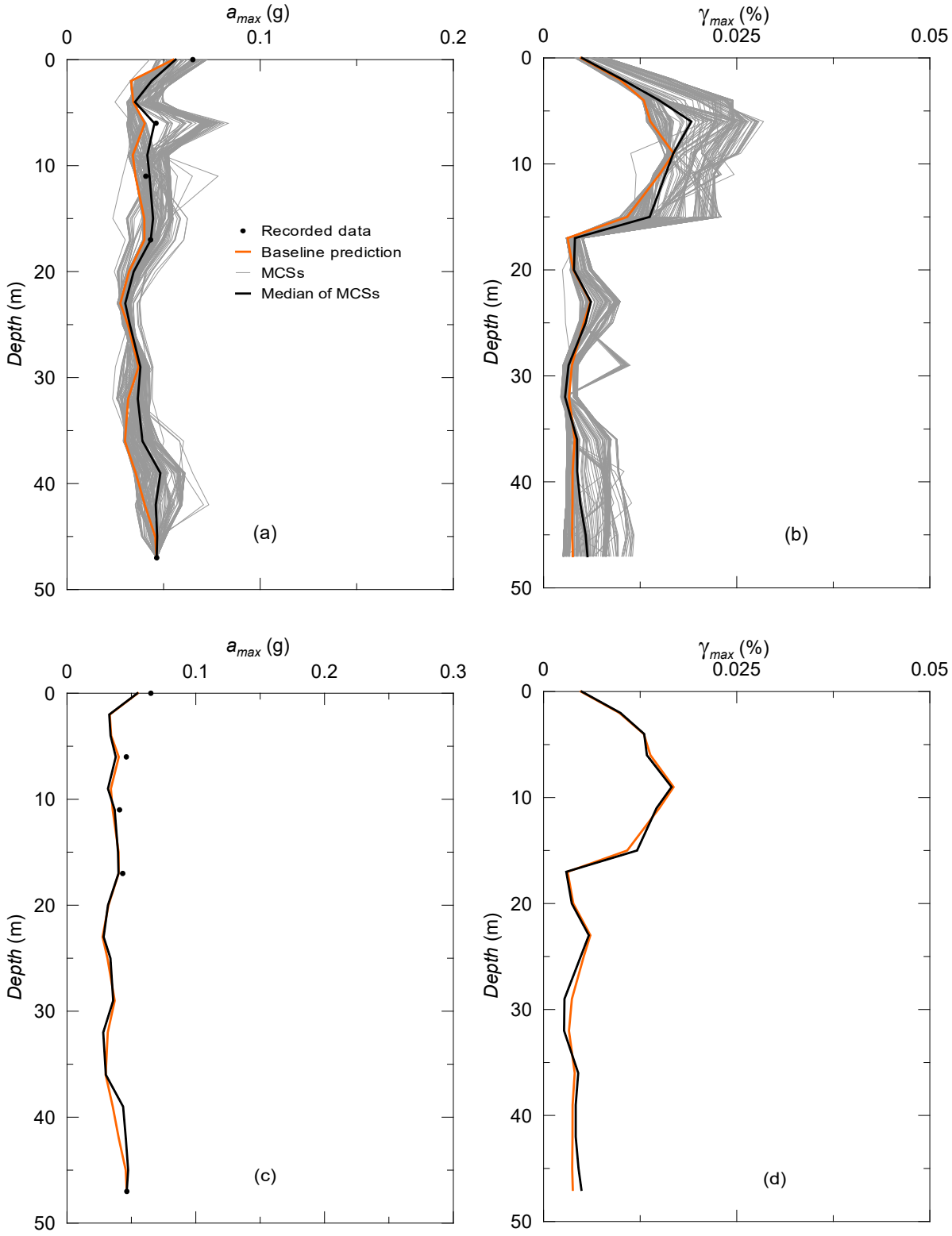

Figure 6.15 Influence of stiffness profile (a-b) and nonlinear curves (c-d) variability on the a_{max} and γ_{max} profiles for the LSST11 event.

When the V_s profile is spatially varied, Figure 6.16 indicates that the prediction is not really affected or diverted from the baseline response, even if the truncation level is changed. Different to what observed in Figure 6.13, the spatial variability of the initial stiffness profile

does not improve the predictions in terms of median surface response. Nevertheless, the σ_{lnSa} variation for each truncation level (Figure 6.16d) is smaller than the corresponding standard deviation distribution obtained considering a point stiffness variability (Figure 6.13d).

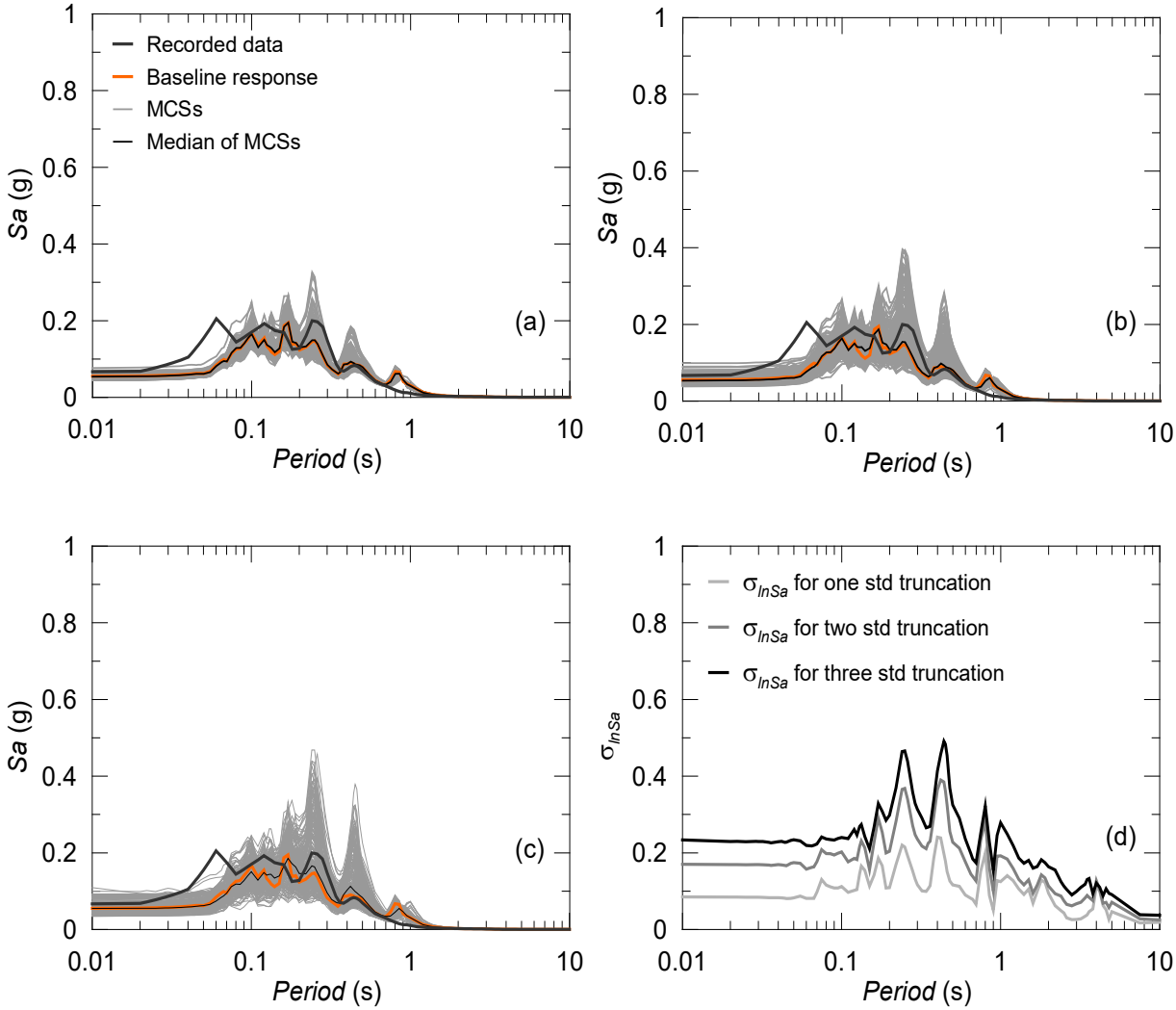

Figure 6.16 Influence of the level of truncation around the baseline V_S profile (based on spatial variability) on site response prediction of the weak input motion: (a) with one std, (b) with two std, (c) with three std and (d) σ_{lnSa} at the ground surface.

6.4.3 Equivalent Linear Monte Carlo Simulations

The impact of variability of shear wave velocity and shear modulus reduction and damping curves is also investigated by conducting equivalent linear MCSs through EERA visco-elastic program EERA (Bardet *et al.*, 2000). Similar V_s profiles and G/G_o and D curves used in the nonlinear MCSs are adopted in the equivalent linear analyses with same statistical distributions considered. Again, the E-W ground motions of LSST7 and LSST11 earthquake events recorded at the Lotung site are simulated.

It can be seen from Figure 6.17 that the variability of V_s profile and G/G_o and D curves contribute to the uncertainty in the site response prediction of the strong input motion at the ground surface. The variability of V_s profile does cause greater uncertainty in the response when it is compared with G/G_o and D curves. Nevertheless, median responses of MCSs are quite similar in both cases with the baseline response showing under-prediction of actual spectral values between 0.4 s and 2 s. From maximum acceleration and shear strain profiles exhibited in Figure 6.18, the influence of the variability through the soil profile can be seen. The variability in the a_{max} profiles (Figure 6.18a-c) increases towards the ground surface. This can be attributed to the nonlinear soil behaviour becoming more evident at the near surface and with this respect the variability in the soil properties affect dramatically the site responses.

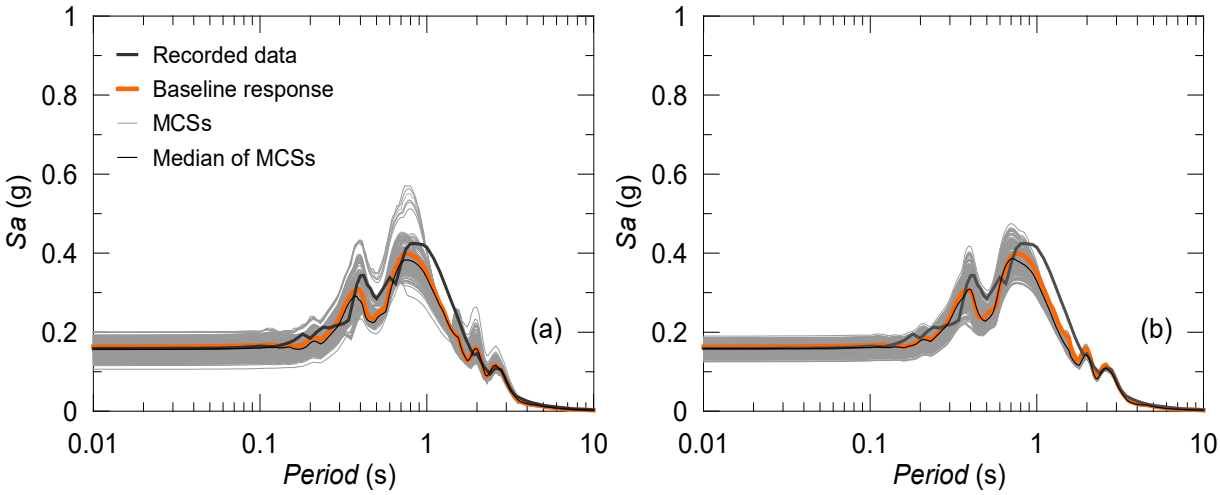

Figure 6.17 Equivalent linear site response prediction under the strong input motion (LSST7): (a) variability of V_s profile and (b) variability of G/G_o and D curves.

Since the soil model consist of sandy and clayey layers having relatively higher and lower values of V_s, this geological formation is obviously reflected in the γ_{max} profiles (Figure 6.18b-d). More precisely, the variability in the shear strain levels at sandy layers are greater than those at clayey layers when the V_s profile is varied. The figure also indicates the influence of stiffness contrast between the layers as rapid changes in the strain values are observed. When the G/G_o and D curves are varied, the variability in a single γ_{max} profile does not necessarily vary with the layers as relatively smooth transition between the layers is seen.

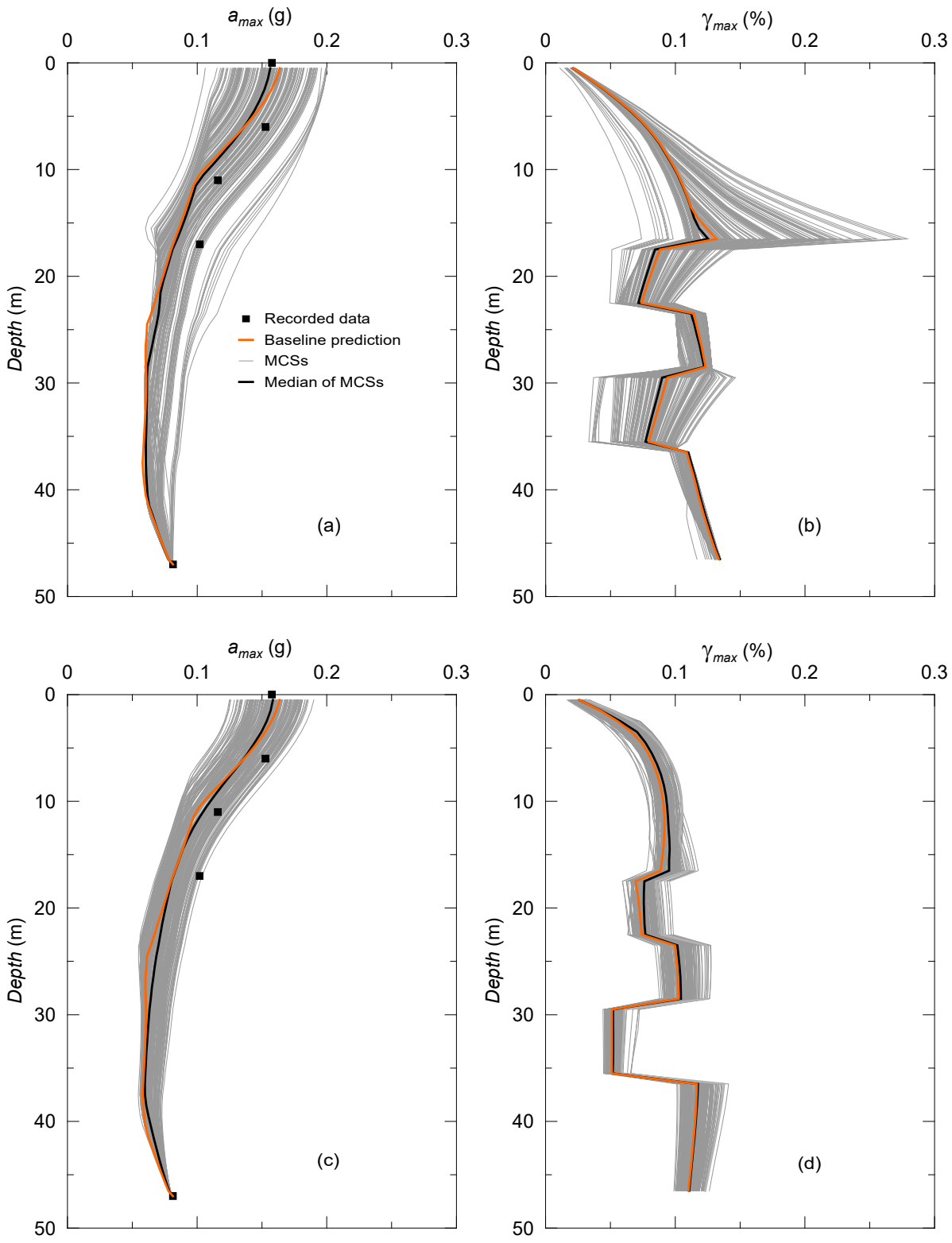

Figure 6.18 Influence of (a-b) stiffness profile and (c-d) nonlinear curves variability on the a_{max} and γ_{max} profiles for the LSST7 event.

When the weak motion is simulated, the variability of V_s profile is the major contributor affecting the site spectral responses at the surface (Figure 6.19a). On the other hand, the variability of G/G_o and D curves has not significant impact on the spectral values at the

interested period ranges, as can be seen in Figure 6.19b. Median response spectra in both cases are reasonably in good agreement with the baseline responses which are higher at the short periods (< 0.2 s) and match well with the actual data above that period.

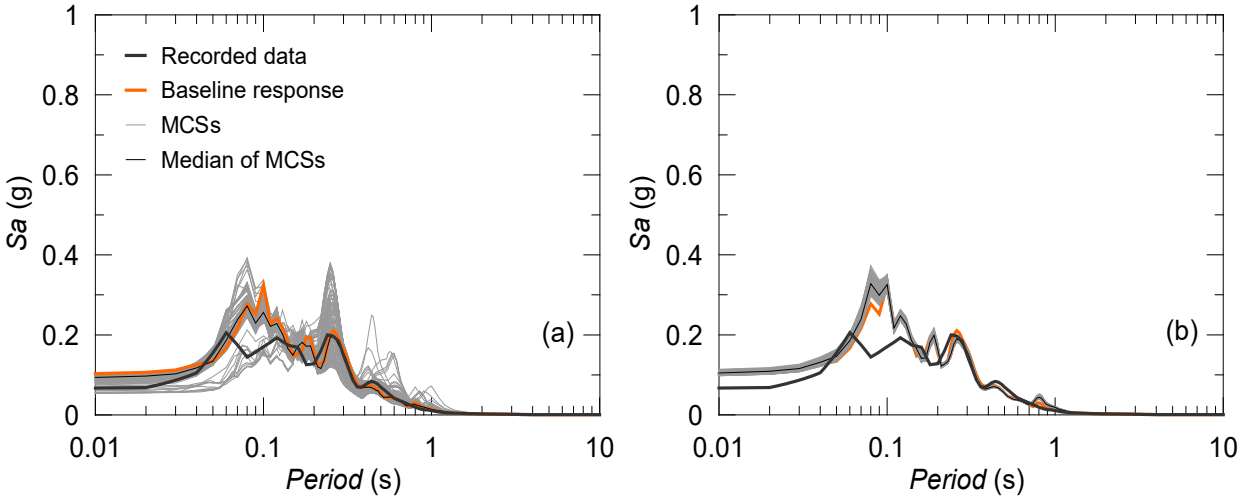

Figure 6.19 Equivalent linear site response prediction under the weak input motion (LSST11): (a) variability of V_s profile and (b) variability of G/G_o and D curves.

Maximum acceleration and shear strain profiles from the MCSs also indicate comparably greater influence of the variability of V_s profile and less of variability of G/G_o and D curves (Figure 6.20). It is important to say that the variability in a_{max} profiles does not increase towards the ground surface when the V_s profile is varied as opposed to the case under the strong input motion (i.e. Figure 6.18a). This is the indication of soil behaviour likely to be linear under the weak input motion, ultimately, the variability in the response becomes less sensitive to the variability of V_s profile. Moreover, although the strain levels at sandy and clayey layers are different but the impact of the variability is quite identical through the soil profile which may, again, be attributed to the seismic intensity level. In case of varying the G/G_o and D curves, not considerable effect on both a_{max} and γ_{max} profiles is observed.

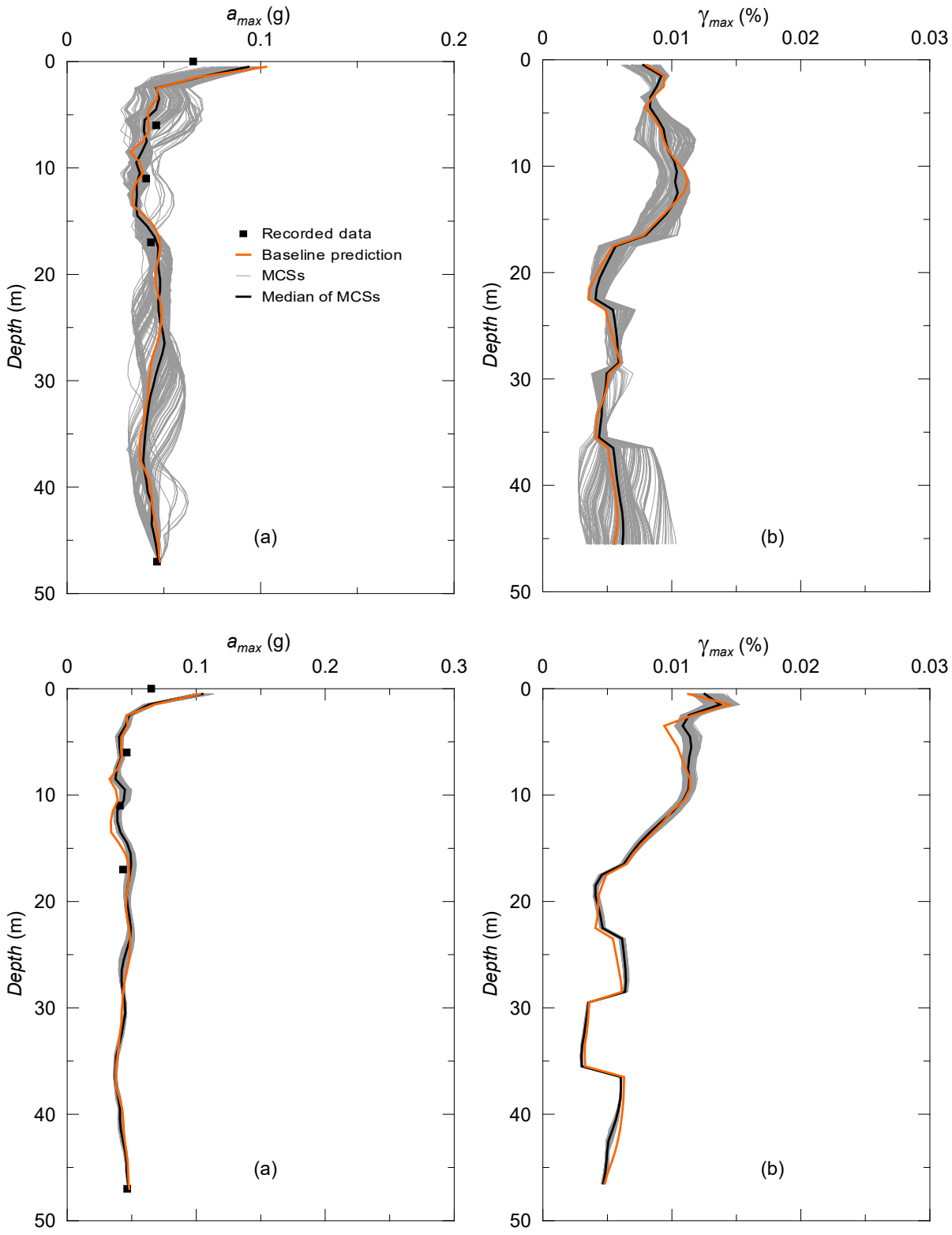

Figure 6.20 Influence of (a-b) stiffness profile and (c-d) nonlinear curves variability on the a_{max} and γ_{max} profiles for the LSST11 event.

6.5 Conclusions

This chapter investigates the influence of variability of elastic and nonlinear soil properties (i.e. shear wave velocity profile, shear modulus reduction and damping curves) on site response predictions through a Monte Carlo approach. For this purpose, the Large Scale Seismic Test site in Lotung is back-analysed using a fully-coupled finite element code and plasticity is introduced in the simulations through a kinematic hardening soil model. Two different input motions recorded at the site, one weak and one strong, are applied at bedrock to investigate the sensitivity of the statistical results to the seismic intensity level. Achieving the variability of V_s profile or G/G_o and D curves in MCSs according to the data from in-situ measurements or laboratory test results is an obvious advantage, in addition to employing a nonlinear FE code, of this study over past studies that implement empirical models with simpler codes to obtain such variabilities. The outputs of the MCSs are interpreted in terms of spectral responses at surface and standard deviation of the logarithmic spectral accelerations. They are also compared to the recorded array data available at the site and to the baseline predictions of deterministic FE analyses performed adopting best-estimate soil properties.

Overall, the results of the statistical approach indicate that the effect of variability in the elastic and nonlinear soil properties on the site response predictions shows a great dependency on the seismic intensity level of the input motion. In the case of a strong input motion, the variability of the stiffness degradation and damping curves has a more pronounced effect on the predicted site response, as nonlinearity is triggered by the high level of induced shear strain. Nevertheless, the median response spectrum of the MCSs is remarkably similar to the baseline prediction, even if the level of truncation is increased.

On the contrary, the results of MCSs at surface are particularly sensitive to the statistical variation in the initial stiffness profile when the weak motion is considered, being nonlinear effects almost negligible. Additionally, accounting for the point variability of the V_s profile in the case of a weak earthquake event can lead to an improved surface response prediction with respect to the deterministic approach. In the case of strong or weak input motions, the spatial variability of the initial stiffness profile does not improve, instead, the baseline predictions in terms of median response at surface.

Finally, equivalent linear MCSs performed with EERA show a quite similar statistical influence of the V_s profile and the G/G_o and D curve distributions on the ground response predictions for the strong earthquake event. In case of simulating the weak earthquake event, the variability of V_s profile affects the spectral response while the variability of nonlinear soil properties does not influence the response considerably. The simpler visco-elastic approach is, in fact, not able to distinctively reproduce the elastic and nonlinear soil behaviour as it cannot capture the continuous change of stiffness and damping properties throughout the motions.

Chapter 7. Summary and Conclusions

7.1 Summary

This thesis investigates the impact of input motion selection strategies and the influence of elastic and nonlinear soil properties (i.e. shear wave velocity profile, V_s, and shear modulus reduction, G/G_o, and damping, D, curves) on the nonlinear site response analysis of soft soil deposits. The ground response analysis is conducted by employing an advanced kinematic hardening soil model which has been implemented in a fully-coupled finite element software.

Chapter 1 briefly explains the background and motivation of the current research. It also includes the aim and objectives of the thesis followed by a description of its structure. In Chapter 2, the earthquake databases, ITACA, ESM, PEER, USGS, COSMOS, Geonet and KiK-net, are explored for the ground motions recorded on soft soil deposits (i.e. soil class D according to EC8). The first part of the chapter demonstrates the influence of factors such as magnitude, distance and local site conditions, on ground motions. In the second part, the types of seismic hazard analysis, used to define a site-specific response spectrum, are considered. Focus is given to the design response spectrum encompassed in EC8, whose suitability is compared with the empirical results from earthquake databases.

In Chapter 3, the development of selection strategies is discussed. The implementation of selection strategies and issues encountered in structural engineering are reviewed. The studies on this topic in the geotechnical engineering field are also presented. By recognising the lack of studies on the selection strategies in geotechnical engineering, the common research focuses are explained (e.g. development of site response analyses and soil models). In the last part of the chapter, the work on the influence of variability of V_s profile and G/G_o and D curves on site response analyses are reviewed with a special reference to the major studies.

In Chapter 4, the performance of the advanced soil model is evaluated by modelling the free-field Large-Scale Seismic Test (LSST) site in Lotung, Taiwan. The mean V_s profile obtained from the V_s values from the in-situ measurements is adopted. The soil material parameters are calibrated against well-documented experimental data (EPRI, 1993)

relative to soil samples retrieved from different depths of the downhole array. Equivalent linear analyses are also conducted for comparison purposes by using the equivalent linear visco-elastic program EERA. Two bedrock input motions from LSST7 and LSST11 earthquake events recorded at the bottom of the array are simulated, which represent relatively strong and weak seismic intensities. The input motions are applied in both horizontal directions (East-West and North-South). The predicted accumulation of pore water pressures at different depths is also compared with the actual data.

In Chapter 5, well-established input motion selection strategies are studied. Namely, PGA scaling, Sa(T_1) scaling, 0.2T_1 and 2T_1 scaling, MSE scaling and spectral scaling selection strategies are investigated. Earthquake events are selected from the European Strong-Motion Database and PEER Ground Motion Database. For each selection strategy, seven input motions are selected and modified, accordingly. Two EC8 target response spectra with 0.15g and 0.35g seismic intensities are adopted. An ideal soft clay soil with 50 m depth is modelled in the FE code and plasticity is described through the *RMW* model, as the model performance has been verified in Chapter 4. The parameters of soil model are calibrated by using G/G_o and D curves given in the literature. The spectral response predictions at surface and the Engineering Demand Parameters (EDPs), i.e. the relative horizontal displacement, peak acceleration and spectral acceleration at the first natural period of the soil deposit (Sa(T_1)), are considered. The influence of the number of bedrock input motions adopted for each scaling strategy and the soil depths on the surface response spectra and EDPs is also studied. Lastly, the t-test is conducted to test whether the median responses at surface can statistically be accepted as equal.

In Chapter 6, the effect of variability of V_s profile and G/G_o and D curves on site response prediction is investigated by using the same free-field FE soil model and input motions used in Chapter 4. The measured V_s values are used to randomise the V_s profile based on logarithmic distributions using Monte Carlo Simulations (MCSs). The V_s profile is also randomised with respect to spatial variability. G/G_o and D curves are varied by lognormally distributing a soil model parameter that has major impact on the dynamic shear modulus and corresponding damping ratio values. This characterisation of nonlinear curves is also in line with the experimental data given in the literature. For the sake of simplicity, only the E-W components of bedrock input motions are simulated. Model-to-model variability is also investigated by employing EERA program in MCSs.

Lastly in Chapter 7, the objectives of chapters are recalled including methodologies. Subsequently, the results are summarised and followed by general findings of the study. Finally, some recommendations are provided for future studies in relation with seismic site response analysis.

7.2 Conclusions from Each Chapter

7.2.1 Chapter 2

The first step in input motion selections is to define a target response spectrum obtained from a site-specific seismic hazard analysis (deterministic or probabilistic) or from a design provision code (e.g. EC8, NEHRP). By closely looking at the input motion selection strategies in the structural engineering discipline, it is recognised that the Intensity Measure (IM) linking the seismic hazard to the building response is the most useful factor to be considered in the selection. Efficiency and sufficiency are the two important features expected from an IM. In the early stages, the peak ground acceleration (PGA) of an input motion was accepted as a good IM reflecting both the characteristic of the motion and the structural response. However, further researches reveal that $Sa(T_1)$ is a better IM candidate than PGA. This chapter also includes studies showing the legitimacy of linear scaling of input motions causing less scatter in the structural response, thus, leading to fewer nonlinear analyses. Furthermore, the use of arbitrary spectral acceleration rather than geometric mean is justified along with consideration of epsilon, ε, and the use of uniform hazard spectrum against conditional mean spectrum.

In the second part of the chapter, the lack of research focusing on the input motion selections in the analyses of geotechnical problems is highlighted by referencing few studies conducted recently. The frameworks of equivalent linear and nonlinear approaches developed for site response analyses are explained with their merits and drawbacks. Following that, early developments of soil models are given and the necessity of more sophisticated soil models that can capture early irreversibility, stiffness degradation and soil structure losses is justified. Specifically, the philosophy of *RMW* model is demonstrated. In the last part, the chapter investigates the role of variability of V_s profile and G/G_o and D curves in site response analyses discussed in the relevant literature.

Overall, this chapter demonstrates the need of further research on the influence of selection strategies on site response analyses. Moreover, it highlights the importance of variability of elastic and nonlinear soil properties on site response analyses. These two conclusions drawn from the literature justify the necessity of the work undertaken in Chapter 5 and Chapter 6.

7.2.2 Chapter 3

This chapter demonstrates that the magnitude of an earthquake event greatly influences the frequency content and duration of ground motions. Moreover, the distance between the epicentre of the earthquake event and the station is shown to have an impact on the spectral values at short, medium and long period ranges. A local site condition (i.e. stiffness profile) is shown to be considerably influential in the ground motion amplifications from the bedrock to the ground surface. Subsequently, the concepts of deterministic and probabilistic site response analyses adopted in modern design codes are explained. Particularly, the benefit of a probabilistic approach, which considers all potential future earthquake events at a specific site, over the use of a deterministic approach, which is recognised to be subjective as only a single worst-case earthquake event is considered, is highlighted.

The results of spectral responses of ground motions recorded in soft soils from the earthquake databases indicate that EC8 design response spectrum can be seen as a good proxy of potential earthquake events for both Type 1 and Type 2 seismic intensity levels. In contrast, by closely checking the spectral accelerations of several individual ground motions, it is found that the spectral peaks over the plateau of the design response spectrum and at the longer periods cannot be represented by the EC8 spectral shapes. In this chapter, hence, it is suggested to conduct site response analyses when a site is located over soft soil deposits and to study ideal soft soil deposits in Chapter 5.

7.2.3 Chapter 4

The results from the equivalent linear and nonlinear site response analyses of the Lotung site show the potential of both approaches when the weak input motion of LSST11 earthquake event is applied at the bottom of the soil model. More precisely, both approaches lead to similar spectral response predictions in the E-W and N-S directions, especially at 11 m and 6 m, and they are in good agreement with the actual recordings. This is also confirmed by the PGA and shear strain profiles. In case of simulating the strong input motion of LSST7

earthquake event, where the soil nonlinearity is expected to be influential in site response predictions, both approaches, again, perform well in the prediction of spectral responses at 11 m and 6 m and at the ground surface in E-W direction, capturing the PGAs.

When the N-S strong input motion is applied, the equivalent linear approach predicts spectral accelerations relatively better than the nonlinear approach at periods lower than T_1. Conversely, the nonlinear approach shows good performance over periods higher than T_1. Both approaches, however, under-predict the PGAs at 11 m, 6 m and at the ground surface. The predictions of accumulation of pore water pressure at different depths agree well with the recorded data under the strong input motion in both directions, indicating the capability of the nonlinear approach. Further research is conducted to better understand the reason of the under-prediction obtained from the FE nonlinear approach in the N-S direction by modelling only a 17 m column with a gradually reduced V_s profile. The spectral predictions in this case improve significantly at all considered depths in the N-S direction, while this causes over-predictions in the E-W direction.

This chapter verifies the performance of the advanced soil model in predicting site response within a FE procedure, especially under strong input motions. Moreover, it emphasises the importance of the V_s profile in site response prediction, especially at the near surface, which leads to the study undertaken in Chapter 6.

7.2.4 Chapter 5

The initial spectral response results from the equivalent linear and nonlinear analyses show that, apart from PGA scaling, the remaining selection strategies result in similar response for both seismic intensity levels. The first two natural periods of soil deposit contribute to the seismic oscillations. The outputs of the simulations also imply that the EC8 design response spectrum may not be a good indicator of a future earthquake event at a 0.15g seismic intensity level. In contrast, it becomes a better proxy according for a 0.35g seismic intensity level, as confirmed by both equivalent linear and nonlinear analyses. It is also found the inappropriateness of the EC8 design response spectrum at the 0.35g seismic intensity level for soil deposits with depths higher than 50 m, due to the considerable amplification in the long period ranges.

EDP results point out that the spectral matching selection strategy is the best candidate amongst the others as it leads to the least scattered response, thus requiring fewer nonlinear

site response analyses. The Sa(T_1) or $0.2T_1$-$2T_1$ selection strategies can be seen as the second-best options to be considered.

Increasing the number of input motions does cause similar median response spectra and introduces greater uncertainty or scatter in terms of EDPs. This, hence, does not suggest to increase the number of input motions from 7 to 14. From the test results for the selection strategies using either 7 or 14 input motions it is concluded that, except from the EDPs from PGA selection strategy, the median EDPs from the remaining selection strategies can be regarded as equal at both 0.15g and 0.35g seismic intensity levels.

7.2.5 Chapter 6

The results of 200 nonlinear MCSs reveal that the variability of G/G_o and D curves does clearly affect the spectral response predictions, while a very small effect is observed when the V_s profile is varied under the strong input motion. Median responses are shown to be remarkably similar to the baseline responses obtained by using mean V_s profile and G/G_o and D curves. Hence, no improvement is observed when the variability of soil property is included in the site response analyses. 50 randomisations of G/G_o and D curves seem to be sufficient to obtain a stable median response at the surface of the soil deposit. Increasing the level of truncation from one std to two and three std around V_s profile and G/G_o and D curves does not change the median responses, but only increase the level of logarithmic standard deviation. This is especially evident at around T_1, where the site amplification tends to be greater and becoming more sensitive to the variability of soil property. Spatial variability of V_s profile does also not show any considerable impact on the median response.

In case of simulating the weak input motion, the variability of V_s profile is the major factor influencing the spectral response values, while no effect of the variability of G/G_o and D curves is observed. Median response prediction in the former case shows better agreement with the actual spectral response than the baseline prediction. This is more strongly evident when the level of truncation is increased, along with the increase of logarithmic standard deviation. Spatial variability of V_s profile also influences the site responses, but does no significantly improve it as opposed to the case observed for the normal probability distribution.

The results of the equivalent linear MCSs under the strong input motion show the influence of variability of both V_s profile and G/G_o and D curves on the spectral response predictions

leading to median responses similar to the baseline response. The effect of the variability of V_s profile is greater than that of G/G_o and D curves. The results under the weak input motion demonstrates only the influence of V_s profile on the spectral response, while the variability of G/G_o and D curves does not affect the response at the surface.

7.2.6 Findings of the Study

In light of the aim and objectives of this research study, Chapter 2 and Chapter 3 depict the necessity of such study in the geotechnical engineering field, particularly for site response analyses. While Chapter 4 tests the performance of the employed nonlinear FE approach with the advanced soil constitutive model, it also highlights the importance of shear wave velocity profile in site response analyses. Chapter 5 analyses the input motion selection strategies with respect to spectral responses and EDPs at the surface and tests the suitability of EC8 design response spectrum. Finally, Chapter 6 investigates the influence of variability of soil properties on equivalent linear and nonlinear site response analyses. Overall, the findings of the thesis can be listed as follows:

1. The equivalent linear and nonlinear FE codes (EERA and SWANDYNE II, respectively) can be useful in predicting site responses when a weak input motion is simulated.
2. The use of a FE code can be particularly recommended in simulating a strong input motion as it captures early irreversibility and accumulation of pore water pressure during seismic oscillations.
3. Spectral matching selection strategy is the best candidate in the selection of bedrock input motions for site response analyses. $Sa(T_1)$ or $0.2T_1$-$2T_1$ selection strategies can be the second best options if only linear scaling is considered appropriate.
4. Consideration of seven bedrock input motions is sufficient to obtain a stable response at the surface, especially for the selection strategies mentioned in the previous point.
5. The influence of variability of elastic and nonlinear soil properties on site responses is dependent on the seismic intensity level of the input motion. The effect of variability also show differences with respect to the numerical model adopted (e.g. equivalent linear or nonlinear numerical approaches).
6. Nevertheless, the inclusion of variability into nonlinear or equivalent linear site response analyses does not tend to improve the response predictions as the median

spectral responses are in good agreement with the baseline predictions, especially in the case of simulating strong input motions.

7.2.7 Recommendations for Future Works

This research mainly studies input motion selection strategies and the influence of variability of soil properties on site response analyses along with the verification of the adopted constitutive model in describing the behaviour of soil deposits in two-dimensions (2D). Equivalent linear analyses are also undertaken for comparison purposes. While the findings of the study are presented in the previous section, the current section intents to give suggestions for future works concerning site response analyses.

2D nonlinear FE analyses is shown to lead to a reasonable response prediction at the Lotung site, especially in the E-W direction. Inefficiency of the numerical model in predicting the N-S component of the earthquake event is further studied in this study by using reduced stiffness profile and some improvement is observed. It is important to note here that the spectral amplification at the top 6 m is far greater in the N-S direction than in the E-W direction. This makes a good prediction in both directions not possible by using the same soil profile. For possible future studies addressing this issue, it is either necessary to modify and adopt different soil profiles in E-W and N-S directions in terms of its elastic and nonlinear soil properties (as, to some extent, applied in Chapter 4). Or, three-dimensional (3D) FE modelling can be used as it will enable to apply the input motions simultaneously in both horizontal directions. Full-scale FE modelling of the site can be an alternative study that will allow to more realistically simulate the seismic wave propagation through the soil layers as the geological formations in the E-W and N-S directions are different (as presented in Chapter 4). This is known in the literature as basin effect on site response analysis (Ince and Yılmazoğlu, 2014) and can be firstly studied in 2D models and then extended to 3D models of the Lotung site.

This study gives preferable input motion selection strategies for site response analyses of soft soil deposits and confirms the inability of EC8 design response spectrum in representing the possible future earthquake event. It is also advised to consider the thickness of soft soil deposits when the design response spectrum is constructed. In order to pronounce these conclusions more strongly, it is necessary to conduct a considerable number of site response analyses with a number of different bedrock input motions and different soil deposits.

Furthermore, the selection strategies studied here can be further examined in terms of structural response by modelling the full soil-foundation-structure interaction problem. This will require a numerical code where the behaviour of the soil, foundation and structure subjected to dynamic loading can be modelled at the same time. It is only in this way that the work will contribute to closing the gap between the geotechnical and structural engineering practitioners in relation to understanding comprehensively seismic hazards of earthquake events to earth structures.

Lastly, this study points out the dependence of site response predictions on the seismic intensity levels and the numerical models considered when a statistical variation of the soil properties is accounted for. It also indicates that the involvement of variability of soil properties does not clearly improve the prediction and, thus, its consideration in site response analysis seems not to be encouraging. To further discretise the uncertainty in site responses, influence of stiffness contrast between the soil layers should be carefully investigated as it can cause great amplification, especially at the near surface. Secondly, the influence of variability in the thickness of soil deposit on site response should be studied to better quantify the uncertainty in the responses. Finally, a deeper insight into the influence of variability of soil properties will be gained by modelling a site in 3D and applying the two horizontal components of an earthquake event simultaneously.

Appendix A

1 EC8 Design Response Spectrum

Horizontal design response spectrum is described with the following parameters, within the corner period ranges (T_B , T_C and T_D):

$$0 \le T \le T_B \rightarrow \ S_e(T) = a_g S \left[1 + \frac{T}{T_B}(\eta 2.5 - 1)\right] \quad \text{A.1}$$

$$T_B \le T \le T_C \rightarrow \ S_e(T) = a_g S \eta 2.5 \quad \text{A.2}$$

$$T_C \le T \le T_D \rightarrow \ S_e(T) = a_g S \eta 2.5 \left[\frac{T_C}{T}\right] \quad \text{A.3}$$

$$T_D \le T \le 4s \rightarrow \ S_e(T) = a_g S \eta 2.5 \left[\frac{T_C T_D}{T^2}\right] \quad \text{A.4}$$

where

$S_e(T)$= elastic response spectrum;

T = vibration period of a linear single-degree-of-freedom system;

a_g= design ground acceleration on type A ground ($a_g = \gamma_I a_{gR}$);

γ_I=importance factor;

a_{gR}=reference peak ground acceleration on type A ground;

T_B=lower bound of the period of the constant spectral acceleration region;

T_C=upper bound of the period of the constant spectral acceleration region;

T_D= period at and beyond which the constant displacement response range of the spectrum;

S=soil factor;

η=damping correction factor with a reference value of η = 1 for 5% viscous damping.

The soil factors and the corner periods (T_B, T_C, and T_D) values for each type of soil in seismicity Type 1 and Type 2 cases are given in the following table:

Ground Type	Seismicity Type 1				Seismicity Type 2			
	S	T_B(s)	T_C(s)	T_D(s)	S	T_B(s)	T_C(s)	T_D(s)
A	1	0.15	0.4	2	1	0.05	0.25	1.2
B	1.2	0.15	0.5	2	1.35	0.05	0.25	1.2
C	1.15	0.20	0.6	2	1.5	0.1	0.25	1.2
D	1.35	0.20	0.8	2	1.8	0.1	0.3	1.2
E	1.4	0.15	0.5	2	1.6	0.05	0.25	1.2

Table A.1 Soil factors (S) and corner periods for each soil class.

2 Horizontal Components of the Records

The median spectral response of the accelerations recorded along two horizontal directions on soil class D and available in each database are represented here.

ITACA

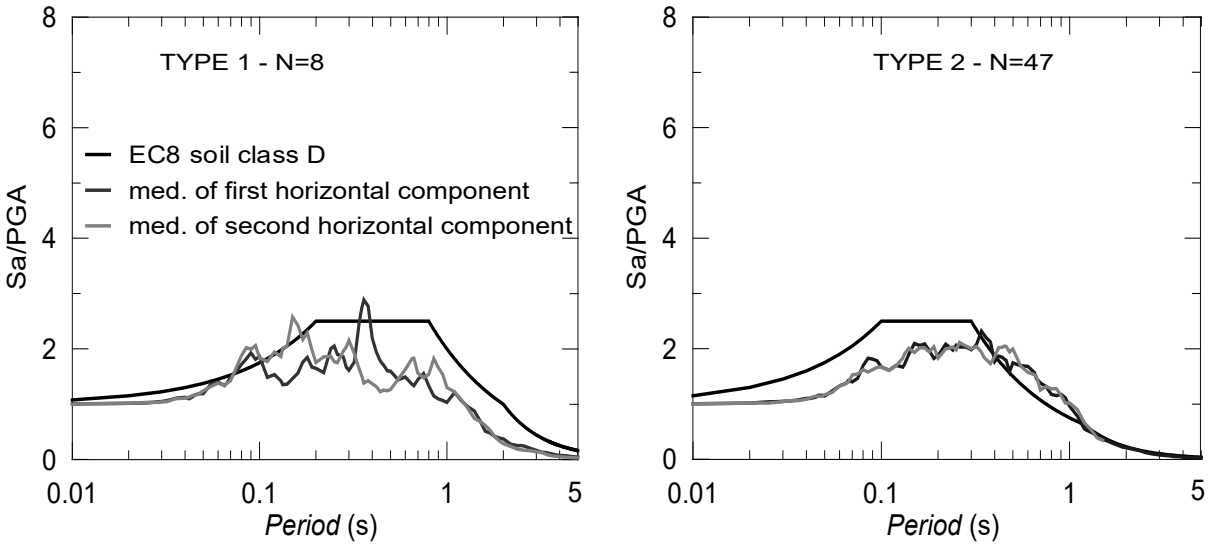

ESMD

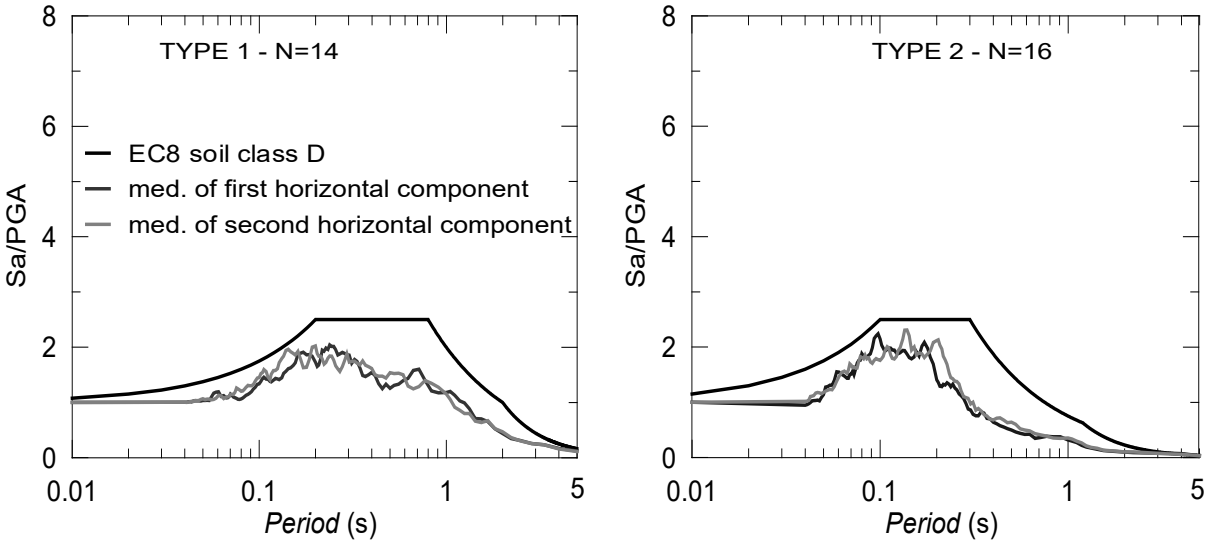

USGS

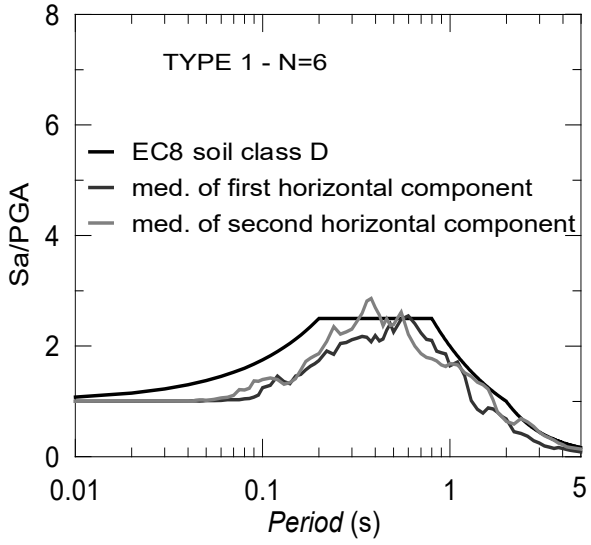
TYPE 1 - N=6
EC8 soil class D
med. of first horizontal component
med. of second horizontal component
Sa/PGA
Period (s)
0
2
4
6
8
0.01
0.1
1
5

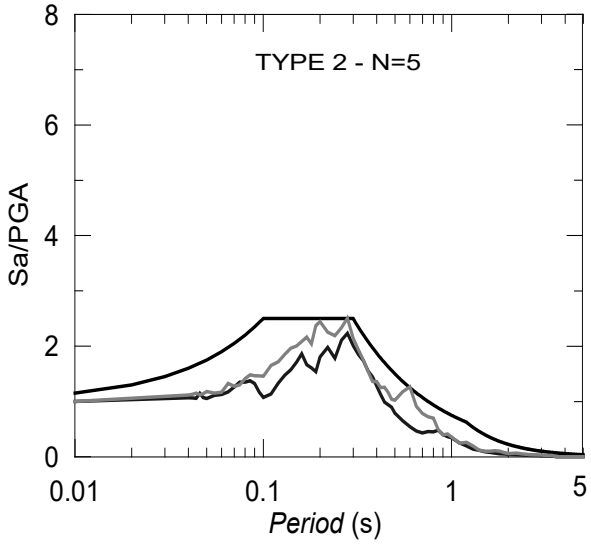
TYPE 2 - N=5
Sa/PGA
Period (s)
0
2
4
6
8
0.01
0.1
1
5

COSMOS

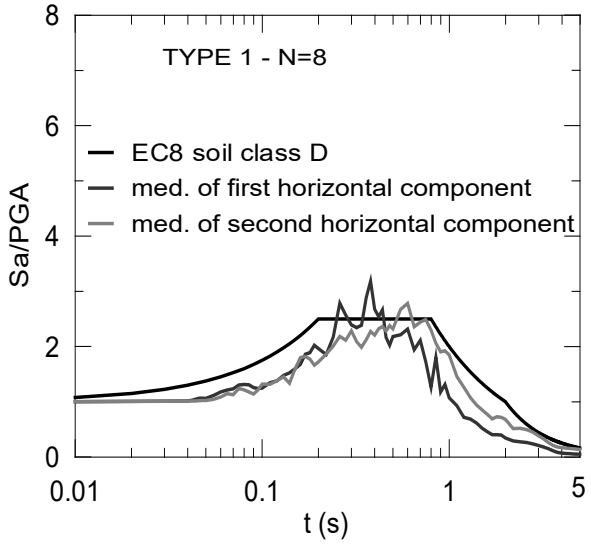
TYPE 1 - N=8
EC8 soil class D
med. of first horizontal component
med. of second horizontal component
Sa/PGA
t (s)
0
2
4
6
8
0.01
0.1
1
5

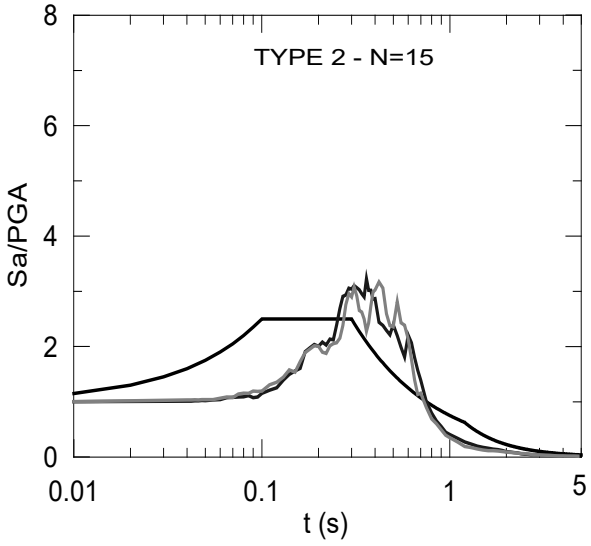
TYPE 2 - N=15
Sa/PGA
t (s)
0
2
4
6
8
0.01
0.1
1
5

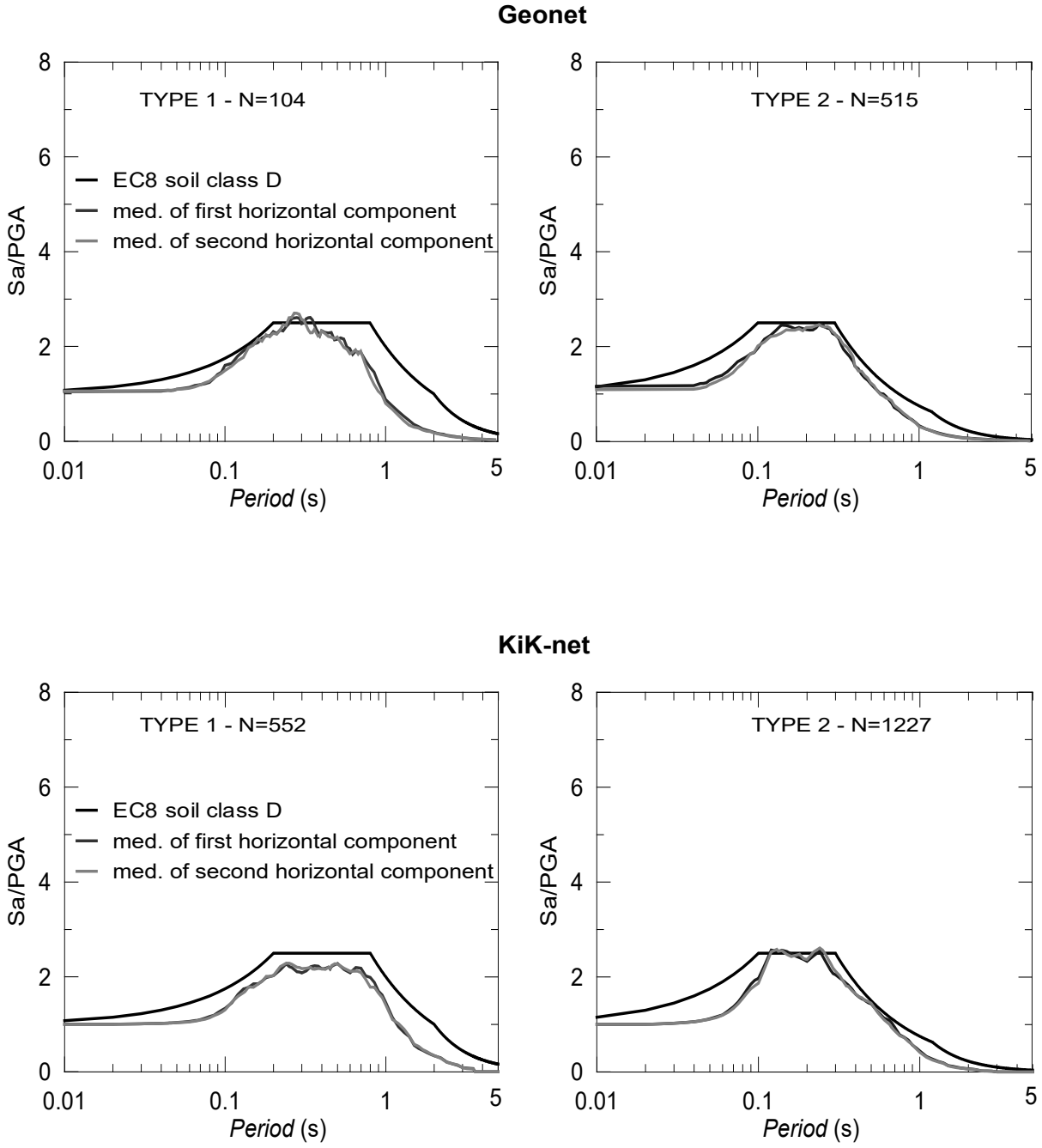

Figure A.1 Median horizontal spectral response of the earthquake events available in the earthquake databases and recorded on soil class D.

Appendix B

Chapter 6 - Application of the N-S Component of the Lotung Earthquake Events

Since the influence of elastic and nonlinear soil properties is presented in Chapter 6 only for the E-W components of the earthquake events, in this Appendix the results under the N-S component of the events are demonstrated. While Figure 1 shows the acceleration-time histories in the N-S direction, the results of the nonlinear MCSs in terms of spectral accelerations are presented in Figure 2 and Figure 3 for the strong and weak input motions, respectively.

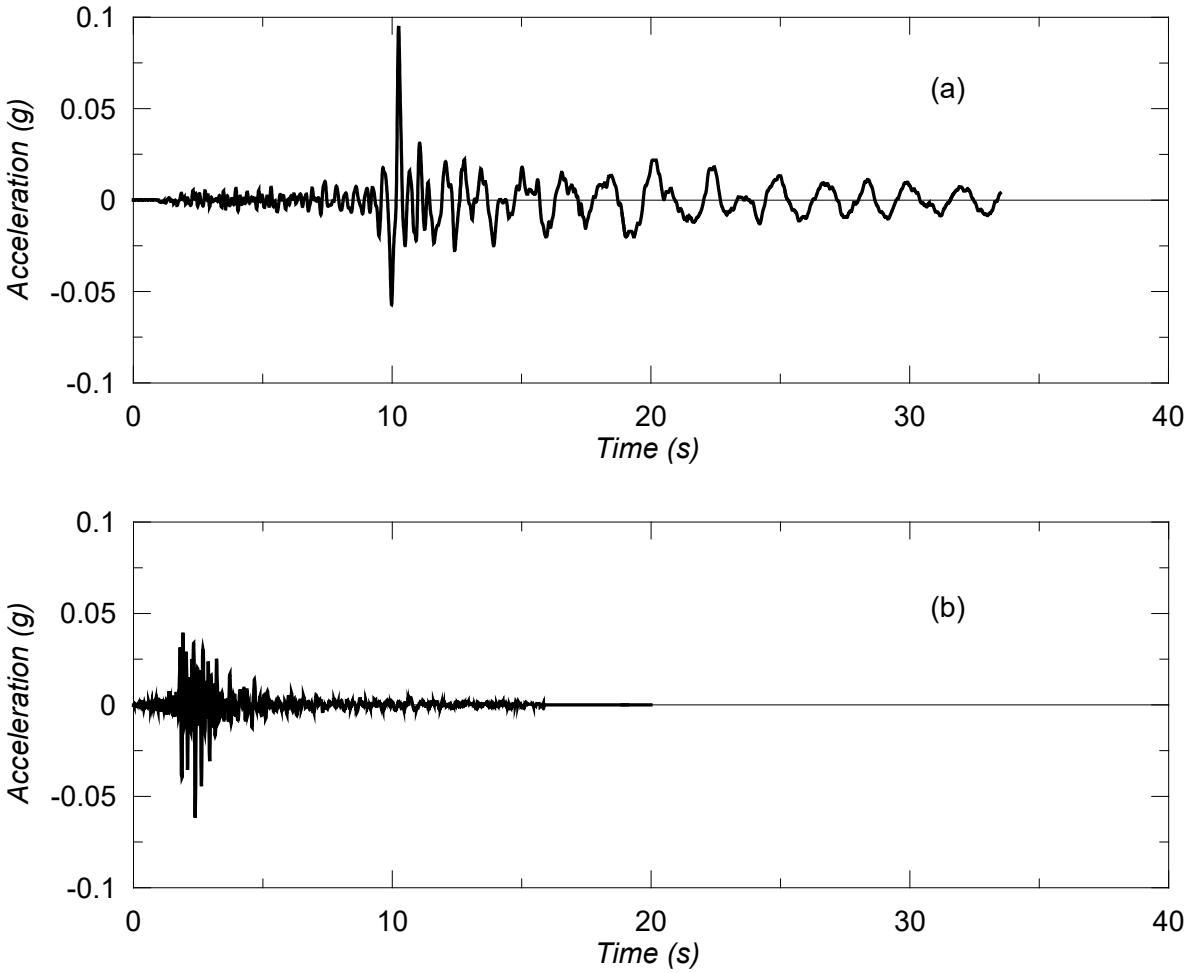

Figure B.1 Recorded input motions at the Lotung site in the North-South (N-S) direction: (a) strong earthquake event (LSST7) and (b) weak earthquake event (LSST11).

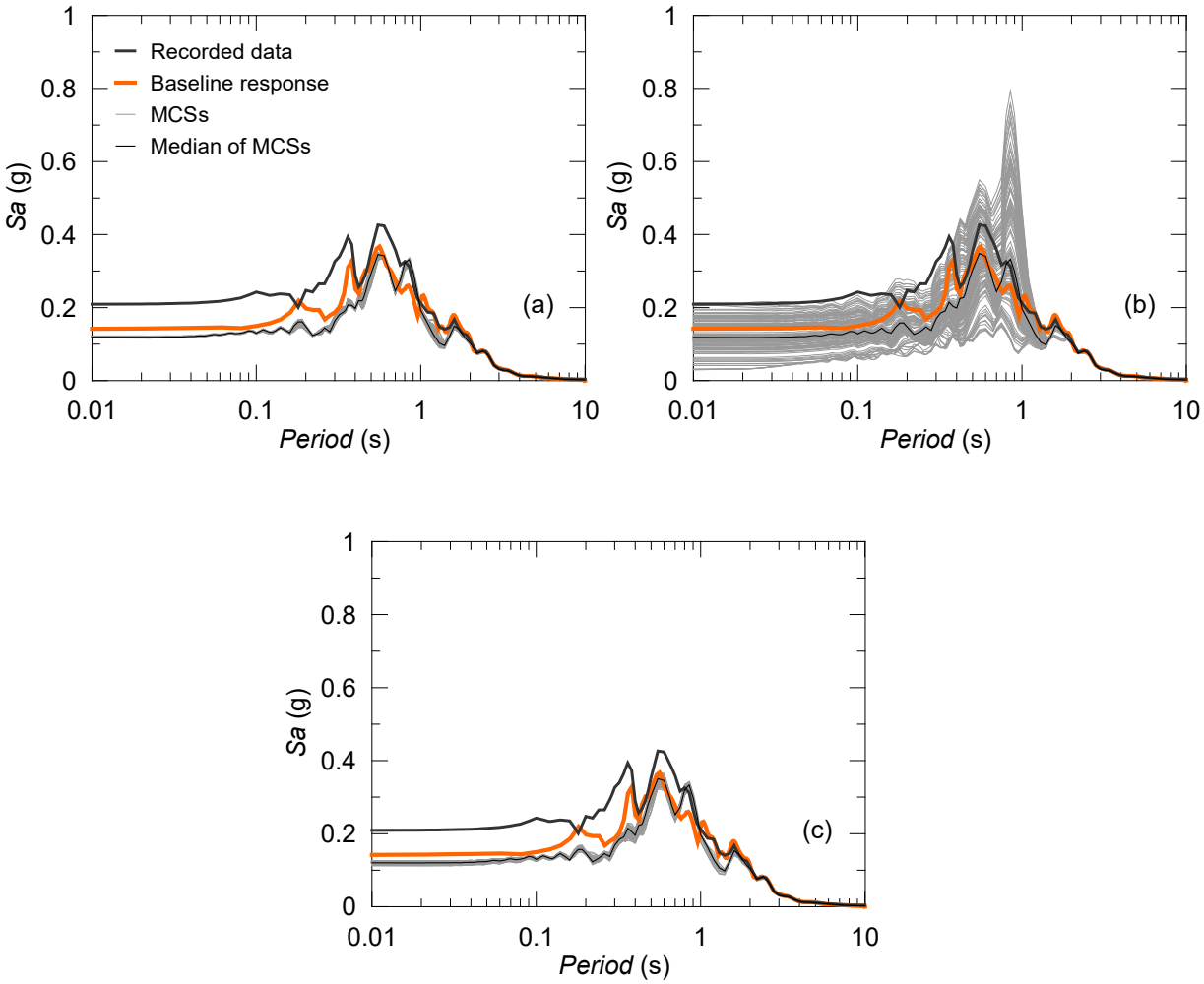

Figure B.2 Site response prediction under the strong input motion (LSST7-NS): (a) variability of V_s profile based on the probability distribution, (b) variability of G/Go and D curves and (c) variability of V_s profile based on the spatial statistics.

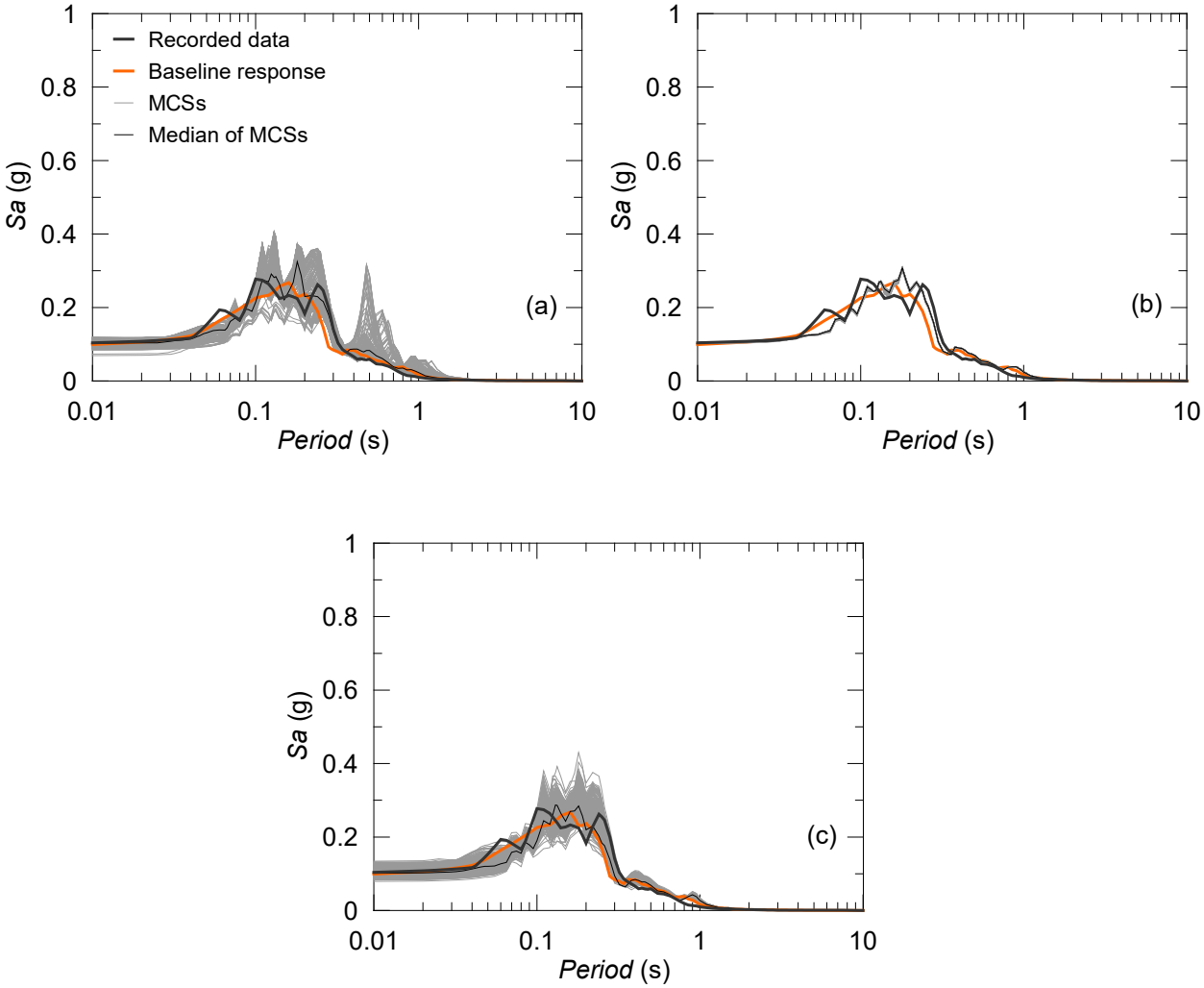

Figure B.3 Site response prediction under the weak input motion (LSST11-NS): (a) variability of V_s profile based on the probability distribution, (b) variability of G/G_0 and D curves and (c) variability of V_s profile based on the spatial statistics.

References

Abrahamson, N.A. (1992). 'Non-stationary spectral matching', *Seismological research letters*, *63*(1), p.30.

Al-Tabbaa, A. and Wood, D.M. (1989) 'An experimentally based bubble model for clay', *In: The 3rd International Symposium on Numerical models in geomechanics (NUMOG III)*. University of Cambridge, pp. 90-99.

Ambraseys, N., Smit, P., Sigbjornsson, R., Suhadolc, P. and Margaris, B. (2002) Internet-site for European String-Motion Data. Available at: http://www.isesd.hi.is/ESD_Local/frameset.htm.

Ambraseys, N., Smit, P., Douglas, J., Margaris, B., Sigbjornsson, R., Olafsson, S., Suhadolc, P. and Costa, G. (2004), 'Internet-Site for European Strong-Motion Data', *Bollettino di Geofisica Teorica ed Applicata*, 45(3), pp. 113-129.

Amirzehni, E., Taiebat, M., Finn, W.D.L. and R.H., D. (2015) 'Ground Motion Scaling/Matching for Nonlinear Dynamic Analysis of Basement Walls', *The 11th Canadian Conference on Earthquake Engineering*. Canadian Association for Earthquake Engineering.

Amorosi, A., Boldini, D. and di Lernia, A. (2016) 'Seismic ground response at Lotung: Hysteretic elasto-plastic-based 3D analyses', *Soil Dynamics and Earthquake Engineering*, 85, pp. 44-61.

Amorosi, A., Boldini, D. and Elia, G. (2010) 'Parametric study on seismic ground response by finite element modelling', *Computers and Geotechnics*, 37(4), pp. 515-528.

Ancheta, T.D., Darragh, R.B., Stewart, J.P., Seyhan, E., Silva, W.J., Chiou, B.S.J., Wooddell, K.E., Graves, R.W., Ko-ttke, A.R. and Boore, D.M. (2013) 'PEER NGA-West2 Database', PEER Report 2013/03. Berkeley: Pacific Earthquake Engineering Research Center, University of California.

Ancheta, T.D., Darragh, R.B., Stewart, J.P., Seyhan, E., Silva, W.J., Chiou, B.S.J., Wooddell, K.E., Graves, R.W., Kottke, A.R. and Boore, D.M. (2014) 'NGA-West2 database', *Earthquake Spectra*, 30(3), pp. 989-1005.

Anderson, D.G. (1993) 'Geotechnical synthesis for the Lotung large-scale seismic experiment', Technical Report No. TR-102362. Palo Alto, California: Electric Power Research Institute.

Anderson, D.G. and Tang, Y.K. (1989) 'Summary of soil characterization program for the Lotung large-scale seismic experiment', *Proc. EPRI/NRC/TPC workshop on seismic soil-structure interaction analysis techniques using data from Lotung, Taiwan,* EPRI NP-6154, 1, 4.1, 4.20. Palo Alto: Electric Power Research Institute.

Anderson, J.G. and Quaas, R. (1988) 'The Mexico earthquake of September 19, 1985—Effect of magnitude on the character of strong ground motion: An example from the Guerrero, Mexico strong motion network', *Earthquake Spectra*, 4(3), pp. 635-646.

Andrade, J.E. and Borja, R.I. (2006) 'Quantifying sensitivity of local site response models to statistical variations in soil properties', *Acta Geotechnica*, 1(1), pp. 3-14.

Archuleta, R.J., Steidl, J. and Squibb, M. (2006) 'The COSMOS Virtual Data Center: A web portal for strong motion data dissemination', *Seismological Research Letters*, 77(6), pp. 651-658.

Assimaki, D., Li, W., Steidl, J. and Schmedes, J. (2008) 'Quantifying nonlinearity susceptibility via site-response modeling uncertainty at three sites in the Los Angeles Basin', *Bulletin of the Seismological Society of America*, 98(5), pp. 2364-2390.

Arias, A. (1970) 'A measure of earthquake intensity', Seismic Design for Nuclear Power Plants, Hansen, R. , MIT Press, Cambridge, Massachusetts, pp. 438-483.

Atkinson, J.H. (1995) 'Stiffness of fine-grained soil at very small strains', *Géotechnique*, 45(2), pp. 249-265.

Aubry, D. and Modaressi, A. (1996) 'GEFDYN Manuel Scientifique'. Ecole Centrale Paris.

AGI (2005) Aspetti geotecnici della progettazione in zona sismica: linee guida. Pàtron Editore.

Baker J.W. (2008). *An Introduction to Probabilistic Seismic Hazard Analysis (PSHA).* White Paper, Version 1.3, p. 72.

Baker, J.W. and Cornell, C.A. (2005) 'A vector-valued ground motion intensity measure consisting of spectral acceleration and epsilon', *Earthquake Engineering & Structural Dynamics*, 34(10), pp. 1193-1217.

Baker, J.W. and Cornell, C.A. (2006a) 'Spectral shape, epsilon and record selection', Earthquake *Engineering & Structural Dynamics*, 35(9), pp. 1077-1095.

Baker, J.W. and Cornell, C.A. (2006b) 'Which spectral acceleration are you using?', *Earthquake Spectra*, 22(2), pp. 293-312.

Barani, S., De Ferrari, R. and Ferretti, G. (2013) 'Influence of soil modeling uncertainties on site response', *Earthquake Spectra*, 29(3), pp. 705-732.

Bardet, J.P., Ichii, K. and Lin, C.H. (2000) 'EERA: a computer program for equivalent-linear earthquake site response analyses of layered soil deposits'. University of Southern California, Department of Civil Engineering.

Bardet, J.P. and Tobita, T. (2001) 'NERA, A Computer Program for Nonlinear Earthquake Site Response Analysis Layered Soils Deposits'. Los Angeles: University of Southern California.

Bathe, K.J. (1982) *Finite element procedures in engineering analysis*. Upper Saddle River, NJ; Prentice.

Baudet, B. and Stallebrass, S. (2004) 'A constitutive model for structured clays', *Géotechnique*, 54(4), pp. 269-278.

Bazzurro, P. and Cornell, C.A. (1999) 'Disaggregation of seismic hazard', *Bulletin of the Seismological Society of America*, 89(2), pp. 501-520.

Bazzurro, P. and Cornell, C.A. (2004a) 'Ground-motion amplification in nonlinear soil sites with uncertain properties', *Bulletin of the Seismological Society of America*, 94(6), pp. 2090-2109.

Bazzurro, P., Sjoberg, B., Luco, N., Silva, W. and Darragh, R. (2004) 'Effects of Strong Motion Processing Procedures on Time Histories, Elastic and Inelastic Spectra', *Invited Workshop on Strong Motion Record Processing, Consortium of Organizations for Strong-Motion Observation Systems (COSMOS)*. Richmond, CA.

Bazzurro, P. and Cornell, C.A. (2004b) 'Nonlinear soil-site effects in probabilistic seismic-hazard analysis', *Bulletin of the Seismological Society of America*, 94(6), pp. 2110-2123.

Berger E., Fierz H., Kluge D. (1989) 'Predictive response computations for vibration tests and earthquake of May 20, 1986 using an axisymmetric finite element formulation based on the complex response method and comparison with measurements—a Swiss contribution', *In: Proceedings of the EPRI/NRC/TPC workshop on seismic soil-structure interaction analysis techniques using data from Lotung, Taiwan*, EPRI NP-6154, vol 2, pp. 15.1–15.47. Palo Alto: Electric Power Research Institute.

Biot, M.A. (1941) 'A mechanical analyzer for the prediction of earthquake stresses', *Bulletin of the Seismological Society of America*, 31(2), pp. 151-171.

Blume, J.A., Sharpe, R.L., Dalal, J.S. and Blume, J.A. (1973) 'Recommendations for shape of earthquake response spectra', Rep. No. WASH-1254. Washington DC: John A. Blume and Associates. Available at: ark:/67531/metadc784186.

Bommer, J.J. and Acevedo, A.B. (2004) 'The use of real earthquake accelerograms as input to dynamic analysis', *Journal of Earthquake Engineering*, 8(spec01), pp. 43-91.

Boore, D.M. and Atkinson, G.M. (1987) 'Stochastic prediction of ground motion and spectral response parameters at hard-rock sites in eastern North America', *Bulletin of the Seismological Society of America*, 77(2), pp. 440-467.

Boore, D.M. and Bommer, J.J. (2005) 'Processing of strong-motion accelerograms: needs, options and consequences', *Soil Dynamics and Earthquake Engineering*, 25(2), pp. 93-115.

Boore, D.M. and Joyner, W.B. (1991) 'Estimation of ground motion at deep-soil sites in eastern North America', *Bulletin of the Seismological Society of America*, 81(6), pp. 2167-2185.

Borja, R.I., Chao, H.-Y., Montáns, F.J. and Lin, C.-H. (1999a) 'Nonlinear ground response at Lotung LSST site', *Journal of Geotechnical and Geoenvironmental Engineering*, 125(3), pp. 187-197.

Borja, R.I., Chao, H.-Y., Montáns, F.J. and Lin, C.-H. (1999b) 'SSI effects on ground motion at Lotung LSST site', *Journal of Geotechnical and Geoenvironmental Engineering*, 125(9), pp. 760-770.

Borja, R.I., Duvernay, B.G. and Lin, C.-H. (2002) 'Ground response in Lotung: total stress analyses and parametric studies', *Journal of Geotechnical and Geoenvironmental Engineering*, 128(1), pp. 54-63.

Borja, R.I. and Wu, W.-H. (1994) 'Vibration of foundations on incompressible soils with no elastic region', *Journal of Geotechnical and Geoenvironmental Engineering*, 120(9), pp. 1570-1592.

Bradley, B.A. (2013) 'A critical examination of seismic response uncertainty in earthquake engineering', *Earthquake Engineering & Structural Dynamics*, 42(11), pp.1717-1729.

Brinkgreve, R.B.J., Engin, E. and Swolfs, W.M. (2013) 'PLAXIS 3D 2013 user manual'. Plaxis bv, Delft.

Brinkgreve, R.B.J., Swolfs, W.M. and Engin, E. (2011) 'PLAXIS 2D Reference manual'. Delft University of Technology and PLAXIS bv The Netherlands.

Burland, J.B. (1990) 'On the compressibility and shear strength of natural clays', *Géotechnique*, 40(3), pp. 329-378.

Campbell, K.W., Bozorgnia, Y. (2013) 'NGA-West2 Campbell-Bozorgnia Ground Motion Model for the Horizontal Components of PGA, PGV, and 5%-Damped Elastic Pseudo-Acceleration Response Spectra for Periods Ranging from 0.01 to 10 s', PEER Report 2013/06. Berkeley: Pacific Earthquake Engineering Research Center, University of California.

Campbell, K.W. and Bozorgnia, Y. (2008) 'NGA ground motion model for the geometric mean horizontal component of PGA, PGV, PGD and 5% damped linear elastic response spectra for periods ranging from 0.01 to 10 s', *Earthquake Spectra*, 24(1), pp. 139-171.

CEN (2005) Eurocode 8: Design of structures for earthquake resistance–Part 1: General rules, seismic actions and rules for buildings. CEN Brussels.

Chan, A.H.C. (1995) 'User's Manual for DIANA-SWANDYNE II'. University of Birmingham, UK.

Chang, S.W.-Y. (1996) Seismic performance of deep soil deposits. Ph.D. thesis. Berkeley: University of California.

Chen, H., Sun, R., Yuan, X. and Zhang, J. (2008) 'Variability of nonlinear dynamic shear modulus and damping ratio of soils', *Proceedings, 14th International Conference on Earthquake Engineering*. Beijing, China.

Clough, R.W. and Penzien, J. (2003) *Dynamics of structures*. Berkeley: Computers and Structures Inc.

Darendeli, M.B., Stokoe, K.H. (2001) '*Development of a new family of normalized modulus reduction and material damping curves*', Geotech. Engrg. Rpt. GD01-1. Austin: University of Texas.

Dawood, H.M., Rodriguez-Marek, A., Bayless, J., Goulet, C.A. and Thompson, E. (2014) *The KiK-net database processed using an automated ground motion processing protocol.* Available at: https://nees.org/resources/7849.

Dawood, H.M., Rodriguez-Marek, A., Bayless, J., Goulet, C.A. and Thompson, E. (2016) 'A Flatfile for the KiK-net Database Processed Using an Automated Protocol', *Earthquake Spectra*, 32(2), pp. 1281-1302.

Depina, I., Le, T.M.H., Eiksund, G. and Benz, T. (2015) 'Behavior of cyclically loaded monopile foundations for offshore wind turbines in heterogeneous sands', *Computers and Geotechnics*, 65, pp. 266-277.

Dobry, R., Idriss, I.M. and Ng, E. (1978) 'Duration characteristics of horizontal components of strong-motion earthquake records', *Bulletin of the Seismological Society of America*, 68(5), pp. 1487-1520.

El-Kadi, A.I. and Williams, S.A. (2000) 'Generating Two-Dimensional Fields of Autocorrelated, Normally Distributed Parameters by the Matrix Decomposition Technique', *Groundwater*, 38(4), pp. 530-532.

Elgamal, A.W., Zeghal, M., Tang, H.T. and Stepp, J.C. (1995) 'Lotung downhole array. I: Evaluation of site dynamic properties', *Journal of Geotechnical Engineering*, 121(4), pp. 350-362.

Elgamal, A.W., Zeghal, M., Tang, H.T. and Stepp, J.C. (1995) 'Lotung downhole array. II: Evaluation of soil nonlinear properties', Journal of Geotechnical Engineering, 121(4), pp. 363-378.

Elia G. (2015) 'Site response for seismic hazard assessment', *In: Encyclopedia of Earthquake Engineering.*Springer (DOI: 10.1007/978-3-642-36197-5_241-1).

Elia, G., Amorosi, A., Chan, A.H.C. and Kavvadas, M.J. (2011) 'Fully coupled dynamic analysis of an earth dam', *Geotechnique*, 61(7), pp. 549-563.

Elia, G., Dimitrios, K. and Rouainia, M. (2015) 'Non-linear finite element analysis of site effects at Lotung (Taiwan)', *SECED 2015 Conference: Earthquake Risk and Engineering towards a Resilient World*. Cambridge, UK.

Elia, G. and Rouainia, M. (2012) 'Seismic performance of earth embankment using simple and advanced numerical approaches', *Journal of Geotechnical and Geoenvironmental Engineering*, 139(7), pp. 1115-1129.

Elia, G. and Rouainia, M. (2014) 'Performance evaluation of a shallow foundation built on structured clays under seismic loading', *Bulletin of Earthquake Engineering*, 12(4), pp. 1537-1561.

Elia, G., Rouainia, M., Karofyllakis, D. and Guzel, Y. (2017) 'Modelling the non-linear site response at the LSST down-hole accelerometer array in Lotung', *Soil Dynamics and Earthquake Engineering*, 102, pp. 1-14.

Engineers (1999) *Response spectra and seismic analysis for concrete hydraulic structures*. US Army Corps of Engineers, Washington, DC.

EPRI (1993) 'Guidelines for determining design basis ground motions-Volume 1: method and guidelinesfor estimating for estimating earthquake ground motion in Eastern North America', Rep. No. TR-102293. Palo Alto, California: Electric Power Research Institute.

Eurocode, C.E.N. (2004) *8: Design of structures for earthquake resistance—Part 1: General rules, seismic actions and rules for buildings (EN 1998-1: 2004).* European Committee for Normalization, Brussels.

Field, E.H., Jordan, T.H. and Cornell, C.A. (2003) 'OpenSHA: A developing community-modeling environment for seismic hazard analysis', *Seismological Research Letters*, 74(4), pp. 406-419.

Finn, W.D.L., Yogendrakumar, M., Yoshida, N. and Yoshida, H. (1986) 'TARA-3: a program for nonlinear static and dynamic effective stress analysis'. Vancouver, BC, Canada: Soil Dynamics Group, University of British Columbia.

Galasso, C. (2010) Consolidating record selection for earthquake resistant structural design. Ph.D thesis. Università degli Studi di Napoli Federico II.

Galasso, C. and Iervolino, I. (2011) 'Relevant and minor criteria in real record selection procedures based on spectral compatibility', *XIV Convegno Associazione Nazionale Italiana di Ingegneria Sismica ANIDIS*. Bari, Italy.

Glaser, S.D. and Leeds, A.L. (1996) Preliminary Processing of the Lotung LSST Data. US National Institute of Standards and Technology.

Gonzalez, N.A., Rouainia, M., Arroyo, M. and Gens, A. (2012) 'Analysis of tunnel excavation in London Clay incorporating soil structure', *Géotechnique*, 62(12), p. 1095.

Gutenberg, B. and Richter, C.F. (1944) 'Frequency of earthquakes in California', *Bulletin of the Seismological Society of America*, 34(4), pp. 185-188.

Hall, J.F. and Beck, J.L. (1986) 'Structural damage in Mexico city', *Geophysical Research Letters*, 13(6), pp. 589-592.

Hancock, J., Watson-Lamprey, J., Abrahamson, N.A., Bommer, J.J., Markatis, A., McCoy, E. and Mendis, R. (2006) 'An improved method of matching response spectra of recorded earthquake ground motion using wavelets', *Journal of Earthquake Engineering*, 10(spec01), pp. 67-89.

Hanks, T.C. and McGuire, R.K. (1981) 'The character of high-frequency strong ground motion', *Bulletin of the Seismological Society of America*, 71(6), pp. 2071-2095.

Haselton, C.B., Whittaker, A.S., Hortacsu, A., Baker, J.W., Bray, J. and Grant, D.N. (2012) 'Selecting and scaling earthquake ground motions for performing response-history analyses', *Proceedings of the 15th World Conference on Earthquake Engineering*. Lisbon, Portugal.

Hashash, Y.M.A., Groholski, D.R., Phillips, C.A., Park, D. and Musgrove, M. (2012) 'DEEPSOIL 5.1', User Manual and Tutorial.

Hashash, Y.M.A. and Park, D. (2002) 'Viscous damping formulation and high frequency motion propagation in non-linear site response analysis', *Soil Dynamics and Earthquake Engineering*, 22(7), pp. 611-624.

Hashiguchi, K. (1989) 'Subloading surface model in unconventional plasticity', *International Journal of Solids and Structures*, 25(8), pp. 917-945.

Hatanaka, M. and Uchida, A. (1996) 'Empirical Correlation between Penetration Resistance and Internal Friction Angle of Sandy Soils', *Soils and Foundations*, 36(4), pp. 1-9.

Housner, G.W. (1941) *An investigation of the effects of earthquakes on buildings*. California Institute of Technology.

Housner, G.W. (1952) *Spectrum intensities of strong-motion earthquakes*. California Institute of Technology.

Hudson, M., Idriss, I.M. and Beikae, M. (1994) 'User's manual for Quad4m: a computer program to evaluate the seismic response of soil structures using finite element procedures and incorporating a compliant base'. Davis, California: Center for Geotechnical Modeling, Dept. Civil&Environmental Engineering, University of California.

Idriss, I.M. (1973) 'Quad-4: A Computer Program for Evaluating the Seismic Response of Soil Structures by Variable Damping Finete Element Procedures', Rep. No. EERC 73-16. Berkeley: Earthquake Engineering Research Center, University of California.

Idriss, I.M. (2004) 'Evolution of state of practise', *Int. Workshop on the Uncertainties in Nonlinear Soil Properties and Their Impact on Modeling Dynamic Soil Response*. Pacific Earthquake Engineering Research Center, Richmond, California.

Idriss, I.M. and Sun, J.I. (1992) 'SHAKE91: A computer program for conducting equivalent linear seismic response analyses of horizontally layered soil deposits'. Davis, California:

Center for Geotechnical Modeling. Department of Civil and Environmental Engineering, University of California.

Iervolino, I. and Cornell, C.A. (2005) 'Record selection for nonlinear seismic analysis of structures', *Earthquake Spectra*, 21(3), pp. 685-713.

Iervolino, I., Galasso, C. and Cosenza, E. (2010) 'Rexel: computer aided record selection for code-based seismic structural analysis', *Bulletin of Earthquake Engineering*, 8, pp. 339-392.

Iervolino, I., Maddaloni, G. and Cosenza, E. (2008) 'Eurocode 8 compliant real record sets for seismic analysis of structures', *Journal of Earthquake Engineering*, 12(1), pp. 54-90.

Iervolino, I. and Manfredi, G. (2008) 'A Review of Ground Motion Record Selection Strategies for Dynamic Structural Analysis', in Bursi, O.S. and Wagg, D. (eds.) Modern Testing Techniques for Structural Systems. *Springer Science & Business Media*, pp. 131-163.

Iervolino, I., Manfredi, G. and Cosenza, E. (2006) 'Ground motion duration effects on nonlinear seismic response', *Earthquake Engineering & Structural Dynamics*, 35(1), pp. 21-38.

Ince, G. and Yılmazoğlu, L. (2014) 'Investigating the influence of topographic irregularities and two-dimensional effects on surface ground motion intensity with one- and two-dimensional analyses', *Natural Hazards and Earth System Sciences*, 14(7), pp. 1773-1788.

Itasca, F. (2012) 'Fast Lagrangian Analysis of Continua, Ver.7.0'. Itasca Consulting Group, Inc., Minn.

Jousset, P. and Douglas, J. (2007) 'Long-period earthquake ground displacements recorded on Guadeloupe (French Antilles)', *Earthquake Engineering & Structural Dynamics*, 36(7), pp. 949-963.

Kaiser, A., Holden, C., Beavan, J., Beetham, D., Benites, R., Celentano, A., Collett, D., Cousins, J., Cubrinovski, M. and Dellow, G. (2012) 'The Mw 6.2 Christchurch earthquake of February 2011: preliminary report', *New Zealand Journal of Geology and Geophysics*, 55(1), pp. 67-90.

Kaklamanos, J., Baise, L.G., Thompson, E.M. and Dorfmann, L. (2015) 'Comparison of 1D linear, equivalent-linear, and nonlinear site response models at six KiK-net validation sites', *Soil Dynamics and Earthquake Engineering*, 69, pp. 207-219.

Katona, M.C. and Zienkiewicz, O.C. (1985) 'A unified set of single step algorithms part 3: The beta‐m method, a generalization of the Newmark scheme', *International Journal for Numerical Methods in Engineering*, 21(7), pp. 1345-1359.

Kavvadas, M. and Amorosi, A. (2000) 'A constitutive model for structured soils', *Géotechnique*, 50(3), pp. 263-273.

Khose, V.N., Singh, Y. and Lang, D.H. (2012) 'A comparative study of design base shear for RC buildings in selected seismic design codes', *Earthquake Spectra*, 28(3), pp. 1047-1070.

Kontoe, S., Zdravkovic, L., Potts, D.M. and Salandy, N.E. (2007) 'The use of absorbing boundaries in dynamic analyses of soil-structure interaction problems', *In: 4th International Conference on Earthquake Geotechnical Engineering*. Thessaloniki, Greece.

Kottke, A. and Rathje, E.M. (2008) 'A semi-automated procedure for selecting and scaling recorded earthquake motions for dynamic analysis', *Earthquake Spectra*, 24(4), pp. 911-932.

Kottke, A.R. and Rathje, E.M. (2009) 'Technical manual for Strata', Rep. No. 2008/10. Berkeley, California: Pacific Earthquake Engineering Research Center.

Krahn, J. (2004) 'Dynamic modeling with QUAKE/W: an engineering methodology'. Alberta, Canada: GEO-SLOPE International Ltd.

Kramer, L.S. (1996) *Geotechnical Earthquake Engineering*. Essex, England: Pearson Education Limited.

Kwok, A.O., Stewart, J.P., Hashash, Y.M., Matasovic, N., Pyke, R., Wang, Z. and Yang, Z. (2007) 'Use of exact solutions of wave propagation problems to guide implementation of nonlinear seismic ground response analysis procedures', *Journal of Geotechnical and Geoenvironmental Engineering*, 133(11), pp. 1385-1398.

Kwok, A.O.L., Stewart, J.P. and Hashash, Y.M.A. (2008) 'Nonlinear ground-response analysis of Turkey flat shallow stiff-soil site to strong ground motion', *Bulletin of the Seismological Society of America*, 98(1), pp. 331-343.

Land, C. E. (1972) 'An evaluation of approximate confidence interval estimation methods for lognormal means', Technometrics, 14, pp. 145-158.

Lee, M.K.W. and Finn, W.D.L. (1978) 'DESRA-2: Dynamic effective stress response analysis of soil deposits with energy transmitting boundary including assessment of liquefaction potential'. Department of Civil Engineering, University of British Columbia.

Li, W. and Assimaki, D. (2010) 'Site-and motion-dependent parametric uncertainty of site-response analyses in earthquake simulations', *Bulletin of the Seismological Society of America*, 100(3), pp. 954-968.

Li, X.S., Shen, C.K. and Wang, Z.L. (1998) 'Fully coupled inelastic site response analysis for 1986 Lotung earthquake', Journal of Geotechnical and Geoenvironmental Engineering, 124(7), pp. 560-573.

Li, X.S., Wang, Z.L. and Shen, C.K. (1992) 'SUMDES: A nonlinear procedure for response analysis of horizontally-layered sites subjected to multi-directional earthquake loading', p. 86. Department of Civil Engineering, University of California, Davis

Lu, J., Elgamal, A.-W.M. and Yang, Z. (2006) 'Cyclic1D: A computer program for seismic ground response', Rep. No SSRP-06/05. San Diego, La Jolla, CA: University of California.

Luzi, L., Hailemikael, S., Bindi, D., Pacor, F., Mele, F. and Sabetta, F. (2008) 'ITACA (ITalian ACcelerometric Archive): a web portal for the dissemination of Italian strong-motion data', *Seismological Research Letters*, 79(5), pp. 716-722.

Lysmer, J., Udaka, T., Tsai, C. and Seed, H.B. (1975) 'FLUSH-A computer program for approximate 3-D analysis of soil-structure interaction problems'. California University, Richmond (USA): Earthquake Engineering Research Center.

Malhotra, P.K. (2006) 'Smooth spectra of horizontal and vertical ground motions', *Bulletin of the Seismological Society of America*, 96(2), pp. 506-518.

Marasco, S. and Cimellaro, G.P. (2017) 'A new energy-based ground motion selection and modification method limiting the dynamic response dispersion and preserving the median demand', *Bulletin of Earthquake Engineering*, pp. 1-21.

Matasovic, N. (2006) 'D-MOD_2: A computer program for seismic response analysis of horizontally layered soil deposits, earthfill dams, and solid waste landfills'. GeoMotions, LLC.

Matasovic, N. and Ordonez, G. (2012) 'D-MOD2000–A computer program for seismic site response analysis of horizontally layered soil deposits, earthfill dams and solid waste landfills', Geomotions, LLC.

Mazzoni, S., Hachem, M. and Sinclair, M. (2012) 'An improved approach for ground motion suite selection and modification for use in response history analysis', *15th World Conference on Earthquake Engineering*. Lisbon, Portugal. Curran Associates, Inc.

McGuire, R.K. (1995) 'Probabilistic seismic hazard analysis and design earthquakes: closing the loop', *Bulletin of the Seismological Society of America*, 85(5), pp. 1275-1284.

McGuire, R.K., Toro, G.R. and Silva, W.J. (1988) 'Engineering model of earthquake ground motion for eastern North America'. Palo Alto, CA (USA): Electric Power Research Institute, Risk Engineering, Inc., Golden.

McKenna, F. and Fenves, G.L. (2001) 'The OpenSees command language manual'. University of California (opensees. ce. berkeley. edu).

Midorikawa, M., Okawa, I., Iiba, M. and Teshigawara, M. (2003) 'Performance-based seismic design code for buildings in Japan', *Earthquake Engineering and Engineering Seismology*, 4(1), pp. 15-25.

Mohraz, B. (1976) 'A study of earthquake response spectra for different geological conditions', *Bulletin of the Seismological Society of America*, 66(3), pp. 915-935.

Mroz, Z., Norris, V.A. and Zienkiewicz, O.C. (1979) 'Application of an anisotropic hardening model in the analysis of elasto–plastic deformation of soils', *Geotechnique*, 29(1), pp. 1-34.

Muir Wood, D. (1990) *Soil behaviour and critical state soil mechanics*. Cambridge: Cambridge University Press.

Muravskii, G. (2005) 'On description of hysteretic behaviour of materials', *International Journal of Solids and Structures*, 42(9), pp. 2625-2644.

Nash, J.C. (1990) *Compact numerical methods for computers: linear algebra and function minimisation*. 2nd edn. Bristol, England: CRC press.

Newmark, N.M., Blume, J.A. and Kapur, K.K. (1973a) 'Seismic design spectra for nuclear power plants', *Journal of the Power Division, Poroceeedings of the American Society of Civil Engineers*, 99(PO2).

Newmark, N.M., Hall, W.J. and Mohraz, B. (1973b) 'A study of vertical and horizontal earthquake spectra'. Richord, California: Earthquake Engineering Research Center.

Newmark, N. M. and Hall, W. J. (1982) 'Earthquake Spectra and Design', *EERI Monograph*. Oakland: Earthquake Engineering Research Institute.

Ordóñez, G.A. (2000) 'SHAKE2000: A computer program for the 1D analysis of geotechnical earthquake engineering problems'. Lacey, Washington, USA: Geomotions, LLC.

Pacor, F., Paolucci, R., Luzi, L., Sabetta, F., Spinelli, A., Gorini, A., Nicoletti, M., Marcucci, S., Filippi, L. and Dolce, M. (2011) 'Overview of the Italian strong motion database ITACA 1.0', *Bulletin of Earthquake Engineering*, 9(6), pp. 1723-1739.

Panayides, S. (2014) Modelling the effects of structure degradation in geotechnical problems. Ph.D thesis. Newcastle University.

Paolucci, R., Rovelli, A., Faccioli, E., Cauzzi, C., Finazzi, D., Vanini, M., Di Alessandro, C. and Calderoni, G. (2008) 'On the reliability of long-period response spectral ordinates from digital accelerograms', *Earthquake Engineering & Structural Dynamics*, 37(5), pp. 697-710.

Park, D. and Hashash, Y.M.A. (2004) 'Soil damping formulation in nonlinear time domain site response analysis', *Journal of Earthquake Engineering*, 8(02), pp. 249-274.

Phoon, K.-K. and Kulhawy, F.H. (1999) 'Characterization of geotechnical variability', *Canadian Geotechnical Journal*, 36(4), pp. 612-624.

Pitilakis, K., Riga, E. and Anastasiadis, A. (2012) 'Design spectra and amplification factors for Eurocode 8', *Bulletin of Earthquake Engineering*, 10(5), pp. 1377-1400.

Pousse, G., Berge-Thierry, C., Bonilla, L.F. and Bard, P.-Y. (2005) 'Eurocode 8 design response spectra evaluation using the K-Net Japanese database', *Journal of Earthquake Engineering*, 9(04), pp. 547-574.

Prevost, J.H. (1981) 'DYNA-FLOW: a nonlinear transient finite element analysis program'. Princeton University, Department of Civil Engineering, School of Engineering and Applied Science.

Pyke, R.M. (1973) Settlement and liquefaction of sands under multi-directional loading. Ph.D thesis. University of California, Berkeley.

Pyke, R.M. (1992) 'TESS: a computer program for nonlinear ground response analyses TAGA Engineering Systems and Software'. Lafayette.

Rathje, E.M., Kottke, A.R. and Trent, W.L. (2010) 'Influence of input motion and site property variabilities on seismic site response analysis', *Journal of Geotechnical and Geoenvironmental Engineering*, 136(4), pp. 607-619.

Rathje, E.M. and Ozbey, M.C. (2006) 'Site-specific validation of random vibration theory-based seismic site response analysis', *Journal of Geotechnical and Geoenvironmental Engineering*, 132(7), pp. 911-922.

Rey, J., Faccioli, E. and Bommer, J.J. (2002) 'Derivation of design soil coefficients (S) and response spectral shapes for Eurocode 8 using the European Strong-Motion Database', *Journal of Seismology*, 6(4), pp. 547-555.

Riddel, R. (1996) 'Use and knowledge of design spectra', *Eleventh World Conference on Earthquake Engineering*. Santiago, Chile.

Robert, E.M. (1999) *Structural reliability analysis and prediction*. Baffins Lane, Chichester, West Sussex, England: Wiley.

Roblee, C., Silva, W., Toro, G., and Abrahamson, N. (1996) 'Variability in site-specific seismic ground-motion design predictions', *Geotechnical Special Publications*, 58(2), pp. 1113–1133.

Roesset, J.M. (1977) 'Soil amplification of earthquakes', Numerical methods in geotechnical engineering, pp. 639-682.

Roscoe, K.H. (1963) 'Mechanical behaviour of an idealised 'wet' clay', *Proceedings of the second European Conference on Soil Mechanics*, pp. 47-54. Wiesbaden, Germany.

Roscoe, K.H. and Burland, J.B. (1968) 'On the generalized stress-strain behaviour of 'wet' clay'. Cambridge: Cambridge University Press.

Rota, M., Lai, C.G. and Strobbia, C.L. (2011) 'Stochastic 1D site response analysis at a site in central Italy', *Soil Dynamics and Earthquake Engineering*, 31(4), pp. 626-639.

Rouainia, M. and Muir Wood, D. (2000) 'A kinematic hardening constitutive model for natural clays with loss of structure', *Géotechnique*, 50(2), pp. 153-164.

Sarma, S.K. and Irakleidis, A.-K. (2007) 'An investigation into the uncertainty of the one dimensional site response analysis', *4th International Conference on Earthquake Geotechnical Engineering*. Thessaloniki, Greece.

Schnabel, P.B., Lysmer, J. and Seed, H.B. (1972) 'SHAKE–A computer program for response analysis of horizontally layered sites', Rep. No. EERC 72-12. Berkeley: University of California.

Scholl, R.E. (1989) 'Observations of the performance of buildings during the 1985 Mexico earthquake, and structural design implications', *International Journal of Mining and Geological Engineering*, 7(1), pp. 69-99.

Seed, H.B. and Idriss, I.M. (1970) 'Soil moduli and damping factors for dynamic response analyses', Rep. No. EERC 70/10. Berkeley: Earthquake Engineering Research Center, University of California.

Seed, H.B., Ugas, C. and Lysmer, J. (1976) 'Site-dependent spectra for earthquake-resistant design', *Bulletin of the Seismological Society of America*, 66(1), pp. 221-243.

Seed, R.B. (1990) 'Preliminary report on the principal geotechnical aspects of the October 17, 1989 Loma Prieta earthquake', Rep. No. UCB/EERC-90/05. Berkeley: Earthquake Engineering Research Center, University of California.

Seifried, A.E. and Baker, J.W. (2016) 'Spectral variability and its relationship to structural response estimated from scaled and spectrum-matched ground motions', *Earthquake Spectra*, 32(4), pp. 2191-2205.

Seismosoft (2016) 'SeismoMatch 2016 – A computer program for spectrum matching of earthquake records'. Available from http://www.seismosoft.com.

Shapiro, S.S. and Wilk, M.B. (1965) 'An analysis of variance test for normality (complete samples)', Biometrika, 52(3/4), pp. 591-611.

Shen, C.K., Chan, C.K., Li, X.S., Yang, H.W., Ueng, T.S., Wu, W.T. and Chen, C.H. (1989) 'Chapter 25: Pore water pressure response measurements at Lotung site', *Proceedings: EPRI/NRC/TPC Workshop on Seismic Soil-Structure Interaction Analysis Techniques using Data from Lotung, Taiwan*, Rep. No. EPRI NP-6154. Palo Alto, California: Electric Power Research Institute.

Shome, N., Cornell, C.A., Bazzurro, P. and Carballo, J.E. (1998) 'Earthquakes, records, and nonlinear responses', *Earthquake Spectra*, 14(3), pp. 469-500.

Silva, W.J. and Green, R.K. (1989) 'Magnitude and distance scaling of response spectral shapes for rock sites with applications to North American tectonic environment', *Earthquake Spectra*, 5(3), pp. 591-624.

Somerville, P.G., Smith, N.F., Graves, R.W. and Abrahamson, N.A. (1997) 'Modification of empirical strong ground motion attenuation relations to include the amplitude and duration effects of rupture directivity', *Seismological Research Letters*, 68(1), pp. 199-222.

Stewart, J.P., Chiou, S.-J., Bray, J.D., Graves, R.W., Somerville, P.G. and Abrahamson, N.A. (2002) 'Ground motion evaluation procedures for performance-based design', *Soil Dynamics and Earthquake Engineering*, 22(9), pp. 765-772.

Stewart, J.P. and Kwok, A.O. (2008) 'Nonlinear seismic ground response analysis: code usage protocols and verification against vertical array data', *Geotechnical Engineering and Soil Dynamics IV*, ASCE Geotechnical Special Publication No. 181, 181.

Stone, W.C., Yokel, F.Y., Celebi, M., Hanks, T. and Leyendecker, E.V. (1987) 'Engineering aspects of the September 19, 1985 Mexico earthquake', Rep. No. NBS BSS 165. Building Science Series, National Institute of Standards and Technology.

Tang, H.T. (1987) 'Large-scale soil structure interaction', Rep. No. NP-5513-SR. Palo Alto, California: Electric Power Research Institute.

Tang, H.T., Tang, Y.K. and Stepp, J.C. (1990) 'Lotung large-scale seismic experiment and soil-structure interaction method validation', *Nuclear Engineering and Design*, 123(2), pp. 397-412.

Tönük, G., Ansal, A., Kurtuluş, A. and Çetiner, B. (2014) 'Site specific response analysis for performance based design earthquake characteristics', *Bulletin of Earthquake Engineering*, 12(3), pp. 1091-1105.

Toro, G. R. (1995) 'Probabilistic models of site velocity profiles for generic and site-specific ground-motion amplification studies', Technical Rep. No. 779574. Brookhaven National Laboratory, Upton, New York.

Trifunac, M.D. (2008) 'Early history of the response spectrum method', *Soil Dynamics and Earthquake Engineering*, 28(9), pp. 676-685.

Viggiani, G. and Atkinson, J.H. (1995) 'Stiffness of fine-grained soil at very small strains', *Géotechnique*, 45(2), pp. 249-265.

Visone, C., Santucci de Magistris, F. and Bilotta, E. (2010) 'Comparative study on frequency and time domain analyses for seismic site response', *Electronic Journal of Geotechnical Engineering*, 15, pp. 1-20.

Vucetic, M. (1986) *Pore pressure buildup and liquefaction at level sandy sites during earthquakes*. Rensselaer Polytechnic Institute.

Vucetic, M. and Dobry, R. (1991) 'Effect of soil plasticity on cyclic response', *Journal of Geotechnical Engineering*, 117(1), pp. 89-107.

Welch, B.L. (1938) 'The significance of the difference between two means when the population variances are unequal', *Biometrika*, 29(3/4), pp. 350-362.

Yang, J. and Yan, X. (2009) 'Factors affecting site response to multi-directional earthquake loading', *Engineering Geology*, 107(3), pp. 77-87.

Youd, T.L. and Croven, T.N. (1975) 'Lateral stress in sands during cyclic loading', *Journal of Geotechnical and Geoenvironmental Engineering*, 101(ASCE# 11093 Tech. Note).

Zalachoris, G. and Rathje, E.M. (2015) 'Evaluation of One-Dimensional Site Response Techniques Using Borehole Arrays', *Journal of Geotechnical and Geoenvironmental Engineering*, 141(12).

Zeghal, M. and Elgamal, A.-W. (1994) 'Analysis of site liquefaction using earthquake records', *Journal of Geotechnical Engineering*, 120(6), pp. 996-1017.

Zeghal, M., Elgamal, A.W., Tang, H.T. and Stepp, J.C. (1995) 'Lotung downhole array. II: Evaluation of soil nonlinear properties', *Journal of Geotechnical Engineering*, 121(4), pp. 363-378.

Zhang, J., Andrus, R.D. and Juang, C.H. (2005) 'Normalized shear modulus and material damping ratio relationships', *Journal of Geotechnical and Geoenvironmental Engineering*, 131(4), pp. 453-464.

Zhao, J., Sheng, D., Rouainia, M. and Sloan, S.W. (2005) 'Explicit stress integration of complex soil models', *International Journal for Numerical and Analytical Methods in Geomechanics*, 29(12), pp. 1209-1229.

Zhou, X.H. and Gao, S. (1997) 'Confidence intervals for the log-normal mean', *Statistics in medicine*, *16*(7), pp.783-790.

Zienkiewicz, O.C., Chan, A.H.C., Pastor, M., Schrefler, B.A. and Shiomi, T. (1999) *Computational geomechanics (with Special Reference to Earthquake Engineering)*. Chichester, England: John Wiley & Sons.

Publications

1 Elia, G., Rouainia, M., Karofyllakis, D. and **Guzel, Y.** (2017) 'Modelling the non-linear site response at the LSST down-hole accelerometer array in Lotung', *Soil Dynamics and Earthquake Engineering*, 102, pp. 1-14.

2 **Guzel, Y.**, Elia, G., Rouainia, M. (2017) 'The effect of input motion selection strategies on nonlinear ground response predictions', *COMPDYN 2017 – 6th International Thematic Conference*. Rhodes Island, Greece: National Technical University of Athens.

3 **Guzel, Y.**, Elia, G., Rouainia, M. (2017) 'Effect of statistical variation in soil dynamic properties on local site response: the case of Lotung', *16th European Conference on Earthquake Engineering*. Thessaloniki, Greece: Hellenic Society of the European Association for Earthquake Engineering and Aristotle University of Thessaloniki.

4 **Guzel, Y.**, Rouainia, M., Elia, G. (2018) 'The effect of soil properties on nonlinear site response predictions: applications to the Lotung site', *Soil Dynamics and Earthquake Engineering* **(under review, submitted on 20/02/2018)**.

5 **Guzel, Y.**, Elia, G., Rouainia, M. (2018) 'Influence of input motion selection and scaling strategies on nonlinear ground response analyses of soft soil deposits', *Acta Geotechnica* **(ready for submission)**.